The Dissertation Committee for Christopher Adam Griffith Certifies that this is the approved version of the following Dissertation:

Colloidal Particles at Fluid Interfaces: from Stabilizing Emulsions to Destabilizing Them

Committee:

Hugh C. Daigle, Supervisor

Larry W. Lake

Kishore Mohanty

Matthew Thomas Balhoff

Charles J. Werth

Colloidal Particles at Fluid Interfaces: from Stabilizing Emulsions to Destabilizing Them

by

Christopher Adam Griffith

Dissertation

Presented to the Faculty of the Graduate School of

The University of Texas at Austin

in Partial Fulfillment

of the Requirements

for the Degree of

Doctor of Philosophy

The University of Texas at Austin

May 2019

Acknowledgements

First, I would like to thank my advisor Dr. Hugh Daigle for being an incredible advisor. Dr. Daigle gave me the flexibility to pursue many of my own research ideas which made working in the lab exciting. I always looked forward to our weekly meetings and I will always be appreciative of how he was able to keep things in perspective when I was struggling with my experiments. For me, he made graduate school a very enjoyable experience and for that, I thank him.

Thank you to my committee members Dr. Larry Lake, Dr. Kishore Mohanty, Dr. Charles Werth, and Dr. Matthew Balhoff. Dr. Mohanty was particularly generous for allowing me to use his lab rheometer, which was instrumental for this work, at all hours of the day. Dr. Balhoff's student's Ke Xu and Peixi Zhu were very helpful with my initial micromodel experiments and discussions in general. Dr. Werth was also very kind with letting me use his centrifuge during this work.

Thank you to the staff members at the Texas Materials Institute for all your help with equipment training and for help with my research. Thank you to Dr. Hugo Celio, Dr. Andrei Dolocan, Dr. Shouliang Zhang, and Kristofer Ohlinger.

Thank you to Ms. Leilani Swafford. You were always so generous with your time when I needed help with administrative issues or ordering chemicals. Also, thank you for always ordering my lab chemicals immediately! I can't thank you enough for that.

Thank you to Dr. Jimmie Baran who graciously provided me with an opportunity to do a summer internship with 3M. I really enjoyed my summer in the Twin-Cities and learned an incredible amount about nanotechnology during the internship.

Thank you to all the members in the Daigle research group. I always enjoyed listening about your research and I was able to learn from each of you. Thank you Nick, Han, Michael, Abhishek, David, Daniel, Rita, and Chunxiao.

I have to thank my good friend Ming for the countless discussions we've had over the years about anything and everything. I wish you the best of luck in the future.

Sean and Kevin, thank you guys for being great friends and regularly calling to see how I was doing with school, research, and how things were going in general. I won't forget it.

I am really lucky to have two amazing parents who have always been supportive of my decisions. Thank you for all the sacrifices that you have made in your lives to make mine better. I also have two incredible older brothers that I have always looked up to. I have learned more from them than they will ever know. Thank you for being the best older brothers that I could ask for and thank you for being hard, but not too hard on me while growing up.

Lastly, I have to thank my wife for always being supportive and patient. Thank you for all the little things that you have done to make graduate school a little bit easier for me, whether it was sneaking snacks into my backpack or calling me during the day to see how experiments were going. And hey, hopefully you learned something about nanoparticles too! I love you.

Abstract

Colloidal particles at fluid interfaces: from stabilizing emulsions to destabilizing them

Christopher Adam Griffith, PhD

The University of Texas at Austin, 2019

Supervisor: Hugh C. Daigle

This work uses silica nanoparticles to stabilize oil-in-water and water-in-water emulsions. These emulsions are called Pickering emulsions and have potential use for enhanced oil recovery.

There are two challenges with using nanoparticles for subsurface applications which are the high salinities and elevated temperatures of reservoir brines. These conditions are problematic because nanoparticles without surface modification are unstable, because of nanoparticle charge screening, which leads to particle agglomeration. Additionally, much of the current research on particle stabilized emulsions focuses on using nanoparticles modified with hydrophobic molecules or surfactants with the sole intent of getting particles to the oil/water interface. Because of this, many of these particles are not applicable for subsurface applications due to their lack of stability in brine.

To address these challenges, I functionalize silica nanoparticles with different concentrations of a hydrophilic silane called (3-glycidyloxypropyl)trimethoxysilane (glymo) and stabilize Pickering emulsions with these particles. Glymo was selected as a

nanoparticle surface modifier because of its ability to sterically stabilize particles in brine. I characterized the static stability of different Pickering emulsion formulations by using a centrifuge and by calculating the emulsion demulsification pressure. I correlate a critical demulsification pressure to emulsions that show little change in emulsion drop size while flowing, which I define as dynamically stable. The critical demulsification pressure is applied to several untested Pickering emulsion formulations to verify its applicability as an emulsion pre-screening tool.

I perform a rheological characterization on emulsions stabilized with low and high surface coverage glymo-coated particles to establish relationships between nanoparticle bridging and the extent of glymo surface modification with different ionic strength brines. I use cryo-scanning electron microscopy to visually assess the bridging behavior of these different Pickering emulsions.

I use fumed silica particles, with different wettabilities, and assess their ability to destabilize a model Pickering emulsion. I determine there is a strong correlation between the wettability of a fumed silica particle and its ability to destabilize a model emulsion. This work is relevant because most of the current research on Pickering emulsions focuses primarily on how to tune the properties of colloidal particles to generate stable emulsions with less overall emphasis on methods to destabilize them.

Lastly, an aqueous, two phase system is stabilized with 6 nm and 50 nm silica particles modified with 2-(methoxy(polyethyleneoxy)6-9propyl)trimethoxysilane (PEG-silane). Stabilization of the water/water interface results in emulsions that have relatively good stability to shear. Water-in-water emulsions do not contain any oil which is often considered a major limitation of Pickering emulsions for EOR, therefore these emulsions are potential candidates for enhanced oil recovery.

Table of Contents

List of Tables

List of Figures

Chapter 1: Introduction

1.1 MOTIVATION

Within the last 20-30 years nanomaterials (particles, wires, crystals) have found their way into a range of industrial products and applications (Otero-Gonzalez et al., 2015). This is because of their small size (<100 nm) which allows for materials to be manipulated at the molecular scale so that the macroscopic properties of a material can be improved (Szczech et al., 2011). One example of this is the inclusion of high aspect ratio carbon-nanotubes into polymer-composites to increase the overall strength of the composite (Arayan and Tour, 2007).

In light of these innovations, the oil and gas industry has also adopted the use of nanomaterials for subsurface applications (ShamsiJazeyi et al., 2014). Some proposed applications are as additives to drilling fluids, as tracers, and for enhanced oil recovery (Ko and Huh, 2019). In the context of the work presented here, I focus on using nanoparticles as additives for enhanced oil recovery and, more specifically, I use colloidal silica as interfacial stabilizers for emulsions. I also explore their use as interfacial destabilizers.

There are two challenges with using nanoparticles for subsurface applications and they are the high salinities and elevated temperatures of reservoir brines (Hwang et al., 2014). These conditions are problematic because nanoparticles without surface modification are unstable, which results in their agglomeration from nanoparticle charge screening (Zhang et al., 2016). Exacerbating this is that much of the current research on particle stabilized emulsions focuses on altering the wettability of nanoparticles with the sole in intent of getting particles to oil/water interfaces (Edgehouse et al., 2019) and, because of this, many of these particles are not applicable for subsurface applications.

Additionally, quantifying the differences in stability of different Pickering emulsions is surprisingly quite challenging given that a large number of particle emulsifiers can stabilize statically stable emulsions (Ashby and Binks, 2000; Vignati and Piazza, 2003; Melle et al., 2005; Yang et al., 2006; Kalashnikova et al., 2011; Briggs et al., 2018; Edgehouse et al., 2019).

Based on this, there are two motivating factors for this work. The first goal of this work was to establish a semi-quantitative method capable of distinguishing differences in the relative stabilities of different Pickering emulsions. The second goal of this work was to modify silica nanoparticles with a well-defined hydrophilic silane and to characterize the rheological properties of the resulting Pickering emulsion as a function of nanoparticle surface modification, nanoparticle concentration, oil volume fraction, salinity, and pH.

1.2 OUTLINE

This dissertation has a total of seven chapters. Chapter 2 is a literature review that highlights the use of macroemulsions for enhanced oil recovery and discusses some of the challenges with using conventional surfactants to stabilize macroemulsions. The literature review provides motivation for using colloidal particles to stabilize emulsions instead of surfactants.

Chapter 3 compares the static and dynamic stability of Pickering emulsions stabilized with silica nanoparticles modified with low and high concentrations of (3-glycidyloxypropyl)trimethoxysilane (glymo). The chapter introduces the demulsification pressure as a screening metric and proposes using it as a predictive indicator for the dynamic stability of a Pickering emulsion. I find a critical demulsification pressure that correlates well with an emulsion that is dynamically stable while flowing through a glass

capillary tube. The critical demulsification pressure criterion was then applied to several untested emulsion formulations to validate its potential use as a predictive indicator for the dynamic stability of Pickering emulsions.

Chapter 4 is a rheological characterization of various Pickering emulsions stabilized with low and high coverage glymo-modified nanoparticles in different concentration brine waters. I show that the zero-shear elastic storage moduli of oil-in-water emulsions could be minimized by using particles with a high coverage of glymo on the particle surface, which reduced the Ca^{2+}/silanol site interactions. Emulsions that were stabilized with low surface coverage particles had noticeably higher zero-shear elastic storage moduli; however, their zero-shear elastic storage moduli could be reduced by a factor of 3.3 by simply lowering the solution pH to 3. Cryo-SEM images showed that nanoparticle bridging was more pronounced with nanoparticles that had low glymo-coverage compared to particles with high glymo-coverage. This chapter illustrates the importance of the extent of surface modification and the impact it can have on the macroscopic properties of a Pickering emulsion.

Chapter 5 investigates whether fumed silica particles with different wettabilities can destabilize a model Pickering emulsion. I show that there is a strong correlation between the wettability of a fumed silica particle and its ability to destabilize a Pickering emulsion, with more hydrophobic particles showing a greater tendency to coalesce the Pickering emulsion. Hydrophilic and partially hydrophobic particles, at all concentrations tested, were unable coalesce the model emulsion. This was because the particles were almost immediately wetted by the continuous phase of the emulsion, which prevented any interactions between the emulsified oil drops and the silica particle surface. The hydrophobic fumed silica particles coalesced 60% of the emulsified oil with just 0.01 wt% added fumed silica, which further increased to 85% with 0.05 wt% added silica.

This chapter is relevant because much of the current research on Pickering emulsions focuses primarily on how to tune the properties of colloidal particles to generate stable emulsions with less overall emphasis on establishing methods to destabilize them.

Chapter 6 assess the stability of a relatively low interfacial tension water-in-water emulsion stabilized with 6 nm and 50 nm silica nanoparticles modified with 2-(methoxy(polyethyleneoxy)6-9propyl)trimethoxysilane (PEG-silane). This chapter is important because one of the main criticisms of macroemulsion enhanced oil recovery is that oil needs to be injected into the ground in the form of an emulsion. This chapter shows that water-in-water emulsions have relatively good stability while being sheared, which suggests that these oil-less emulsions could have some use for subsurface applications.

Chapter 7 is the concluding chapter and highlights the relevant findings from this work and proposes future work.

Chapter 2: Literature review

2.1 EMULSIONS IN UPSTREAM OIL AND GAS

Emulsions are frequently encountered in upstream oil and gas operations, from being used as drilling fluids (Kirsner et al., 2009) to being produced from reservoirs (Umar et al., 2018). In some cases, like with drilling fluids, the goal is to tailor the emulsion to meet some design criteria, for example a specific mud weight (Nicora et al., 2001). In other cases, like with the production of water-in-oil emulsions, having a fundamental understanding on what is stabilizing the emulsion and how best to destabilize it is the goal (Pena et al., 2005).

The purpose of this chapter is to go over the two types of emulsions that are used for enhanced oil recovery, which are micro and macroemulsions. First, I go over their similarities and differences and then focus on key aspects of surfactant stabilized macroemulsions and how they are used as an EOR technology. This is done in an attempt to motivate the use of solid particles, as opposed to chemical surfactants, to stabilize macroemulsions. I then provide detailed information on the different methods that can be used to alter the wettability of colloidal particles so that they can stabilize emulsions. The purpose of this is to highlight previous work on Pickering emulsions, but it also serves the purpose of highlighting some of the major limitations associated with Pickering emulsions stabilized with colloidal particles modified with conventional methods (surfactants or hydrophobic silanes), which provides motivation for my work.

Here, I define an emulsion following Binks (1997): an emulsion may be defined as “a heterogeneous system of two immiscible liquid phases (‘oil’ and ‘water’) where one of the phases is dispersed in the other as drops”.

2.2 MICROEMULSIONS

Surfactants are commonly used to stabilize emulsions. By definition, a surfactant is an amphiphilic molecule that consists of a hydrophilic head and lipophilic tail (Pichot et al., 2009). Surfactants can be anionic, cationic, nonionic, or zwitterionic (Umar et al., 2018). The type of emulsion that a surfactant stabilizes (water-in-oil, oil-in-water, or bicontinuous) depends on the properties of the surfactant, which is often characterized by the surfactants hydrophilic-lipophilic balance (HLB) (Umar et al., 2018). The HLB is the ratio of the hydrophilic contributions from the surfactant head to the lipophilic contributions from the surfactant tail (Pasquali et al., 2008). Therefore, if a surfactant has a high HLB, it will prefer to stabilize an oil-in-water emulsion, whereas if a surfactant has a low HLB it will prefer to stabilize a water-in-oil emulsion (Binks, 2002).

Microemulsions are a specific type of emulsion that are thermodynamically stable and exist as clear, translucent fluid (Healy and Reed, 1974). The translucent nature of a microemulsion is due their ultra-low interfacial tensions, which leads to emulsion drops that are nanometer in size and do not significantly scatter light (Hwan et al., 1978). The ultralow interfacial tension is achieved by mixing (1) a surfactant, (2) at least one co-surfactant that, in combination with the primary surfactant, has the appropriate amphiphilic properties to match (3) a particular oil of interest. These emulsions form spontaneously (Ruckenstein and Chi, 1975), and therefore do not external shear.

The use of microemulsions to recover oil from subsurface reservoirs (tertiary oil recovery) has been studied for over 40 years (Healy and Reed, 1974). Because oil is trapped in rocks with small pore spaces, the flow behavior of fluids (oil/gas/water) is controlled by capillary and interfacial forces, which is generally quantified using the dimensionless capillary number (N_C):

$$N_c = \frac{-k\left(\Delta\Phi_p/\Delta L\right)}{\sigma}, \tag{2.1}$$

where k is permeability, $\Delta\Phi_p/\Delta L$ is the potential gradient, and σ is the oil/water interfacial tension (Sheng, 2015). For siliciclastic reservoirs, capillary desaturation curves show that ~30% of the original oil in place can be produced under normal field conditions, where normal field conditions are defined by capillary numbers that are on the order of 10^{-6}-10^{-4} (Sheng, 2015; Qi et al., 2016). These same capillary desaturation curves show that almost all of the oil from a reservoir can be produced if the capillary number is increased by a factor of ~1000 (Sheng, 2015).

In practice, the only way to increase the capillary number by 1000 is to reduce the interfacial tension between oil and water by appropriately selecting the correct surfactant, co-surfactant, and co-solvent for a specified reservoir (Sheng, 2015).

2.3 MACROEMULSIONS

Macroemulsions are characterized by their large emulsion drop size (Arab et al., 2018), which are typically much larger in size than microemulsion drops. Moreover, the surfactants that are used to stabilize macroemulsions do not lower the oil/water interfacial tension to ultra-low levels. Nevertheless, macroemulsions are still considered as an EOR technology and there are two unique ways macroemulsion based EOR can be implemented.

2.3.1 Macroemulsions: flow diversion

Macroemulsions can be used to divert the flow of injected fluids from thief zones of high permeability (which are depleted of oil) to zones of lower permeability with bypassed oil (McAuliffe, 1973; Jennings et al., 1974; Salatheil et al., 1980; Schmidt et al., 1984; Soo and Radke, 1985; Mandal et al., 2010; Kumar et al., 2017; Xu et al., 2017;

Yu et al., 2018; Pandey et al., 2018). Typically for this application, macroemulsions are injected as dilute suspension (~5 wt% oil) which gives the injected fluid a low viscosity and good injectivity (Yu et al., 2018). The idea is that macroemulsion droplets can block high permeability pore throats and divert subsequent injected water to unswept portions of a formation. This can lead to better overall displacement sweep efficiency and better oil recovery during water flooding (McAuliffe, 1973).

It is generally thought that the mechanism responsible for diverting fluid is the physical straining of emulsion drops at pore restrictions (McAuliffe, 1973). However, for high permeability rock, there is some debate as to whether straining of emulsion drops is the primary mechanism responsible for fluid flow diversion, particularly when dilute macroemulsions are used (Yu et al., 2018).

Yu et al. (2018) suggested that other mechanisms could be at play for flow diversion, which include: emulsion jamming (Yu et al., 2018) and interception (Soo and Radke, 1984). Jamming refers to pore throat blockage when several emulsion drops (that are individually smaller than the pore restriction) arrive at a restriction at the same time and 'jam' that restriction. This has the ability to reduce the relative permeability to water at the pore restriction and potentially divert flow during water flooding. Interception refers to the interaction of emulsion drops to grain surfaces either through charge interactions (Daigle and Griffith, 2018) or due to low velocity flow fields (Soo and Radke, 1984).

Yu et al. (2018) studied the relationship between emulsion drop size and the peak pressure drop across high permeability sand packs (~1 D). They measured the peak pressure to infer how the differently sized emulsion drops impacted the ability for an emulsion to divert/block high permeability pathways. The authors were interested in

using their results to develop a physics-based model capable of capturing their experimental observations.

In their work, dilute emulsions with 5 wt% oil were used. The emulsions were stabilized using a combination of two nonionic surfactants: Span 60 (0.1 wt%), Tween 80 (0.1 wt%), and a small fraction of sodium hydroxide (0.025 wt%). The size of the emulsion drops was controlled by varying the shear rate of their homogenizer or by varying the emulsification time. They stabilized emulsions with drops that ranged from 1.57 μm to 10.19 μm.

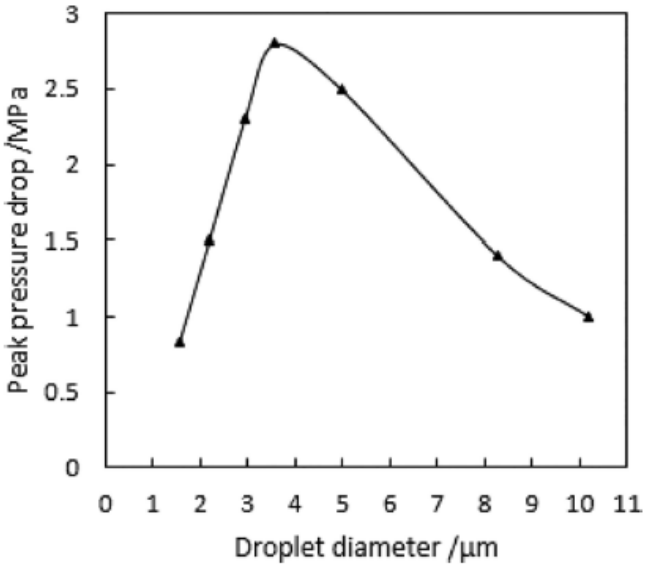

Figure 2.1 – Peak pressure drop versus emulsion drop size for an emulsion flow through a high permeability (~1 D) sand pack (Yu et al., 2018).

Figure 2.1 shows a plot of peak pressure drop versus emulsion drop size from their experiments. For small to intermediately sized emulsion drops (1.57 μm to 3.58 μm), they showed that there was a linear increase in peak pressure drop with increasing emulsion drop size, with larger emulsion drops leading to larger peak pressure drops. The authors suggested that the low peak pressure drops during experiments with small

emulsion drops was due to these drops easily passing through the pore throats of their sand packs. However, when the emulsions with larger drops were used (3.58 μm), the authors hypothesized that the larger drops were able to reduce the effective pore throat size by adsorbing to grain surfaces, which then enabled subsequent drops to be physically strained, leading larger overall peak pressure drops.

Interestingly, as the average emulsion drop size further increased (>3.58 μm), they observed a pronounced decrease in the peak pressure drop (Figure 2.1). This experimental observation was somewhat surprising. The explanation that they gave was: the ability for emulsion drops to plug pore throats is a function of two parameters: (1) emulsion drop size and (2) the total number of drops in an emulsion. At a fixed oil volume fraction, an emulsion with larger average emulsion drops will have fewer total drops than an emulsion with smaller drops. Because of this, an emulsion with larger drops will have fewer total drops available to block a pore restriction and therefore will be less likely to block the restriction. One weakness to this argument is that the authors do not acknowledge that for surfactant stabilized macroemulsions it is relatively well known that emulsions with larger drops have a tendency to be weaker than those with smaller drops (Walstra, 1993; Chevalier and Bolzinger, 2013). So their experimental observation could potentially be due to the larger emulsion drops partially coalescing while flowing through the sand pack. They do not mention the characteristics of the emulsion after flooding. Additionally, the stability of their emulsion was characterized with respect to creaming only.

2.3.2 Macroemulsions: mobility control

Macroemulsions can also be used as a high viscosity mobility control fluid (Zhang et al., 2010; Kaminsky et al., 2010; Sharma et al., 2015a; Sharma et al., 2015;

Griffith et al., 2016; Pei et al., 2018). The high viscosity of these macroemulsions can aid in the production of heavy oils that are very viscous, but still mobile (Kaminsky et al., 2010). Because these macroemulsions are so viscous, they provide a more favorable mobility ratio between the injected fluid and in-situ oil (Zhang et al., 2010). Macroemulsions have been targeted as an EOR technology for viscous oil recovery because of limitations associated with other EOR techniques (Arab et al., 2018).

For example, a large portion of heavy oils are found within thin reservoirs that are deep in the subsurface. Because of this, thermal methods are not applicable due to excessive heat loss to the formations that are above and below the reservoir rock (Arab et al., 2018), which can make thermal EOR un-economic. Moreover, conventional polymer flooding is really only applicable in reservoirs where the viscosities are less than ~150 cP (Taber et al., 1997), which is too low for viscous oil recovery because of the high viscosities associated with these oils (30-3,000 cP or higher) (Kaminksy et al., 2010).

A major disadvantage of using an emulsion as a mobility control fluid is that a large volume of emulsion is required ~1 PV (Baldygin et al., 2014). Because these emulsions are typically 50% by volume, this in turn means a large volume of oil is injected into a formation, which many would argue does not make sense.

In an attempt to address this issue, Baldygin et al. (2014) studied a novel water-alternating-emulsion (WAE) injection scheme to test if emulsion flooding could be tuned to recover more oil by injecting less emulsion during the process (thus requiring less injected oil). They alternated water and emulsion injection patterns into highly permeable sand packs (~7 D) that had pore diameters that were ~25 μm. They varied their WAE injection scheme from 2:1 (water to emulsion) up to 5:1. Their emulsions had a mean drop size of 2.46 μm, which resulted in an emulsion drop size to pore throat size ratio ~0.1. Their results were quite promising. They showed that over 80% of the original oil

in place could be recovered by using their WAE injection scheme, even when using a 5:1 injection ratio.

2.3.3 Macroemulsions: challenges with conventional surfactant stability

In most of the examples listed above, surfactants were used to stabilize the macroemulsion oil/water interface. However, because oil reservoirs are typically at elevated temperatures and have high salinities, the long term stability of these surfactant stabilized macroemulsions is questionable. This is because conventional surfactants are typically small (low molecular weights), which means they can spontaneously desorb from the oil/water due to thermal fluctuations (Binks, 2002; Kundu et al., 2013; Abedi et al., 2019).

To highlight the lack of thermal stability of macroemulsions stabilized with conventional surfactants, I summarize several recent papers which studied how surfactant stabilized emulsions respond to changes in temperature and salinity.

Kundu et al. (2013) studied the stability of oil-in-water emulsions stabilized with sodium dodecyl benzene sulphonate (SDBS). The authors were interested in understanding the relationship between temperature, salinity, and emulsion stability. They characterized the stability of their emulsions by measuring the electrical conductivity of the continuous phase. The idea behind this characterization technique was that because the continuous phase of their model emulsions was water (with or without salt), the conductivity of these emulsions should be relatively high if the emulsions were stable. However, as the emulsion loses its stability, either due to phase inversion or coalescence, the conductivity of the emulsion should change (decrease).

Their results clearly showed that all of their conventional oil-in-water macroemulsions were susceptible to thermally induced coalescence. The authors

quantified the stability of these using a term called the ‘phase inversion temperature’, which they defined as the temperature at which the emulsion began to rapidly destabilize. As an example, an emulsion with a low phase inversion temperature would be more susceptible to temperature-induced coalescence than an emulsion with a high phase inversion temperature.

Figure 2.2 shows experimental results from their experiments. The plot shows a variety of oil-in-water emulsions prepared with a range of different NaCl brine solutions. These results showed that as the concentration of salt in a formulation increased, the phase inversion temperature decreased, indicating a strong correlation between emulsion coalescence and salt concentration.

In Figure 2.2, we highlight the conductivity profile of an emulsion prepared with 0.01 M NaCl (filled circles). This emulsion had a phase inversion temperature of just 60 °C. This is important for two reasons: first, the salt concentration of the emulsion is rather low and lower in ionic strength than many reservoir brines (Worthen et al., 2016). Secondly, the temperature at which the emulsion destabilizes is also lower than what is typical of subsurface reservoirs (Levitt and Pope, 2008). Therefore, the use of macroemulsions for high temperature and high salinity reservoirs is potentially problematic.

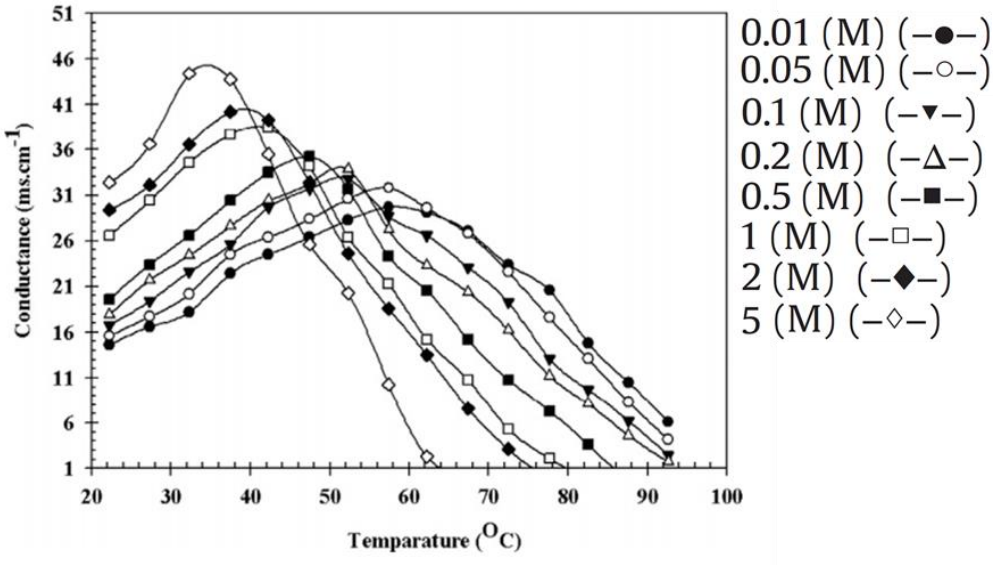

Figure 2.2 – Conductivity versus temperature for emulsions stabilized with different concentrations of sodium chloride. Open diamonds corresponds to an oil/water emulsion stabilized with 5 M sodium chloride. The filled circles correspond to an oil-in-water emulsion stabilized with 0.01 M sodium chloride. These salt concentrations span the range of salt concentrations tested. From Kundu et al. (2013).

Another example that illustrates the lack of thermal stability for a surfactant-stabilized macroemulsion is from the work of Abedi et al. (2019). In their work, they used a micromodel to show how a two-dimensionally constrained hexadecane-in-water emulsion stabilized with 2 wt% sodium dodecyl sulfate destabilized with an increase in temperature from just 16.8 °C to 17.5 °C (Figure 2.3). The very low destabilization temperature of this sodium dodecyl sulfate stabilize emulsion is not unexpected given that the surfactant is relatively small and its hydrophobic dodecyl chains do have very good penetration into oil (Kundu et al., 2013).

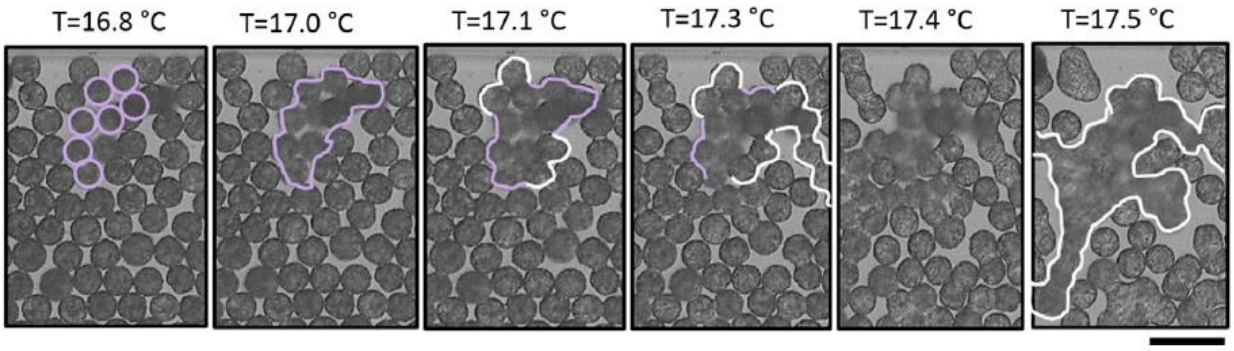

Figure 2.3 – Hexadecane-in-water emulsion stabilized with 2 wt% sodium dodecyl sulfate anionic surfactant. From left to right shows the destabilization of the emulsion as it is heated from an initial temperature of T = 16.8 °C to T = 17.5 °C. Scale bar is 100 μm. From Abedi et al. (2019).

2.3.4 Macroemulsions: particles as an alternative interfacial stabilizer?

Due to their lack of thermal stability, colloidal particles have been proposed as an attractive alternative to conventional surfactants for interfacial stabilizers. Colloidal particles are capable of stabilizing an oil/water interface to form an emulsion that, if properly designed, can be very stable for long periods of time, even in the harsh conditions of subsurface reservoirs (Zhang et al., 2010). This long term stability is directly the result of the large attachment energies associated with getting nanoparticles to the oil/water interface, which prevents their subsequent desorption due to temperature changes (Binks, 2002).

Additionally, nanoparticles are made of inert materials, like silica, which means they should not degrade even when they exposed to reservoir conditions for extended periods of time. Moreover, because these particles are typically tens of nanometers in size, they should be able to freely flow within the pore spaces of a reservoir rock (Zhang et al., 2010; Wang et al., 2012; Griffith et al., 2016).

Stabilizing emulsions and foams with colloidal particles is currently a very active and very rich area of research. Because of this, it is also necessary to fundamentally understand how the different parameters of colloidal particles impact the macroscopic properties of particle stabilized emulsions (emulsion drop size, rheology, and dynamic stability), which ultimately allow for better design of particle stabilized emulsions. Some of these fundamental aspects are covered in the following sections.

2.4 PARTICLE STABILIZED MACROEMULSIONS

Emulsions that are stabilized with colloidal particles are referred to as Pickering emulsions, which were first observed by Ramsden in 1903 (Ramsden, 1903) and Pickering in 1907 (Pickering, 1907). These emulsions are stabilized with solid particles instead of chemical surfactants.

Interest in Pickering emulsions has increased in last 10-20 years. Much this interest is due to advancements in materials science which has led to a wide range of well-defined colloidal particles that can act as Pickering emulsifiers (Wu and Ma, 2016). There are also technical advantages of using Pickering emulsions instead of surfactant stabilized emulsions, which has also helped drive this renewed interest. Some of these advantages (described by Chevalier and Bolzinger (2013)) are: (1) particle stabilized emulsions exhibit good long term stability to coalescence even at elevated temperature, (2) they are attractive for the pharmaceutical and cosmetic industries where surfactants can be skin irritants and this skin irritancy can be eliminated by using a Pickering emulsion, and (3) very large macroemulsions (large drops) can be stabilized using colloidal particles, which is typically very difficult to do with surfactants (Chevalier and Bolzinger, 2013).

In general, solid particles have the ability to localize at the interface between two fluids when the following conditions are met: (1) their surface properties allow for the particle to be wetted by both fluids (Ngai and Bon, 2014), (2) there is enough mechanical energy to form dispersed drops (usually in the form of shear), and (3) this mechanical energy is sufficient to get the particle to attach to the liquid/liquid interface (Melle et al. (2005)). When these three conditions are met, a Pickering emulsion is formed.

The energy that is required to get a particle to the oil/water interface is a function a particles size, wettability, and the interfacial tension between the two phases (Chevalier and Bolzinger, 2013; Worthen et al., 2013). The attachment energy of a single particle is calculated using equation (2.2):

$$E = \pi R^2 \gamma_{\alpha\beta}(1 - |cos\Theta|)^2, \quad (2.2)$$

where R is the particle radius, γ is the interfacial tension between the two phases, and θ is the contact angle of the particle at the interface of the two fluids.

2.4.1 Nanoparticle Size

The International Organization for Standardization (ISO) defines a nanoparticle as "a nano-object with all three external dimensions in the nanoscale, where nanoscale is defined as the size range from approximately 1 – 100 nm" (Boeverhof et al., 2015).Within the context of this definition, there are two generally accepted methods for producing nanoparticles. These methods include (1) the "top down" and (2) the "bottom up" approach (Boverhof et al., 2015). The "top down" approach refers to the process of mechanically degrading a bulk material that starts out much larger in size than a nanomaterial, common examples include using a ball mill to grind a material like fly ash (Lee et al., 2015), graphene (Kneike et al., 2010; Boverhof et al., 2015), or biochar (Griffith and Daigle, 2016) to produce nanoparticles.

The “bottom up” approach refers to using a chemical process to manufacture nanoparticles (Boverhof et al., 2015). Two common examples of the “bottom up” manufacturing process are the production of silica nanoparticles from a solution by precipitation or the production of silica using flame hydrolysis (Boverhof et al., 2015; Evonik, 2018).

In general, silica particles produced by flame hydrolysis consist of primary particles (~12 nm) that are fused together into aggregates, which can form even larger agglomerates (Evonik, 2018). The fused aggregates are typically 100-500 nm in size and cannot be broken down to be smaller (Evonik, 2018). Figure 2.4 shows a sketch of a fumed silica particle and shows the relationship between primary particles and aggregates.

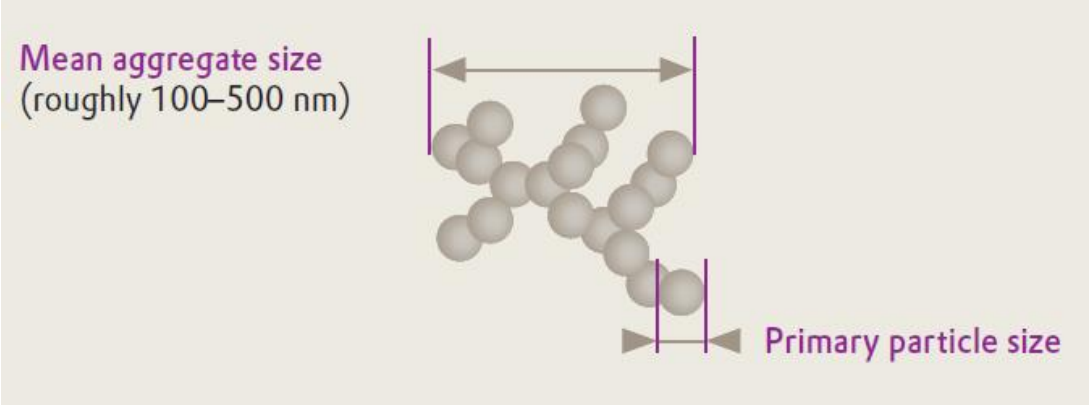

Figure 2.4 – Illustration of a fumed silica particle that is produced via the flame hydrolysis method. The image shows the relationship between a primary particle and larger aggregates that form during the flame hydrolysis. From Evonik Technical Bulletin (2018).

Silica particles produced by the sol-gel (precipitation) process are usually much smaller in size, have narrower size distributions, contain much larger specific surface areas, and can be manufactured to very specific size requirements (Evonik, 2016).

Because of this high specificity, they are commonly used for a range of industrial applications.

The attachment energy of a particle of radius R to the oil water interface scales as R^2. Therefore, particle size has a profound impact on particle attachment/detachment energy. Figure 2.5 shows a plot of particle attachment versus nanoparticle radius. For this calculation, I assumed a constant three-phase contact angle of 90^o and a constant interfacial tension of 30 mN/m. The plot reveals that relatively small particles can be used to achieve very large particle attachment energies, where a particle with a radius of 10 nm has a particle attachment energy of ~600 kT (Dickinson, 2010).

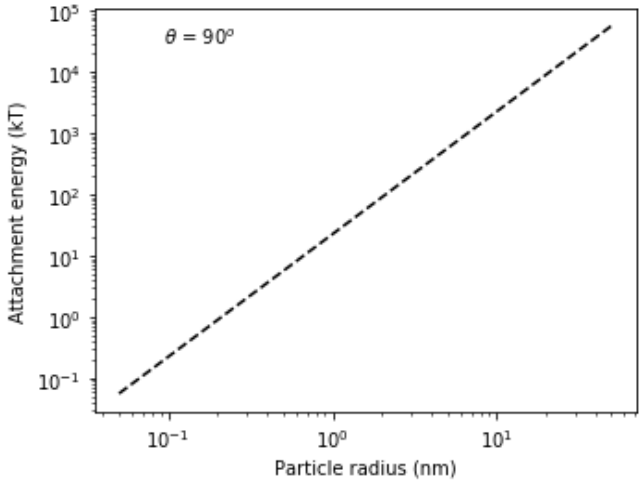

Figure 2.5 – Attachment energy versus particle size for nanoparticles with a constant three phase contact angle of 90°.

For most practical applications, the size of the colloidal particle has less of an impact on the stability of a Pickering emulsion (in oil/water systems) than the wettability of the particle, which is discussed in detail below. This is because once the attachment energy is $\gtrsim$ several hundred kT, the particle for all practical purposes is irreversibly adsorbed (Binks, 2002). I would like to point out that particle size does appear to play a much more significant role in stabilizing interfaces of low interfacial tension systems, for

example in water-in-water emulsions, which will be discussed later in my dissertation. Nevertheless, researchers are still interested in the fundamental relationship between particle size and emulsion properties and this is illustrated by the work of Kim et al. (2016).

Kim et al. (2016) studied the impact of nanoparticle size on the properties of decane-in-water Pickering emulsions. They used particles with diameters of 5, 12, 25, and 80 nm. The particles were surface-modified with an undisclosed silane. They showed that emulsions stabilized with smaller nanoparticles had smaller emulsion droplets, which resulted in emulsions with much higher viscosities. Moreover, they also showed that good stability of the emulsions could be achieved even with small particle emulsifiers.

Although larger particles have larger attachment energies compared to smaller ones, the reality is that particle wettability is of more practical interest and therefore much more studied than particle size (in terms of affecting properties of Pickering emulsions). This is because the wettability of a particle controls whether or not the particle can actually adhere to the interface. Additionally, attachment energies of 100s kT are sufficiently large to satisfy the requirement of irreversible adsorption to an interface (Binks, 2002).

2.4.2 Nanoparticle wettability

The wettability of a nanoparticle is described by the three-phase contact angle that it makes with a fluid/fluid interface (for example oil/water/nanoparticle) and is a key parameter that researchers can tune to improve the attachment energy of a particle to fluid/fluid interfaces (Binks and Lumsdon, 2000, Binks, 2002, Aveyard et al., 2003, Horozov et al., 2007).

Figure 2.6 qualitatively illustrates the importance of particle wettability and its impact on particle attachment energy. In this example, the particle wettability is varied from 0° to 180° and the particle size is assumed to be 50 nm and the an oil/water interfacial tension (IFT) is 30 mN/m. Figure 2.6 reveals three important features: (1) the optimum particle attachment occurs at a three phase contact angle of $\theta = 90°$, (2) the attachment energy at this contact angle is very high, ~14,000 kT and (3) the particle attachment energy is still relatively high ($\gtrsim$100 kT) with contact angles $\sim 30° < \theta < \sim 150°$.

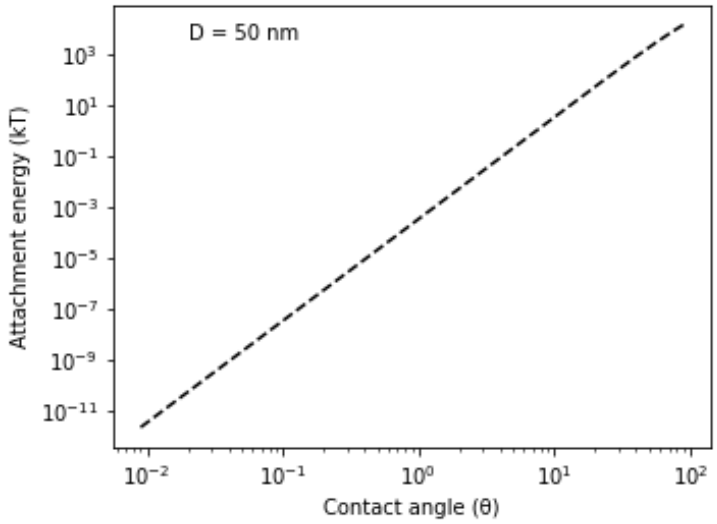

Figure 2.6 – Particle attachment energy versus contact angle for a D = 50 nm spherical particle with an oil/water IFT of 30 mN/m.

At $\theta = 90°$ the particle attachment energy is four orders of magnitude greater than kT, which means if a particle is at a fluid/fluid interface, it will not detach, even if very large temperature fluctuations are present (Binks, 2002). This is in contrast to many surfactant-stabilized emulsions, in which the surfactants are in dynamic equilibrium and can readily desorb from the interface (Binks, 2002). Moreover, we highlight the 100 kT

attachment energy criterion because this appears to be around the threshold that is necessary to prevent particles from detaching from a fluid interface due to externally imposed shear, which I will show later with water-in-water emulsions stabilized with PEGylated nanoparticles.

The contact angle is also important because it determines what phase a particle will be dispersed in. For a two-phase oil/water system, it is generally assumed that if a particle has a contact angle of less than 90°, then the particle will be dispersed in the aqueous phase (Horozov et al., 2007). Additionally, if the particle is able to stabilize an emulsion, the emulsion will be and oil-in-water emulsion (o/w) with water being the continuous phase (Horozov et al., 2007). The alternate of this situation is also true, where if a particle has a contact angle >90 °, then the particle will prefer to reside in the oil phase, and the emulsion the particle stabilizes will be a water-in-oil emulsion (w/o) with oil as the continuous phase (Horozov et al., 2007).

In practice, measuring the three-phase contact angle is very challenging and therefore is usually not reported. However, there are some scenarios, for example if very large particles are used (>1 μm) where high magnification optical microscopy can be used to directly visualize a particle at an interface (Balakrishanan et al., 2012). Figure 2.7 shows an example of this. In this image, there is a large, 2 μm diameter latex particle that is the interface between two fluids. The authors used confocal laser microscopy to measure a three phase contact angle of 145° ± 5° (Balakrishanan et al., 2012).

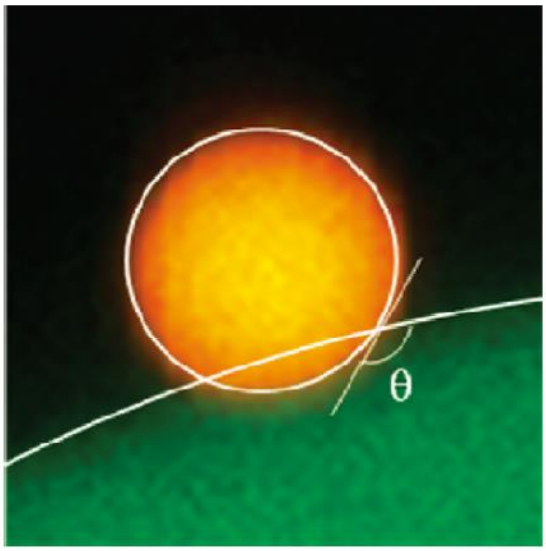

Figure 2.7 – The yellow particle is a 2 μm diameter latex particle resting at the interface of two aqueous phases (polymer/polymer system). The green in the image is a dextran-rich polymer solution (MW = $5x10^5$ g/mol) and the black phase is a polyethylene glycol-rich phase (MW = $2x10^5$ g/mol). From Balakrishan et al. (2012).

Generally, indirect methods are used to estimate the contact angle a particle makes with oil and water. Yan et al. (2000) outlined several of these methods. The first is the modified capillary rise technique, in which a capillary tube is packed with dry particle powder. The packed bed is assumed to be a bundle of capillary tubes and the Washburn equation is then modified by combining Poiseulle's equation and capillary forces to obtain the contact angle of the particles. This is also referred to as the Washburn technique. The second is compressing particles into a pellet/disk and measuring the contact angle that a fluid makes with the disk, which is the most common method used in the literature. The third is the enthalpy of immersion technique, which was the focus of Yan et al. (2000) can be used to get repeatable contact angle measurements.

Despite the availability of these methods, it appears that researchers typically prefer to relate surface properties of a particle to the type of emulsion that is formed,

which has been done in detail by Binks and Lumsdon (2000), Binks (2002), Aveyard et al. (2003), and Horozov et al. (2007). This will be highlighted in the following sections.

2.4.2.1 Nanoparticle surface modification by surfactant

Here I briefly review how silica nanoparticles can be modified by surfactants (cationic, zwitterionic, anionic, and nonionic), which alter the wettability of the particle so that they are capable of stabilizing Pickering emulsions. I go into detail on how silica particles can be modified with cationic surfactants through electrostatic interactions mainly because of its similarity to covalent attachment of molecules to a silica particle surface through siloxane bonds – both of which are surface area-driven. However, I do not go into as much detail on the surface modification of silica particles by zwitterionic, anionic, and nonionic surfactants. This is because this information has already been reviewed in sufficient detail in Chevalier and Bolzinger (2013) and Arab et al. (2018).

2.4.2.2 Cationic surfactant

Bare silica particles contain silanol groups on their surface (Binks, 2000), which means they are too hydrophilic to stabilize emulsions without some sort of surface modification (Binks and Whitby, 2005). When silica particles are dispersed in DI water above pH 2-4 (which is near the isoelectric point for silica (Ma et al., 2010)) the particles carry a negative surface charge that is on the order of – 40 mV at pH 9.5 (Figure 2.8).

Therefore, cationic surfactants are a natural choice as a particle surface modifier because the positively charged surfactant heads can electrostatically bind to the negatively charged surface silanol groups. If the proper ratio of cationic surfactant to available silanol groups is achieved, it is possible to stabilize Pickering emulsions.

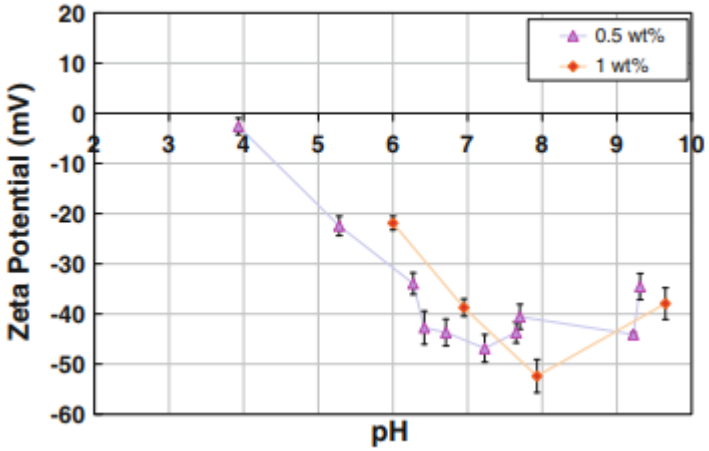

Figure 2.8 – Silica nanoparticle zeta potential versus solution pH for 25 nm particles dispersed as 0.5 wt% or 1 wt% dispersions. From Metin et al. (2010).

Because of this, understanding the interactions between cationic surfactants and silica nanoparticles and how these interactions affect the type and stability of emulsion that is formed is a very active area of research (Hassander et al., 1989; Binks and Lumsdon, 1999; Binks and Whitby, 2005; Binks et al., 2007; Lan et al., 2007; Eskandar et al., 2007; Zhu et al., 2015; Maurya and Mandal, 2018).

Figure 2.9 qualitatively illustrates how a cationic surfactant interacts with a silica particle surface. The left-hand side of Figure 2.9 shows a bare silica particle that is occupied with silanol groups. The right-hand side of Figure 2.9 shows how a cationic surfactant binds to the silica particle surface through electrostatic interactions.

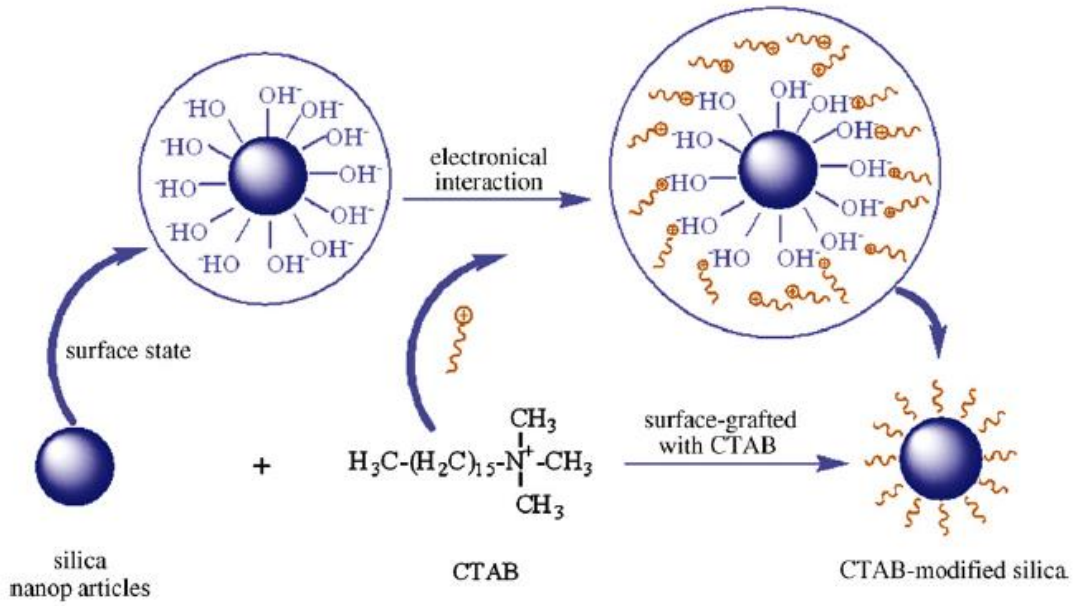

Figure 2.9 – Schematic illustrating the modification of a silica nanoparticle surface by addition of cationic surfactant, cetyltrimethylammonium bromide (CTAB). From Ma et al. (2010).

At low surfactant concentrations, once the surfactant is bound to the particle surface, the hydrophobic surfactant tail can protrude radially away from the silica particle, which makes the surface modified particle partially hydrophobic and interfacially active (Binks et al., 2007). At these low surfactant concentrations, because the nanoparticle surface is not 100% saturated by cationic surfactant, the silica particle still carries residual surface charge, which allows the particle(s) to remain stably dispersed in an aqueous solution. However, as the concentration of surfactant is increased to the point where the silanol groups on a silica particle are 100% saturated the silica particles no longer carry a sufficiently large surface charge to electrostatically stabilize the particles. Because of this, the particles become unstable, flocculate, and eventually settle out from the dispersion (Binks et al., 2007).

If the concentration of cationic surfactant is increased again, tail-tail interactions between surface-bound surfactant and free surfactant in solution transition the particle from being unstable to electrostatically stabilized due to the newly added surfactant heads (positively charge) protruding away from a particle surface (Binks et al., 2007). This can produce electrostatically stable particle dispersions that are positively charged (from the surfactant head) (Binks et al., 2007).

In 2007, Binks et al. studied this behavior in detail and characterized the relationship between surface modification and the ability of these surface-modified particles to stabilize emulsions. They demonstrated that dodecane-in-water Pickering emulsions could be stabilized if the hydrophilic/lipophilic interactions were properly tuned by the extent of surface modification with CTAB. They highlighted several important results from their work. First, they showed that silica nanoparticles (modified with CTAB) decreased the air/water surface tension with increasing adsorption of CTAB to a silica particle surface. This result shows that surface modification of a non-interfacially active silica particle can make the particle interfacially active, which is directly the result of the particle surface modifier. Moreover, the extent of interfacial activity was shown to increase with the amount of surface modification.

Binks et al. (2007) also showed that CTAB surfactant was capable of screening the negative charges of a silica particle surface, even when the silica particle was above its pH point of zero charge. They experimentally showed that silica dispersions at high pH (~9) could become neutrally charged if 10^{-2} M CTAB was added to the dispersion, resulting in an unstable, flocculated particle mixture. What was remarkable about this result was that they showed that these highly flocculated dispersions were capable of producing very stable dodecane-in-water emulsions. Lastly, they showed that surface modification of silica with cationic surfactant was only capable of producing oil-in-water

emulsions. This result suggests that silica particles modified with surfactants (CTAB) could not become sufficiently hydrophobic to stabilize water-in-oil emulsions.

In a very similar paper, Lan et al. (2007) studied the interaction between CTAB surfactant and fumed silica particles. One difference in their work from that of Binks et al. (2007) was that they were able to measure contact angles between fumed silica particle pellets (modified with CTAB) and their light paraffin oil. Their results showed that emulsions stabilized with fumed silica particles modified with CTAB were the most stable when the three phase contact angle 90°. As the concentration of surfactant was increased beyond the optimum, the emulsions became less stable. To summarize the interaction between CTAB and silica: (1) with the appropriate CTAB concentration, silica particles can be tuned to have a favorable three phase contact angle; (2) CTAB induces particle flocculation, which aids in emulsion stabilization; and (3) CTAB reduces the IFT between the oil and water phase so that particles can attach to the interface.

2.4.2.3 Zwitterionic surfactant

Zwitterinoic surfactants, which are surfactants that carry a positive, negative, or neutral charge depending on physicochemical conditions, have also been studied as nanoparticle surface modifiers for Pickering stabilization (Worthen et al., 2013; Worthen et al., 2014; Liu et al., 2017; Kim et al., 2017).

The interaction between a silica nanoparticle and zwitterionic surfactant is similar to a cationic surfactant when the zwitterionic surfactant is in its protonated state. Liu et al. (2017) showed that when a zwitterionic carboxyl betaine surfactant was in its positively charged state (i.e., acting as a cationic surfactant) it was capable of electrostatically binding to a silica particle surface in the same manner as a cationic surfactant, but only at low pH (< 5). At high pH, the surfactant was negatively charged,

and unable to bind to a silica particle surface due to charge repulsion between the surfactant and nanoparticle surface. This resulted in very weak emulsions that rapidly coalesced. This behavior occurred at elevated pH (>8.5).

2.4.2.4 Nonionic surfactant

Nonionic surfactants without ethylene oxide (EO) units in the presence of bare silica particles have shown the ability to stabilize Pickering emulsions (Pichot et al., 2009). Pichot et al. (2009) suggested that for these systems, each species plays a discrete role in the emulsion stabilization process where it was hypothesized that the surfactant reduces the interfacial tension between oil/water and the colloidal particle acts as an emulsion stabilizer.

Nonionic surfactants with ethylene oxide can also interact with bare silica particles to stabilize Pickering emulsions. However, the mechanism of stabilization differs from nonionic surfactants without EO groups. This is because it is well known that ethylene oxides interact with silanol groups through hydrogen bonds (Howard and McConneil, 1967; Rubio and Kitchener, 1976; Katepalli et al., 2016), which results in particle surface modification. Therefore, using a nonionic surfactant with ethylene oxide units in some sense is qualitatively analogous to using a cationic surfactant to alter the wettability of a bare silica particle. This behavior between nonionic surfactants with EO groups and silica particles and their ability to stabilized Pickering emulsions has been studied by Binks et al. (2007)

2.4.2.5 Anionic Surfactant

Anionic surfactants in combination with bare silica particles are also capable of stabilizing emulsions. Mauraya and Mandal (2018) studied the interaction between

sodium dodecyl sulfate (SDS) with 20-30 nm spherical silica particles and their ability to stabilize decane-in-water emulsions. They demonstrated that stable emulsions could be generated at a fixed silica particle concentration (0.5 wt%) using a range of SDS concentrations (0.1-0.5 wt%).

Similar in behavior to nonionic surfactants without EO groups, the anionic surfactant first formed small oil droplets via interfacial tension reduction and the nanoparticles were restricted to the continuous phase of the emulsion where they aided in emulsion stabilization through charge repulsion (Pilapil et al., 2016). Because the nanoparticles are not actually adsorbed to the oil/water interface, there is some debate as to whether these emulsions are actually Pickering emulsions.

For these anionic/nanoparticle stabilized emulsions, as salt is included into a formulation, there is a tendency for the emulsions to lose stability (with respect to emulsion creaming). For example, when high salt concentrations were used (5 wt%) in Mauraya and Mandal (2018), their nanoparticle/anionic surfactant stabilized emulsions became highly unstable. They attributed this behavior to the sodium cations screening the negatively charged silica particles, which reduced the magnitude of repulsive forces between silica particles and SDS, ultimately allowing for the emulsion drops to flocculate and cream (Mauraya and Mandal, 2018). This enhanced creaming with increased salt concentration is shown in Figure 2.10.

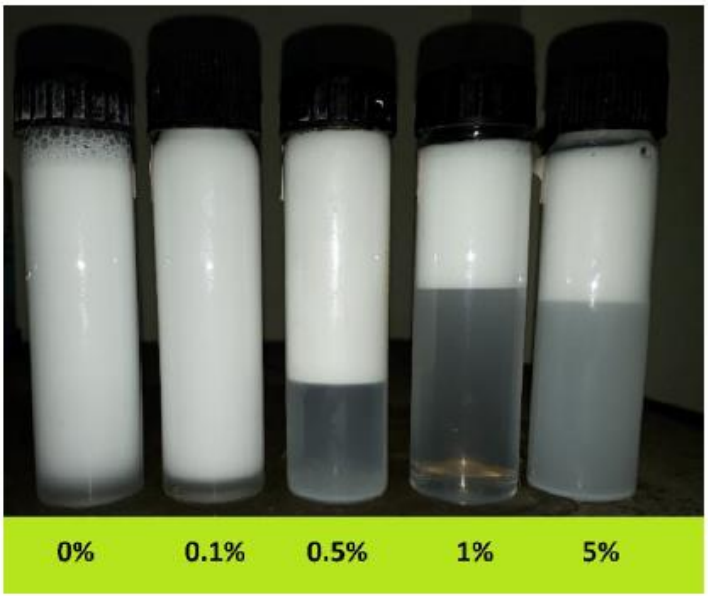

Figure 2.10 – Oil-in-water emulsions stabilized with 0.5 wt% silica nanoparticles, 0.4 wt% sodium dodecyl sulfate, and varying concentrations of sodium chloride (0 wt%, 0.1 wt%, 0.5 wt%, 1 wt% and 5 wt%). This image was taken 10 days after the emulsions were made. From Mauraya and Mandal (2018).

2.5 Some practical challenges with Pickering emulsion stability when using surfactant-modified nanoparticles

While surface modification of nanoparticles (with surfactants) accomplishes the task of changing the wettability of a particle so that it can stabilize a Pickering emulsion, one potential limitation of using surfactants is their lack of permanent adsorption to a particle surface when physicochemical conditions change (Chevalier et al., 2013).

This is typically not an issue for Pickering emulsions designed for the food or cosmetic industries where physicochemical conditions do not significantly change (i.e., salt concentration and temperature). However, for subsurface applications where there can be drastic changes in temperature, variable salinity gradients, and where emulsions will come into contact with in-situ surfactants from crude oils, it is not well understood if

these physicochemical changes will degrade the electrostatic interactions between surfactant and nanoparticle surface.

However, there has been some recent work that suggests physicochemical changes could alter the properties of a surfactant modified particle, enabling surfactant desorption from the particle surface and leading to emulsion destabilization (i.e., coalesence). The work of Zhu et al. (2015) highlights an example of a silica particle that has been modified with surfactant that was capable of stabilizing a Pickering emulsion. In their work, toluene-in-water or tricaprylin-in-water emulsions were stabilized with silica nanoparticles modified with varying concentrations of cationic surfactants: cetyltrimethylammonium bromide (CTAB) or dodecyltrimethylammonium bromide (DTAB). These emulsions were classified as stable due to the observation that there was no coalesced oil during six months of monitoring and because there was no change in emulsion drop size after one month.

The stability of the emulsions was investigated in the presence of varying concentrations of sodium dodecyl sulfate (anionic surfactant). Interestingly, they were able to show that when sodium dodecyl sulfate was added to their oil-in-water emulsions stabilized with CTAB- (or DTAB-) modified silica nanoparticles and gently shaken, the emulsions rapidly degraded and were demulsified (Figure 2.11). The authors noted that destabilization was only possible when sodium dodecyl sulfate was added in equimolar concentrations as cationic surfactant.

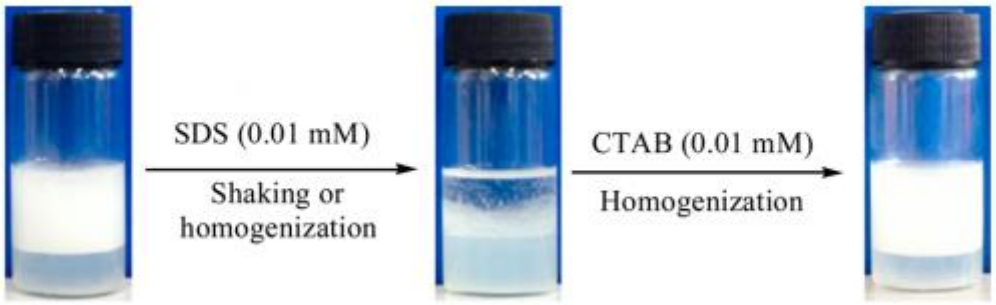

Figure 2.11 – Left: A 50 vol% toluene-in-water emulsion stabilized with 0.5 wt% 20 nm silica nanoparticle modified with 0.01 mM cetyltrimethylammonium bromide cationic surfactant. Middle: The emulsion after addition of 0.01 mM anionic sodium dodecyl sulfate surfactant. Note that the emulsion has been hand shaken. Right: Re-homogenization and re-emulsification of toluene-in-water Pickering emulsion by addition of 0.01 mM cetyltrimethylammonium bromide. From Zhu et al. (2015)

This experimental result is quite remarkable given that Pickering emulsions are thought to be extremely stable to coalescence due to the irreversible adsorption of particles to the oil/water interface. The authors hypothesized that this destabilization was due to a competition between the adsorption of: (1) the cationic surfactant to deprotonated silanol groups on the silica particle surface and (2) the cationic surfactant adsorbing directly to the negatively charged sodium dodecyl sulfate surfactant.

Their results clearly indicate that when sodium dodecyl sulfate was added at equimolar concentrations to CTAB (or DTAB), CTAB (or DTAB) preferred to form ion pairs with the negatively charge sulfate surfactant instead of the silanol groups on the silica particle surface. The result of this was desorption of CTAB from the particle surface, which modified the wettability of the silica particle so that it was no longer capable of stabilizing an emulsion. This resulted in complete destabilization of their emulsion. Somewhat surprisingly, they showed that this process was reversible, where if a new aliquot of CTAB was added to the destabilized emulsion and it was re-homogenized, a stable Pickering emulsion was re-formed.

This idea of using surfactants to stabilize Pickering emulsions is appropriate for situations where little changes physicochemical conditions can be anticipated. This is just one example where an emulsion stabilized with surfactant modified silica particle can destabilize due to changes in physicochemical conditions. This type of destabilization behavior can be mitigated with colloidal particles that are modified by covalent attachment of chemicals to the particle surface. This is because the surface modifiers are permanently altered through chemical bonds and not electrostatic interactions.

2.6 NANOPARTICLE SURFACE MODIFICATION BY COVALENT ATTACHMENT OF SURFACE MODIFIER

The Binks research group, led by Dr. Bernard Binks at the University of Hull, has pioneered the field of Pickering emulsions. A large portion of their work has dealt with understanding fundamental relationships between silica particles (that have been covalently modified) and the properties of the Pickering emulsions that these particles stabilize.

In their work, they almost exclusively use colloidal silica manufactured by Wacker-Chemie. These silica particles are produced using the "bottom up" flame hydrolysis method, where $SiCl_4$ is fed into a flame hydrolysis reactor and silica particles are produced. As an aside, silica particles produced by the flame hydrolysis are frequently referred to as "fumed" silica. Fumed silica particles produced by the flame hydrolysis method are bare, consist of silanol groups, and very hydrophilic.

To make the particles more hydrophobic, they can be post-treated by silanization using organosilanes. The Wacker-Chemie particles are typically modified with dichlorodimethylsilane. Figure 2.12 qualitatively illustrates what a modified silica surface looks like.

In the context of particle surface modification, silanization with small molecules (such as what is done here) is referred to as the "grafting to" functionalization method, where a molecule is directly attached to a particle surface. However, when larger molecules (e.g., MW > 1,000s g/mol) need to be attached to a particle surface, the "grafting from" approach can be used, where a small initiator molecule is first attached to the particle surface, followed by polymerizing the molecule to a desired molecular weight (Saleh et al., 2005).

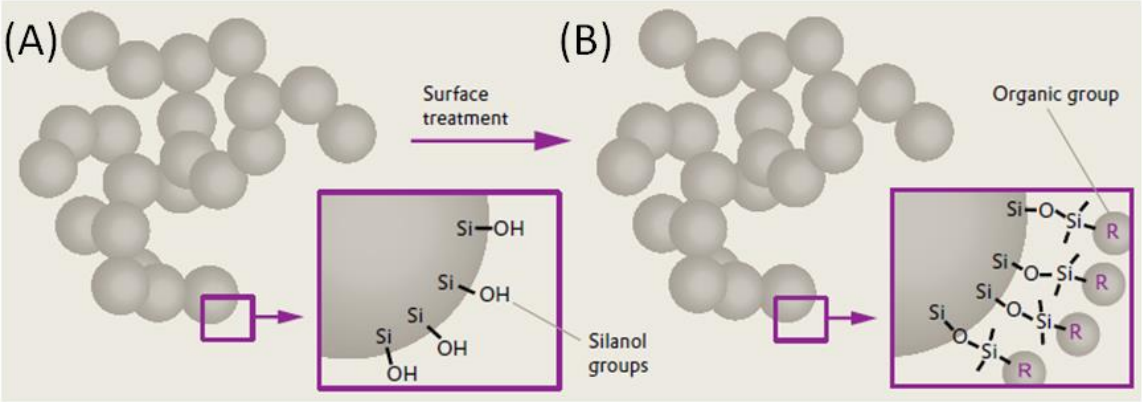

Figure 2.12 – (A) qualitative illustration of an aggregated fumed silica particle that has not been surface treated. The aggregated fumed silica particle only contains silanol groups on its surface. (B) a qualitative illustration of a post treated fumed silica particle. The inset of the image shows that the particle surface has been silanized through siloxane bonds. The "R" in the image refers to any organic constituent. From Evonik Technical Bulletin (2018).

The fumed silica particles produced by Wacker-Chemie are modified with varying concentrations of dichlorodimethysilane. This has the effect of producing particles with different wettabilities/hydrophobic/hydrophilic properties (Binks and Lumsdon, 2000; Binks, 2002; Aveyard et al., 2003; Horozov et al., 2007).

What makes the Wacker-Chemie particles ideal for fundamental Pickering emulsion research is that they are well characterized with respect to the amount (%) of free silanol groups on the particle surface, for example 70% free silanol groups. This is

important because it allows for basic relationships between the modified particles and macroscopic properties of the Pickering emulsions to be established. The silanol content is determined by titrating the particles with sodium hydroxide solutions (Binks and Lumsdon, 2000).

Previously I had discussed some of the challenges associated with experimentally measuring the three phase contact angle that a particle makes with the oil/water interface and how it is a parameter that is typically not reported in papers. Here, because the silanol content of the Wacker-Chemie particles are so well characterized, researchers instead prefer to correlate the extent of silica silanization with the type of emulsion that is formed (Binks and Lumsdon, 2000; Binks, 2002).

The work of Aveyard et al. (2003) emphasizes this. In their work, they studied the relationship between particle surface modification and the impact this had on the type of emulsion that was formed (oil-in-water (o/w) or water-in-oil (w/o)). The particles they used had surface silanol concentrations that ranged from 100% (bare) to 14% (modified with dicholordimethylsilane). Their results demonstrated that if silica particles were highly hydrophilic (SiOH > 76%), oil-in-water emulsions were formed. Conversely, if the particles were very hydrophobic (SiOH < 36%) then water-in-oil emulsions were formed. If however, the particles contain intermediate wettabilities, they showed that there exists the possibility to form oil-in-water or water-in-oil which depended on the initial phase the particles were dispersed in and the physicochemical conditions of the different phases (i.e., concentration of particles, pH, and if salt was present).

Another common particle that is used to stabilized Pickering emulsions are Evonik's Aerosil R816 particles, which has shown a tremendous ability to stabilize a wide range of Pickering emulsions (Whitby et al., 2009; Vashisth et al., 2010; Priest et

al., 2011; Whitby et al., 2011; Whitby et al., 2012; Juarez and Whitby, 2012; Whitby and Onnink, 2014; Whitby and Krebsz, 2014; Katepalli et al., 2017).

The R816 particle is unique due to its surface modification, which is covalently modified with a hexadecylsilane (C16). The C16 chains make the particles partially hydrophobic so that they are both water- and oil-dispersible. One drawback of these particles is that Evonik does not disclose the extent of surface modification like Wacker-Chemie.

Based on the initial work of the Binks group, many researchers have followed suit and studied the relationship between different organic surface modifiers and the impact they have on the properties of Pickering emulsions. Saleh et al. (2005) studied Pickering emulsions stabilized with silica particles that were covalently modified with highly charged poly(styrenesulfonate) brushes, which were modified using the "grafting from" method, where the bare silica particles were first functionalized with 2-bromoisobutyrate followed by using the atom transfer radical polymerization (ATRP) method to grow polystyrene brushes away from the silica particle surface.

The authors demonstrated that even though their silica particles had a highly negative surface charge (due to the polystyrene ligand,-77 mV at neutral pH), the particles were still able to stabilize a toluene/water interface. They suggest this was because the polystyrene ligand is interfacially active (because of its chemical structure) and because of this has a relatively strong affinity for the oil phase (trichloroethylene or TCE). They quantified the interfacial activity of the surface modified particles by measuring the TCE/water IFT. The particles were capable of reducing the IFT from 30 to 14.5 mN/m.

Up to this point, the discussion of Pickering emulsions has mainly focused on the static properties of emulsions stabilized with either surfactant or covalently modified silica particles and understanding the static properties of the emulsions, i.e., no

coalescence. Here I briefly go over some of the rheological properties of Pickering emulsions stabilized with silica particles in the presence of salt solutions.

2.7 PICKERING EMULSION RHEOLOGY

In most practical situations, not all of the particles used to stabilize a Pickering emulsion will be adsorbed to the oil/water interface (Chevalier and Bolzinger, 2013) and because of this there will be excess particles that remain in the continuous phase of the emulsion.

Recall that silica particles have silanol groups on their surface. In most cases, not all of these silanol groups are capped with a surface modifier and with pH >2-4, the silanol groups are deprotonated and carry a strong negative charge. This results in electrostatic repulsion between particles so that stable dispersions in DI water can be formed. However, when salt is included in a dispersion, the electrostatic repulsive forces between particles are screened (Figure 2.13), which compresses the electrical double layer of the particles, resulting in strong attractive forces which can result in particle bridging in the continuous phase of the emulsion, which is shown in Figure 2.14.

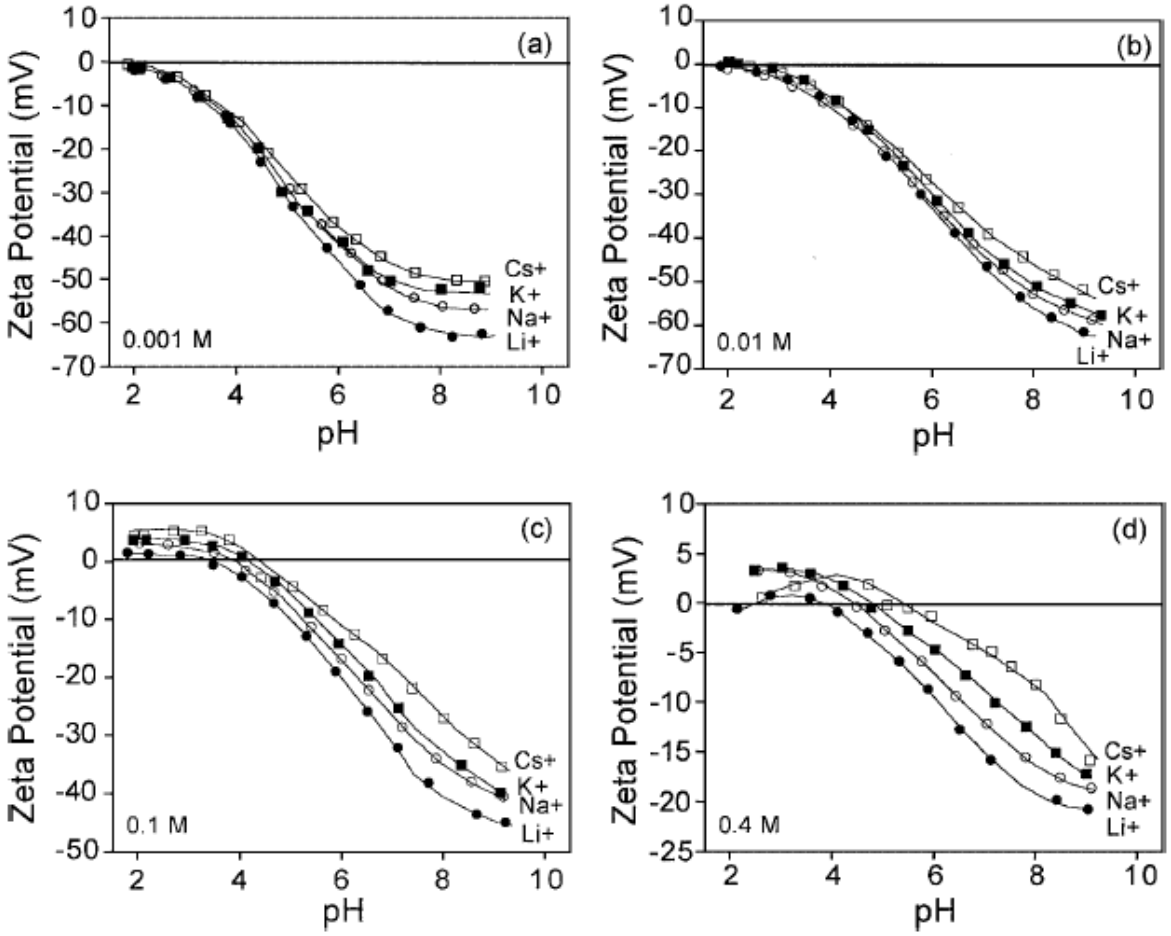

Figure 2.13 – Influence of monovalent salt concentration (lithium, sodium, potassium, and cesium) on silica nanoparticle zeta potential for (a) 0.001 M, (b) 0.01 M, (c) 0.1 M, (d) 0.4 M ionic strength solutions. From Franks (2002).

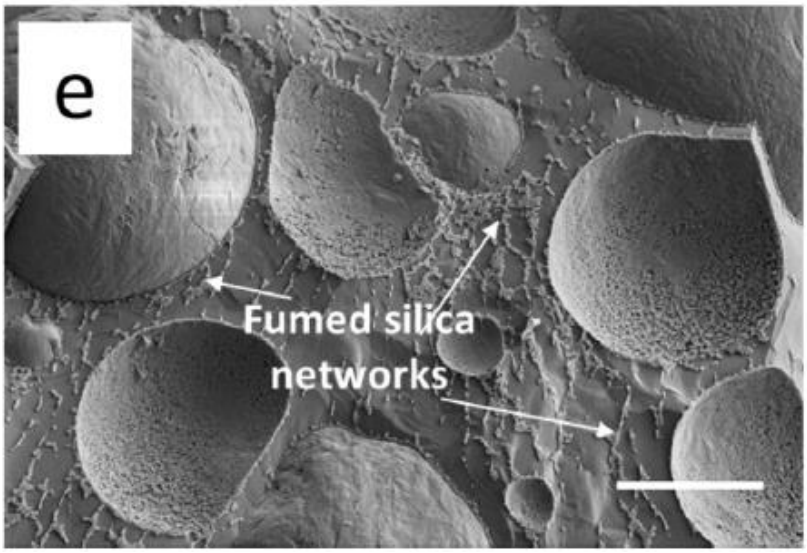

Figure 2.14 – Cryo-SEM image of a bromohexadecane-in-water Pickering emulsion stabilized with 2 wt% Evonik R816 fumed silica particles. The emulsion formulation contained 50 mM NaCl. Scale bar is 20 μm. From Katepalli et al. (2017).

This behavior of flocculated/bridged silica particles in a Pickering emulsion is actually a very desirable property for the food or cosmetic industries. This is because "stability" for the food or cosmetic industry is simply defined by the lack of macroscopic phase separation (emulsion creaming). For an oil-in-water emulsion, creaming is defined as the density driven phase separation of emulsified oil drops from the continuous water phase. The result of creaming is a dense emulsion phase, referred to as "cream" that rests on top of a resolved aqueous phase. By including excess fumed silica particles that are flocculated, emulsion creaming can be reduced or even completely eliminated. Eliminating creaming with conventional surfactant-stabilized emulsions is very difficult because conventional surfactants do not form bridges or associate with one another in the continuous phase (Chevalier and Bolzinger, 2013).

Understanding the relationship between salt concentration and the strength of the particle network that forms has been studied (Horozov et al. 2007; Whitby et al., 2011;

Lee et al., 2011; Whitby et al., 2012; Katepalli et al., 2017; Derakhshandeh et al., 2018; Pandey et al., 2018). Researchers have investigated the rheological properties of these emulsions in the context of salt concentration, type of nanoparticle, concentration of nanoparticles, and oil volume fraction in a formulation. Here I highlight several articles and their efforts to characterize these behaviors.

Horozov et al. (2007) studied the behavior of a model Pickering emulsion that was stabilized with Wacker-Chemie fumed silica particles (85% silanol content). They included sodium chloride (NaCl) in their formulations. They stabilized polydimethyl silicone oil-in-water emulsions (o/w). They assessed the creaming behavior of their emulsions (4 wt% particles, 50 vol% oil) and found that emulsions prepared without salt rapidly creamed (< 6 minutes). Interestingly, they found that by including just 1-2 mM NaCl, that the creaming behavior of their emulsions was significantly retarded, where very little creaming was observed 36 hours of monitoring. Figure 2.15 highlights the results from their work and shows the profound impact that salt can have on minimizing emulsion creaming.

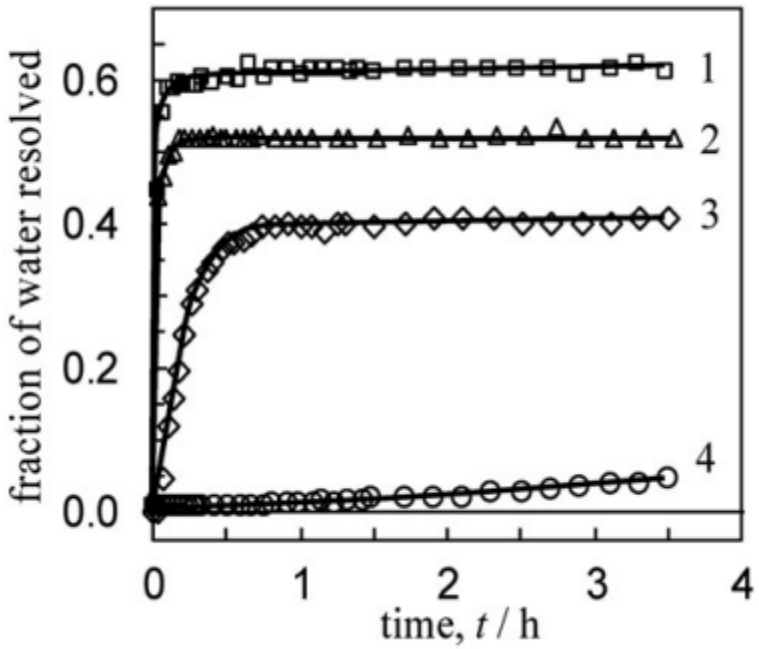

Figure 2.15 – Fraction of water resolved versus monitoring time for 50 % (by volume) polydimethyl silicone oil-in-water emulsions (o/w) stabilized with 4 wt% Wacker-Chemie fumed silica particles (84% SiOH) with (1) DI water, (2) 0.005 mM NaCl, (3) 1 mM NaCl, and (4) 2 mM NaCl. From Horozov et al. (2007).

To quantify the origin of this behavior, the authors measured the viscoelastic properties of their different emulsion formulations. The term viscoelasticity defines a material that exhibits both liquid- and solid-like properties (Malvern, 2016). The tendency for that material to be solid- or liquid-like depends on the external conditions that are imposed on the sample (Malvern, 2016).

Using standard rheometry, they characterized the elastic (G') and viscous (G") components of their emulsions using a cone and plate geometry. Their measurements were done at a shear rate of 10 s^{-1} and they showed a clear relationship between salt concentration and emulsion viscoelasticity, with more viscoelastic emulsions being

produced at higher salt concentrations (Figure 2.16). This was characterized by the magnitude of the elastic storage modulus or by the relative viscosity of the emulsion.

Horozov et al. (2007) explained these observations by suggesting that in low-ionic strength brines, electrostatic repulsion between particles dominated and no particle bridges formed in the continuous phase of the emulsion. This macroscopically manifests itself in very fast emulsion creaming. However, at high ionic strengths, which they define as those above the critical flocculation concentration (cfc) of salt (~2 mM NaCl), attractive forces between particles became dominant, which resulted in interparticle attractions and the formation of a structured network of particles in the continuous phase of the emulsion.

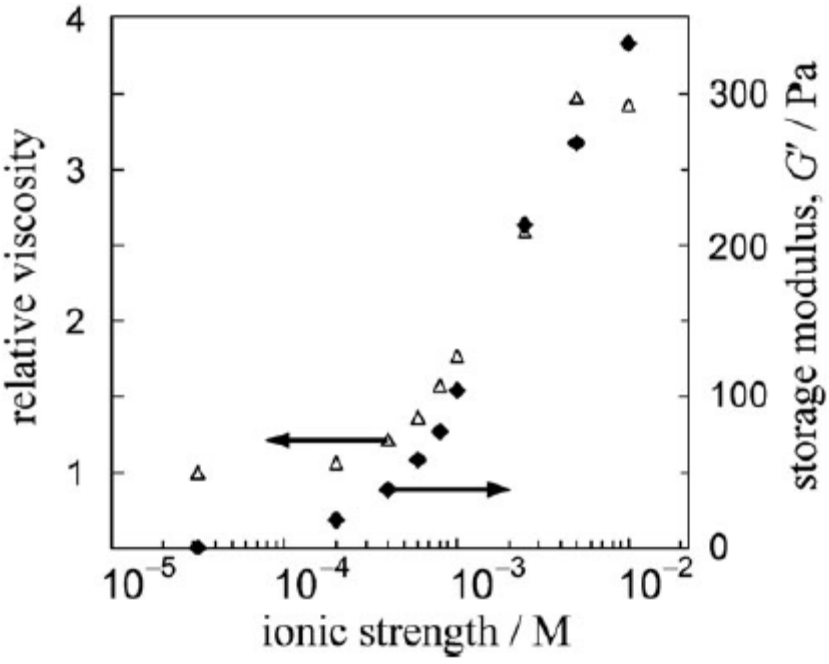

Figure 2.16 – Emulsion viscoelasticity versus sodium chloride for 50 % (by volume) polydimethyl silicone oil-in-water emulsions (o/w) stabilized with 4 wt% Wacker-Chemie fumed silica particles (84% SiOH). The left axis plots the relative viscosity of the emulsion and the right axis plots the storage modulus (G') of the emulsion. The measurements were done at a shear rate of 10 s^{-1}. From Horozov et al. (2007).

In a similar study, Katepalli et al. (2017) investigated the effect of particle shape and aqueous phase salt concentration on the viscoelastic properties of a Pickering emulsion. They used two different particles in their work: (1) R816 fumed silica particles produced by Evonik and (2) bare spherical silica particles from Fiber Optic Center.

Recall the R816 particles are partially modified with a linear C16 molecule, so to make the bare silica particles have similar properties to the R816 particles, the authors modified their particles with hexylamine through electrostatic interactions. The authors stabilized bromohexadecane-in-water emulsions with these particles. It is important to point out their choice of bromohexadecane as a model oil because it has a specific gravity of 0.999. This high specific gravity minimizes the impact of density driven phase separation on their rheological measurements and ensures they were truly quantifying the impact of particle shape and salt concentration.

In their formulations, they used 2 wt% particles with either 0.1 mM or 50 mM NaCl. They suggested that interparticle interactions were repulsive with 0.1 mM NaCl and attractive with 50 mM NaCl, which was calculated using standard DLVO theory (Figure 2.17). The emulsions stabilized with the fractal-like R816 particles had smaller emulsion drops than the emulsions prepared with spherical particles. They suggest that this result was due to the ability of the fractal particles to be “pinned” to the interface more quickly than the spherical particles because of their irregular shape.

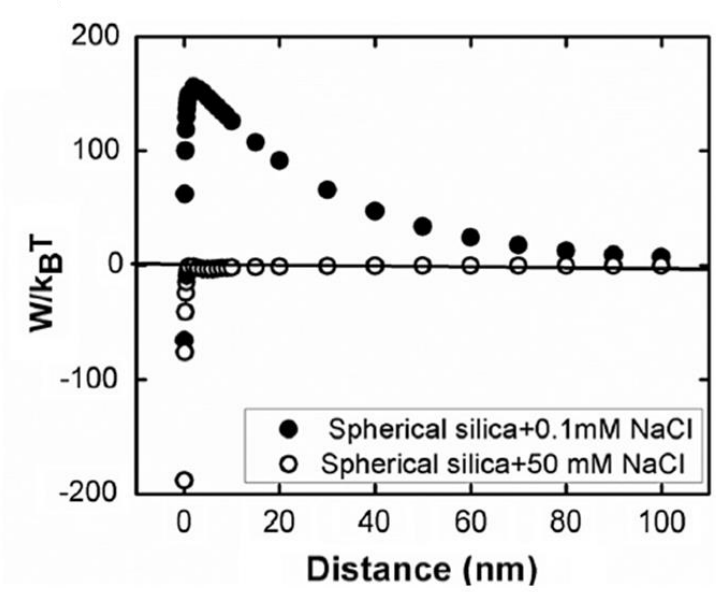

Figure 2.17 – Total interaction potential (kT) versus separation distance for a spherical silica particle (D = 210 nm) in the presence of 0.1 mM NaCl or 50 mM NaCl. Positive interaction potentials indicate repulsion whereas negative interaction potentials indicate attraction. From Katepalli et al. (2017).

They showed that their emulsions had significantly different responses to small oscillatory shear amplitude measurements (SAOS) which were attributed to: (1) particle geometry and (2) concentration of salt in the formulation (Figure 2.18). The authors showed that increased salt concentrations led to an increase in the zero shear elastic storage modulus of both emulsions, which was in agreement with Horozov et al.'s (2007) results. The zero-shear elastic storage modulus was calculated by averaging the elastic storage moduli data in the linear viscoelastic regime of a strain sweep measurement. The authors also showed that the emulsions stabilized with spherical particles with 50 mM NaCl had a zero shear elastic storage modulus of 9 Pa whereas the R816 fractal particles had a zero shear elastic storage modulus of about 200 Pa.

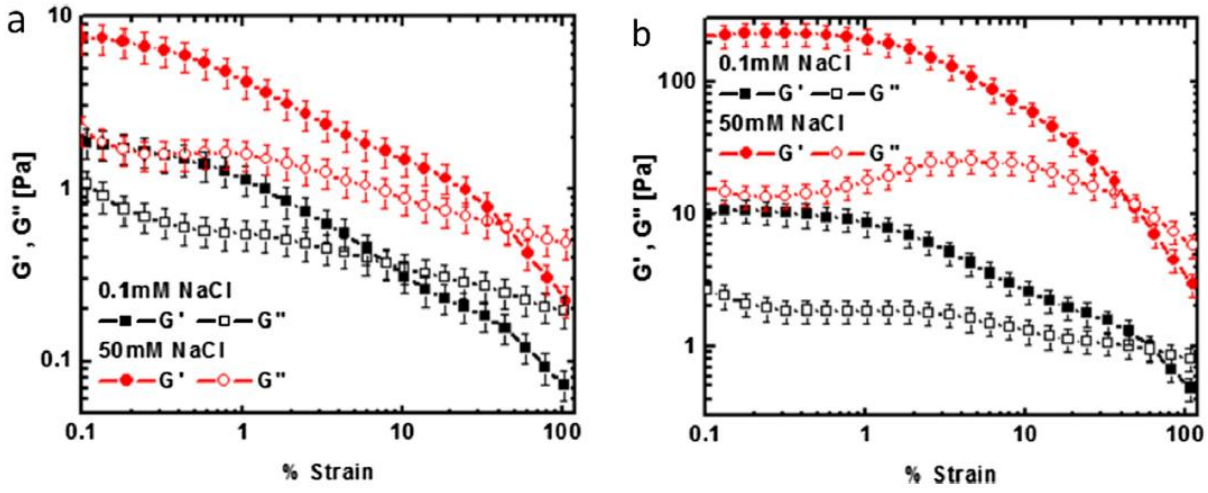

Figure 2.18 – Strain sweep profiles for Pickering emulsions prepared with 2 wt% (a) spherical silica particles and (b) fractal like R816 fumed silica particles with 0.1 mM (black) and 50 mM (red) sodium chloride. From Katepalli et al. (2017).

The results presented by Katepalli et al. (2017) are interesting for a couple of reasons. First, the authors were able to clearly show that nanoparticle shape plays a rather significant role in the viscoelastic properties of a Pickering emulsion. This is important because it provides experimentalists with another design parameter that they can use to tailor the properties of their emulsions. Second, their results amplify the impact that salts play in interparticle attractions and the highly viscoelastic properties that result from.

To further emphasize this, in the work of Horozov et al. (2007), the highest salt concentration used was 100 mM NaCl. Moreover, their measurements showed that interparticle attractions became detectable at about 1mM NaCl. In Katepalli et al. (2017) used only 50 mM NaCl and their emulsions also showed strong viscoelastic behavior. To put this into perspective, many subsurface reservoirs have salinities that are comparable to that of sea water (Kharaka et al., 2006), which has a concentration of approximately 600 mM NaCl (Saha et al., 2013).

Clearly, the experimental results from Horozov et al. (2007) and Katepalli et al. (2017) are problematic for subsurface applications because of the relationship between emulsion viscoelasticity and salinity for fumed silica particles. Because of this, it is highly unlikely that fumed silica particles could act as Pickering emulsifiers due to their lack of stability in low ionic strength and as a result, these emulsions have viscoelastic properties. This calls into question whether or not these emulsions could actually flow through a reservoir. Therefore, there is a need to find nanoparticles, with well-defined surface modifiers that are capable of minimizing interparticle attractions, especially in highly concentrated salt waters.

One important aspect of my work is that I attempt to address this issue of interparticle attractions and how viscoelasticity of an emulsion can be minimized (in brine) by careful selection of a nanoparticle surface modifier. I also show how that minimization of viscoelasticity is not only dependent on the nanoparticle surface modifier but also it is dependent on the extent of nanoparticle surface modification. This needs to be highlighted because most of the research on Pickering emulsions (or foams) completely neglects the extent of surface modification as a design parameter.

2.8 PICKERING EMULSION STABILITY

2.8.1 Static stability

Pickering emulsions are frequently described by their long term static stability and are often said to have better long term stability compared to surfactant-stabilized macroemulsions. In most cases, the definition that is used to describe the stability of a Pickering emulsion is the lack of macroscopic coalescence with respect to time (Saleh et al., 2007; Worthen et al., 2014;Kim et al., 2017; Bjorkegren et al., 2017; Tyowua et al.,

2017; Rincon-Fontan et al., 2019; Edgehouse et al., 2019). However, because there are so many particle emulsifiers that meet this definition of “stability”, it makes it difficult to compare the relative stabilities of different Pickering emulsion formulations. Here I try to highlight some common definitions that are used to describe the stability of Pickering emulsions and why these definitions make it difficult to compare different Pickering emulsifiers.

When describing the “static” stability of a Pickering emulsion, stability can refer to two different components of an emulsion. Stability can be described using the definition that was given above, which is the lack of macroscopic coalescence with respect to time and for a Pickering emulsion to satisfy this definition of stability, the emulsified oil drops should be sufficiently populated with particles so that the drops do not coalesce with respect to time (Schroder et al., 2018). Figure 2.19 (center) shows an example of a Pickering emulsion that shows long term static stability, which is based on the observation that the emulsion did not coalesce during 1.5 years of monitoring (Bjorkegren et al., 2017). This emulsion was stabilized with 2.5 wt% silica particles modified with propyl-e and mPEG.

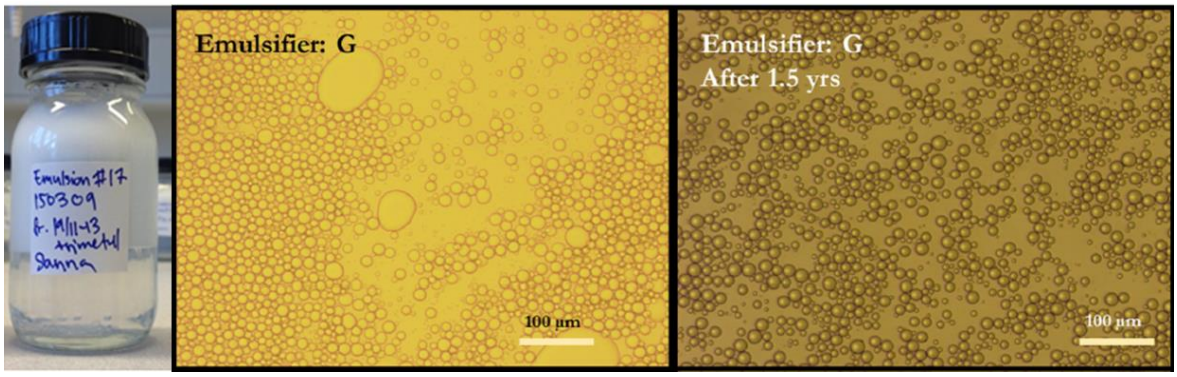

Figure 2.19 – Oil-in-water emulsion stabilized with surface modified silica nanoparticles. (left) Emulsion resting in a storage container. (middle) Emulsion initially after emulsification. (right) Emulsion 1.5 years after emulsification. Note the lack of significant change in emulsion drop size with time. From Bjorkegren et al. (2017).

The second definition of stability refers to an emulsion's ability to resist creaming. Creaming is the physical phase separtation of emulsified oil from the continuous water phase and occurs due to the density difference between oil and water (Katepalli et al., 2017). Creaming is quantified using the Stokes settling velocity (equation (2.3)) where $\Delta\rho$ is the density difference between oil and water, $R_{emulsion}$ is the radius of the emulsion drops, and η is the viscosity of the continuous phase of the emulsion:

$$v_{stokes} = \frac{2\Delta\rho g R_{emulsion}^2}{9\eta}. \qquad (2.3)$$

The leftmost image in Figure 2.19 shows that this emulsion is not stable to creaming. This is because there is a creamed, emulsified phase that is resting on top of a clear aqueous phase.

Based on equation (2.3), minimizing emulsion creaming is done by decreasing the density difference between oil/water, decreasing the diameter of the emulsion drops, or

by increasing the viscosity of the continuous phase of the emulsion. In most practical applications, the type of oil that is used in an emulsion is fixed and cannot be altered. Changing the emulsion drop size by including more emulsifier is possible, but there is typically a finite limit to how much the size of an emulsion drop can be reduced. Altering the continuous phase viscosity, by addition of polymer or with excess particles with salt, is the easiest way to minimize emulsion creaming. Minimizing creaming is particularly important for emulsion drops that are not sufficiently populated with emulsifier. This is because once the emulsified oil drops cream, the drops begin to compress against one another and coalesce.

Compared to surfactant-stabilized emulsions, for a Pickering emulsion, there is no relationship between emulsion drop size and their long term static stability to coalescence. The only criterion that matters for long term static stability is that emulsified oil drops be sufficiently populated with particles (Frelichowska et al., (2010)). This was experimentally shown by Frelichowska et al. (2010). This behavior is in contrast to macro-emulsions stabilized with surfactants, where it has been shown there is a strong correlation between stability of an emulsion and its initial drop size, with emulsions that have smaller drops having greater long-term stability (Abedi et al., 2019).

2.8.2 Dynamic stability

The dynamic (orthokinetic) stability to coalescence of Pickering emulsions is far less studied compared their static stability. This is likely due to the fact many of the proposed applications for Pickering emulsions are static in nature – for example cosmetic or food emulsions.

To date, the most comprehensive article on the shear stability of Pickering emulsions is by Whitby et al. (2011). In their article, they assessed the stability of a well-

formulated Pickering emulsion stabilized with 2 wt% partially hydrophobic R816 fumed silica particles. Salt (sodium chloride) was used in their formulations to ensure that their emulsion drops were well covered with silica particles. They characterized the coverage of particles on their emulsion drops using laser confocal microscopy (Figure 2.20). Additionally, the authors used bromhexadecane as their oil to minimize emulsion creaming during their rheological assessment.

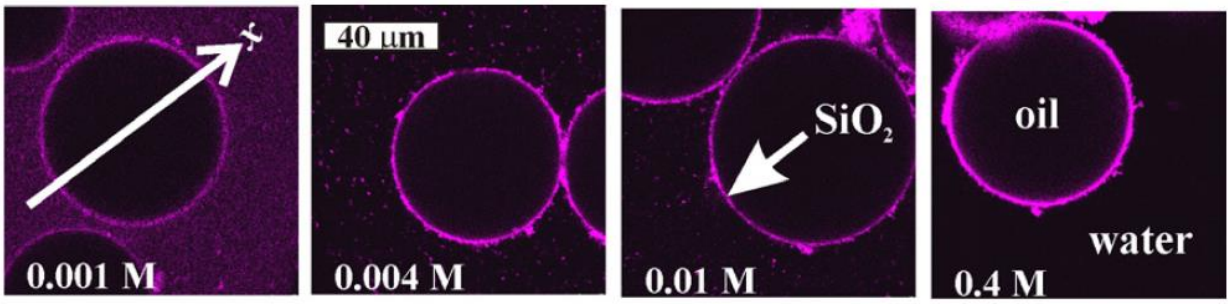

Figure 2.20 – Laser confocal microscopy images of bromohexadecane-in-water emulsions stabilized with 2 wt% R816 fumed silica particles with varying salt concentrations. The image qualitatively shows the relationship between particle coverage on an emulsion drop surface and salt concentration, which is indicated at the bottom of each panel. Image from Whitby et al. (2011).

Whitby et al. (2011) analyzed the orthokinetic stability of their emulsions using a rheometer. This was done by monitoring the change in emulsion drop size with respect to shearing time (at a fixed shear rate). Figure 2.21A shows results from a shear-induced coalescence experiment that was done at a constant shear rate of 10 s^{-1}. The left axis of the plot shows the emulsion drop size and the right axis of the plot shows the emulsion uniformity index, which measures how polydisperse the emulsion drops are. Their results show that for this emulsion formulation (which was prepared with only 0.001 M NaCl), the drops did not significantly change in size during the first 20 minutes of shear, but they showed rapid coalescence after 20 minutes of shear.

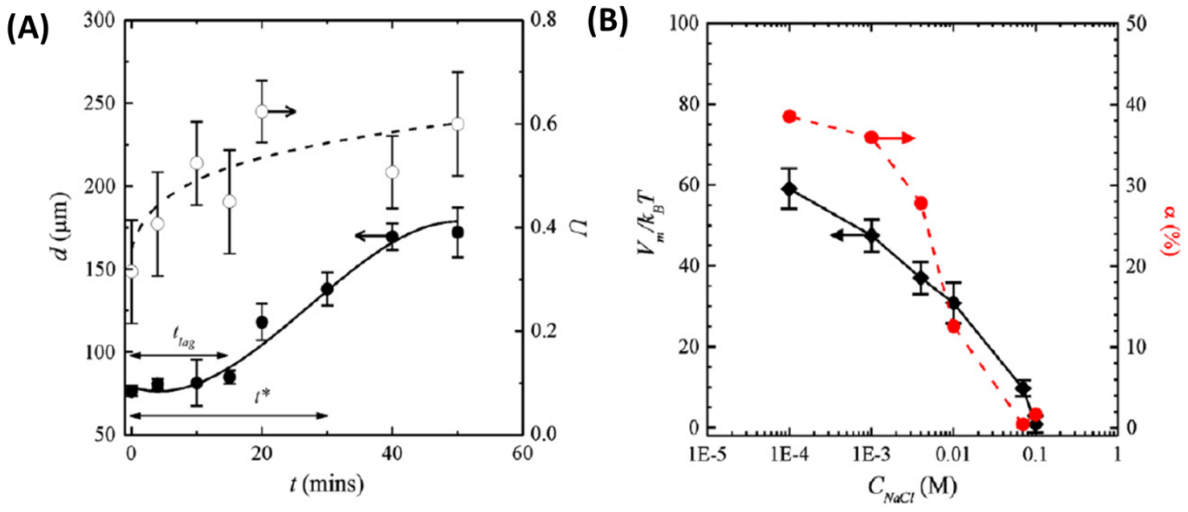

Figure 2.21 – (A) (left axis) Change in emulsion drop size versus stirring time at a shear rate of 10 s^{-1} for a bromohexadecane-in-water emulsions stabilized with R816 fumed silica particles with 0.001 M NaCl in the continuous phase. (right axis) Emulsion drop uniformity versus time. (B) (left axis) Interaction potential of R816 fumed silica particles versus sodium chloride concentration (black markers). (right axis) Volume of coalesced oil during 1 minute of shear at 1000 1/s for bromohexadecane-in-water emulsions stabilized with 2 wt% R816 silica particles (red markers). Image from Whitby et al. (2011).

Whitby et al. (2011) also performed a set of shear experiments where they measured volume of oil coalesced from an emulsion while it was sheared for 1 minute at 1000 1/s (Figure 2.21B). In these experiments, they were attempting to quantify the relationship between salt concentration and emulsion stability. At low salt concentrations, the emulsions released large volumes of oil (~40%), which suggested that the emulsions were not orthokinetically stable. At high salt concentrations, the emulsions released much less oil, indicating much better orthokinetic stability.

The authors correlated the stability of their Pickering emulsions to the interaction potential between silica particles using DLVO theory. They suggested that the low orthokinetic stability for emulsions prepared with low salt concentrations was due to

repulsive forces dominating particle-particle interactions. They calculated an interaction potential of ~60/kT for an emulsion with 0.1 mM NaCl. The implication of this is that because strong repulsive forces dominate at low salt concentrations, a large majority of the silica particles appear to reside in the continuous phase of the emulsion, which leaves oil drops that were not densely populated with particles on their surface (Figure 2.20). Because of this, the emulsions prepared with low salt concentrations were susceptible to shear-induced coalescence.

However, as the concentration of salt increased (up to 0.4 M NaCl), the stability of their emulsions also increased. With 0.4 M NaCl, the particle-particle interactions were attractive due to charge screening, which led to a dense layer of particles at the oil/water interface (Figure 2.20). This produced an emulsion that did not significantly coalesce while being sheared (Figure 2.21B).

Recently, Schroder et al. (2018) published results on the relationship between the adsorption rate of colloids to the oil/water interface (to form Pickering emulsions) and its impact on the dynamic stability of their Pickering emulsion. These authors were interested in forming "food" grade Pickering emulsions, so they used stripped sunflower oil for their emulsified phase and colloidal lipid particles as their Pickering emulsifiers. The adsorption rate of particles to the oil/water interface was controlled by the total volumetric flow rate in the flow focusing T-junction of their model with low flow rates corresponding to low shear rates and therefore to low particle adsorption rates. Their results clearly demonstrated that there was a strong correlation between the dynamic stability of their emulsions and the adsorption rate (flow rate) of particles to the oil/water interface, with higher particle adsorption rates leading to more stable Pickering emulsions (at a fixed particle concentration). They experimentally showed this by monitoring the number of coalescence events that occurred within their micromodel as a function of total

flow rate. They found there was a much higher probability of emulsion coalescence at low particle adsorption rates. Moreover, they also showed there was a strong correlation between the dynamic stability of their Pickering emulsions and the concentration of particles that were used in a formulation. They showed that at low particle concentrations, ~ 0.005%-0.05% w/w, that there were more coalescence events, which was attributed to the lack of sufficient particle coverage on an emulsion drop surface.

2.9 NANOPARTICLE SURFACE MODIFICATION WITH HYDROPHILIC MOLECULES

The methods described above are commonly used to alter the wettability of a silica particle. However, they are not applicable for stabilizing emulsions for subsurface applications. This is because those particle modifications are done with the sole intent of altering particle wettability and are not designed to take into account the high salinity of oil reservoirs. Because of this, these surface modifications (with surfactants or hydrophobic silanes) will not prevent particle agglomeration/aggregation in the presence low ionic strength brines, which could result in unwanted plugging/loss of reservoir permeability (Zhang et al., 2010). To address this issue, nanoparticles need to be modified with hydrophilic molecules that can sterically stabilize the nanoparticles in brine.

Much of the early work on nanoparticle surface modification, for applications in salty environments, was driven by the biomedical industry. Two frequently cited biomedical uses for nanoparticles are for selectively targeting cancer cells or as contrast agents for medical imaging (Estephan et al., 2010). However, in order to get nanoparticles to achieve these tasks, they must be able to exist as stable dispersions in high ionic strength solutions (0.5 – 3 M NaCl) or high concentration protein solutions, like fetal bovine solution (Esephan et al., 2010).

Estephan et al. (2010) functionalized silica nanoparticles with a hydrophilic zwitterionic silane called 3-(dimethyl-(3-(trimethyoxysilyl)propyl)ammonio)propane-1-sulfonate and characterized the stability of these particles as a function of different reaction parameters. The motivation for their work was to find a biologically acceptable alternative to polyethylene glycol (PEG) salinized silica particles (which is often referred to as PEGylation). This is because PEGylation is known to have several prominent limitations, which are protein adsorption to PEG, lack of stability in the presence of oxygen and transition metals, and large increases in particles functionalized with PEG due to the physical size of PEG molecules (Estephan et al., 2010)

The two reaction parameters that were varied in Estephan et al. (2010) were temperature (ambient versus 80^{o}C) and silane concentration (0.16 – 8 μmol/m^2). The dispersion stability of the particles was assessed by monitoring their turbidometric response in different ionic strength brine waters (0.5 M – 3 M NaCl). They found that particles silanized at 80 °C with 1.7 μmol/m^2 silane (which resulted in 1.0 μmol/m^2 attached to the particle surface) produced the most stable particle dispersions. These particles showed no change in hydrodynamic diameter for over 15 days in 0.5 M NaCl at pH 7.4. Moreover, when tested under the harsh conditions of 3 M NaCl, the particles showed no signs of agglomeration during 15 days of monitoring. This achievement was quite remarkable. One limitation of this study was that the stability of the dispersions was tested at relatively low temperatures: 25 °C for the sodium chloride solutions and 37 °C for the fetal bovine solution.

Numerous articles have used (3-glycidyloxypropyl)trimethoxysilane (glymo) to modify silica substrates (Daniels and Francis, 1998; Daniels et al., 1999; Yang and Liu, 2010; Greenwood and Gevert, 2011; Schonherr et al., 2012; He et al., 2013; Worthen et al., 2016; Behzadi and Mohammadi, 2016; Torrico et al., 2018; Jang et al., 2018) and

some have shown that glymo is capable of preventing agglomeration of silica sols with ions present (Greenwood and Gevert, 2011; Worthen et al., 2016; Jang et al., 2018). Because of glymo's low cost, wide use, and proven ability to stabilize silica dispersions in salt water, it is a highly attractive silane for subsurface applications.

Worthen et al. (2016) performed a detailed study on the ability for four different hydrophilic silanes to stabilize silica nanoparticles in brine water. The silanes that they studied were: (1) glymo, (2) 3-(dimethyl-(3-(trimethyoxysilyl)propyl)ammonio)propane-1-sulfonate, and (3-4) two PEG silane derivatives (a methyl terminated silane with 6-9 EO groups and one alcohol terminated silane with 8-12 EO groups).

The approach to their work was very similar to that of Estephan et al. (2010). They tested how different reaction conditions (reaction temperature and silane concentration) affected the dispersion stability of the sterically stabilized particles. They evaluated the stability of their dispersions by monitoring the change in particle size (using DLS) with respect to time and showed that only glymo and SB were capable of stabilizing 6 nm particles for over 30 days at 80 °C in American Petroleum Institute (API) brine (8 wt% NaCl + 2 wt% $CaCl_2$). The results from this work are important because they have identified two silanes, with well-defined structures, that can provide steric stabilization in highly saline environments. Moreover, this provides two unique particle surface modifiers that could potentially be used to aid in stabilizing foams or emulsion for EOR.

Worthen et al. (2016) also used extended DLVO theory to semi-quantitatively predict the dispersion stability of particles. We highlight these calculations below.

2.10 DLVO SURFACE CALCULATIONS

DLVO theory (Derjaguin and Landau, 1941; Verwey and Oeverbeek, 1948) can estimate the dispersion stability of bare nanoparticles in different ionic strength waters, whereas extended DLVO theory can be used to semi-quantitatively predict the stability of particles with surface modification.

It is well known that silica nanoparticles are not aqueously stable in high ionic strength brines, which is well described by DLVO theory (Metin, 2012). To illustrate this, I calculate the total interaction potential between two equally sized spheres without any surface modification. I then compare these results to a sterically stabilized nanoparticle in the same ionic strength solution to highlight the importance of nanoparticle surface modification, and how it can impart the stability of nanoparticles, which is necessary for particles that are to be used in briny waters. Extended DLVO theory includes an additional term in the total interaction potential calculation, which is the steric contribution of the nanoparticle surface modifier. Note: these equations are based on the work of Binks and Lumsdon (1999), Metin (2012) and Worthen et al. (2016) and are only valid for spheres of equal size (Hoxha et al., 2017)

The total interaction potential between two spheres is the sum of their electrostatic (repulsive) and van der Waals (attractive) and steric forces which are shown in equation (2.4):

$$V_T(d) = V_R(d) + V_{vdW}(d) + V_S(d), \quad (2.4)$$

where V_T is the total interaction potential in units of k_BT, where k is Boltzmann's constant, and T is temperature (K). V_R is the electrostatic component, V_{vdW} is the van der Waals contribution, and V_S is the steric contribution from surface modification. d is the separation distance between the two particles. V_R is calculated using equation (2.5):

$$V_R(d) = 2\pi R\varepsilon_o\varepsilon_r\psi_o^2 LN(1 + e^{-\kappa d}) \quad (2.5)$$

where R is the radius of the particle, ε_o is the permittivity of vacuum, ε_r is the relative permittivity of an electrolyte solution, ψ_o is the surface potential of a silica particle which is generally assumed to be the zeta potential of a silica sol, and κ is the inverse Debye length. The inverse Debye length is calculated using equation (2.6)

$$\kappa = \sqrt{\frac{2N_A e^2 I}{\varepsilon_o\varepsilon_r kT}} \quad (2.6)$$

where N_A is Avogadro's number, e is the elementary charge, and I is the ionic strength of the solution. The van der Waals (V_{vdW}) attractive component is calculated using equation (2.7)

$$V_{vdW}(d) = -\frac{(R+L)\left(\sqrt{A_m}-\sqrt{A_p}\right)^2}{12d} \quad (2.7)$$

where R is the core nanoparticle radius, L is the thickness of the surface modifier, A_m is the Hamaker constant for the fluid medium and A_p is the Hamaker constants for the particle (Worthen et al., 2016). The steric component is calculated using equation (2.8)

$$V_s(d) = V_e(d) + V_o(d) \quad (2.8)$$

where V_e is the entropic/elastic and V_o is the osmotic contribution. Both of these are the result of the nanoparticle surface modifier. The entropic/elastic component contribution (V_e) is calculated using (2.9):

$$V_e(d) = 0, \qquad d \geq L, \quad (2.9)$$

$$V_e(d) = \frac{2\pi R}{M_W}\phi d^2 \rho_p \left[\frac{d}{L}\ln\left(\frac{d}{L}\left(\frac{3-d/L}{2}\right)^2 - 6\ln\left(\frac{3-d/L}{2}\right) - 3\left(1+\frac{d}{L}\right)\right)\right] d$$

$$< L,$$

where M_W is the molecular weight of the silane/polymer surface modifier, φ is the volume coverage of silane/polymer on the particle surface, and ρ_p is the density of pure silane/polymer in solution. The osmotic contribution (V_o) is calculated using (2.10):

$$V_o(d) = 0 \qquad d \geq 2L, \qquad (2.10)$$

$$V_o(d) = \frac{4\pi R}{\upsilon_1}\phi^2(0.5-\chi)\left(L-\frac{d}{2}\right)^2 \qquad L \leq d < 2L,$$

$$V_o(d) = \frac{4\pi R}{\upsilon_1}\phi^2(0.5-\chi)L^2\left(\frac{d}{2L} - 0.25 - \ln\left(\frac{d}{2}\right)\right)^2 \qquad d < L,$$

where υ_1 is the volume occupied by one silane/polymer molecule and χ is the Flory-Huggins interaction parameter.

The volume fraction that a surface modifier occupies on a particle surface and the Flory-Huggins interaction parameter are both qualitative and therefore add some uncertainty to the calculation.

The volume fraction is often estimated by determining the organic content on a nanoparticle surface using thermogravimetric analysis (Worthen et al., 2016), where a sample is heated to a high temperature (~900 °C) under an inert atmosphere (typically N_2) and the weight that is lost is attributed to the particle surface modifier and called the 'organic' content of a particle. Calculating the coverage of a modifier on a particle

surface is done assuming that only a monolayer of 'organic' material deposits on the particle surface.

According to Metin (2012) and Worthen et al. (2016), the Flory-Huggins interaction parameter indicates how compatible the surface modifier is to a particular solvent, where for my work, solvent refers to a solution of brine water with varying ionic strengths. It is assumed that if the surface modifier is compatible with a particular solvent, then a Flory-Huggins parameter < 0.5 is acceptable (Metin, 2012). Aqueous stability tests can be done to verify this compatibility between surface modifier and solvent. Worthen et al. (2016) further suggests that the Flory-Huggins parameter ranges from 0.1 (very good), 0.25 (intermediate), and 0.45 (poor). For my calculation to compare the stability of a 6 nm silica particle (with and without surface modification) in 100 mM monovalent salt solution, we assume very good compatibility between our solvent glymo surface modifier (χ = 0.1).

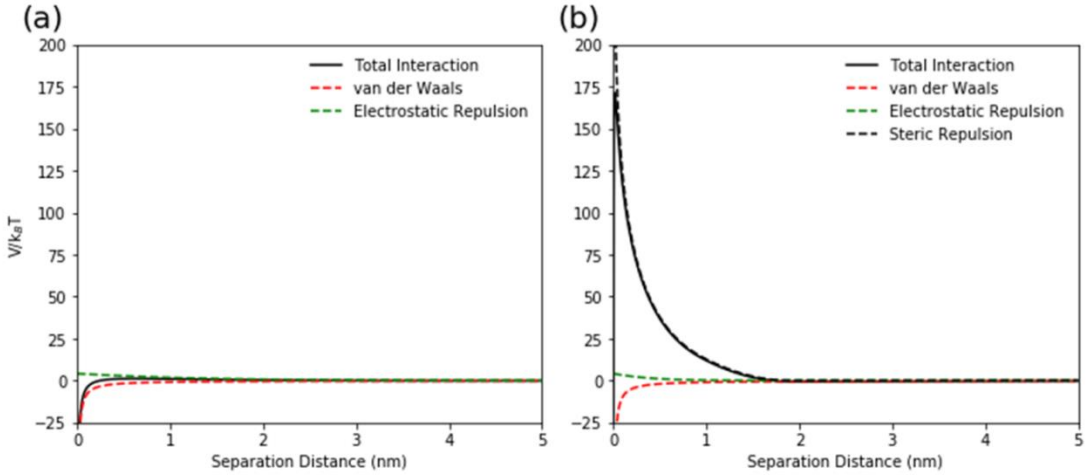

Figure 2.22 – DLVO calculations for 6 nm silica nanoparticles in a monovalent salt solution with an ionic strength of I = 100 mM (a) bare silica particle and (b) glymo surface modified silica particle. Black is the total interaction potential between two 6 nm particles. The red dashed line is the van der Waals interaction. The green dashed line is the electrostatic repulsion component. The black dashed line is the steric contribution from nanoparticle surface modification.

Figure 2.22(a,b) show the interaction potentials for 6 nm bare and glymo modified silica nanoparticles in a monovalent salt solutions with an ionic strength of 100 mM as a function of separation distance between the particles. The bare silica particles have a maximum interaction potential of ~ 0/ k_BT, which indicates the particles are unstable and will eventually agglomerate in this idealized 100 mM brine solution. Not surprisingly, the modified DLVO calculations suggest that the glymo surface modification increases the maximum total interaction potential to ~ 175/ k_BT. This implies there is a sufficiently large energy barrier that prevents particles from coming into close contact with one another and agglomerating. These plots also show that these DLVO calculations are sufficiently accurate at predicting the dispersion stability of bare and surface modified particles.

Given that there is a very large body of literature on how colloidal silica modified with surfactants or hydrophobic silanes, with varying extents of surface modification affect the stability, drop size, and rheology of Pickering emulsions, there is much less work dedicated to understanding how hydrophilic silanes impact the properties of Pickering emulsions.

Because of this, there is a need to study how hydrophilically modified particles and physicochemical conditions impact various properties of the Pickering emulsions – if any.

2.11 SOME PRACTICAL IMPLICATIONS OF THIS WORK

Some parallels can be drawn between my work on Pickering emulsions and previous work on polymer and micellar flooding for EOR, which can help highlight the practical importance of the work presented here.

2.11.1 Emulsion stability using centrifugation and the polymer filtration ratio:

Hydrolyzed polyacrylamide (HPAM) is a polymer commonly used for EOR (Seright, 1983; Putz et al., 1994). When dispersed in an aqueous solution, it increases the viscosity of the injected fluid and lowers its mobility. This leads to better overall displacement sweep efficiency (Huh and Pope, 2008) and oil recovery (Koh et al., 2016). The general idea of using an HPAM polymer solution is to tune the rheological properties of the solution so that it has the appropriate mobility ratio to a particular oil (Taber et al., 1997). This is done by selecting the correct polymer concentration (Gao, 2013), its molecular weight (Qi et al., 2017), and degree of hydrolysis (Levitt and Pope, 2008).

Once the HPAM parameters have been selected, polymer pre-screening tests are done to predict the stability of a polymer solution before it is tested in a core. This is done by measuring the filtration ratio of the polymer using a 1.2 μm Millipore cellulose filter under a 15 psi argon blanket (Levitt and Pope, 2008). The filtration ratio is defined by equation (2.11)

$$Filtration\ ratio = FR = \frac{(t_{200\ mL} - t_{180\ mL})}{(t_{80\ mL} - t_{60\ mL})} \tag{2.11}$$

where t is the time it takes for the specified volume of fluid has passed through the filter. The filtration ratio is a powerful pre-screening tool because it ensures a polymer solution is properly hydrated (Lee et al., 2009) and gives some indication as to whether it successfully be transported through a porous core (Driver, 2018). As a general rule of thumb, filtration ratios that are less than or equal to 1.5 are desired (Espinosa et al., 2018) and if they are higher, it is unlikely the polymer formulation will be successful as it will plug pore throats within a core (Driver, 2018).

The polymer filtration ratio is highlighted because it is a pre-screening tool that helps experimentalist's select optimal polymer formulations *prior* to running a core flood. This must be emphasized because, to the best of my knowledge, there is no such pre-

screening method that has been proposed for assessing the stability of different Pickering emulsion formulations. This is important because there are such a wide range of tunable parameters for stabilizing Pickering emulsions. These include the nanoparticle core material, its size, the surface modifications (disclosed or undisclosed), and the physicochemical conditions of the formulation.

Therefore, it is necessary to have a tool that can successfully distinguish differences in the relative stability of these different emulsion formulations. By determining differences in the relative stability of emulsions, only the best formulations can then be tested in time consuming core floods.

One of my contributions to Pickering emulsion science is that I have successfully shown that the demulsification pressure of an emulsion can be used to compare the relative stability of different Pickering emulsion formulations. Additionally, I also show that it can be used to predict the dynamic stability of a Pickering emulsion as it flows through a glass capillary tube.

2.11.2 Tuning the viscosity of Pickering emulsions and microemulsion rheology

During EOR micellar flooding, emulsions are formed in-situ when a surfactant formulation comes into contact with a reservoir oil. Great care is taken to ensure these emulsions have the appropriate rheological properties to maximize oil recovery, i.e., prevent the formation of liquid crystals, no macro-emulsions, and no gels (Walker et al., 2012; Fortenberry et al., 2015; Tagavifar et al., 2018). This is accomplished by tailoring the micellar solutions so that they include some (or all) of the following chemicals: branched surfactants, twin-tailed surfactants, mixtures of dissimilar surfactants, and one or more co-solvents (Walker et al., 2012).

Given the amount of research dedicated to controlling the rheological properties of microemulsions, there should be an equal amount of effort on understanding the parameters that control the rheological properties of Pickering emulsions.

It is well-known that salts can induce interparticle attractions between excess particles in a Pickering emulsion, which will result in particle bridging and an emulsion with a yield stress. Somewhat surprisingly, very little attention has been given to minimizing these interparticle attractions using appropriately selected nanoparticle surface modifiers and how these interactions can be tuned to control the rheological properties of a Pickering emulsion (or foam).

Interparticle interactions can be tuned by first selecting an appropriate surface modifier followed by modifying the surface of a silica nanoparticle with varying degrees of surface silanization, which is exactly what we have done in this work. For a very general comparison, most Pickering emulsions stabilized with nanoparticles (for subsurface applications) completely neglect the structure of the surface modifier (Gabel, 2014; Xue et al., 2016; Kim et al., 2016; San et al., 2017), the extent of surface modification (Roberts, 2011; Spisak, 2011; Hariz, 2012; Gabel, 2014; Ahmad, 2015; Xue et al., 2016; San et al., 2017) and the rheological properties of the Pickering emulsion (or foam) (Kim et al., 2016).

In the work I present here, I show, through a detailed rheological characterization, that the extent of surface modification of a silica particle, using a well-defined silane, play an important role in the rheological properties of a Pickering emulsion. This is significant because this work highlights another design parameter that can be leveraged to control the rheological behavior of a Pickering emulsion.

2.11.3 Destabilizing Pickering emulsions

A large portion of the research on Pickering emulsions focuses on modifying colloidal particles and making stable Pickering emulsion. This is typically followed by characterizing the properties of the emulsion, like the drops size and rheological properties. In general, there is much less effort dedicated to understanding how to destabilize Pickering emulsions. This is particularly important because many of the common methods used to destabilize surfactant stabilized emulsions (adding salt to alter the HLB and heating to enhance destabilization) are generally not applicable to destabilizing a properly formulated Pickering emulsions. Because of this, there is a gap in the literature on methods capable of destabilizing Pickering emulsions.

In this dissertation, I used fumed silica particles with different wettabilities and studied the relationship between particle wettability and for their ability to macroscopically induce emulsion coalescence. This was done by simply adding varying mass fractions of fumed silica particles to an emulsion and stirring on a conventional laboratory stir plate for just 20 minutes. For my destabilization experiments, special care was taken to formulate a Pickering emulsion that was not susceptible to coalescence by my selected stirring method.

The end result of the work was that I found there was a strong relationship between the wettability of added fumed silica and its ability to destabilize my model Pickering emulsion. My results showed that fumed silica particles that were hydrophilic were unable to destabilize the model Pickering emulsion. This was because the hydrophilic particles were immediately wetted by the continuous phase of the emulsion, forming a water film around the particle surface which prevented interaction between emulsified oil drops and the silica particle surface. However, hydrophobic fumed silica particles showed a remarkable ability to destabilize my model Pickering emulsion. This

was because the emulsified oil drops preferred to wet the particle surface instead of remaining as emulsified drops. This behavior was driven by the hydrophobic nature of the silica particle surface.

2.11.4 Water-in-water emulsions

One of the main criticisms of macroemulsions for EOR is that you have to inject oil into a reservoir to get oil out, which many would argue does not make economic sense. This concern is legitimate. However, Kaminsky et al. (2010) suggested that overall recovery should be higher when using macroemulsion based EOR, but the tradeoff is that production rates will be lower because oil needs to be re-injected into a formation (in the form of an emulsion). However, they also suggest that under the right economic conditions using macroemulsion based EOR could be justified because it is considered to be more environmentally friendly than say, thermal EOR for heavy oils.

Water-in-water emulsions appear to be a potential alternative to traditional oil/water macroemulsion based EOR because they do not contain any oil, but instead, consist of two aqueous phases. Another potential application for water-in-water emulsions is for their use in encapsulating materials of interest (i.e., acids) so that they can be delivered to locations within a reservoir without having to use highly hydrophobic silica particles (Singh et al., 2017; Panthi et al., 2017). This could be an advantage because very hydrophobic particles need to be dispersed within an oily carrier fluid whereas with these water-in-water this could be avoided.

Water-in-water emulsions form when the interface of an aqueous, two phase system (ATPS) is stabilized. These two phase systems originate when two incompatible solutes are added to a solution above some minimum concentration (Song et al., 2013; Ganley et al., 2017) and above this concentration, the free energy of mixing is positive

(Frith, 2010). When this condition is met, the two solutes cannot physically coexist in solution with one another, which leads to their separation, and the formation of two discrete aqueous phases, each enriched in one of the solutes.

Stabilizing the interface of an ATPS is typically very difficult and can only be done with nanoparticles or very large block chain copolymers (Buzza et al., 2013). However, if the correct interfacial stabilizer is selected, these emulsions could potentially accomplish many of the same tasks as a more traditional oil/water Pickering emulsion. Furthermore, their use for subsurface applications has not been studied in any great detail. In fact, there was only one reference that proposed using an ATPS for a subsurface application, which was for conformance control (Sullivan et al., 2010).

In this patent (Sullivan et al., 2010), the authors proposed using an ATPS made from two incompatible polymers as a conformance control technology. Their ATPS system consisted of emulsified guar polymer dispersed into a continuous phase of hydroxypropyl cellulose (HPC) polymer. The general idea for this invention was to disperse a highly viscous polymer into a much less viscous continuous phase so as to improve the injectivity of the emulsion and because of the thermodynamic properties of the guar polymer/dhyroxypropyl ceullulose ATPS, temperature induced phase inversion occurred at a temperature of 45 °C – 50 °C. Therefore, as the emulsion is heated by the geothermal gradient, it will eventually invert into a highly viscous hydroxypropyl cellulose polymer-in-guar polymer emulsion, which could act as a conformance control fluid. This is because guar polymer solution has such a high viscosity.

My work on water-in-water emulsions was much more fundamental as I was concerned with understanding the relationship between nanoparticle size and its impact on the dynamic stability of a water-in-water Pickering emulsion while it was sheared. I carefully selected a model ATPS that had a low, but not too low interfacial tension, and

varied the particle attachment energy by using different sized nanoparticles to stabilize the water/water interface.

The results from this work are relevant because I have shown that a simple water-in-water emulsion can be stabilized using appropriately modified silica nanoparticles. I also show that these emulsions have relatively good stability to shear, which implies there could be some use for these emulsion as a novel EOR technology.

Chapter 3: A comparison of the static and dynamic stability of Pickering emulsions

3.1 INTRODUCTION

One advantage of using particles, as opposed to surfactants, to stabilize emulsions (Pickering emulsions) is that particles are thought to be irreversibly adsorbed to the oil/water interface (Binks, 2002). Theoretical calculations suggest that the attachment energy of these particles is many orders of magnitude greater than kT (Aveyard and Binks, 2003), which means that if there is a dense monolayer of particles are on an emulsion drop surface, the emulsion should not destabilize over long periods of time or coalesce due to thermal fluctuations.

This unique advantage of Pickering emulsions relative to surfactant stabilized emulsions is one of their desirable attributes for subsurface applications (Arab et al., 2018), where an emulsion that originates on the surface will experience a wide range of temperature fluctuations that could potentially destabilize a surfactant stabilized emulsion (Kundu et al., 2013; Abedi et al., 2019), but presumably not a Pickering emulsion. Pickering emulsions have been proposed as conformance (Pandey et al., 2018a; Daigle and Griffith, 2018) or mobility control (Kim et al., 2017) technologies to improve the recovery of oil from oil and gas reservoirs.

Based on our literature review, the term "stable" is frequently used to describe the macroscopic behavior of Pickering emulsions and, in many cases, it simply refers to the lack of macroscopic coalescence with little to no change in emulsion drop size with respect to time, under static conditions. However, because there are so many particle emulsifiers that meet this definition of stability (Destribats et al., 2014; Dong et al., 2014; Derakhshandeh et al., 2018; Briggs et al., 2018; Pandey et al., 2018b; Edgehouse et al., 2019; Xu et al., 2019), it can be difficult to distinguish differences in their stability

without some additional characterization beyond static monitoring. The criteria of long-term static stability are even possibly met when very low particle concentrations are used to stabilize emulsions (Horosov and Binks, 2006; Saha et al., 2013; Kim et al., 2016).

This definition of stability is particularly problematic for designing Pickering emulsions for subsurface applications, where an emulsion needs to be both statically and dynamically stable for long periods of time. Moreover, coreflood experiments are commonly used as a pre-screening testing method for enhanced oil recovery treatments, where fluids (or emulsions) are injected into small rock cores, which represent an experimental analog for fluid flow in a reservoir. However, in many cases, cores can only be used one time, which makes it difficult to run a large number of repeatable experiments to systematically test the impact of select parameters on the stability of a Pickering emulsion while flowing within a porous material. Further complicating this is the fact that core flood experiments can be time consuming and typically require large volumes of fluids which makes it difficult to screen new materials. Therefore, it is highly desirable to have some screening parameter that is at least semi-quantitative in nature that can reduce the number of coreflood experiments that are required to test a Pickering emulsion formulation. This is the motivation of the present work.

Characterizing the stability of Pickering emulsions by centrifugation (forced coalescence) is, surprisingly, only sparingly found in the literature (Binks and Lumsdon, 2000; Gautier et al., 2007; Lan et al., 2007; Frelichowska et al., 2010; Saha et al., 2013; Varanasi et al., 2018). This is in spite of its ease of use and its ability to directly quantify the stability of different Pickering emulsion formulations. Recently, Varanasi et al. (2018) used centrifugation to systematically study how salt, pH, and cellulose nanocrystal (CNC) concentration impacted the stability of their 20 vol% canola oil (or hexadecane)-in-water Pickering emulsions. By using a centrifuge, they were able to directly probe and

quantify differences in the stability of their emulsions. They showed that an emulsion prepared with 1 wt% CNC with 50 mM NaCl was 3 times more stable than the same formulation in the absence of salt. In their work, they typically centrifuged emulsions at 4,000 x g for 10 minutes to assess their stability.

Similarly, Saha et al. (2013) used a centrifuge to characterize the stability of their octane-in-water emulsions stabilized with para-amino benzoic acid-modified carbon black (CB) particles. One of their goals was to correlate the stability of their emulsions to the zeta potential of their particles by altering the dispersion pH with the addition of acid (1 N HCl) or by adding salt (NaCl) to their nanoparticle dispersions. Their experimental results showed that emulsions stabilized with lower zeta potentials, by addition of salt, were more stable than those modified with acid. Their explanation was that salt-modified particles were more hydrophilic than those modified by acid, which allowed for some of the particles to remain in the continuous phase of the emulsion, as opposed to the oil/water interface, and form particle bridges. The particle bridges helped minimize droplet coalescence. One important outcome from their work was that they used the demulsification pressure to characterize the stability of their different emulsions, where the demulsification pressure is calculated by using equation (2.1):

$$P_{demulsification} = \frac{\Delta\rho g_k (V_{oil} - V_{released})}{A}, \tag{3.1}$$

where $\Delta\rho$ is the density difference between oil and aqueous phase, g_k is the gravitation acceleration of the centrifuge, V_{oil} is the total volume of oil in the emulsion, $V_{released}$ is the volume of oil released after centrifugation, and A is the cross sectional area of the centrifuge tube.

Saha et al. (2013) demonstrated that their 0.015 wt% CB emulsion stabilized in the presence of salt (0.6 M NaCl) had a demulsification pressure of 4.6 kPa whereas the same emulsion without salt (but at pH 3.3) had a demulsification pressure of 2.2 kPa. Using the demulsification pressure as a parameter to characterize the stability of different Pickering emulsion formulations is much more rigorous than benchtop static stability tests, which is typically used to assess Pickering emulsion stability.

The demulsification pressure also appears to be a potentially useful metric for correlating the static stability of a Pickering emulsion to its flowing stability in porous media. This is because the process of centrifugation, qualitatively, simulates what happens to an emulsion as it flows within a reservoir. As an emulsion flows in an oil reservoir, at some point an emulsion drop will be retained at a pore throat that is physically smaller than the emulsion drop. When this happens, the emulsion will accumulate at the restriction and the drops will compress against one another (e.g., Xu et al., 2017a), similar to how emulsion drops compress against one another during centrifugation. If the emulsion drops are inadequately populated with nanoparticles, the drops will begin to coalesce and the emulsion will lose its properties and be unable to accomplish its intended application. Therefore, there should be some correlation between the demulsification pressure of a Pickering emulsion and its flowing stability.

Herein we stabilized decane-in-water Pickering emulsions using 6 nm silica particles modified with low and high concentrations of (3-glycidyloxypropyl)trimethoxysilane (glymo). We characterized the static properties of the different emulsions as a function surface functionalization and nanoparticle concentration. We characterized the following emulsion properties: emulsion drop size with respect to time, emulsion creaming behavior, and the emulsion demulsification pressure. Next, we flowed different emulsions through a 0.75 mm ID glass capillary tube.

We monitored the change in emulsion drop size at different flow rates. We then correlated the demulsification pressures of our emulsions to the dynamic behavior of the emulsions. We did this to establish a critical demulsification pressure that could predict the flowing stability of a Pickering emulsion. Lastly, we showed that we could increase the demulsification pressure of a 2.8 wt% HSC glymo-stabilized emulsion from 10.2 kPa (when prepared with DI Water) to 18.6 kPa by including calcium chloride in the formulation (10 wt%). The increased demulsification pressure led to a dynamically stable emulsion, which was predicted to occur given the results from our previous capillary tube experiments.

3.2 MATERIALS AND METHODS

3.2.1 Materials

NexSil 6 nanoparticles (6 nm silica particles) were purchased from Nyacol Technologies. The stock solution contained 17.1 wt% nanoparticles at a pH of approximately 10. The particles have a specific surface area of 445 m^2/g (provided by the manufacturer). (3-glycidyloxypropyl)trimethoxysilane (>98%) (glymo) was purchased from Sigma-Aldrich. n-decane was purchased from MP Biomedical (>99%). 1 N hydrochloric acid was purchased from Fisher Scientific. Deionized (DI) water was generated from a Barnstead E-Pure Ultrapure water Purification System. All chemicals were used as received.

3.2.2 Methods

3.2.2.1 Nanoparticle functionalization

Silica nanoparticles were modified with glymo using the same procedure outlined in our previous work (Griffith and Daigle, 2018). We added glymo into reaction mixtures at

concentrations of 1.85 or 4.00 μmol/m² of nanoparticle surface area to make low (LSC) and high surface coverage (HSC) modified nanoparticles, respectively. Prior to adding glymo to the nanoparticle dispersion, the glymo epoxide was opened with an acid-catalyzed ring opening reaction. This was done by reacting glymo for several minutes in DI water that had an adjusted pH of 2 (using 1N HCl). The ring-opened glymo was then added to the nanoparticle dispersion and heated overnight at 60°C to complete the hydrolysis condensation reaction. In some cases, a small amount methanol was used to prevent the self-condensation of glymo oligomers which eventually precipitate out of solution. The methanol was removed from the final reaction mixture by evaporation. The final concentration of nanoparticles in the mixture was approximately 10 wt% and the final pH of the reaction mixture was 10-10.1. Batches with 20 g of nanoparticles were surface modified. The particles were used without purification.

3.2.2.2 Dynamic light scattering and zeta potential

A Malvern Zetasizer Nano ZS was used to measure the hydrodynamic diameter and zeta potential of the LSC and HSC glymo functionalized nanoparticles. Samples were prepared with 1 wt% nanoparticles in the aqueous phase.

3.2.2.3 Interfacial tension measurements

The pendant drop method was used to determine the interfacial tension (IFT) between the different LSC and HSC nanoparticle dispersions and decane. A droplet of nanoparticle dispersion was suspended for 1 minute in a quartz container filled with decane to equilibrate the two phases. After this, 3 successive measurements were taken each lasting 30 s. We report the average of these three measurements, with error bars representing the range of the three measurements.

3.2.2.4 Emulsion preparation

Emulsions were prepared in 40 mL batches using a 30 W Branson Digital Tip Sonifier with a 5 mm microtip. In a typical emulsion procedure, 20 mL of n-decane and 20 mL of nanoparticle dispersion were added to a 50 mL centrifuge vial and sonicated for 10 s. The emulsion was gently shaken, followed by repeating this process two more times so that all of the oil was emulsified.

3.2.2.5 Emulsion centrifugation

Each of our emulsions was centrifuged to assess their stability to coalescence. All of the centrifugation experiments were performed within one hour of the emulsion being generated. Initial pre-screening of the different emulsions was performed to determine an appropriate gravitational acceleration to run the tests. We performed all of our centrifugation experiments with a gravitational acceleration of 5000 x g and tested each emulsion two times. Following the work of Saha et al. (2013) we centrifuged our emulsions for 15 minutes. Upon completing the centrifugation experiments, we used a volumetric pipette to remove the coalesced oil from the emulsions so that we could calculate demulsification pressures.

3.2.2.6 Flowing experiments

A 250 μL Hamilton Gastight syringe (Part# 81120) was placed on a Chemyx Fusion 200 series two channel syringe pump (Model # 720). A female luer microlectric adapter (1.0 mm OD) (Word Precision Instruments, Item# MPH6S10) was connected to the Gastight syringe. A 0.75 mm ID (1.0 mm OD, L = 152.4 mm) borosilicate glass capillary tube (World Precision Instrument, Item# TW100-6) was connected to the microelectric adapter – see Figure B4. Emulsion effluent was collected from the glass capillary tube and analyzed using light microscopy.

3.2.2.7 Light microscopy

A Nikon Labophot-Pol microscope with a Nikon Digital Sight DS-Fil camera was used to obtain optical micrographs for drop size analysis. For static drop analysis, 50-100 µL of emulsion was diluted with 1 mL of DI water. The diluted emulsion was placed on a glass microscope slide and covered with a glass cover slip. We analyzed 150-300 emulsion drops for each sample. ImageJ was used to determine the pixel area of each emulsion drop. The Sauter mean diameter (D[3,2]) for each emulsion was then calculated, using equation (3.2). We report the standard deviation in our measurements as error bars in the plots.

$$\mathrm{D}[3,2] = \frac{\sum_i^n D_i^3}{\sum_i^n D_i^2} \; [=] \; \mu m, \tag{3.2}$$

3.3 RESULTS AND DISCUSSION

3.3.1 Emulsion drop size and creaming behavior for low (LSC) and high surface coverage (HSC) glymo-stabilized emulsions

We previously determined that bare NexSil 6 particles are unable to stabilize oil-in-water emulsions. This is because the surfaces of bare silica particles are occupied with silanol groups, which are known to be too hydrophilic to attach to the oil/water interface and stabilize an emulsion. Therefore, to stabilize a Pickering emulsion, some sort of surface modification is required. We modified our particles by covalent attachment of glymo silane through siloxane bonds. We selected glymo as a nanoparticle surface modifier because of its ability to prevent nanoparticle agglomeration in the presence of 12.5 wt% NaCl brine (Greenwood and Gevert, 2011) and at an elevated temperature of 80 ^{o}C (Worthen et al., 2016; Jang et al., 2018), which are desirable attributes for subsurface applications. In our previous work, we determined that low (1.85 µmol

silane/m^2) and high (4.0 µmol silane/m^2) glymo concentrations were sufficient enough to stabilize bromohexadecane-in-water emulsions (Griffith and Daigle, 2018), so we use those same concentrations here.

The size and zeta potential of the LSC and HSC glymo functionalized particles were measured using a Malvern Zetasizer Nano ZS. The LSC glymo-coated particles had volume average hydrodynamic diameter of 8.1 ± 0.2 nm and a surface zeta potential of -38 ± 1.3 mV, whereas the HSC glymo-coated particles had a volume average hydrodynamic diameter of 9.3 ± 0.1 nm and a surface zeta potential of -29 ± 2.3 mV. These results are what we would expect given that increased concentrations of glymo are expected to reduce the number of free silanol groups and decrease the surface zeta potential particles of HSC glymo-modified silica nanoparticles compared to the LSC glymo-modified particles.

Decane-in-water Pickering emulsions were prepared with LSC and HSC glymo coated nanoparticles. The concentration of nanoparticles (C_p) in our formulations ranged from 0.34 wt% – 6.9 wt% and our analysis started by comparing the drop sizes of the different emulsions.

Figure 3.1A-F show select optical micrographs for these Pickering emulsions (see Figure B5 and B6 for all micrographs). The micrographs show that the emulsion drops are relatively monodisperse, aside from the 0.34 wt% LSC glymo-stabilized emulsion, which shows a range of small, medium, and large emulsion drops.

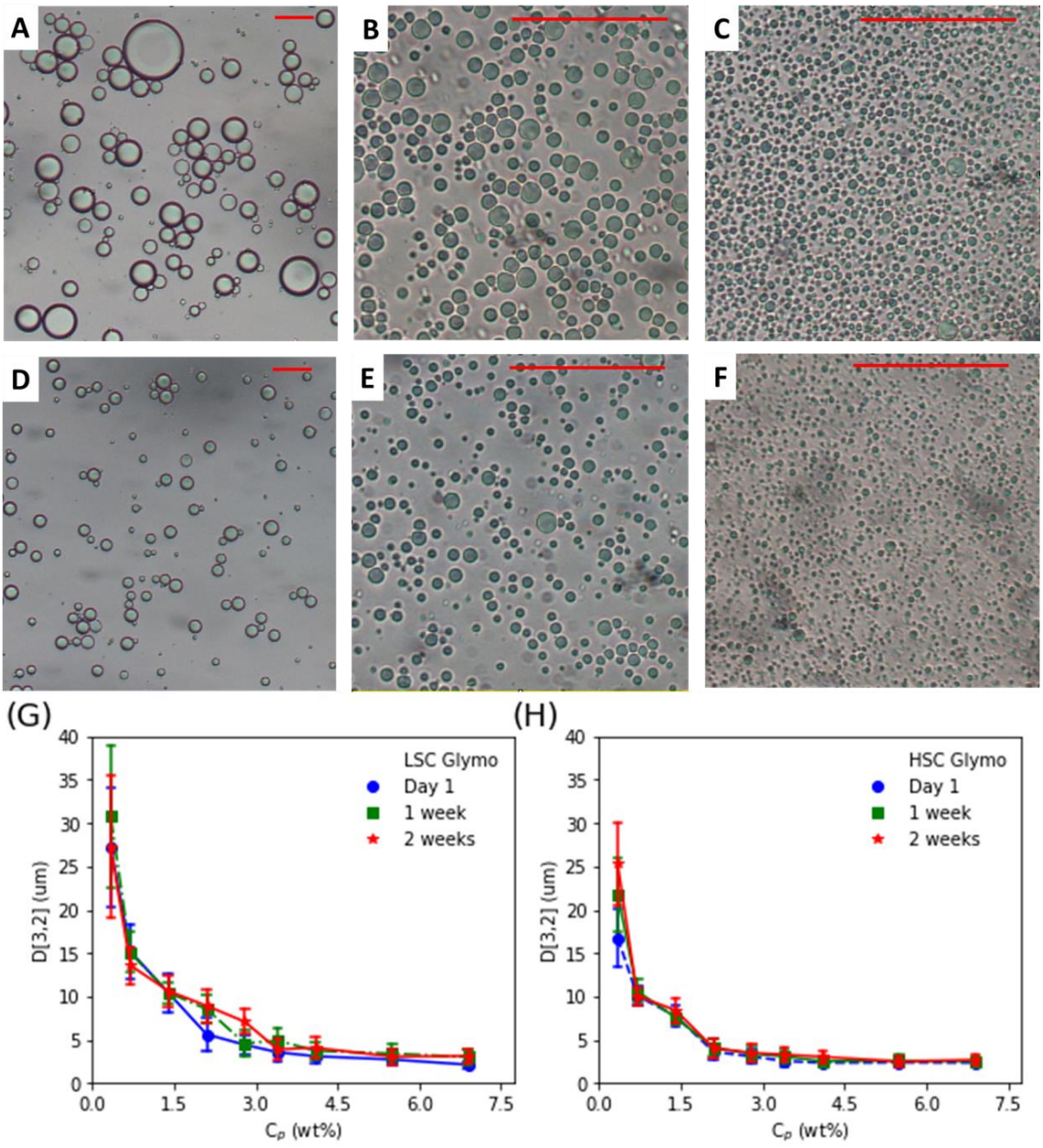

Figure 3.1 – Optical micrographs of emulsions stabilized with 0.34 wt%, 2.8 wt%, and 6.9 wt% LSC (A-C) and HSC (D-F) glymo-stabilized emulsions. Scale bar represents 50 µm. (G) Sauter mean diameter (D[3,2]) versus nanoparticle concentration for LSC particle stabilized emulsions and (H) HSC particle stabilized emulsions.

Figure 3.1G and H plot the Sauter mean diameters (D[3,2]) for the LSC and HSC Pickering emulsions versus C_p for emulsion drops analyzed: (1) immediately, (2) one week, and (3) two weeks after preparation (Figure B7 and B8). The emulsion drops ranged in size from 2.4 μm (C_p = 6.9 wt% HSC glymo) to 24 μm (C_p = 0.34 wt% LSC glymo). The plots show that the emulsion drop size decreases with increasing nanoparticle concentration (for both LSC and HSC particles), which is consistent with previous work on Pickering emulsions (Aveyard et al., 2003; Chevalier and Bolzinger, 2013).

Direct comparison of D[3,2] values for the LSC and HSC glymo-stabilized emulsions show that when $C_p \leq 5.5$ wt%, the HSC glymo-stabilized emulsions had, on average, smaller D[3,2] (by 20 – 43%) than the LSC glymo-stabilized emulsions. However, at C_p greater than 5.5 wt%, both the LSC and HSC glymo-stabilized emulsions had drop sizes that were similar in size (Figure 3.1C,F).

This difference in emulsion drop size for the LSC and HSC glymo-stabilized emulsions was likely due to several related factors. First, there was a small but detectable difference in the interfacial tension between the various LSC and HSC nanoparticle dispersions and decane. We determined that the HSC glymo coated particles had interfacial tensions that were 4-6% lower than the LSC glymo coated particles (Figure B9). The lower interfacial tension for the HSC particles, at a fixed nanoparticle concentration, could potentially enable for more particles to attach to the decane/water interface allowing for stabilization of smaller emulsion drops.

We also acknowledge that we are using unfiltered nanoparticle dispersions in this work and we had previously determined that the unfiltered HSC glymo particles had an organic fraction of 15.3 wt% whereas the LSC glymo-coated particles had an organic fraction of 10.1 wt% (Griffith and Daigle, 2018). Because of this, it is entirely possible

that the ungrafted silanes could be acting as small particle emulsifiers that help promote the formation of smaller emulsion drops. We did not study this behavior in detail, but we did make several oil/water mixtures with glymo silane that were treated using same reaction procedure as our functionalized particles, but without the nanoparticles in these reactions. We found that glymo silane (alone) was capable of stabilizing decane-in-water emulsions at all concentrations we tested. However, these emulsions were very weak and when glymo was included at concentrations $\leq$ 2.8 wt% equivalent nanoparticle dispersions, the emulsions completely coalesced within 48 hours. At higher glymo concentrations, >2.8 wt%, there was a very small fraction of emulsion that remained after 48 hours of monitoring (Figure B10).

Next, we monitored the creaming velocities for the LSC and HSC glymo-stabilized emulsions, both as a function of nanoparticle concentration. The creaming distance versus time for the different emulsions is plotted in Figure 3.2 (A)-(F). We determined the creaming position by placing 10 mL of emulsion sample into a glass vial and imaging the emulsion every 2 minutes over the course of 24 hours. The results from the creaming velocity experiment are consistent with our drop size analysis, where at all nanoparticle concentrations tested, the HSC glymo-stabilized emulsions had slower creaming velocities than the LSC glymo-stabilized emulsions. This behavior is due to the HSC glymo-stabilized emulsions having smaller drop sizes.

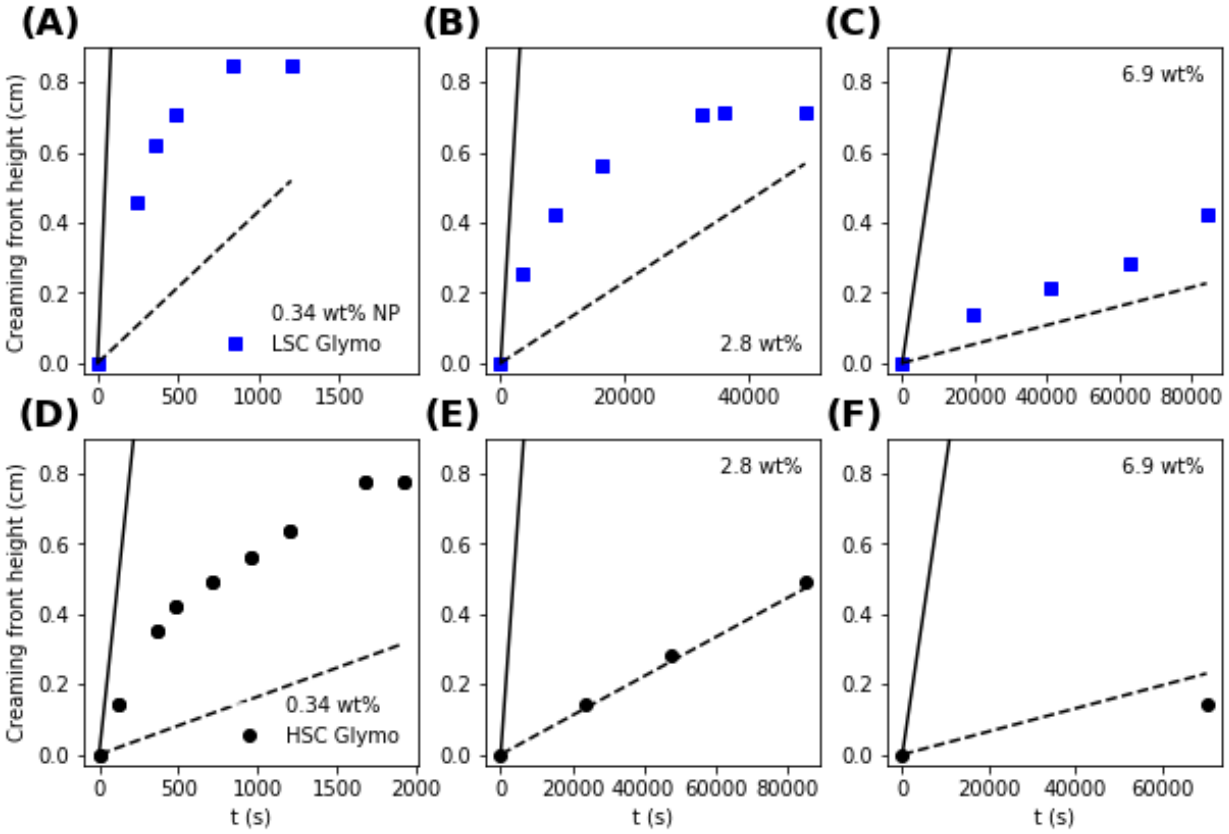

Figure 3.2 – (A) – (C) Creaming front velocities for (A) 0.34 wt%, (B) 2.8 wt%, and (C) 6.9 wt% LSC particle stabilized emulsions (blue, squares). (D) – (E) Creaming front velocities for (D) 0.34 wt%, (E) 2.8 wt%, and (F) 6.9 wt% HSC particle stabilized emulsions (black, circles). The solid, black line is the ideal Stokes law creaming front and the dashed, black line is the modified Richardson-Zaki model.

Our experimental creaming velocities were compared to the ideal Stokes settling velocity (equation (2.3)) and to the modified Richardson-Zaki creaming model (equation (3.4))(Lettieri et al., 2001; Worthen et al., 2014) to gain insight into how these emulsions behave relative to common creaming models. The Stokes settling velocity is calculated using equation (2.3),

$$v_{stokes} = \frac{2\Delta\rho g R^2}{9\eta}, \tag{3.3}$$

where $\Delta\rho$ is the density difference between decane and the aqueous phase, R is the radius of an emulsion drop, g is the gravitational acceleration, and η is the viscosity of the aqueous phase of the emulsion. The Richardson-Zaki model is calculated by modifying the Stokes settling calculated using equation (3.4)

$$v = v_{stokes}(1-\phi)^{4.65}, \quad (3.4)$$

where φ is the dispersed phase volume fraction. This analysis that we have done is similar to Worthen et al. (2014), where the creaming velocities for dodeceane-in-synthetic sea water emulsions were monitored. The Richardson-Zaki model is included in the analysis because it takes into account the nondilute nature of an emulsion by empirically modifying the Stokes settling velocity (Worthen et al., 2014). For our creaming front calculations, we assumed a constant continuous phase viscosity of 1 cP (Figure B11).

Upon inspecting the relationship between our experimental creaming fronts and the Stokes and Richardson-Zaki velocity models, several trends became apparent. First, Figure 3.2A,D show that at low nanoparticle concentration (C_p = 0.34 wt%) the creaming velocities for both the LSC and HSC glymo were very fast relative to the other emulsions. Complete creaming for these emulsions occurred in just 14 (LSC) and 28 (HSC) minutes, and their creaming behavior was bound by both models. The fast creaming of these emulsions is due to their large initial emulsion drop size at C_p = 0.34 wt%.

Figure 3.2B shows that at C_p = 2.8 wt%, the creaming behavior of the LSC glymo-stabilized emulsion was still well described by both theoretical creaming models. However, Figure 3.2E shows that the HSC glymo-stabilized emulsion was no longer

bounded by both models, but instead correlated well with the Richardson-Zaki model. At C_p = 6.9 wt%, the creaming velocity for the LSC particle stabilized emulsion was bounded by both models, in contrast to the the HSC particle stabilized emulsion which now fell below the lower threshold described by the Richardson-Zaki model (Figure 3.2C,F).

Given that the emulsion drops for LSC and HSC glymo-stabilized emulsions are not significantly different in size, this difference in creaming behavior when using emulsions stabilized with HSC glymo coated particles ($C_p \geq 2.8$ wt%) supports our earlier idea that the ungrafted glymo silanes are contributing to the properties of the HSC particle stabilized emulsions. This is because with $C_p \geq 2.8$ wt%, the creaming behavior of the LSC glymo-stabilized emulsions was always bounded by both creaming models (Figure B12). This was not the case for the HSC glymo-stabilized emulsions (Figure B13).

After letting the LSC and HSC emulsion statically rest on the lab bench for one week, all of the emulsions had a resolved water layer beneath the creamed emulsion (Figure B7b,c and Figure B8,b,c). The 0.34 wt% and 0.69 wt% LSC and HSC glymo-stabilized emulsions had a thin film of coalesced oil resting on top of the creamed emulsion layer (Figure B14), indicating that these formulations were not completely stable to coalescence under static conditions.

We also monitored the D[3,2] values for these emulsions. The 0.34 wt% LSC particle stabilized emulsion increased in size by 13%. The 0.34 wt% HSC particle stabilized emulsions increased by 30%. The 0.69 wt% LSC and HSC formulations did not show any significant change in emulsion drop size during this time period. Overall, there was relatively little change in emulsion drop size for the other emulsion formulations during the two weeks we monitored them.

3.3.2 Emulsion stability to forced coalescence

Next, we assessed the stability of our Pickering emulsions to centrifugation at 5,000 g for 15 minutes. Figure 3.3A and B show LSC and HSC glymo-stabilized Pickering emulsions after centrifugation and show that there is a decrease in the amount of coalesced oil with increasing nanoparticle concentration.

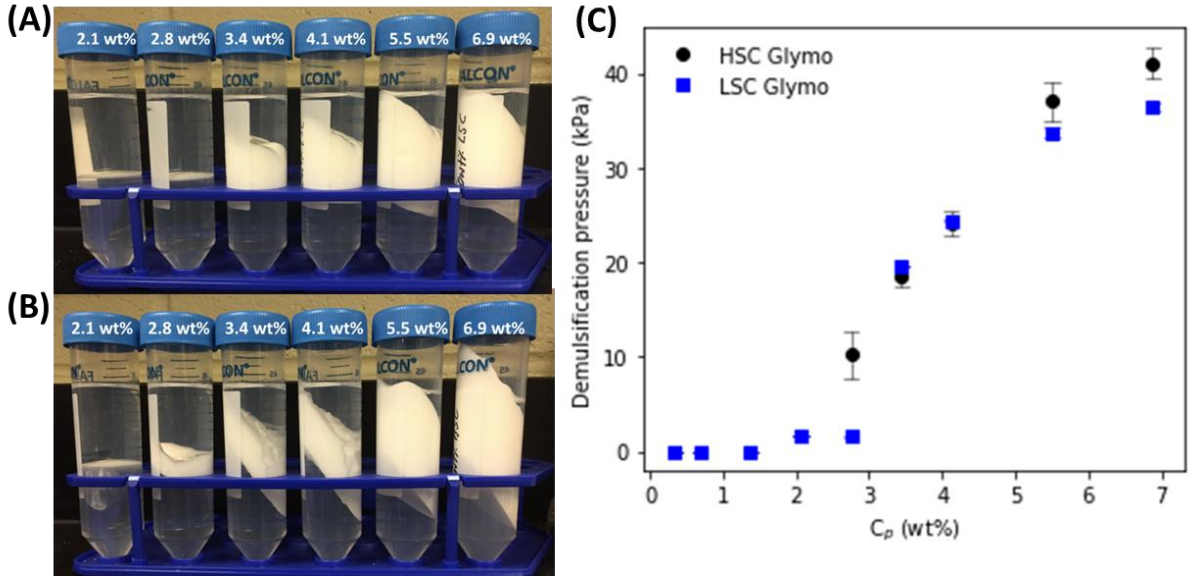

Figure 3.3 – (A) LSC and (B) HSC glymo-stabilized emulsions after centrifugation for 15 minutes at 5,000 g. (C) Calculated demulsification pressures for LSC (blue squares) and HSC (black circles) glymo-stabilized emulsions.

In all of the emulsions, we saw a layer of coalesced oil resting on top of a creamed emulsion layer, which was resting atop a resolved aqueous phase. After centrifugation, the creamed emulsion was found to be in a gelled state, which is attributed to the emulsion having a high oil fraction after centrifugation. The emulsions were also found to be resting at an angle (Frelichowska et al. 2010), which is a due to the angle of the centrifuge rotor.

We calculated the demulsification pressures for our different emulsion formulations by measuring the volume of oil released after centrifugation. Figure 3.3C

plots the demulsification pressure versus nanoparticle concentration for the LSC and HSC glymo-stabilized emulsions. The demulsification pressures that we obtained ranged from 0 kPa ($C_p \leq 1.4$ wt%) to 41.1 kPa ($C_p = 6.88$ wt%). We note that for our emulsions stabilized with low nanoparticle concentrations, they should have a finite, nonzero demulsification pressure. However, because we centrifuged all of our emulsions at 5,000 x g, this acceleration was above their critical demulsification acceleration. Because of this, these weak emulsions completely coalesced and we did not attempt to quantify their stability by centrifugation any further.

Figure 3.3C shows that there is a trend of increasing demulsification pressure with increasing nanoparticle concentration. This trend is valid for both the LSC and HSC glymo-stabilized emulsions. The improved stability at higher initial nanoparticle concentrations is due to the emulsions having better coverage of nanoparticles on their surface. In general, the LSC and HSC glymo-stabilized emulsions had demulsification pressures that were very comparable to one.

For a general comparison, Saha et al. (2013) presented demulsification pressures for octane-in-water Pickering emulsions stabilized with carbon black particles (1:1 by volume) that ranged from 1.4 – 4.6 kPa. Frelischowska et al. (2010) presented limited centrifugation data on their 2-ethylhexyl stearate-in-water emulsions (7% oil, 93% water by weight) that were stabilized with fumed silica particles. They showed that emulsions stabilized with hydrophilic fumed silica (Wacker Chemie, HKSD, 71% SiOH) did not release any oil upon being centrifuged for 30 minutes at 15,557 x g. They also mentioned that emulsions stabilized with hydrophobic H30 particles showed partial coalescence, but they did not report the volume of oil that was released from those experiments.

It is difficult to compare the stability of our emulsions to those in Frelischowska et al. (2010). Although their experiments were performed at significantly higher

gravitational accelerations, using the gravitational acceleration as the only parameter to compare our emulsions to theirs is not accurate because the gravitational acceleration neglects key differences between our experiments: the total volume of emulsion tested, the volume of oil that was emulsified, differences in the density of oils used, and the geometry of the centrifuge vial. All of these differences are taken into account with the demulsification pressure, which makes it a more quantitative metric for comparing the relative strength of different emulsion formulations.

Similarly, Lan et al. (2007) performed centrifugation experiments on paraffin oil-in-water emulsions stabilized with fumed silica particles modified with cetyltrimethylammonium bromide (CTAB). They do show some data that suggest their emulsions were stable to centrifugation (Figure 5a), but it is difficult to directly compare the relative stability of our emulsions to theirs without knowing the total volume of emulsion tested in their experiments and the size and geometry of their centrifuge vials.

An interesting result from Frelischowska et al. (2010), which is worth highlighting, is that they determined there was no correlation between the stability of a Pickering emulsion (when centrifuged) and to its initial emulsion drop size. The key factor in determining the stability of an emulsion is the coverage of nanoparticles on an emulsion drop surface. Their emulsions stabilized with hydrophilic particles (HKSD) had larger initial drop sizes than the emulsions stabilized with hydrophobic particles (H30), but they were more stable to centrifugation because of better coverage of particles on the emulsion drop surface.

3.3.3 Flow of emulsions through a 0.75 mm glass capillary tube – deionized water

In the previous section, we stabilized decane-in-water Pickering emulsions using LSC and HSC glymo modified nanoparticles. We characterized their drop size, creaming

behavior, and stability to coalescence by centrifugation as a function of nanoparticle concentration.

In this section, we attempt to correlate the demulsification pressure of our Pickering emulsions to their stability while flowing (i.e., dynamic stability). We tested the dynamic stability of these emulsions by flowing them through a glass capillary tube (ID = 0.75 mm; L = 152.4 mm).

For our flowing experiments, we varied the volumetric flow rate from q = 50 µL/hr, which is comparable to the rate of fluid flow in oil and gas reservoirs (Xu et al., 2017b; Mejia et al., 2019) to 10,000 µL/hr, which was the upper limit of what our experimental apparatus could handle. At a flow rate of 10,000 µL/hr, all 250 µL of our emulsion was depleted in roughly 90 s.

To ensure that we sampled emulsion effluent at the correct time interval, we calculated the residence time τ for each flow rate using equation (3.5):

$$\tau = \frac{V_{tube}}{q_{emulsion}}, \tag{3.5}$$

where V_{tube} is the total volume of the capillary tube and q is the volumetric flow rate of the emulsion through the capillary tube. Table 3.1 shows the calculated residence times for each of the flow rates tested, which is an indication of the average time an emulsion resides within the capillary tube.

Flow Rate [µL/hr]	τ [s]	τ [min]
50	4850	80.8
500	485	8.1
5,000	49	0.8
10,000	24	0.4

Table 3.1 – Calculated residence times for different volumetric flow rates in a glass capillary tube with ID = 0.75 mm and L = 152.4 mm.

To start our analysis, we focused primarily on characterizing the dynamic behavior of our HSC glymo-stabilized emulsions. We started by flowing our weakest emulsions first, which was our formulation with C_p = 0.34 wt%. This was done so that we could systematically move along our demulsification pressure curve and establish a critical pressure that corresponds to an emulsion formulation that is dynamically stable.

At the start of our first experiment (C_p = 0.34 wt%), it was visually obvious that this emulsion was very weak and unable to flow through the glass capillary tube. Figure 3.4A shows the emulsion in the Hamilton syringe. The emulsion in the figure is slightly opaque with large, coarsened emulsion drops. These qualitative observations are in contrast to Figure 3.4B, which shows a 1.4 wt% HSC glymo-stabilized emulsion that is milky white and free of any large, visible, emulsion drops. This observation of immediate and significant emulsion coarsening while flowing is quite interesting given that the emulsion had not completely coalesced over two weeks of monitoring under static conditions.

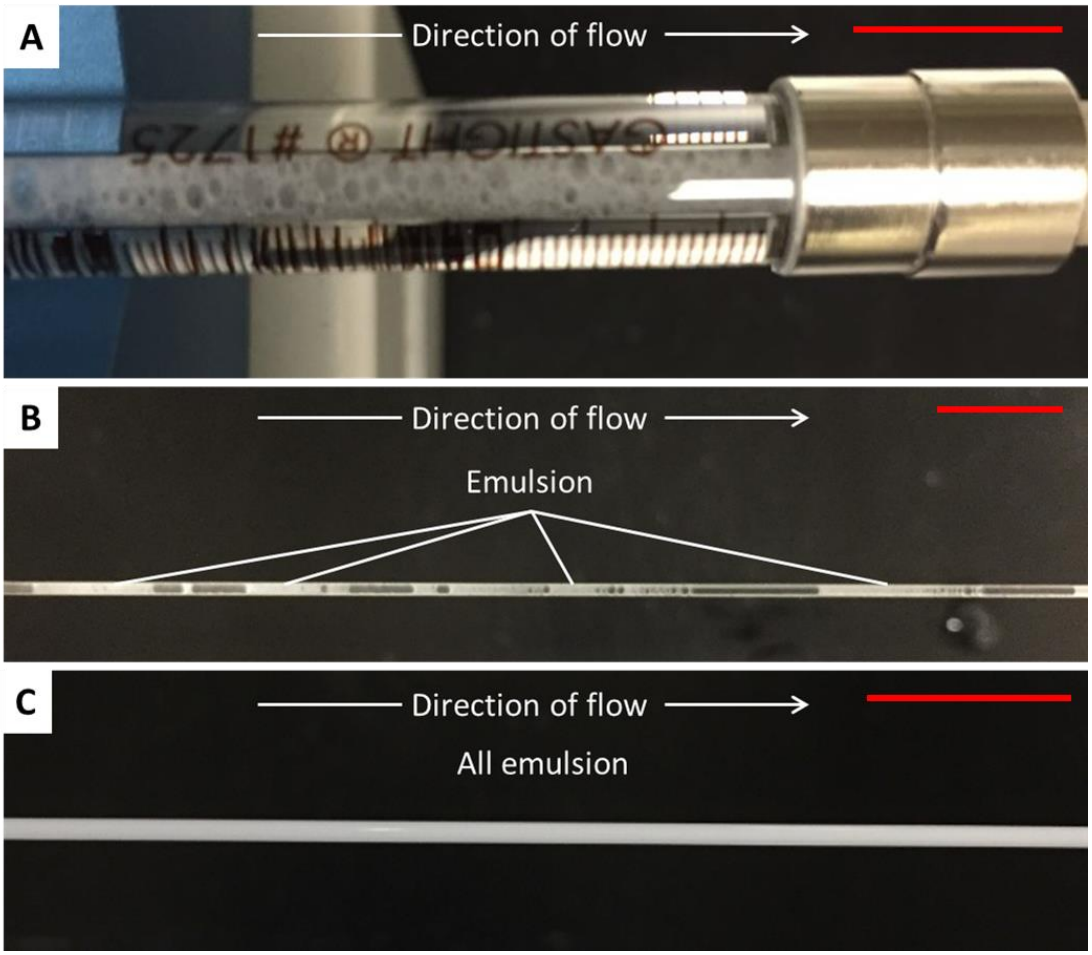

Figure 3.4 – HSC glymo-stabilized emulsions using (A) 0.34 wt% particles in a 250 µL Hamilton gastight syringe, (B) 0.69 wt% HSC glymo particles in a glass capillary tube and, (C) 1.4 wt% HSC glymo particles in a glass capillary tube. The flow direction was from left to right and the flow rate was 50 µL/hr. The red scale bar in all of the images is 10 mm.

The 0.69 wt% HSC glymo-stabilized emulsion behaved very similarly to the 0.34 wt% HSC glymo-stabilized emulsion. The emulsion was unstable while flowing through the capillary tube and Figure 3.4B shows the emulsion in the capillary tube. The image shows the emulsion flowing as a discontinuous mixture of emulsion, coalesced oil, and water.

The lack of dynamic stability for the 0.34 and 0.69 wt% HSC glymo nanoparticles can be explained as follows: first, the concentration of nanoparticles used in these formulations was low and, because of this, the coverage of nanoparticles on the emulsion drop surface was likely also low (see Figure 2 a and b in Griffith and Daigle (2018)). At a flow rate of q = 50 µL/hr, the emulsions are in the capillary tube for 81 minutes. From our creaming experiments, we know that it took 28 and 74 minutes for the 0.34 and 0.69 wt% emulsions to completely cream, respectively. This means the emulsions creamed within the capillary tube while they were flowing. This combination of low nanoparticle coverage on an emulsion drop along surface along with creaming while flowing likely enabled bare portions of emulsion drops to contact one another, which resulted partial coalescence of our emulsion drops while flowing. This lack of stability, at low particle concentrations, is qualitatively in agreement with the results from Schroder et al. (2018), where they suggest increased coalescence events for their colloidal lipid particle (CLP) stabilized emulsions (while flowing) occurred when low concentrations of CLPs adsorbed to the oil/water interface of their emulsions.

As the concentration of particles in our formulations increased, progressively more stable flow patterns were observed, which agreed well with our demulsification pressure data. Figure 3.4C shows a 1.4 wt% HSC glymo-stabilized emulsion in a glass capillary tube. Macroscopically, the emulsion showed no signs of coarsening/coalescence. This was the first instance in which we observed semi-stable flow of emulsion through the glass capillary tube and we were able to assess the stability of the emulsion at different flow rates by inspecting the effluent emulsion drop size.

Figure 3.5A-D plots the normalized D[3,2] versus flow rate for capillary tube experiments with 1.4 wt%, 2.8 wt%, 3.4 wt% HSC glymo-stabilized emulsions and a 3.4 wt% LSC glymo-stabilized emulsion. For these plots, we normalized the effluent D[3,2]

to the static emulsion D[3,2] to aid in data visualization. For a dynamically stable emulsion, there should be little change in emulsion drop size with respect to flow rate and the normalized D[3,2] should be close to unity.

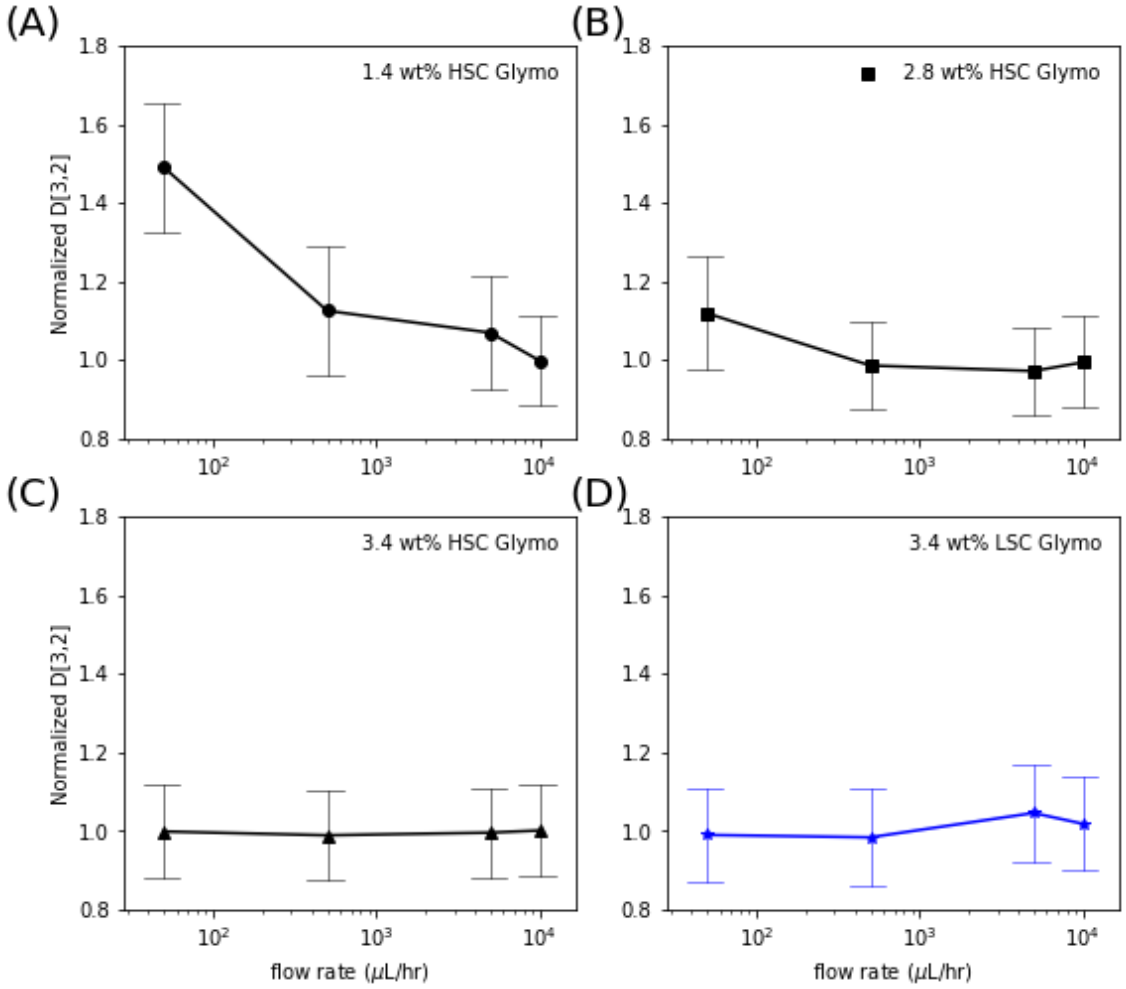

Figure 3.5 – Normalized D[3,2] versus flow rate for (A) 1.4 wt% HSC glymo, (B) 2.8 wt% HSC glymo, (C) 3.4 wt% HSC glymo, and (D) 3.4 wt% LSC glymo.

For the 1.4 wt% HSC glymo-stabilized emulsion (Figure 3.5A), we saw a 50% difference between the static emulsion drop size and the effluent drops when using a flow rate of q = 50 µL/hr. This difference in emulsion drop size is quite large. However, as we increased the flow rate, the difference between the static D[3,2] and effluent D[3,2]

decreased. Our creaming experiments show that complete creaming took about 4 hours. Although this emulsion does not completely cream in the capillary tube, at a flow rate of q = 50 μL/hr, creaming is clearly playing a role in the instability of the emulsion, where it appears this concentration of particles is not sufficiently decorating the emulsion drop surface to suppress coarsening. The consequence of this is that at low flow rates, creaming is playing a dominant role and the result is that we see larger emulsion drops in the effluent. This same behavior was observed with our 2.8 wt% HSC glymo-stabilized emulsions (Figure 3.5B).

For our 3.4 wt% HSC glymo-stabilized emulsions (Figure 3.5C), we observed a constant D[3,2] versus flow rate. This constant emulsion drop size with flow rate indicates this emulsion formulation was both statically and dynamically stable. Because the 3.4 wt% LSC and HSC glymo-stabilized emulsions had the same demulsification pressures (Figure 3.3C), the 3.4 wt% LSC stabilized emulsion should also be dynamically stable. Consistent with the demulsification pressures (for the two formulations), the 3.4 wt% LSC glymo-stabilized emulsion showed little change in emulsion drop size with respect to flow rate, with the largest difference between the static drop size and flowing drop size occurring at a flow rate of q = 5,000 μL/hr, where there was only a 4.6% difference.

In our previous flowing experiments (0.34 wt% - 2.8 wt% HSC glymo-stabilized emulsions), creaming played a dominant role in their lack of dynamic stability. This was because at a flow rate of 50 μL/hr, the residence time was 81 minutes, which was long enough to allow the emulsions to cream within the capillary tube. For the 3.4 wt% LSC and HSC glymo-stabilized emulsions creaming took place on the order of 11 hours, therefore at a flow rate of 50 μL/hr creaming was not a factor. To test the stability of this

emulsion while it was creaming and flowing, we used a flow rate of 5 μL/hr, which had a residence time of ~14 hours.

At a flow rate 5 μL/hr, the 3.4 LSC glymo-stabilized emulsion had an effluent drop size of 3.76 μm. Their static drop size was 3.85 μm. For the HSC glymo-stabilized emulsion, the initial drop size was 2.68 μm and the drop size after completing the experiment was 2.82 μm. The change in drop size for both of these experiments was 2.3 and 5.2%, respectively. These results clearly demonstrate that at this nanoparticle concentration, there is sufficient coverage of nanoparticles on the emulsion drop surface to prevent emulsion drop coarsening, even if creaming is taking place.

3.3.4 Flow of emulsions through a 0.75 mm glass capillary tube – effect of salt on emulsions stability

In the previous section, we focused on the relationship between the demulsification pressure and its ability to predict the flowing stability of our model Pickering emulsions. We determined that if an emulsion had a demulsification pressure of approximately 18.5 kPa, that the emulsion drops would be sufficiently protected by interfacially adsorbed nanoparticles and prevent the emulsion drops from coarsening while flowing. These emulsions would be characterized as dynamically stable, which we define as less than 10% change in emulsion drop size while flowing through a capillary tube.

In this section, we are testing whether the demulsification pressure can predict the stability of an untested emulsion formulation. We are using a formulation with 2.8 wt% HSC glymo particles. This formulation previously failed our tube flow experiment when it was prepared using DI water. Moreover, this formulation also has a relatively high demulsification pressure of 10.2±2.4 kPa. So in theory, we should be able to improve the stability of the emulsion by including salt in the formulation, which was shown to be the

case in the work of Whitby et al. (2011), Saha et al. (2013), and Varanasi et al. (2018). Additionally, the change in stability of the emulsion should be quantifiable using the demulsification pressure.

Figure 3.6A shows the demulsification pressure of a 2.8 wt% HSC glymo-stabilized emulsion versus calcium chloride concentration (wt%). The plot shows that as the concentration of calcium chloride increases, so too does the demulsification pressure. This behavior is expected given that it is well known that salts screen electrostatic charges on colloidal particles (Whitby et al., (2011), which allows for more particles to pack on an emulsion drop surface (Creighton et al., 2016).

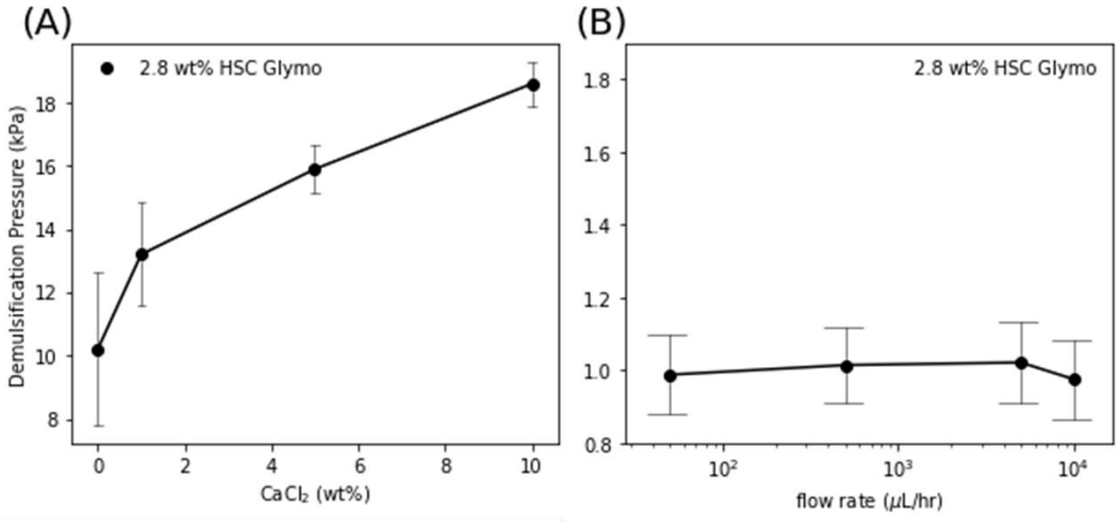

Figure 3.6 – (A) demulsifcation pressure for a 2.8 wt% HSC glymo-stabilized emulsion versus calcium chloride concentration. (B) D[3,2] for a 2.8 wt% HSC glymo-stabilized emulsion with 10 wt% CaCl2 versus flow rate.

For our flowing experiment we selected a formulation with 10 wt% $CaCl_2$ because it had a demulsification pressure of 18.6 ± 0.7 kPa. Recall, our 3.4 wt% HSC glymo-stabilized emulsion prepared with DI water was dynamically stable and had a demulsification pressure of 18.5 ± 1.1 kPa. Therefore, a 2.8 wt% HSC glymo-stabilized

emulsion with 10 wt% $CaCl_2$ should be stable while flowing through the glass capillary tube.

Figure 3.6B plots emulsion drop size versus flow rate for a 2.8 wt% HSC glymo-stabilized emulsion with 10 wt% $CaCl_2$. The plot is consistent with what we have predicted, which is a formulation with a demulsification pressure ~ 18.5 ± 1.1 kPa should be dynamically stable while flowing through a glass capillary tube. This plot shows there is little change in emulsion drop size during these flowing experiments. We see a maximum emulsion drop size change of 2.5%.

3.3.5 Is this testing method general?

In the previous sections, I focused on the properties of emulsions stabilized with glymo-modified silica nanoparticles with varying degrees of surface functionalization. I characterized the static and dynamic stability of these decane-in-water emulsions as a function of nanoparticle concentration (with or without added salt). This was done to establish some basic relationships between the static properties (emulsion drop size, creaming behavior, and demulsification pressure) and the dynamic properties of the different glymo-stabilized emulsions. I successfully showed that there was a relationship between the critical demulsification pressure and the dynamic stability of glymo-stabilized emulsions, which was done by injecting the emulsion into a 0.75 mm glass capillary tube. One problem with this analysis is that it is on a very specific nanoparticle core with a very specific nanoparticle surface modifier, so a natural question to ask is, does this testing method more broadly apply to other oil/water Pickering emulsion systems?

In order to answer this question, I performed the same set of experiments using a different hydrophilic salt tolerant nanoparticle. The particles were provided by 3M

Corporation and were modified with a polyethylene glycol silane (PEG-silane). The exact structure of the silane is unknown. However, PEG-silane modified silica nanoparticles are quite versatile because they have previously shown the ability to stabilize foams (Worthen et al., 2013), o/w emulsions (Zhang et al., 2011), and w/w emulsions (Griffith and Daigle, 2018).

The particles that I used were provided as a 19.7 wt% aqueous dispersion. The particles had a hydrodynamic diameter of 11.4 nm and a surface zeta potential of -28.8 ±1.8 mV. The size and zeta potential of these 3M PEG coated particles are similar to the glymo-modified particles that I synthesized. Figure 3.7(A)-(C) show optical micrographs for 0.34 wt%, 2.8 wt%, and 6.9 wt% 3M PEG stabilized emulsions. Figure 3.7D shows the emulsion drop size (D[3,2]) versus nanoparticle concertation for the 3M PEG decane-in-water emulsions. In general, the emulsion drops for the PEG stabilized emulsions were larger than in size than the emulsion drops for the LSC and HSC glymo-stabilized emulsions. We are unsure of this origin; however, it is worth noting that this difference could be used as a design constraint.

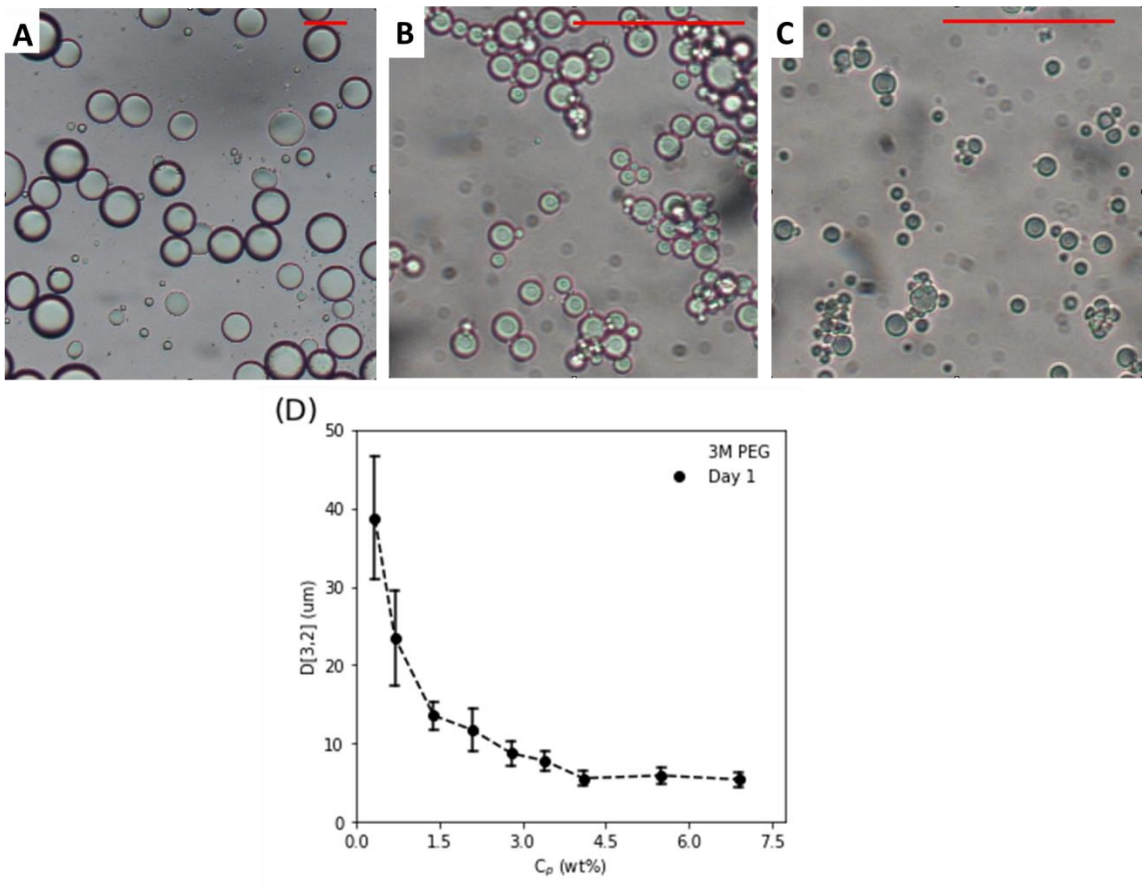

Figure 3.7 – Optical micrographs of emulsions stabilized with 0.34 wt%, 2.8 wt%, and 6.9 wt% 3M PEG nanoparticles (A-C). Scale bar represents 50 µm. (D) Sauter mean diameter (D[3,2]) for decane in water emulsions stabilized with 3M PEG particles versus nanoparticle concentration.

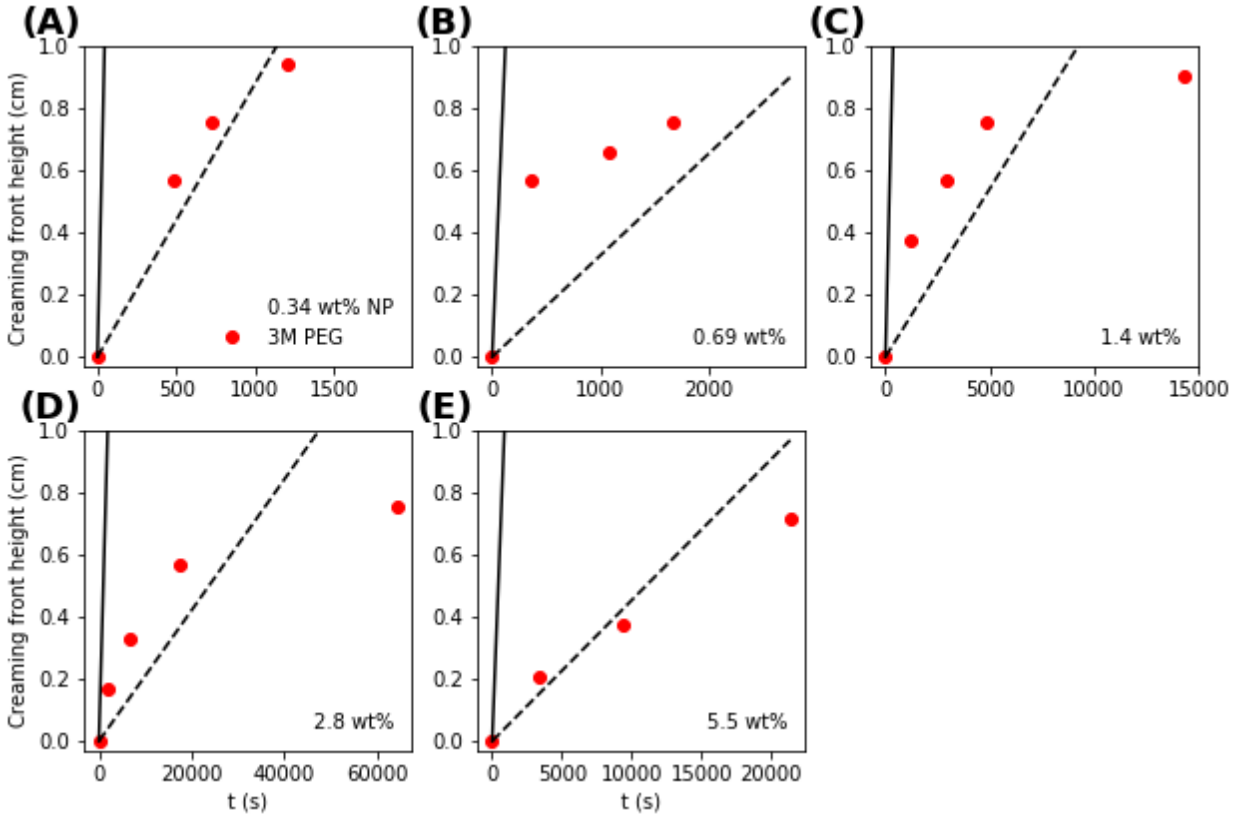

Figure 3.8 – (A) – (E) Creaming front velocities for (A) 0.34 wt%, (B) 0.69 wt%, (C) 1.4 wt%, (D) 2.8 wt%, (E) 5.5 wt% 3M PEG particle stabilized emulsions (red, circles). The solid, black line is the ideal Stokes law creaming front and the dashed, black line is the modified Richardson-Zaki model.

Figure 3.8 shows the creaming profiles for the different PEG stabilized Pickering emulsions. Figure 3.8 shows that even though the PEG stabilized emulsion drops were larger in size when compared to the LSC and HSC glymo-stabilized emulsions; their creaming times were on the same time scale as the LSC and HSC glymo-stabilized emulsions. One potential explanation for this is that there could be particle induced bridging from the emulsification method that we used in this work – which is tip sonication.

Figure 3.9 shows demulsification pressures versus nanoparticle concentration for the 3M PEG nanoparticle stabilized emulsions. The results from these experiments reveal

that the 3M PEG-stabilized emulsions are more stable than the LSC and HSC glymo-stabilized emulsions. To highlight this, at 2.1 wt%, the 3M PEG stabilized emulsions had a demulsification pressure of 17.2 kPa, whereas the LSC and HSC glymo-stabilized emulsions both had demulsification pressures ~1.6 kPa. This suggests that the 3M PEG nanoparticles are capable of stabilizing stronger emulsions at lower nanoparticle concentrations than the LSC and HSC glymo-coated particles. Moreover, at 5.5 wt% nanoparticles, the 3M PEG-stabilized emulsions did not release any oil after centrifugation. Whereas both the LSC and HSC glymo-stabilized emulsions released some oil (Figure 3.3A,B).

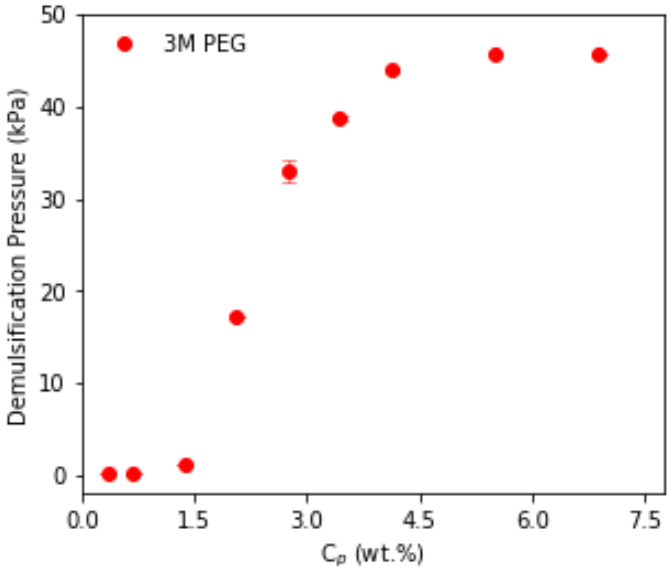

Figure 3.9 – Calculated demulsification pressures for 3M PEG (red circles) decane-in-water emulsions.

For our flowing experiments, we only tested 3M PEG-stabilized emulsions with 2.1 wt% and 2.8 wt% nanoparticles. This is because both of these emulsion formulations satisfied our critical demulsification pressure threshold requirement. Figure 3.10A, B show that both of these 3M PEG stabilized emulsions were dynamically stable because

their emulsion drops did not change by more than 10% while flowing through the glass capillary tube.

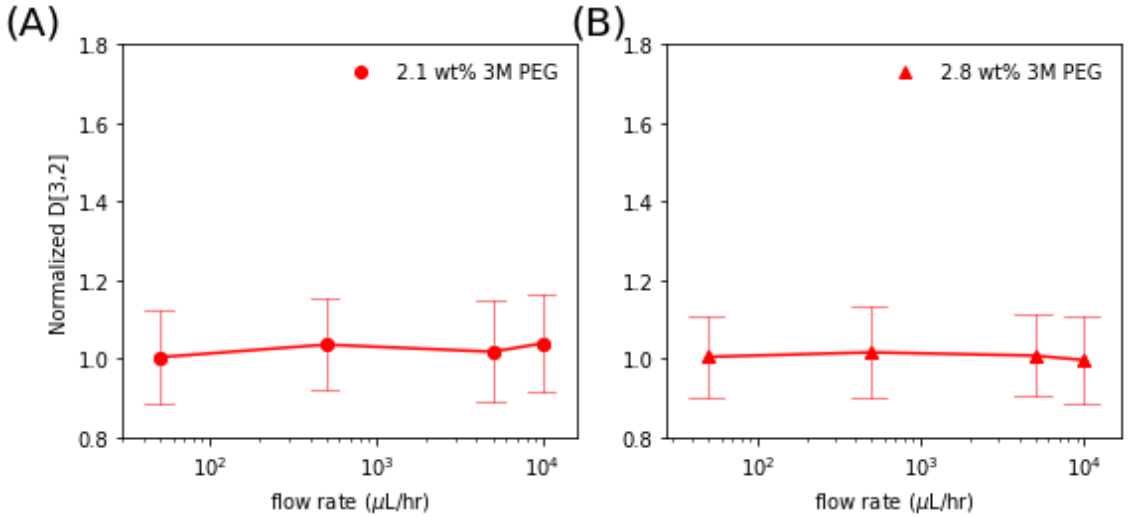

Figure 3.10 – Normalized D[3,2] versus flow rate for (A) 2.1 wt% and (B) 2.8 wt% 3M PEG-stabilized emulsions.

3.3.6 What about other particles?

Now that we have established that the demulsification pressure predicts the dynamic stability of an emulsion fairly well, this characterization method should be able to predict the stability of other particle stabilized emulsions. To compare the relative stabilities of other Pickering emulsions I have formulated emulsions using other common particles that our department has used in the past. These include Nissan EOR5XS particles and Nyacol DP9711 particles. Both particles have silica cores but are modified with unspecified silanes.

As a quick screen, I prepared emulsions using only DI water to see how the relative stabilities of these emulsions compare to the 3M PEG nanoparticles and my LSC and HSC glymo-coated nanoparticles. Figure 3.11 clearly shows that the EOR 5XS and Nyacol DP9711 have much lower demulsification pressures than the 3M PEG and LSC

and HSC glymo-stabilized emulsions. It must be pointed out that both the EOR 5XS and Nyacol DP9711 particles are more than 2years old, therefore it is unknown if this has any impact on the stability of these emulsions.

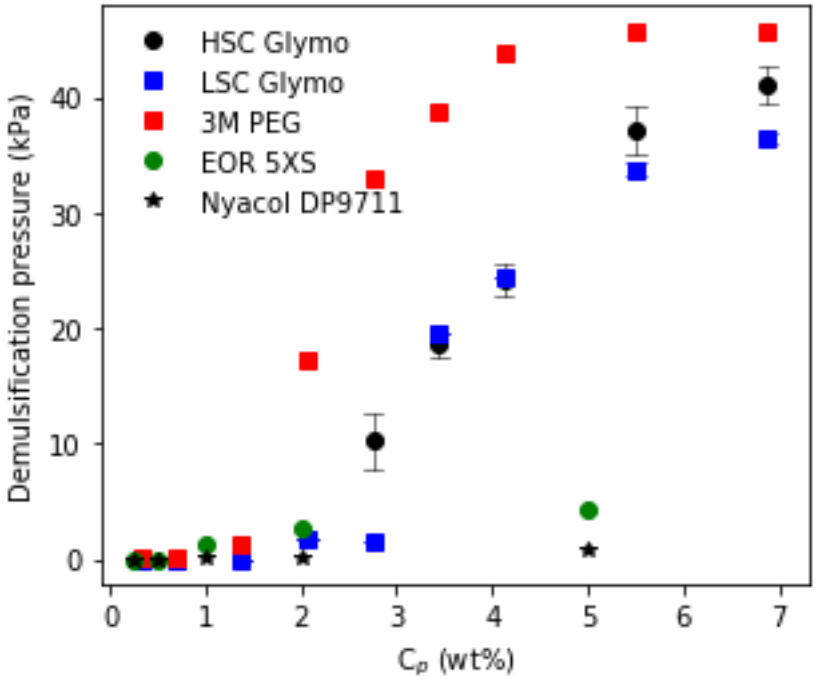

Figure 3.11 – Demulsification pressure versus nanoparticle concentration for LSC glymo-stabilized, HSC glymo-stabilized, 3M PEG stabilized, EOR 5XS stabilized, and Nyacol DP9711 stabilized emulsions.

Figure 3.12 shows a decision tree for the steps that can be taken to assess the stability of a new particle stabilized emulsion. This tree can aid in the rapid assessment of new nanoparticles and if they are capable of forming “stable” Pickering emulsions.

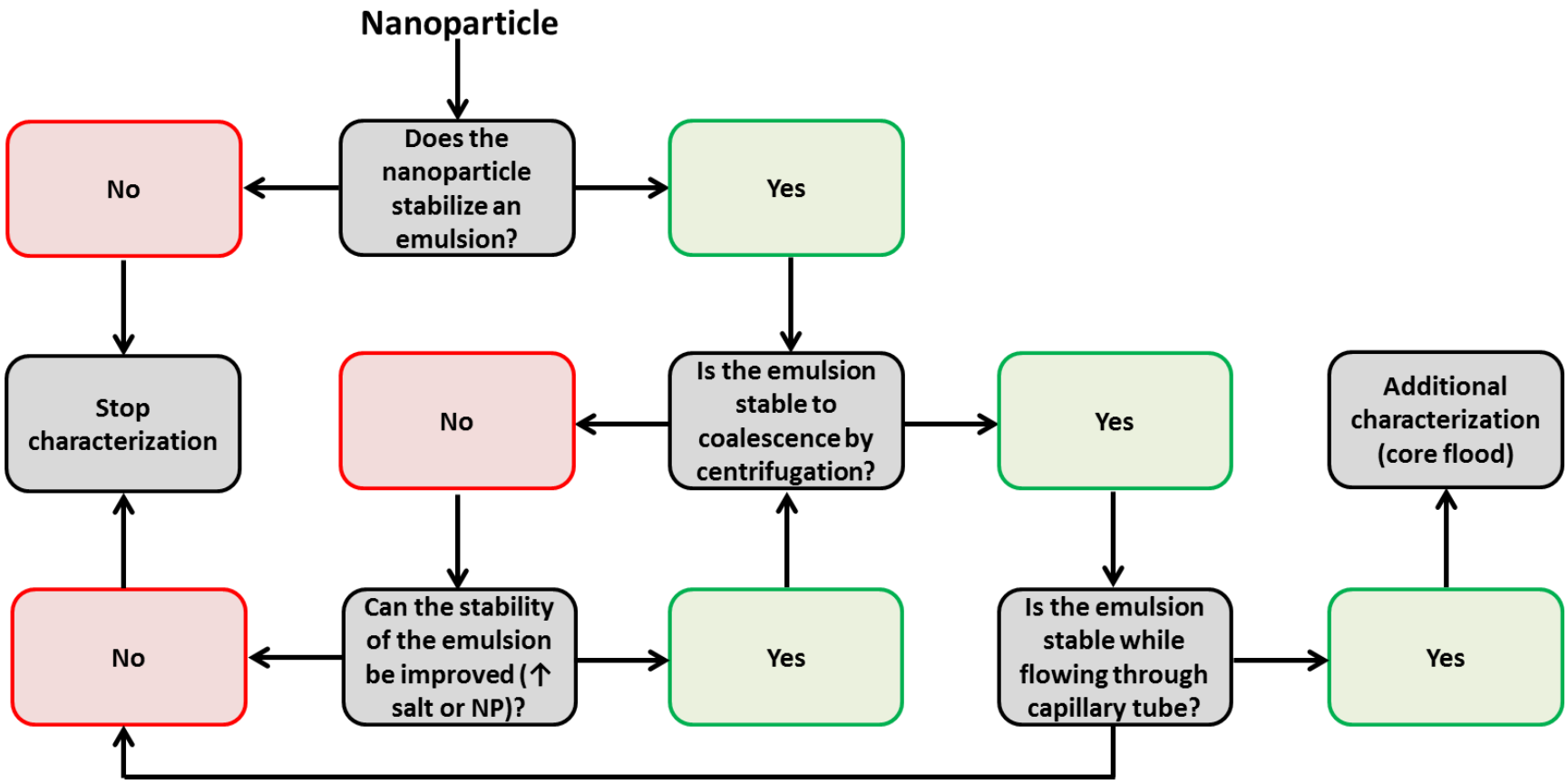

Figure 3.12 – Decision tree for assessing new Pickering emulsifiers and their ability to stabilize emulsions.

3.4 CONCLUSIONS

Because there are a wide range of particle emulsifiers capable of producing statically stable Pickering emulsions, a current challenge in the literature is being able to distinguish differences in their stability and to correlate their static stability to their dynamic stability. This is important for applications where emulsions are required to flow.

We have demonstrated that the concept of the demulsification pressure, which has previously been used to characterize the relative strength of different oil-in-water Pickering emulsions, is a sufficiently good metric that can predict the flowing stability of a Pickering emulsion. We demonstrated this by preparing a wide range of decane-in-water emulsions using low and high surface coverage glymo modified silica nanoparticles with different nanoparticle concentrations. We found that the demulsification pressure increased with increasing nanoparticle concentration. We injected different model emulsions through a 0.75 mm glass capillary tube and found that a demulsification pressure ~ 18.5 kPa was required for an emulsion to be dynamically stable as it flowed through the glass capillary tube.

We validated this critical demulsification pressure by using a previously untested emulsion formulation. This was done by stabilizing an emulsion with 2.8 wt% high surface coverage glymo coated nanoparticles and 10 wt% calcium chloride. The use of calcium chloride increased the demulsification pressure of this emulsion from 10.2 kPa (DI water) to 18.6 kPa (10 wt% calcium chloride). Moreover, the emulsion did not show any change in emulsion drop size while flowing through the glass capillary tube. This work outlines a promising screening method that can serve as an aid for selecting appropriate emulsions for more thorough coreflood tests.

Chapter 4: Manipulation of Pickering emulsion rheology using hydrophilically modified silica nanoparticles in brine[1]

4.1 INTRODUCTION

Pickering emulsions are emulsions stabilized with solid amphiphilic particles as opposed to chemical surfactants (Dong et al., 2014) and are kinetically stable to coalescence due to the irreversible adsorption of solid particles to the interface between two immiscible fluids (Cui et al., 2011). The appropriate selection of a nanoparticle surface modifier plays an integral role in how well particles are dispersed in a particular system (Schmidt and Malwitz, 2003; Weston et al., 2015) and is one of the key parameters that influence the stability and rheological properties of a solid particle-stabilized (Pickering) emulsion (Ngai and Bon, 2014).

For aqueous systems consisting of particles dispersed in pure water, two effective routes for altering the wettability of silica particles and controlling the type of emulsion that is formed (oil-in-water vs. water-in-oil) are modifying the surface by covalent attachment of hydrophobic alkoxysilanes and adsorbing surfactants by electrostatic interactions (Aveyard et al., 2002). For example, Binks and Lumsdon (2000) characterized emulsions stabilized with partially hydrophilic silica particles (76% silanol coverage) by reacting the particles with dimethyldichlorosilane and found they were capable of stabilizing toluene-in-deionized water emulsions, and conversely, those with intermediate wettabilites (50-67% silanol coverage) or hydrophobic (20% silanol coverage) could stabilized deionized water-in-toluene emulsions.

[1]This chapter was published in the Journal of Colloid and Interface Science as: C. Griffith, H. Daigle, Manipulation of Pickering emulsion rheology using hydrophilically modified silica nanoparticles in brine, Journal of Colloid and Interface Science. 509 (2018) 132-139.

Adding salts to the aqueous phase of an oil-water system (containing nanoparticles) complicates the fate and destination of particles at the fluid interface. Whitby et al. (2011) illustrated this with bromohexadecane-in-water emulsions (1:1) stabilized with partially hydrophilic fumed silica particles that were modified with hexadecyl chains. These dilute emulsions, which were well below the random close packing of hard spheres (ϕ = 0.635), developed a yield stress of 1 Pa in the presence of just 1 mM NaCl which further increased to 10 Pa in 400 mM NaCl. The positively charged sodium ions interacted with deprotonated particle silanol sites (Horozov et al., 2007). This process imparted hydrophobicity and reduced the particle electrical double layer, which promoted particle flocculation and their arrangement into a dense monolayer at the interface between droplets of oil and water. In addition, because the particle concentrations were high (~2 wt%) and the anchored hexadecyl groups were poorly solvated in brine (Arditty et al., 2005), an aggregated network of particles formed in the continuous phase. This network was responsible for the yielding behavior of the emulsions and provided additional emulsion stability by retarding creaming/coalescence (Horozov et al., 2007). These properties have been observed elsewhere with emulsions stabilized with clay (Ganely and Duijneveldt, 2017), silica (Horozov et al., 2007; Katepalli et al., 2017), alumina (Muth and Lews, 2017), and layered double hydroxide particles (Zhang et al., 2015).

For subsurface applications, where the salinity of brines is comparable to seawater (0.6 M NaCl) and can be as high as 22% total dissolved solids (Worthen et al., 2016), silica particles modified with hydrophobic alkoxysilanes are a poor choice as foam or emulsion stabilizers for enhanced oil recovery. This is because the formation of a percolating network of particles can be detrimental in propagating an emulsion deep into a formation, where pressure drops are low and on the order of several to ten psi/ft (Qi et

al., 2016). In addition, if the foam or emulsion were to de-stabilize, the hydrophobically modified particles would precipitate out of solution and potentially block pore throats, which could reduce reservoir permeability (Griffith and Daigle, 2017). Therefore, there is a need to explore particles modified with hydrophilic silanes that are stable against aggregation in concentrated brine waters (Worthen et al., 2016), but also capable of adsorbing to the oil/water interface such that foams or emulsions can be stabilized.

At present, Pickering emulsion research has focused on using silica particles to stabilize emulsions with low concentrations of mono- (<400 mM NaCl) and divalent (< 10 mM) ions in solution with the intent of improving emulsion stability (Binks et al., 2005; Horozov et al., 2007; Frelichowska et al., 2010; Whitby et al., 2012; Katepalli et al., 2017; Pilapil et al., 2016). Significantly less attention has been given to emulsions stabilized with sterically stabilized hydrophilic particles in concentrated brines. In the limited studies that do explore these conditions, the information on the structure and the amount of surface modifier is minimal (Kim et al., 2016) and the rheological properties of the generated emulsions are often neglected (Salah et al., 2005; Bjorkegren et al., 2017).

Therefore, in this work, we stabilized oil-in-water (o/w) emulsions with 6 nm silica nanoparticles modified with low and high concentrations of hydrophilic, ring-opened (3-glycidyloxypropyl)trimethoxysilane (glymo). The selection of glymo as a surface modifier was due to its stability in American Petroleum Institute (API) brine (8 wt% NaCl, 2 wt% $CaCl_2$) for up to 30 days at 80 °C (Worthen et al., 2016). In addition, glymo-modified silica nanoparticles have yet to be tested as emulsifying agents and are therefore an attractive particle to evaluate for subsurface applications. We characterized the emulsion properties by monitoring their elastic storage moduli as a function of particle surface coverage, pH, salt concentration ($CaCl_2$), and aqueous phase nanoparticle

concentration and show that emulsion rheology can be tuned primarily by augmenting the particle surface with different concentrations of glymo. In addition, we made observations of the microstructure of the emulsions using cryogenic scanning electron microscopy (cryo-SEM).

4.2 MATERIALS AND METHODS

4.2.1 Materials

NexSil 6 nanoparticles (6 nm silica particles) were purchased from Nyacol Technologies. The stock solution contained 17 wt% nanoparticles at a pH of approximately 10. The particles have a specific surface area of 445 m^2/g (provided by the manufacturer). (3-glycidyloxypropyl)trimethoxysilane (>98%) (glymo) and 1-bromohexadecane (97%) were purchased from Sigma-Aldrich. Calcium chloride, basic alumina, and 1N hydrochloric acid were purchased from Fisher Scientific and used as received.

4.2.2 Methods

4.2.2.1 Nanoparticle functionalization

Nanoparticles were surface modified with (3-glycidyloxypropyl)trimethoxysilane (glymo) following previous work (Yang and Liu, 2010; Worthen et al., 2016). Glymo was added into reaction mixtures at a concentration of 1.85 or 4.00 $\mu mol/m^2$ of nanoparticle surface area for low and high surface coverage, respectively. An acid-catalyzed ring opening of the glymo epoxide was performed before adding it to the nanoparticle dispersion. This was done by reacting glymo for several minutes in DI water

adjusted to pH 2 using 1N HCl. The ring-opened glymo was added to the nanoparticle dispersion and heated overnight at 60°C to complete the hydrolysis condensation reaction. In some cases, a small amount methanol was used to prevent glymo oligomers from precipitating out of solution, and was removed by evaporation upon completing the reaction. The final concentration of nanoparticles in the mixture was approximately 10 wt% and the final pH of the reaction mixture was 10-10.1. Batches containing 20 grams of nanoparticles were surface modified and used without purification.

4.2.2.2 Emulsion preparation

Oil-in-water (o/w) emulsions were prepared using a Branson Digital Tip Sonifier (30 W) equipped with a 5 mm microtip. Prior to generating emulsions, bromohexadecane was passed through basic alumina (2x) to remove polar impurities (Whitby et al., 2011). Bromohexadecane was selected as a model oil due to its high specific gravity (SG = 0.999), which eliminates the possibility of density driven creaming during rheological measurements (Whitby et al., 2011; Katepalli et al., 2017). Emulsions with 50% oil (by volume) were prepared by adding 5 mL of bromohexadecane and 5 mL of nanoparticle dispersion into a 20 mL glass vial. The solutions were tip sonicated for 10 seconds, gently shaken, and then tip sonicated for an additional 10 seconds. Emulsions with higher oil volume fraction (70%) were prepared by adding 3 mL of bromohexadecane and 3 mL of the nanoparticle dispersion into a 20 mL glass vial. The solution was tip sonicated for 10 seconds, gently shaken, and then 1 mL of oil was added, followed by tip sonicating. This was repeated until the total volume of the emulsion was 10 mL (7 mL bromohexadecane and 3 mL nanoparticle dispersion). The presence of o/w emulsions was confirmed with the drop test method (Simon et al., 2010).

4.2.2.3 Dynamic Light Scattering and Zeta Potential

A Malvern Zetasizer Nano ZS was used to record the z-average particle hydrodynamic diameter and zeta potential of various dispersions. Samples were prepared with 1 wt% nanoparticles in the aqueous phase.

4.2.2.4 Rheometer

Rheological measurements were performed with a TA Instruments AR-G2 magnetic bearing rotational rheometer with a 40 mm bead-blasted parallel plate set to a gap width of 0.75 mm. Samples were conditioned by pre-shearing for 30 seconds at rate of 10 s^{-1}. Oscillatory strain sweeps were then performed by varying the strain amplitude from γ = 0.1-1000% at a fixed frequency of 1 Hz. The temperature was maintained at 25 °C. The loss (G") and storage (G') moduli were monitored throughout the measurements. The zero-shear elastic modulus (G'_0) was calculated by averaging G' from γ = ~0.1-0.5% (Lee et al., 2011).

4.2.2.5 Cryogenic-Scanning Electron Microscope

A FEI Quanta 650 SEM equipped with a Quorum Cryo-stage was used for high resolution imaging of frozen emulsion drops. A small volume of sample was placed into a copper rivet and flash frozen in a slushed liquid nitrogen bath. Samples were transferred to the Quorum Cryo-stage and then fractured using a flat knife, followed by sputter coating for 60 seconds with a current of 8 mA. Analysis was done in vacuum at a temperature of -135°C.

4.2.2.6 Thermogravimetric Analysis

The organic fraction of low and high surface coverage silica particles was characterized using thermogravimetric analysis (TGA). The procedure to filter and perform TGA followed Worthen et al. (2016). Particles were purified by washing four times with 30k molecular weight cut-off (MWCO) centrifuge filters for 15 minutes at 5,500 rpm and dried in an oven at 80 ^{o}C, overnight. The samples were analyzed for organic content by heating at a rate of 20 ^{o}C/min under N_2 in a Mettler-Toledo instrument. First, the samples were heated from 30 ^{o}C to 110 ^{o}C and held 110 ^{o}C for 20 minutes to remove water. Second, the samples were heated from 110 ^{o}C – 800 ^{o}C. The mass that was lost during this step was attributed to the glymo ligand.

4.3 RESULTS AND DISCUSSION

4.3.1 Nanoparticle Functionalization

We evaluated the change in Pickering emulsion rheology based on the extent of nanoparticle surface modification with the silane, glymo. We selected low (1.85 µmol/m²) and high (4 µmol/m²) concentrations of glymo as appropriate silane quantities based on our experimentation with the particles in different brines. Particles with low surface concentration were designated as LSC nanoparticles whereas those with high surface concentration were designated as HSC nanoparticles. We assumed a complete monolayer of silane was 7.6 µmol/m² of nanoparticle surface, which was calculated by assuming 4.6 silanol sites/nm^2 of particle surface (Worthen et al., 2016). Table 1 contains the organic fraction of filtered and un-filtered nanoparticles and the ligand coverage of the filtered particles and their associated monolayer fraction. The ligand coverage of glymo on the particle surface was calculated using equation 4.1 (Worthen et al., 2016):

$$\phi_l = \frac{f_o}{(1-f_o)S_A M_{TGA}} * 10^6 \; [=] \frac{\mu mol}{m^2}, \tag{4.1}$$

where f_o is the particle organic fraction by TGA, S_A is the particle specific surface area (445 m^2/g), and M_{TGA} is the molecular weight of the portion of glymo removable by TGA (133 Da) (see Figure S1 in Worthen et al., (2016)) for additional details). The monolayer fraction was calculated by taking the ligand coverage and dividing by 7.6 µmol/m². The HSC particles contained 3 wt% more coverage on their surface which resulted in a 9% increase in monolayer fraction over the LSC particles.

Particle	Glymo concentration (µmol/m²)	Organic fraction of un-filtered particles by TGA, wt.%	Organic fraction of filtered particles by TGA, wt.%	Ligand coverage of filtered particles, µmol/m² (monolayer fraction)
LSC	1.85	10.1	9.3	1.7 (23%)
HSC	4	15.3	12.3	2.4 (32%)

Table 4.1 – Nanoparticle properties determined by thermogravimetric analysis

Figure 4.1a shows a dispersion of 1 wt% modified silica nanoparticles with HSC (left vial) and LSC (right vial) nanoparticles in 1 wt% $CaCl_2$ water (pH ~9.5) at room temperature after 48 hours. The 1wt% HSC dispersion was clear with no signs of particle aggregation or sedimentation, suggesting the 9% increase in monolayer fraction on the particle surface was sufficient to provide particle steric stabilization. The 1wt% LSC nanoparticle dispersion (in 1.0 wt% $CaCl_2$ brine water) was cloudy, which was a sign that particle agglomerates formed due to the interaction of Ca^{2+} and free silanol sites on the nanoparticle surface. The dispersion was monitored for 1 week and showed signs of particle settling and we suspect that given enough time, there would be complete particle settling.

We used dynamic light scattering and zeta potential measurements to monitor the change in particle size and surface zeta potential in different ionic strength solutions. 1 wt% bare NexSil 6 particles in DI water at pH ~9.5 had a z-average hydrodynamic diameter of 19.6 nm. After functionalization, both the LSC and HSC particles had a hydrodynamic diameter of ~23.5 nm with a polydispersity of 0.24. The size of the HSC particles increased to ~26 nm in 0.5 wt% $CaCl_2$ solution and remained constant up to 2.5 wt% $CaCl_2$ (Figure 4.1b, black markers). Accurate size measurements of the LSC particles were difficult to obtain even in the lowest brine concentration tested (0.25 wt% $CaCl_2$), which was due to increased light scattering from particle aggregates, and therefore not reported. The zeta potential of the HSC particles in DI water was -28 mV compared to -42 mV for unmodified particles, further suggesting the condensation of glymo with silanol moieties on the particle surface (Estephan et al., 2010). As the concentration of $CaCl_2$ was increased, the corresponding zeta potential decreased exponentially to a maximum of ~0 mV in 2.5 wt% $CaCl_2$ (Figure 4.1b, green markers), consistent with other surface modified silica nanoparticles in brine waters (Kim et al., 2015).

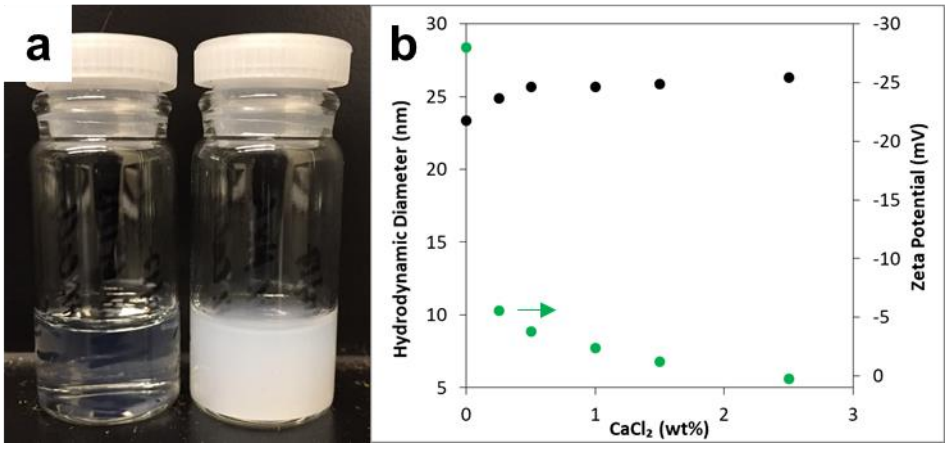

Figure 4.1 – (a) dispersions of: 1 wt% high surface coverage nanoparticles (HSC) in 1 wt% $CaCl_2$ (left vial) and 1 wt% low surface coverage nanoparticles (LSC) in 1 wt% $CaCl_2$ (right vial). (b) Dynamic light scattering (black) and zeta potential (green) measurements of 1 wt% HSC nanoparticles vs. $CaCl_2$ concentration.

4.3.2 Macroscopic and microscopic emulsion behavior

Our initial experiments showed that bare NexSil 6 particles were unable to stabilize o/w emulsions and that surface modification was required to stabilize emulsions. Therefore, we first prepared emulsions with 1 wt% silica nanoparticles (either HSC or LSC) dispersed in DI water (pH 9.5) with 50% oil using the Branson Digital Tip Sonifier. After sonication, the entire volume of oil was emulsified and there were no visible signs of emulsion creaming/coalescence (over the course of a month) and this was despite a small density difference ($\Delta SG=0.03$) between the DI water and nanoparticle dispersion and oil. This observation can be supported by Zhang et al. (2015) and was attributed to the high input energy from the sonicator, which helps to induce nanoparticle bridging between oil droplets and provides a mechanism to prevent droplet coalescence (Ganley and Duijneveldt, 2017).

The role of ions in stabilizing Pickering emulsions has been well studied (e.g., Dong et al., (2014) and Kaganyuk and Mohraz, 2017). Cations screen charges on the particle surface, reducing the Debye length, and depending on the structure of the surface modifier, ions can aid in promoting the formation of a dense monolayer of particles on an oil drop surface. Katepalli et al. (2017) experimentally showed that dilute emulsions (50% bromohexadecane by volume) stabilized with 2 wt% 210 nm fumed silica particles (Evonik Aerosil R816) had a high coverage of particles on drops of oil in low salt concentrations (1 mM NaCl) and formed particle bridges in the presence of 50 mM NaCl, which led to emulsion viscoelasticity. In light of this, we investigated the micro-structure of our emulsions using cryo-SEM and qualitatively characterized their behavior as the concentration of glymo on the nanoparticle surface was altered (LSC vs. HSC particles) and by changing the aqueous phase salt concentration from DI water to 1 wt% $CaCl_2$.

Figure 4.2a shows a cryo-SEM image of a 50% oil emulsion with an aqueous phase of DI water with 1 wt% LSC nanoparticles and provides evidence of interfacially adsorbed nanoparticles on the oil drop surface, although at low densities (Figure 4.2a,b). This low coverage was likely due to particles carrying significant electrostatic charges from deprotonated silanol groups. However, despite the low coverage of nanoparticles on the drop surface, the stable macroscopic nature of the emulsions was expected, given that previous work has shown that a dense monolayer of particles is not required to create stable emulsions (Vignati et al., 2003). Figure 4.2c (red-dashed box) shows the same 1 wt% LSC in DI water emulsion, and highlights the presence of a bridged network of nanoparticles in the continuous phase of the emulsion, which was responsible for inhibiting long term emulsion creaming and coalescence (Ganley and Duijneveldt, 2017).

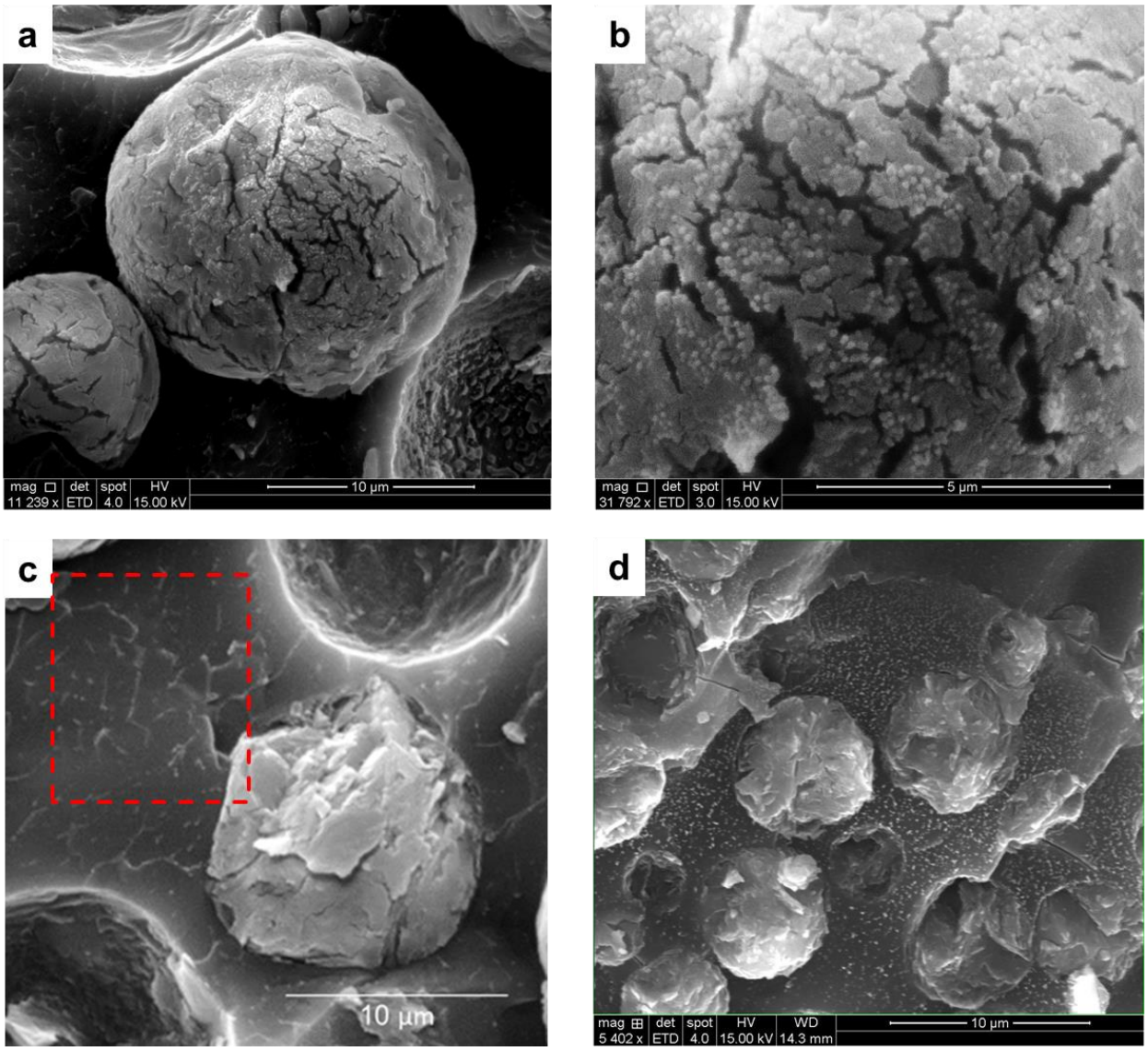
a
mag
11 239 x
det
ETD
spot
4.0
HV
15.00 kV
10 µm
b
mag
31 792 x
det
ETD
spot
3.0
HV
15.00 kV
5 µm
c
10 µm
d
mag
5 402 x
det
ETD
spot
4.0
HV
15.00 kV
WD
14.3 mm
10 µm

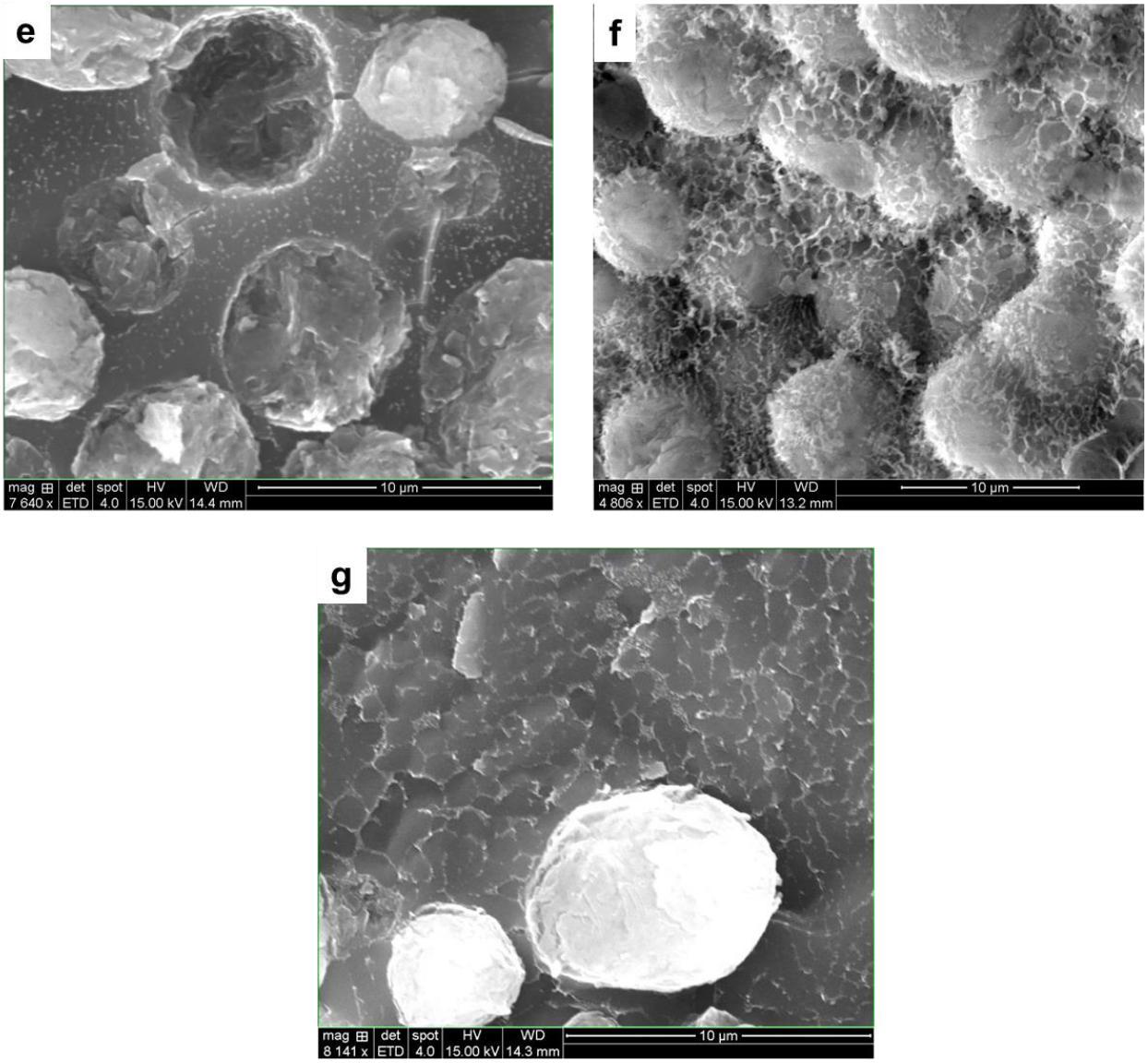

Figure 4.2 – Bromohexadecane-in-water emulsions stabilized with: (a)-(c) 1wt% low surface coverage (LSC) nanoparticles in DI water at high pH, (d)-(e) 1 wt% high surface coverage nanoparticles (HSC) in 1 wt% $CaCl_2$ at high pH, and (f) 1wt% LSC nanoparticles in 1 wt% $CaCl_2$ at high pH, and (g) 1wt% LSC nanoparticles in 1 wt% $CaCl_2$ at low pH.

As Ca^{2+} cations were introduced into the system, there was a distinct relationship between glymo coverage and the number of bridged networks participating in the emulsion microstructure, which was characterized by cryo-SEM. Qualitatively, there

were more structured networks present in emulsions stabilized with LSC particles (Figure 4.2f, g) than with emulsions stabilized with HSC nanoparticles (Figure 4.2d, e) and we observed the most bridging in emulsions stabilized with LSC particles at high pH (Figure 4.2f).

We performed oscillatory measurements on emulsions (50% oil) stabilized with either 1 wt% LSC or HSC particles while in the presence of 1 wt% $CaCl_2$ (Figure 4.3) to macroscopically characterize particle bridging. The HSC particle stabilized emulsions had a zero shear elastic storage modulus (G'_0) of 2 Pa and a crossover strain amplitude of 10% whereas the LSC particle stabilized emulsions had a G'_0 of 20 Pa and crossover strain amplitude of 25%. The increase in G'_0 and the crossover strain amplitude in the rheological measurements were in agreement with our cryo-SEM images that there were showed more particle bridges in emulsions stabilized with LSC particles.

To ensure that our rheological measurements were consistent with previously published literature, we formulated an emulsion that was comparable to the emulsion used in Katepalli et al. (2017). Recall that their work used Evonik R816 fumed silica particles at 2 wt% to stabilize bromohexadecane-in-water emulsions (50% by volume oil) with 50 mM NaCl in their formulation. Here, we stabilized a 50% by volume bromohexadecane-in-water emulsion using 1 wt% R816 fumed silica particles with 0.25 wt% $CaCl_2$ (Figure 4.3, blue markers).

Our R816 bromhexadecane-in-water emulsions compared very favorably to the results presented in Katepalli et al. (2017). In their work, their R816 bromohexadecane-in-water emulsions had a zero shear elastic storage modulus of ~ 200 Pa. The emulsion that we have stabilized had a zero shear elastic storage modulus of ~200 Pa.

It is important to highlight these differences in zero shear elastic storage moduli between our emulsions (stabilized with the HSC and LSC glymo coated particles) and

those that were stabilized with the R816 fumed silica particles. This is because our glymo-coated particles are much more effective at screening particles from cations in solution. Moreover, we also show that the extent of these interactions can be controlled by the concentration silane on a nanoparticle surface. We capture this behavior by monitoring the change in zero shear elastic storage moduli of these different emulsions.

The rheology of emulsions with 70% oil by volume was further probed. We selected 70% oil because of the high repeatability in the rheological measurements (Figure 4.4a). We monitored emulsion behavior in response to glymo coverage on the nanoparticle surface, the concentration of nanoparticles in the aqueous phase, the solution pH, and solution ionic strength. These emulsions were stable at room temperature for periods of months with no signs of creaming or release of emulsified oil unless otherwise noted.

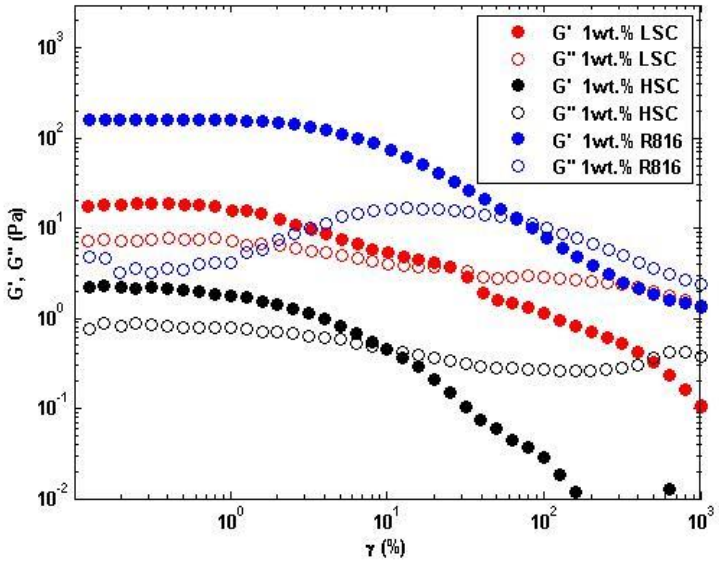

Figure 4.3 – The storage (G' – filled symbols) and loss (G" – open symbols) moduli for 50% o/w emulsions with an aqueous phase of 1 wt% $CaCl_2$ and a pH of 9.5 stabilized with high surface coverage (HSC) [black markers] and low surface coverage (LSC) [red dots] nanoparticles.

4.3.3 Effect of nanoparticle concentration, salinity, and pH on emulsion rheology

4.3.3.1 Oscillatory Rheology of HSC nanoparticle stabilized emulsions

Our oscillatory measurements showed distinct trends in emulsion elasticity and it was found the trends were dependent on the extent of glymo coverage on the nanoparticle surface. In general, emulsions stabilized with HSC particles (pH 9.5) in 1.0 wt% $CaCl_2$ brine had larger zero shear elastic storage moduli (G'_0) compared to emulsions stabilized with HSC particles in brine with 0.25 wt% $CaCl_2$ (Figure 4.4b). However, regardless of salinity, the emulsions stabilized with HSC particles exhibited almost identical qualitative trends when G'_0 was plotted vs. nanoparticle concentration in the aqueous phase (C_p) (Figure 4.4b). Based on these observations, their behavior was divided into two different regimes.

The first regime was graphically represented by a linearly relationship between G'_0 and C_p, and occurred when C_p was increased from 0.5 to 2.5 wt% (Figure 4.4b). In this regime, at a fixed salinity, C_p alone was responsible for increasing G'_0 by a factor of 2.1 (in 0.25 wt% $CaCl_2$ brine) and 2.4 (in 1.0 wt% $CaCl_2$ brine). The second regime was characterized by a reduction in G'_0 and occurred as particle concentrations were increased from 2.5 wt% to the end of our testing at 5.0 wt%. In this regime, G'_0 was reduced by 85% (in 0.25 wt% $CaCl_2$) and 84% (in 1.0 wt% $CaCl_2$) from the maximum G'_0, which occurred at a C_p of 2.5 wt% (for both salt concentrations), to the minimum G'_0 with a C_p of 5.0 wt%.

The strengthening of emulsions in these experiments was due to increasing the number of particle bridges, which was the result of having a higher concentration of nanoparticles in the aqueous phase (Zhang et al., 2008; Zhang et al., 2015; Muth and Lewis, 2017). This behavior was captured by our oscillatory rheology measurements and

enhanced by the addition of $CaCl_2$, which screened electrostatic charges (Figure 4.4b) (Metin et al., 2010). One important aspect of these emulsions was the bridging behavior was due to the emulsification method as opposed to ions inducing attractive interactions between nanoparticles (Simon et al., 2010; Fuma and Kawaguchi, 2015).

Weakening of the emulsions with C_p greater than 2.5wt% was thought to be a result of driving bridged particles to the oil/water interface, which reduced the number of nanoparticles participating in the aqueous phase particle network, and as a result, led to a decrease in the zero shear elastic storage modulus for a given emulsion system (Kaganyuk and Mohraz, 2017). This result was somewhat surprising given that a number of articles have suggested there is an increase in elasticity with more particles in solution (Muth and Lewis, 2017).

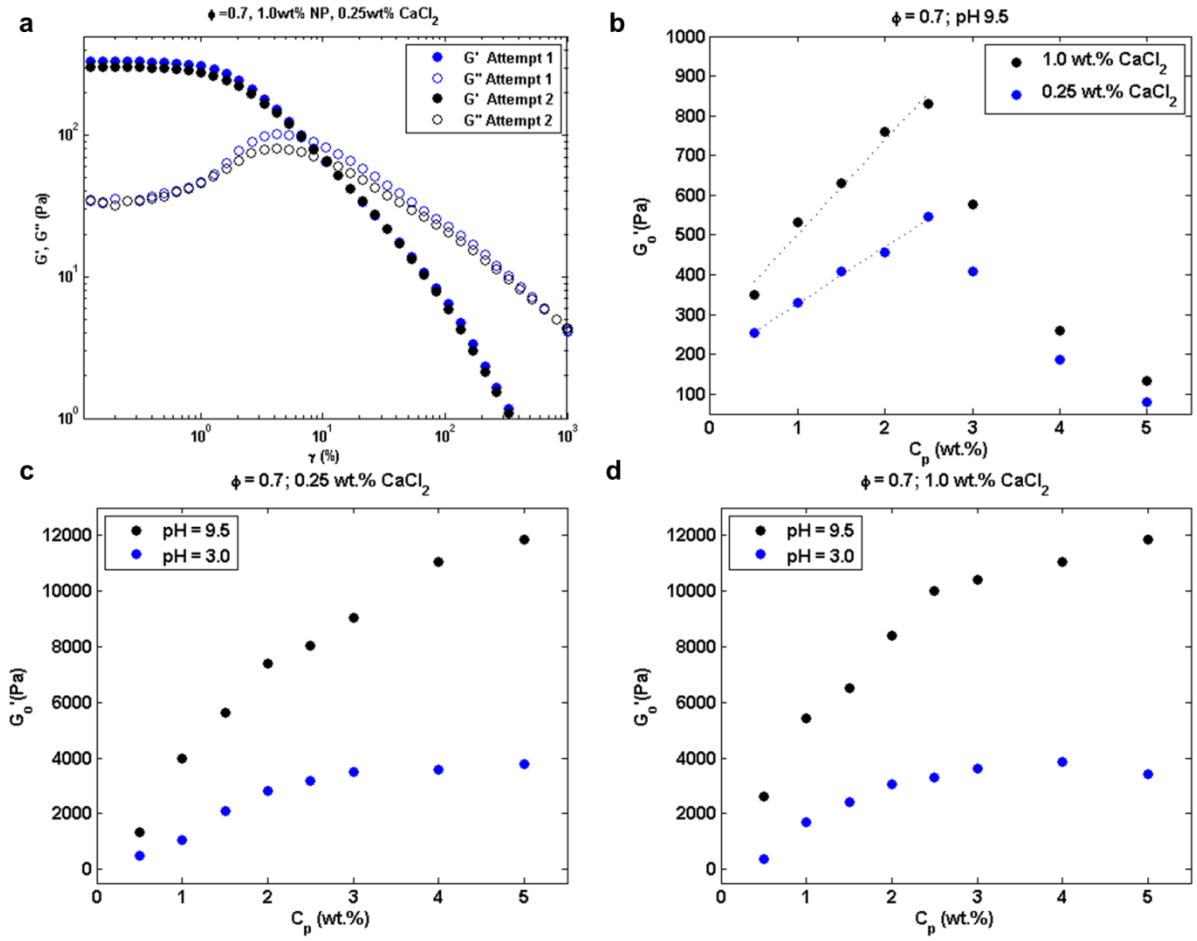

Figure 4.4 – (a) Strain sweep profile for 1wt% HSC nanoparticles in 0.25 wt% $CaCl_2$ with 70% oil. The blue and black markers show the same measurement performed twice. (b) – (c) The zero shear elastic storage modulus of 70% oil by volume emulsions vs. nanoparticle concentration stabilized with: (b) High Surface Coverage (HSC) nanoparticles at pH 9.5 in 0.25 wt% $CaCl_2$ (blue) and 1.0wt% $CaCl_2$ (black). (c) Low Surface Coverage (LSC) nanoparticles in 0.25 wt% $CaCl_2$ at high pH (black) and low pH (blue) and (d) LSC nanoparticles in 1 wt% $CaCl_2$ at high pH (black) and low pH (blue).

4.3.3.2 Oscillatory rheology of LSC nanoparticle stabilized emulsions

Emulsions stabilized with LSC nanoparticles showed different rheological properties than emulsions stabilized with HSC nanoparticles (Figure 4.4c,d). The first

noticeable difference was that at high pH (~9.5) (Figure 4.4c,d - black dots), G'_0 for emulsions stabilized with LSC particles, in almost all cases, were an order of magnitude larger than emulsions stabilized with HSC particles. At low nanoparticle concentrations (less than 2.5 wt%) the 70% oil by volume emulsions showed a linear increase in G'_0 with C_p, which was similar to emulsions stabilized with HSC particles. However, as C_p was further increased, the emulsions transitioned into a second linear regime with a different slope from the first. Moreover, it was found the concentration of $CaCl_2$ in the aqueous phase had little impact on the magnitude of G'_0 between the two different emulsion systems. For example, emulsions stabilized with 5.0 wt% nanoparticles had approximately the same zero shear elastic storage modulus (11,835 vs. 11,841 Pa) in 0.25 wt% or 1.0 wt% $CaCl_2$, respectively.

We found that by adjusting the pH of the aqueous phase to 3, we could manipulate the elasticity of the LSC particle stabilized emulsions (Figure 4.4c,d - blue dots) which resulted in different behavior at higher particle concentrations compared to the LSC stabilized emulsions at high pH. At low pH, the emulsions exhibited a linear increase in G'_0 up to a C_p of 2 wt%, that was followed by a plateauing of G'_0 with C_p greater than 2 wt%. At low pH G'_0 of the emulsions were reduced by an average of 65% (with 0.25 wt% $CaCl_2$) and an average of 70% for emulsions (with 1.0 wt% $CaCl_2$) compared to the high pH cases. This behavior was in contrast to emulsions stabilized with HSC particles which showed emulsion weakening and to emulsions stabilized with LSC particles at high pH which transitioned into a second linear regime.

The enhanced elasticity of emulsions stabilized with LSC particles (at high pH) over those stabilized with HSC particles (also at high pH) was attributed to the low coverage of glymo on the nanoparticle surface, which allowed for more interactions between Ca^{2+} and deprotonated silanol sites, producing attractive inter-particle

attractions, and forming a strong percolating/aggregated particle network (Figure 4.2f). The result of this was much larger G'_0 compared to emulsions stabilized with HSC particles. Moreover, the reduced elasticity of LSC emulsions stabilized at low pH was a result of minimizing inter-particle attractions by protonation of silica silanol groups, subsequently reducing the interaction with Ca^{2+}. Lastly, these measurements suggest that G'_0 had little dependence on salt concentration for emulsions prepared with LSC particles. This would imply that 0.25 wt% $CaCl_2$ was a sufficient concentration of calcium to saturate calcium/silanol interactions and presumably why there were no further increases in G'_0 with additional ions in the aqueous phase.

4.4 CONCLUSION

In this work, we demonstrated that 6 nm silica nanoparticles modified with the hydrophilic silane glymo can stabilize bromohexadecane-in-water emulsions. We characterized the rheological properties of the emulsions by probing their response to different concentrations of glymo on the nanoparticle surface and found that the trends in emulsion elasticity were predominantly dependent on this variable (low vs. high glymo coverage). Our cryo-SEM images showed that emulsions stabilized with low surface coverage of glymo and with $CaCl_2$ (at high pH), exhibited an intense network of bridged nanoparticles in the aqueous phase. The network of particles was responsible for the zero shear elastic storage modulus when 50% oil emulsions were prepared. At 70% oil volume fraction, the elastic storage modulus of emulsions could be reduced by lowering the solution pH to 3, or by using particles with a higher concentration of glymo on the particle surface. Lowering the solution pH reduced the elasticity of emulsions by an average of 65-70% whereas increasing the amount of glymo on the particle surface minimized the interaction between calcium ions and deprotonated silanol sites. We

believe this mechanism was responsible for reducing the elastic storage modulus of emulsions by an order of magnitude compared to emulsions stabilized with nanoparticles with low coverage of glymo.

This work, in contrast to others using silica particles modified with hydrophobic alkoxysilanes (Binks et al., 2005; Horozov et al., 2007; Whitby et al., 2011; Whitby et al., 2012; Katepalli et al., 2017; Pilapil et al., 2016), demonstrates that particles modified with hydrophilic silanes are capable of stabilizing o/w emulsions. We also show that these particles are responsible for reducing the viscoelastic behavior of emulsions with 50% oil and 1 wt% $CaCl_2$ in the aqueous phase. This reduction is significant when compared to similar emulsions prepared in Katepalli et al. (2017) where only 1 and 50 mM NaCl are present. Future work should emphasize the flowing behavior of emulsions stabilized with glymo coated particles through porous cores and to test the nanoparticles ability to stabilize foams at low pH and high temperature, which is also of use for enhanced oil recovery.

Chapter 5: Destabilizing Pickering emulsions using fumed silica particles with different wettabilities[2]

5.1 INTRODUCTION

Pickering emulsions are known for their high degree of stability (Chevalier and Bolzinger, 2013; Xu et al., 2017). This is due to the irreversible adsorption of particles to the oil/water interface (Aveyard et al., 2017), which provides a steric barrier to droplet coalescence (Binks, 2002). Over the past decade, there has been a significant amount of research on how particle size (Binks and Lumsdon, 2001; Kim et al., 2016), shape (Ashby and Binks, 2000; Madivala et al., 2009), concentration (Frelichowska et al., 2010), wettability (Simovic and Prestidge, 2004), and aqueous phase composition (Horozov et al., 2007) affect the type and stability of Pickering emulsion that is formed. There has also been a relatively large amount of work on establishing methods for destabilizing Pickering emulsions (Yan et al., 1993; Whitby et al., 2009; Juarez and Whitby, 2012; Zhao et al., 2018), which is of practical interest to a range of industrial applications (Whitby and Wanless, 2016).

Recently, Whitby and Wanless (2016) wrote a review paper that discussed several mechanisms responsible for destabilizing Pickering emulsions, which broadly fall into three categories: (1) detaching particles from fluid interfaces, (2) transferring mass between liquid phases, and (3) coalescing emulsion drops. Typically, surfactants can be added to a Pickering emulsion to alter the wettability of interfacially adsorbed particles (Whitby and Wanless, 2016) or to competitively displace them from the oil/water interface (Vashisth et al., 2010). Altering the solvent quality of the continuous phase, to

[2]This chapter was recently published in the Journal of Colloid and Interface Science as: C. Griffith, H. Daigle, Destabilizing Pickering emulsions using fumed silica particles with different wettabilities, Journal of Colloid and Interface Science. 2019.

induce emulsion drop flocculation, is another method capable of coalescing a Pickering emulsion (Whitby et al., 2016).

Whitby and Wanless (2016) briefly discussed using particles, in the form of fat crystals, as a method to partially coalesce food emulsions. The ability of a fat crystal to induce partial coalescence is driven by its wettability, with the idea that a fat crystal consisting of intermediate wettability will move from the interior of an oil globule to the oil/water interface (Bookde and Walstra, 1993). This will allow the fat crystal to protrude radially outward from the oil drop surface and to interact with neighboring drops, leading to partial coalescence (Boode and Walstra, 1993). If the crystals are too hydrophobic, however, they will prefer to reside at the center of an oil globule and be unable to interact with other oil drops. This idea of using particles to destabilize emulsions could potentially be used as a method to destabilize Pickering emulsions.

The concept of using colloidal silica to destabilize fluid interfaces has been studied in the context of destabilizing air/liquid interfaces for defoaming applications (Denkov, 2004). In the process described by Denkov (2004), colloidal silica particles are first dispersed into an oily carrier fluid which is then brought into contact with foam. The particles then form bridges between film interfaces and, if the particles are sufficiently hydrophobic, they can destabilize the foam by dewetting the liquid film. This is referred to as the "bridging-dewetting" mechanism. The term "sufficiently" hydrophobic has been studied in relationship to the three phase (air/water/solid particle) contact angle of hydrophobic particles. In general, particles must consist of three phase contact angles in excess of 90° for foam destabilization to occur, but other factors, such as particle shape (Frye and Berg, 1989), can change the contact angle requirement (Frye and Berg, 1989, Denkov, 2004).

In this work, we attempt to use colloidal silica particles, with different wettabilities, as a method to destabilize a model Pickering emulsion. We are interested in using colloidal silica to destabilize Pickering emulsion because of their well-defined hydrophobicity (Yan et al., 2000), fractal like structure (Aerosil, 2018), and because of the practical limitations associated with using surfactants or solvents to destabilize Pickering emulsions (Vashisth et al., 2010; Whitby et al., 2016). For example, in order to competitively displace particles from the oil/water interface (using surfactants), the surfactant needs to be added above its critical micelle concentration (CMC) and the emulsion mixture needs to be mixed at high shear rates in order to detach particles from the oil/water interface. In the work of Vashisth et al (2010), a mixing rate of 13,000 rpm for 2 minutes was required. Moreover, using a solvent to alter the quality of the continuous of an emulsion phase can require large volumes of solvent, which was the case for Whitby et al. (2016). In their work, isopropyl myristate was added to a Pickering emulsion at a volume fraction ~84%, which was necessary for inducing droplet flocculation. These large volumes of solvent might be impractical for some applications.

Fumed silica (Katepalli et al., 2016; Kumar et al., 2018) and latex (Aveyard et al., 1999) particles have been used to destabilize surfactant-stabilized emulsions, but their use in destabilizing Pickering emulsions is unexplored. In the work of Katepelli et al. (2016), it was shown that fumed silica particles were capable of destabilizing an oil-in-water emulsion stabilized with a non-ionic surfactant (Triton X-100). Two fumed silica particles were used in their experiments: (1) a bare hydrophilic fumed silica particle called Aerosil 200, and (2) a partially hydrophobic fumed silica particle covalently modified with hexadecyl (C16) chains, called Aerosil R816. The mechanism responsible for coalescence was hydrophobic interactions between the surfactant tail and C16 chain on the R816 particle surface, which depleted surfactant from the oil/water interface.

The goal of this work was to test if fumed silica particles (with different wettabilities) could potentially destabilize a model Pickering emulsion. To accomplish this, we first generated a stable oil-in-water Pickering emulsion stabilized with polyethylene glycol-modified silica nanoparticles and characterized its stability to coalescence by centrifugation and by stirring on a stir plate for 20 minutes. Next, fumed silica particles, with different wettabilites, were added to the continuous phase of the model emulsion and stirred (on a stir plate) for 20 minutes, after which they were macroscopically assessed for the volume of coalesced oil. Optical microscopy was used to study the mechanisms that were responsible for emulsion destabilization.

5.2 MATERIALS AND METHODS

5.2.1 Materials

Three different fumed silica particles were used in this study. They are commercially available and were obtained from Evonik Corporation. The particles are produced by the flame hydrolysis method and consist of primary particles (7 – 20 nm) that are fused together to form larger aggregates that are 100-500 nm in size (Saleh et al., 2011; Aerosil, 2018). The particles arrive as a dry, white, fluffy powder. The three particles we used (listed in increasing hydrophobicity) were: Aerosil A200 (bare, no surface treatment, most hydrophilic), Aerosil R816 (hexadecylsilane modified, intermediate hydrophobicity), and Aerosil R805 (octylsilane modified, most hydrophobic).

The A200 and R816 particles are water dispersible whereas the R805 particles are not. The A200 particles have a three phase contact angle (toluene-water-solid) of 0° (Yan et al., 2000). The R816 and R805 particles have a three phase contact angle of 60° and

75°, respectively (Yan et al., 2000). The contact angle estimate for the R805 particles comes from the fact they have the same methanol wettability as Evonik R974 particles, which is 45 (Michael et al., 2014. The R974 particles have a measured contact angle of 75° (Yan et al., 2000).

Silica nanoparticles (5 nm) modified with polyethylene glycol silane were supplied by 3M Corporation as a 19.7 wt% aqueous dispersion. Table 1 summarizes the properties of the different silica particles that were used in this work.

n-decane was purchased from MP Biomedical (>99% purity) and used as received. DI water was generated from a Barnstead E-Pure Ultrapure water Purification System.

Particle Name	Primary particle size (nm)	Particle specific surface area (SSA) [m²/g]	Surface modified	Modifier	Water dispersible	Decane dispersible	Methanol wettability	Air/water/silica contact angle, Θ_{aw} (°)	Toluene/water/silica contact angle, Θow (°)
A200	12[a]	175 - 225[a]	No	-	Yes	No	-	14[d]	0[d]
R816	12[a]	170 - 210[a]	Yes	$Si\text{-}C_{16}\text{-}H_{36}$[b]	Yes	Yes	-	23[d]	60[d]
R805	12[a]	125 - 175[a]	Yes	$Si\text{-}(CH_2)_7\text{-}CH_3$[b]	No	Yes	45[c]	117[d]	75[d]
3M PEG	11.4[*]	~233 - 243[**]	Yes	Polyethylene glycol	Yes	No	-	-	-

[a] [29], [b] [23], [c] [28], [d] [22], [*]measured by dynamic light scattering, [**] SSA = 6/(Dρ)

Table 5.1 – Properties of Aerosil A200, R816, R805, and 3M PEG silica particle.

5.2.2 Methods

5.2.2.1 Dynamic light scattering and zeta potential

A Malvern Zetasizer Nano ZS was used to measure the hydrodynamic diameter and zeta potential of the 3M PEG functionalized nanoparticles. Samples were prepared with 1 wt% nanoparticles in the aqueous phase. The particles had an estimated hydrodynamic diameter of 11.4 nm and a zeta potential of – 28.8 ± 1.8 mV.

5.2.2.2 Emulsion preparation

Oil-in-water Pickering emulsions were prepared in 40 mL batches using a 30 W Branson Digital Tip Sonifier with a 5 mm microtip. In a typical emulsion procedure, 20 mL of n-decane and 20 mL of nanoparticle dispersion were added to a 50 mL centrifuge vial. The 20 mL nanoparticle dispersion was a 5 wt% aqueous dispersion of 3M PEG nanoparticles. The mixture was sonicated for 10 s followed by gentle hand shaking. This was repeated two more times so that all of the oil was emulsified.

5.2.2.3 Emulsion stability to centrifugation

A centrifuge was used to assess the stability of the model Pickering emulsion. All centrifuge experiments were done within one hour of generating the emulsion. Emulsions were centrifuged for 20 minutes at 5000 x g.

5.2.2.4 Emulsion destabilization experiments

To prepare emulsions for the destabilization experiments, approximately 10 mL of the model emulsion was pipetted into a glass vial (D = 25 mm; H = 52 mm) with a

magnetic stir bar (L = 13 mm; W = 6.4 mm). The mass of the emulsion was recorded followed by adding known quantities of fumed silica powder to the emulsion. The emulsion was then stirred for 20 minutes using a stir plate. We report the mass fraction of silica added to the formulation as

$$w_{SiO_2} = \left(\frac{m_{SiO_2}}{m_{SiO_2} + m_{emulsion}} \right) * 100 \,, \tag{5.1}$$

where m_{SiO_2} is the mass of fumed silica added and $m_{emulsion}$ is the total mass of the emulsion.

To ensure the model emulsion was stable to shear induced coalescence (in the absence of added fumed silica), we monitored the change in emulsion drop size while the emulsion was stirred for 20 minutes. This was done by sampling approximately 100 µL of emulsion every five minutes and diluting the emulsion ~ 10x for drop size analysis (Figure 5.1A,B). A Nikon Labophot-Pol microscope with a Nikon Digital Sight DS-Fil camera was used to image emulsion drops.

We analyzed the size of the emulsion drops using ImageJ. We report the emulsion Sauter mean diameter (D[3,2]) which is calculated using equation 5.2. The error bars in our graph represent the standard deviation in the measurements.

$$\mathrm{D}[3,2] = \frac{\sum_i^n D_i^3}{\sum_i^n D_i^2} \,, \tag{5.2}$$

where D_i is the diameter of emulsion drop i.

5.2.2.5 Emulsion interaction with fumed silica

To visualize the interaction between the fumed silica particles and the model emulsion, we used a Nikon Labophot-Pol microscope with the Nikon Digital Sight DS-

Fil camera. Fumed silica particles were first placed on a glass microscope slide followed by contacting the model emulsion with the fumed silica particles. Images were recorded during this process.

5.3 RESULTS

The hypothesis of this work is that destabilizing a Pickering emulsion should be possible with colloidal particles provided they are sufficiently hydrophobic, which will enable the particles to dewet an emulsion film and induce coalescence. To test this hypothesis, we first had to generate a model Pickering emulsion that was stable to coalescence.

The first step in testing this hypothesis was to select a nanoparticle that was capable of stabilizing the decane/water interface. We selected silica nanoparticles modified with polyethylene glycol as an emulsion stabilizer because of their demonstrated ability to stabilize oil-in-water Pickering emulsions (Zhang et al., 2010; Bjorkegren et al., 2017).

After preliminary experimentation, we selected a formulation with a high mass fraction of 3M PEG silica nanoparticles (5 wt%) so that a stable emulsion could be generated. Figure 5.1A shows an optical micrograph of the emulsion drops after the original emulsion was dilution (10x) with deionized water. The Sauter mean diameter was ~ 6 μm, which is comparable in size to the diameters reported in (Zhang et al., 2010).

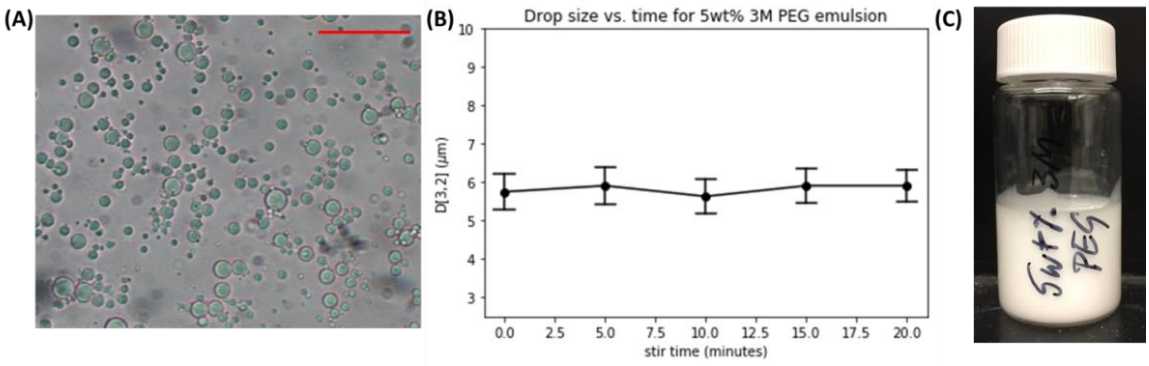

Figure 5.1 – (A) Optical micrograph of a 5 wt% 3M PEG Pickering emulsion diluted ten times (scale bar is 50 μm) (B) Change in emulsion drop size vs. stirring time (C) decane-in-water emulsion stabilized with 5 wt% 3M PEG nanoparticles after 20 minutes of stirring.

The stability of the model emulsion was characterized by centrifugation and by stirring on a stir plate. During the centrifugation experiment, no oil was released after centrifuging for 20 minutes at 5000 x g. Figure 5.1B shows a plot of emulsion drop size versus stirring time. The plot shows that there was little change in emulsion drop size with stirring time. Figure 5.1C shows a macroscopic image of the emulsion immediately after stirring for 20 minutes and shows that no oil was released. These results suggest that, in the absence of added fumed silica particles, this model Pickering emulsion was stable to coalescence both by centrifugation and stirring on a stir plate for 20 minutes.

Next, different mass fractions of fumed silica particles (0.01 – 0.34 wt%) were added to the emulsion, followed by stirring for 20 minutes. This was done to test how the wettability of the fumed silica particles affected the stability of the model emulsion. Figure 5.2A and B are images from experiments performed with the A200 (bare) and the R816 (hexadecyl-modified) fumed silica particles, respectively. It should be clear from these images that neither the bare (A200) nor the hexadecyl-modified (R816) silica

particles had any impact on the stability of this Pickering emulsion. This is because no oil was released after completing the experiments.

Figure 5.2C shows results from experiments using different mass fractions of hydrophobic R805 (octyl modified) fumed silica. The leftmost vial in Figure 5.2C shows that about 60% of the oil in the emulsion was released with just 0.01 wt% added fumed silica. This result is in contrast to emulsions stirred with the A200 and R816 particles, where no oil was released after 20 minutes of stirring. These results also show there was a relationship between the mass fraction of added R805 fumed silica and the volume of oil released during an experiment, with higher mass fractions leading to more coalesced oil. This observation occurred in the range of 0.01 wt% to 0.05 wt% R805 fumed silica particles. As the particle mass fractions were increased beyond 0.05 wt%, there was a noticeable decrease in the volume of coalesced oil, with large volumes of emulsion remaining at mass fractions above 0.13 wt%. This behavior was unexpected and explored in more detail using optical microscopy.

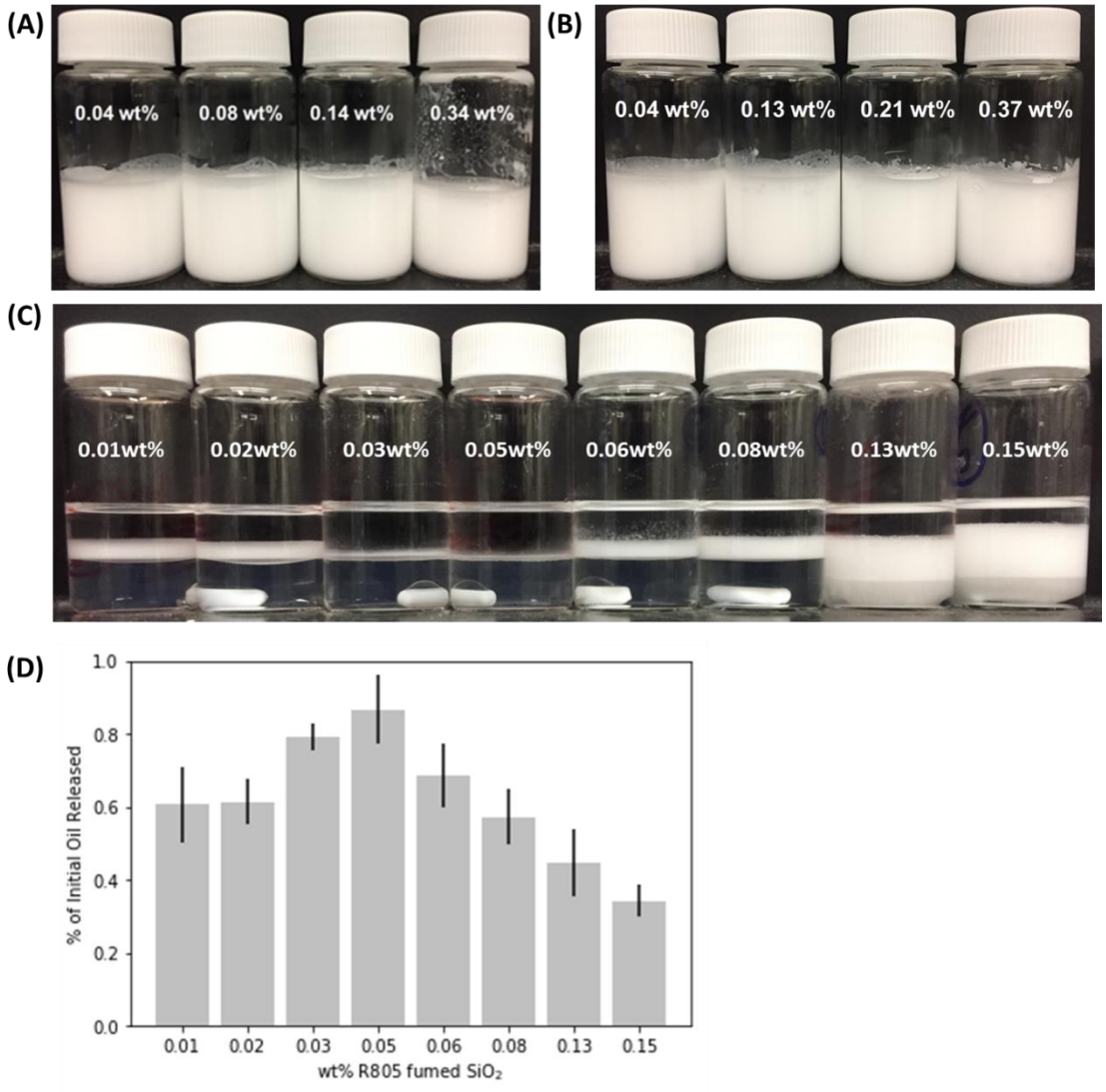

Figure 5.2 – Emulsions after 20 minutes of stirring with different mass fractions of (A) A200 (bare) fumed silica particles, (B) R816 (partially hydrophobic) fumed silica particles, (C) R805 (hydrophobic) fumed silica particles, and (D) average volumes of oil released from repeat experiments of (C).

Figure 5.3A is an optical micrograph of emulsion drops that remain after a stirring experiment with 0.01 wt% added R805 fumed silica particles and shows that the emulsion drops are not only larger in size (compared to the original emulsion, Figure

5.1A) but are also flocculated. This behavior could potentially be from the hydrophobic particles acting as a bridge between the emulsion drops.

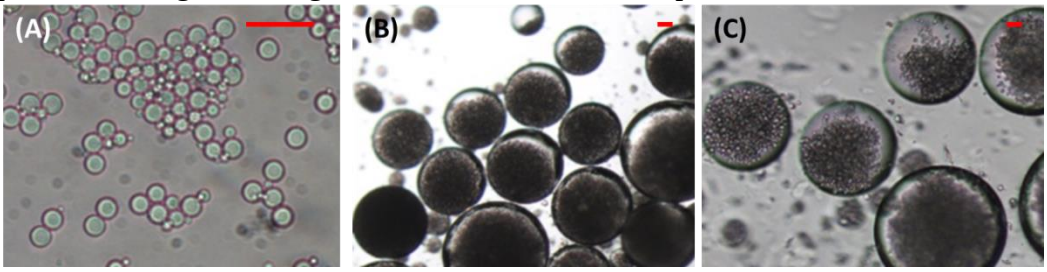

Figure 5.3 – Emulsion after 20 minutes of stirring with hydrophobic R805 fumed silica particles (A) 0.01 wt% fumed silica, (B) 0.13 wt% fumed silica, and (C) 0.13 wt% fumed silica. The red scale bar is 50 µm.

Figure 5.3B and C are optical micrographs of emulsion drops that remain after stirring for 20 minutes with 0.13 wt% R805 fumed silica particles. Both images show the emulsion drops are very large (~200 µm) and are much larger than the emulsion drops in Figure 5.3A. Upon closer inspection, the emulsion drops that remain appear to be a double emulsion consisting of the original decane-in-water Pickering emulsion but now dispersed in a continuous phase of coalesced decane oil.

Next, we used optical microscopy to monitor how the different fumed silica particles interacted with the model Pickering emulsion. Figure 5.4A-C show a time sequence of a bare A200 fumed silica particle (unmodified, hydrophilic) interacting with the emulsion. Figure 5.4A is annotated with important features, which include: the fumed silica particle, the model Pickering emulsion, and the continuous phase (water) of the emulsion on the slide.

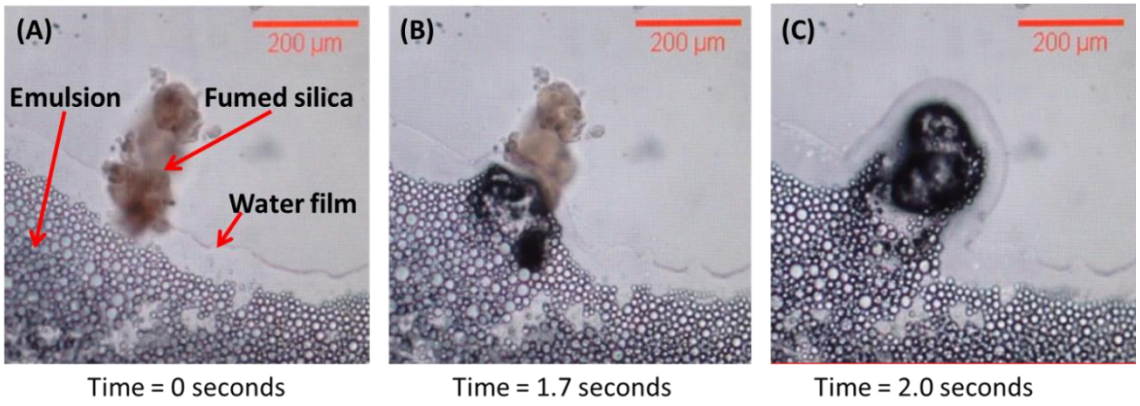

Figure 5.4 – Time lapse sequence of A200 fumed silica particles (hydrophilic, bare) interacting with the model Pickering emulsion stabilized with 1 wt% 3M PEG nanoparticles.

In general, the behavior of the A200 (bare, hydrophilic, θ=0°) fumed silica particle can be described as follows (video S1): first, a small flocculated piece of an A200 fumed silica particle was placed onto a glass slide and contacted by the model emulsion. At early time, the continuous (water) phase of the emulsion spread onto the glass microscope slide and came into contact with the fumed silica particle (Figure 5.4A). Upon this initial contact, the continuous phase of the emulsion began to wet the fumed silica particle (Figure 5.4B) and shortly after this, the particle was completely wetted by continuous phase of the emulsion (Figure 5.4C). During this process, we did not see any emulsion drops coalesce onto the silica particle surface. This observation was consistent with the results from our macroscopic stirring experiments. One important outcome from this experiment was the time it took for the A200 particle to be wetted by the continuous phase of the emulsion, which was just several seconds.

Figure 5.5A-E show optical micrographs of a time sequence of a R816 fumed silica particle (hexadecyl silane modified, intermediate hydrophobicity, θ=60°) interacting with the Pickering emulsion (video S2). Qualitatively, the R816 particle

behaved similarly to the A200 particle with the exception for the time it took for the continuous phase of the emulsion to wet the R816 fumed silica particle, which was on the order of ~5 seconds. This increase in wetting time was expected given the increased hydrophobicity of the R816 particle.

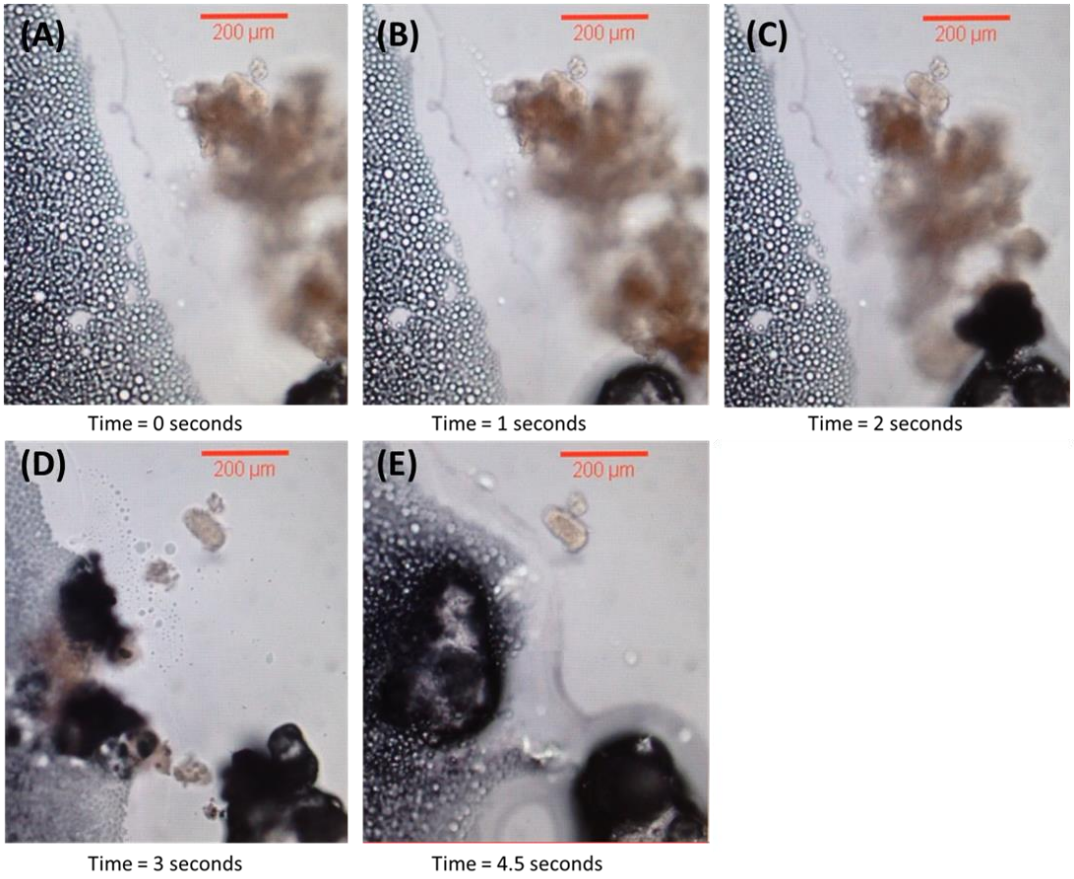

Figure 5.5 – Time lapse sequence of R816 fumed silica particles (intermediate hydrophobicity, hexadecyl silane-modified) interacting with our model Pickering emulsion stabilized with 1 wt% 3M PEG nanoparticles.

Figure 5.6A-E show optical micrographs of the R805 fumed silica particle (octyl silane modified, hydrophobic, θ=75°) interacting with the model Pickering emulsion (video S3). It should be clear from these micrographs that there was a distinct difference in how the R805 particles interacted with the model emulsion compared to the A200 and

R816 fumed silica particles and highlight two major differences. First, the R805 particle was never completely wetted by the continuous phase of the emulsion, which was due to the hydrophobicity of the particle. Second, although the R805 particle was never wetted by the continuous phase of the emulsion, there were still significant interactions between the emulsified oil drops and the R805 particle surface and we highlight these interactions by comparing Figure 5.6B and C. Figure 5.6B is an image of the emulsion after it was exposed to an R805 particle for about six seconds. In this image, the particle was free of dark spots. Figure 5.6C, which was taken 18 seconds later, shows that the R805 particle increased in darkness compared to Figure 5.6B . This change in color from light to dark was due to the emulsified oil drops wetting the R805 particle surface and was consistently seen throughout these experiments.

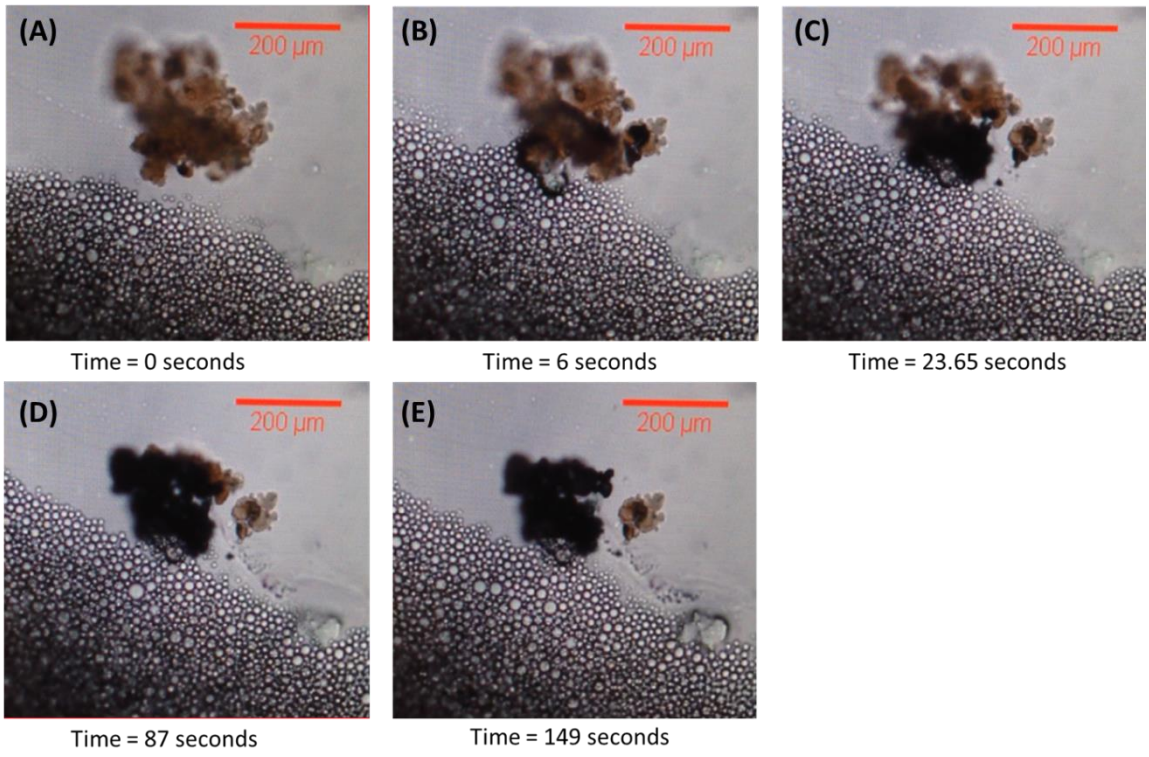

Figure 5.6 – Time lapse sequence of R805 fumed silica particles (hydrophobic, octyl silane-modified) interacting with our model Pickering emulsion stabilized with 1 wt% 3M PEG nanoparticles.

5.4 DISCUSSION

The results from our destabilization experiments show that there is a strong correlation between the wettability of a particle and its ability to destabilize this model Pickering emulsion, with more hydrophobic particles showing a greater tendency to coalesce the emulsion. Our macroscopic stirring experiments (Figure 5.2A,B) clearly indicate that the hydrophilic fumed silica particles (A200 and R816) were unable to destabilize the Pickering emulsion. This is because the particles were almost instantly (<5 seconds) wetted by the continuous phase (water) of the emulsion (see Figure 5.4C and Figure 5.5E), which resulted in a thin film of water around the particle and prevented any

interaction between the emulsified oil drops and silica particle surface. The lack of macroscopic coalescence in the experiments with the bare, A200, and the partially hydrophobic, R816, particles was not completely unexpected. This is because increased concentrations of A200 fumed silica particles are known to act as emulsion stabilizers (Santos et al., 2018) by forming three dimensional networks in the continuous phase of an emulsion and because R816 particles are known to strongly adsorb to the oil/water interface to stabilize oil-in-water Pickering emulsions (Katepalli et al., 2017).

The R805 fumed silica particles, on the other hand, coalesced ~60% of the emulsified oil with just 0.01 wt% in the formulation, which increased to ~85% with 0.05 wt% R805 particles. Our optical micrographs (Figure 5.6A-E) show that the interactions between the hydrophobic particles and the model Pickering emulsion were significantly different compared to the water dispersible A200 and R816 fumed silica particles. Because the R805 particles are very hydrophobic, they were never wetted by the continuous phase of the emulsion (Figure 5.6E). However, we still observed significant interactions between the emulsified oil drops and the fumed silica particle surface, which resulted in the emulsified oil drops wetting the silica particle surface and eventually macroscopic coalescence.

Our results also show that at high concentrations of R805 particles (> 0.05 wt%), there was a sharp decrease in the volume of coalesced oil. This was due to the formation of a double emulsion (Figure 5.3B, C), which was composed of the original oil-in-water Pickering emulsion but now dispersed in coalesced decane oil. The interface of this double emulsion was likely stabilized with the excess R805 particles. We note that this double emulsion was very weak, as it was easily destabilized under the force of a glass cover slip (as it was placed onto the emulsion). We did not explore these double emulsions in more detail.

Based on these results, it appears the mechanism responsible for emulsion coalescence (of this Pickering emulsion) differs from what is reported in the literature on destabilizing surfactant stabilized emulsions (with fumed silica particles). In Katepelli et al. (2016), emulsions were destabilized due to hydrophobic interactions between the surfactant tail and C16 chains on the R816 fumed silica particle surface. These interactions depleted surfactant from the oil/water interface and led to an increase in interfacial tension between oil and water. This was experimentally characterized by surface and interfacial tension measurements. The result of depleting surfactant from the oil/water interface was complete coalescence of their dilute model emulsion. Based on what was described in their work, the fumed silica particles only interacted with the surfactant (Triton X-100) and not the emulsified oil, like in the case of our experimental results.

In our work, nanoparticles were used to stabilize the oil/water interface rather than surfactants. This is an important difference between our system and the one presented in Katepelli et al. (2016) and we highlight this difference to argue that we are not displacing particles from the oil/water interface, but instead using the hydrophobicity of the silica particles to wick/remove oil from the emulsified oil drops.

Because we use nanoparticles to stabilize this model emulsion, we can assume they are irreversibly adsorbed to the oil/water interface (Aveyard et al., 2003). This assumption is justified based on the attachment energy of a single polyethylene glycol-modified silica particle, which we calculate using equation 5.3

$$\Delta G_{adsorption} = \pi r^2 \gamma_{o/w} (1 \pm cos\theta)^2, \quad (5.3)$$

where r is the nanoparticle radius, $\gamma_{o/w}$ is the interfacial tension between decane and a 5 wt% dispersion of polyethylene glycol-modified silica nanoparticles, and θ is the three phase contact angle the particle forms at the oil/water interface. The radius of these

nanoparticles is estimated to be ~5.7 nm and the interfacial tension between decane and a 5 wt% nanoparticle dispersion is ~20 mN/m (Metin et al., 2012). We assume a three phase contact angle of 60°, which is reasonable given the particles are water dispersible and prefer to reside in the aqueous phase. Using these values, we obtain a particle attachment energy of ~100 kT, which is sufficiently high to justify the irreversible adsorption of particles to the oil/water interface. Moreover, we experimentally showed that the stirring method we have selected had no effect on the emulsion drops size (Figure 5.1B), indicating the shear rate that we used was low enough to not desorb particles from the oil/water interface.

We can also assume that the addition of hydrophobic fumed silica particles to the emulsion had little impact on the interfacial tension between decane and the nanoparticle dispersion. This is a valid assumption because hydrophobic fumed silica particles are known to have little effect the interfacial tension of oil/water systems (Drelich et al., 2010). Therefore, our assumption of the irreversible adsorption of polyethylene glycol-modified particles to the oil/water interface is still valid even with the addition of fumed silica particles.

We also point out that this Pickering emulsion was made in the absence of salt. Because of this, the polyethylene glycol-modified silica nanoparticles carry significant surface charge, which we determined to be -28.8 ±1.8 mV. This high particle surface charge implies the particles likely did not form hexagonally close packed arrangements on the oil drop surface due to lateral electrostatic repulsion between particles (Ridel et al., 2016). The consequence of this is that the emulsified oil drops likely contained free interstitial sites which provide access points for the fumed silica particles to interact with the emulsified oil drop (Griffith and Daigle, 2018; Derakhshandeh et al., 2018).

Based on this analysis, it is reasonable to assume that the destabilization of this model Pickering emulsion was driven by the wettability of a fumed silica particle and not from particles detaching from the oil/water interface. This is experimentally supported by the fact that in all of our experiments we never coalesced all of the emulsified oil (in any experiment), which would have occurred if the particles were desorbed from the oil/water interface. This behavior of emulsion destabilization being driven by particle wettability appears to closely align with how hydrophobic silica particles destabilize foams (Denkov, 2004) and how fat crystals partially coalesce food emulsions (Boode and Walstra, 1993).

5.6 CONCLUSIONS

In this work, we used commercially available fumed silica particles to destabilize a model Pickering emulsion. Our results show that there is a strong correlation between the wettability of a fumed silica particle and its ability to destabilize the model emulsion, with more hydrophobic particles showing a greater tendency to induce coalescence. The hydrophilic (A200) and partially hydrophobic (R816) particles were unable to destabilize the model emulsion. This is because they were almost immediately wetted by the continuous phase of the emulsion which resulted in a thin film of water around the particle surface, preventing the emulsified oil drops from interacting with the fumed silica particles. Only the very hydrophobic (R805) particles were capable of destabilizing the model emulsion. We determined that destabilization was the result of the emulsified oil (stabilized by polyethylene glycol-modified nanoparticles) preferring to wet the surface of the hydrophobic particles instead of remaining as emulsified oil. This qualitative description of our system differs from how fumed silica particles destabilize surfactant stabilized emulsions (Katepalli et al., 2016; Aveyard et al., 1999). However, our results appear to closely align with how colloidal particles destabilize foams

(Denkov, 2004) and how fat crystals partially coalesce food emulsions (Boode and Walstra, 1993).

This work highlights that fumed silica particles are capable of destabilizing a Pickering emulsion, which has previously not been described in any detail in the literature (Whitby and Wanless, 2016). Additionally, this work shows that some of the practical limitations with using surfactants or solvents to destabilize Pickering emulsions (i.e., high shear rates (Vashisth et al., 2010) and large volumes of solvent (Whitby et al., 2016)) can be overcome by using colloidal silica particles. Interesting future work could focus on the relationship between nanoparticle surface coverage (on an emulsion drop surface) and the ability for the fumed silica particle to destabilize the emulsion.

Chapter 6: On the shear stability of water-in-water emulsions stabilized with silica nanoparticles[3]

6.1 INTRODUCTION

Recently, researchers have used nano- (Murray and Phisarnchananan, 2014; Vis et al., 2015; Hann et al., 2017; Ganley et al., 2017)and micron- (Balakrishnan et al., 2012) sized particles to stabilize water-in-water (w/w) emulsions using many of the same concepts developed for immiscible Pickering emulsions. W/w emulsions originate from aqueous, two-phase systems (ATPS) and form when two incompatible solutes (e.g., polyethylene glycol (PEG)/dextran, PEG/magnesium sulfate, etc.) are added to a solution above some minimum concentration (Song et al., 2013; Ganley et al., 2017). Above this concentration, the free energy of mixing is positive (Frith, 2010) and the two solutes cannot physically coexist, leading to their separation and the presence of two aqueous phases, each enriched in one of the solutes.

Stabilizing a ATPS is difficult because of the length scale of the interface (Ayed et al., 2018), which is often much larger and more diffuse than systems of two immiscible fluids (Vis et al., 2015). This prevents surfactant molecules from being used as a interface stabilizer (Gonzalez-Jordan et al., 2018). Therefore, stabilization is only possible with solid particles or large block chain copolymers which are capable of spanning the length of the interface (Buzza et al., 2013).

Two questions that frequently arise regarding the stability of w/w emulsions are whether particles are irreversibly adsorbed to the interface and whether the emulsions are stable to shear (orthokinetically stable). These questions are legitimate and stem from the

[3]This chapter was published in the Journal of Colloid and Interface Science as: C. Griffith, H. Daigle, On the shear stability of water-in-water emulsions stabilized with silica nanoparticles, Journal of Colloid and Interface Science. 532 (2018) 83-89.

low interfacial tensions (IFT) between the two aqueous phases (Nguyen et al., 2015). The IFTs, which can be as low as 10^{-3}mN/m, can lead to low particle attachment energies that are on the order of just several kT (Nguyen et al., 2015).

The issue of orthokinetic stability was briefly discussed in Balakrishnan et al. (2012). In that work, the authors studied an emulsion system of $2x10^5$ g mol^{-1} PEO and $5x10^5$ g mol^{-1} dextran stabilized with polystyrene particles. They mentioned that systems with high interfacial tensions (>0.1 mN/m) required "strong shear" to destabilize the w/w Pickering emulsions whereas those with low interfacial tensions ($\lesssim$0.01 mN/M) only needed "gentle stirring" for destabilization. Numerous articles have characterized the static stability (change in drop size vs. time under static conditions) of w/w emulsions (Vis et al., 2014; Nguyen et al., 2015; Ganley et al., 2017; Gonzalez-Jordan et al., 2018), but very few have studied the orthokinetic stability of w/w emulsions, which is the motivation of this work.

We studied the behavior of w/w emulsions made from the ATPS of polyethylene glycol and magnesium sulfate. This system was selected because of its low cost (Azevedo et al., 2009) and the low interfacial tensions that can be achieved between the two phases (Jafarabad et al., 1992; Wu et al., 1996). We first defined the boundary of the aqueous two phase region followed by establishing tie lines and their lengths so interfacial tensions could be estimated from published correlations (Wu et al., 1996). We then demonstrated that it was possible to stabilize emulsions with 6 nm and 50 nm silica particles silanized with 2-(methoxy(polyethyleneoxy)6-9propyl)trimethoxysilane. The drop sizes of the different particle-stabilized emulsions were characterized as a function of particle size, particle concentration, and their static stability vs. time. We used results from optical microscopy and rheological measurements to select an emulsion system that had similar properties (drop size and viscosity) regardless of the nanoparticle size. We

then studied the orthokinetic stability of these emulsions using published protocols (Whitby et al., 2011).

6.2 MATERIALS AND METHODS

6.2.1 Materials:

6 nm (NexSil 6, 17 wt%, pH 10) and 50 nm (NexSil 85-40, 40 wt%, pH 10) silica nanoparticles were supplied by Nyacol Technologies. The specific surface area (SSA) of the particles were 445 m^2/g (6 nm) and 60 m^2/g (45 nm) (provided by Nyacol). 2-(methoxy(polyethyleneoxy)6-9propyl)trimethoxysilane (PEG-silane) was purchased from Gelest (Cat No: 65994-07-2, 90%). BioUltra Polyethylene glycol (PEG) with an average molecular weight of 20,000 g mol^{-1} (16,000-24,000 g mol^{-1}) was purchased from Sigma Aldrich (Cat No: 95172-250G-F). Anhydrous magnesium sulfate was purchased from Fisher Scientific (Cat No: M65-500). Deionized (DI) water was generated from a Barnstead E-Pure Ultrapure water Purification System. PEG polymer dispersions were centrifuged to remove silica impurities (Nguyen et al., 2015). All other materials were used as received.

6.2.2 Methods

6.2.2.1 Nanoparticle functionalization

Silica nanoparticles were modified with 2-(methoxy(polyethyleneoxy)6-9propyl)trimethoxysilane (PEG-silane) following others (Worthen et al., 2016; Bjorkegren et al., 2017). 2 μmol PEG-silane/m^2 of nanoparticle surface area was used to functionalize the nanoparticles. For a typical reaction, the appropriate mass of PEG-silane

was added to DI water and stirred for 5 minutes at room temperature. This mixture was added dropwise to a dispersion of nanoparticles so the combined weight percent of nanoparticles and PEG-silane was approximately 19-20 wt%. The solution was stirred overnight at 60°C to complete the hydrolysis condensation reaction. The pH of the mixture upon completion of the reaction was approximately 10-10.1. The functionalized particles were used without purification.

6.2.2.2 Dynamic light scattering

A Malvern Zetasizer Nano ZS was used to measure the volume average hydrodynamic diameter and zeta potential of the bare and PEGylated functionalized nanoparticles. Samples were prepared with 1 wt% nanoparticles in the aqueous phase.

6.2.2.3 Determination of polyethylene glycol and magnesium sulfate two-phase boundary

The PEG/$MgSO_4$ phase envelope was constructed using the turbidometric titration method (Kaul, 2000). Concentrated stock solutions of 40 wt% PEG (unadjusted pH = 10.5) and 23 wt% $MgSO_4$ (unadjusted pH = 8.5) were prepared by mixing PEG polymer flakes or $MgSO_4$ with DI water. The mixtures were stirred overnight at room temperature. Five mixtures with different mass ratios of stock PEG and $MgSO_4$ solutions were prepared and placed on a stir plate. The solutions were diluted with DI water until a clear, turbid free solution was obtained (Kaul, 2000; Ganley et al., 2017). The five mixtures had initial PEG:$MgSO_4$ mass ratios of 5:1, 4:2, 3:3, 2:4, and 1:5, and correspond to points (1)-(5) in Figure 6.1A. The mass of DI water used to obtain a clear solution for each of the five mixtures was recorded and used to calculate the final mass ratios of PEG and $MgSO_4$ in each mixture so points on the two phase boundary could be established

(Figure 6.1A, solid black line). We performed the turbidometric titration experiment three times.

6.2.2.4 Tie line determination

Tie lines were established by preparing mixtures with different concentrations of PEG and $MgSO_4$ in the two phase region. The top and bottom phases were analyzed using the gravimetric method (de Araujo Sampaio, 2016). This was done by using a volumetric pipette and pipetting a known volume of sample (4 ml) and measuring its mass. Because it was difficult to accurately measure the density of the viscous PEG-phase, we also measured its viscosity. This was done by shearing samples for two minutes at a constant shear rate of 10 s^{-1} and recording the viscosity. Solutions of different total mass ratios were tested until solutions had the same top phase density and viscosity and bottom phase density (Figure 6.1A, points 6 and 7), which is a requirement for solutions on the same tie line. For a more detailed description see (Raja et al., 2011; de Araujo Sampaio, 2016). We did not measure the viscosity of the bottom $MgSO_4$ phase because of how low it was (μ_{bottom} = ~10^{-3} Pa-s) which made it difficult to reliably detect viscosity differences of the different $MgSO_4$ phases (Mei et al., 1995). The tie line length (TLL) was used to estimate the interfacial tension between the two phases.

6.2.2.5 Emulsion preparation

Emulsion samples (10 grams total) were prepared by pipetting the appropriate mass of the stock PEG, $MgSO_4$, and DI water into glass vials (D = 2.5 cm; H = 5.2 cm) and gently shaking to equilibrate the two aqueous phases. Nanoparticles were added to the PEG phase to achieve the desired nanoparticle wt%. Emulsions were prepared with nanoparticle concentrations (Cp) that ranged from 0-6wt%. The ATPS mixtures were

emulsified using an IKA T18 Digital Ultra Turrax rotor stator homogenizer for 1 minute at 5,000 rpm.

6.2.2.6 Light microscopy

A Nikon Labophot-Pol microscope with a Nikon Digital Sight DS-Fil camera was used to obtain optical micrographs for drop size analysis. Approximately 50 µl of emulsion was placed on a glass microscope slide and covered with a glass cover slip. For emulsions with 6 wt% nanoparticles, the emulsions were sometimes diluted with an equilibrated continuous phase from the ATPS to enable drop size analysis. We analyzed approximately 300 emulsion drops and used ImageJ to calculate their Sauter diameters (D[3,2]) using equation 6.1. The error bars represent the standard deviation in the measurements.

$$\mathrm{D}[3,2] = \frac{\sum_i^n D_i^3}{\sum_i^n D_i^2}, \tag{6.1}$$

6.2.2.7 Rheology

Rheological measurements were performed with a TA Instruments AR-G2 magnetic bearing rotational rheometer using a 40 mm 2° cone and plate geometry. Samples (1 ml) were placed on the Peltier plate using a spatula and pre-conditioned by shearing for 10s at a rate of 10 s^{-1}, followed by 1 minute of rest. Oscillatory strain sweep measurements were performed by varying the strain amplitude from γ=0.5-1000% using a constant frequency of 1 Hz. All measurements were performed at 25 °C. Error bars represent the minimum and maximum data points from two measurements. For the shear induced coalescence experiments, we did not pre shear the emulsions.

6.3 RESULTS

6.3.1 Nanoparticle functionalization

We modified 6 nm and 50 nm silica particles with 2-(methoxy(polyethyleneoxy)6-9propyl)trimethoxysilane (PEG-silane). These particles will be referred to as PEGylated particles for the remainder of this work. We selected this modifier because previous work has proven it to be quite versatile in stabilizing various emulsions (Zhang et al., 2010; Espinosa et al., 2010; Worthen et al., 2013; Bjorkegren et al., 2017). Additionally, upon our initial experimentation, these particles demonstrated the ability to stabilize the PEG/ $MgSO_4$ interface. Table 6.1 shows results of the volume average dynamic light scattering measurements (DLS) for bare and PEGylated silica nanoparticles. The bare 6 nm and 50 nm particles had hydrodynamic diameters of 9.5 and 48.5 nm with a zeta potential of approximately -42 mV. After modification, the particles increased in size to 12.2 and 50.7 nm and the zeta potential decreased to -34 mV.

	Hydrodynamic Diameter DLS		Zeta Potential (mV)	
Particle	Bare	2 µmol m^{-2} PEG	Bare	2 µmol m^{-2} PEG
NexSil 6	9.5 (0.218)	12.2 (0.237)	-42.1±23.2	-33.5±20.6
NexSil 85	48.5 (0.066)	50.7 (0.083)	-41.3±21.4	-35.0±22.0

Table 6.1 – Size and zeta potential of bare and PEGylated functionalized silica nanoparticles. The volume weighted particle size is reported. The numbers in parenthesis next to the particle size is the particle distribution index (PDI).

6.3.2 Magnesium sulfate and polyetheylne glycol binodal and tie lines

The goal of this work was to assess the stability of w/w Pickering emulsions (under simple shear flow) stabilized with nanoparticles of different size and to correlate the relationship between emulsion stability and particle size. The low IFT between the PEG and $MgSO_4$ phases (Song et al., 2013) allows for low particle attachment energies to be achieved. The target range of attachment energies for this study was several 10 of kT to 100 of kT, which meant that an IFT of about 1 mN/m was needed if particles with diameters of 6 nm and 50 nm were used. This was determined from equation 1 where R is the particle radius, γ is IFT, and θ is the three phase contact angle. We assumed a contact angle of 80° and selected this based on the observation that the PEGylated particles prefer to reside in the PEG phase and therefore we anticipate the contact angle will be less than 90°. A conservatively high value of 80° was chosen.

$$E = \pi R^2 \gamma (1 - |cos\theta|)^2, \quad (6.2)$$

In order to identify a set of PEG and $MgSO_4$ compositions that produced an IFT close to 1 mN/m, we first defined the two phase boundary for the system (Figure 6.1A, solid black line), and then established tie lines and their respective lengths. The tie line length is an important parameter to characterize because it defines final mixture compositions where the top and bottom phase have the same compositions on a particular tie line. This leads to a constant IFT along a single tie line (de Freitas et al., 2016). The IFT of an ATPS generally scales with the TLL to some power with longer tie lines associated with larger IFTs (Wu et al., 1996).

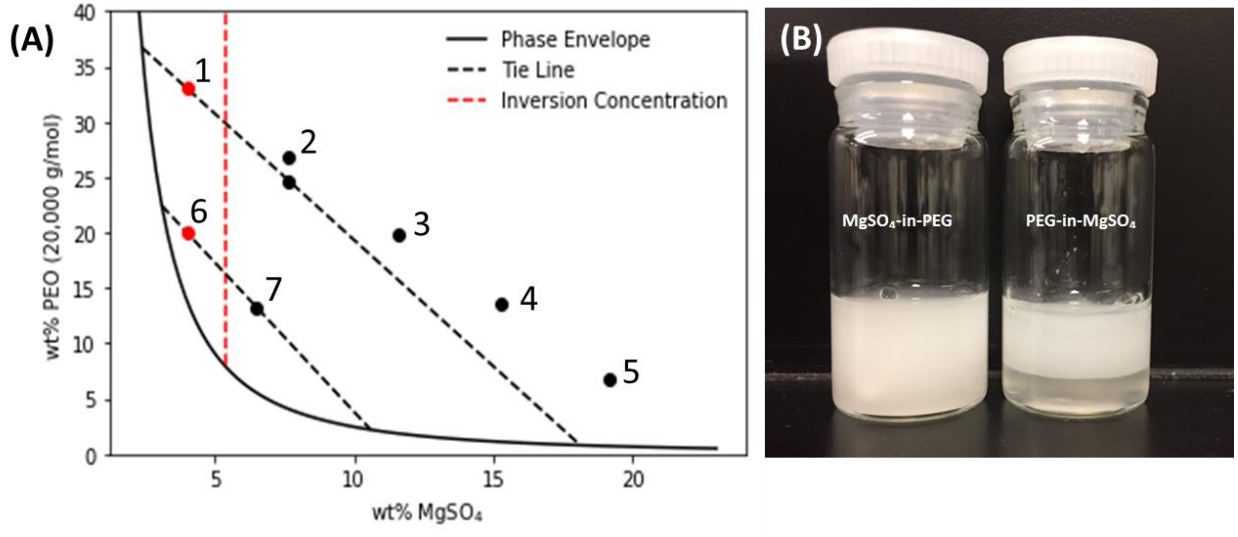

Figure 6.1 – (A) Phase envelope of the $MgSO_4$/PEG aqueous two phase system. Numbers (1)-(5) represent the starting compositions of the solutions used to generate the two phase boundary (black solid line). The black dashed lines are tie lines. The red, dashed vertical line, represents the inversion $MgSO_4$ concentration. Mixtures to the left of the line are $MgSO_4$-in-PEG emulsions whereas mixtures to the right are PEG-in-$MgSO_4$ emulsions. (B) Left: image of point 6 in (A) the emulsion is $MgSO_4$-in-PEG. Right: image of point 7 in (A) the emulsion is PEG-in-$MgSO_4$.

For this work, we established two tie lines (Figure 6.1A, dashed black lines) which were determined by gravimetric analysis and rheological measurements. The top and bottom tie lines in Figure 6.1A have lengths of 38.8 wt% (TL slope = -2.83; μ_{top} = 0.90 Pa-s) and 21.5 wt% (TL slope = -2.70; μ_{top} = 0.14 Pa-s), respectively. The IFTs associated with these TLLs were estimated to be 1.60 mN/m (TLL = 38.8wt%) and 0.77 mN/m (TLL = 21.5wt%) and were calculated using the following empirical correlation from (Wu et al., 1996):

$$\log(\sigma) = a_1 + b_1 \log(\mathrm{TLL}), \quad (6.3)$$

where σ is the interfacial tension in units of mN/m and TLL is in units of wt%. a_1 and b_1 are empirical constants and were 1.76 and 1.24, respectively, and determined from log-

log plots using the data in Table 2 of (Wu et al., 1996) and linearly extrapolating to a PEG MW of 20,000 g mol^{-1}. The IFTs reported here are only estimates and were not experimentally determined. More accurate methods for determining the IFT are the spinning drop (Wu et al., 1996), droplet relaxation (Ganley et al., 2017), or single wall methods (Aarts et al., 2003).

6.3.3 Emulsion type determination

Determining if a PEG-in- $MgSO_4$ or $MgSO_4$-in-PEG emulsion was formed was done by qualitative inspection of the Stokes settling velocity equation and has been used by others (Asenjo and Andrews, 2012) to aid in emulsion type determination of polymer/salt systems. The Stokes settling velocity is given by:

$$v_{Stokes} = \frac{2}{9}\frac{\Delta\rho R^2 g}{\eta}, \quad (6.4)$$

where R is the radius of an emulsion drop, g is gravitation acceleration, $\Delta\rho$ is the density difference between the two phases, and η is the viscosity of the continuous phase. Equation 4 implies that if the two aqueous phases have large viscosity differences, then the emulsion type can be determined by the rate of droplet creaming/sedimentation, which is controlled by the viscosity of the continuous phase. In a polymer/salt ATPS the difference in viscosity can vary by several orders of magnitude ($\eta \sim 1$ Pa-s for 40 wt% 20,000 g mol^{-1} PEG; $\eta \sim 10^{-3}$ Pa-s for 23 wt% $MgSO_4$). Therefore, if the continuous phase is the PEG phase, the rate of sedimentation of emulsified $MgSO_4$ drops will be slow, while if the $MgSO_4$ phase is continuous, the emulsified PEG drops will rapidly cream and drainage of the $MgSO_4$ phase will be fast.

Figure 6.1B shows two w/w emulsions prepared on the same tie line (TLL = 21.5 wt%) approximately one minute after the mixtures were removed from a stir plate. The

emulsion on the left (20 wt% PEG, 4 wt% $MgSO_4$) was determined to be an $MgSO_4$-in-PEG emulsion due to the presence of slowly settling $MgSO_4$ drops whereas the emulsion on the right (13.3 wt% PEG, 6.5 wt% $MgSO_4$) was determined to be a PEG-in- $MgSO_4$. Phase separation occured on the order of tens of minutes for the $MgSO_4$-in-PEG emulsion and in minutes for PEG-in- $MgSO_4$ emulsions.

Using this same method of analysis, emulsions were prepared along the same tie line (TLL = 21.5 wt%) so the inversion point of the system could be defined. The inversion point occurred at a constant $MgSO_4$ concentration of 5.4 wt% (Figure 6.1A, red vertical dashed line). Therefore, emulsions prepared with $MgSO_4$ concentrations below 5.4 wt% were $MgSO_4$-in-PEG whereas those prepared above this concentration were PEG-in-$MgSO_4$ emulsions. The constant salt inversion concentration obtained here is consistent with the PEG/salt system described in (Asenjo and Andrews, 2012). This contrasts polymer/polymer systems where the inversion point is instead determined by which phase has a larger volume and typically occurs somewhere near the midpoint of a particular tie line (Esquena, 2016).

For the remainder of this work, we studied $MgSO_4$-in-PEG emulsions that fell on a tie line with a length of 21.5 wt% and had an estimated IFT of 0.77 mN/m. The final composition of PEG and $MgSO_4$ was 20 wt% and 4 wt%, respectively. The volume fraction of $MgSO_4$ was 17%. These emulsions are considered dilute. The top phase had 0.5 wt% $MgSO_4$, which was determined by conductivity measurements. The top, PEG-rich phase had a viscosity of 0.14 Pa-s. We note these nanoparticles did not show any ability to stabilize PEG-in-$MgSO_4$ emulsions.

6.3.4 Properties of nanoparticle stabilized emulsions

Emulsions were prepared by mixing PEG, $MgSO_4$, and DI water into glass vials followed by gentle shaking to equilibrate the phases. The PEGylated nanoparticles were then introduced into the PEG-rich/ $MgSO_4$ phase. Upon their addition, it was observed the particles began to flocculate. We determined the critical flocculation concentration (cfc) of $MgSO_4$ in a 20 wt% PEG polymer dispersion with 6 wt% PEGylated nanoparticles to be approximately 0.12 wt%. This was done by visual inspection by monitoring different dispersions and observing the salt concentration required for increased turbidity. We note that for the nanoparticle concentrations studied here (0-6 wt%), the PEGylated particles were stable in concentrated solutions of PEG in the absence of $MgSO_4$. Additionally, the particles did not immediate flocculate when they were added into DI water with 0.5 wt% $MgSO_4$, implying that a combination of $MgSO_4$ and PEG polymer was necessary for particle flocculation. The ATPS mixtures were then emulsified using a rotor stator (Figure C3 A,B).

Figure 6.2A shows a flocculated dispersion of 2 wt% (6nm) PEGylated particles, 20 wt% PEG, and 0.5 wt% $MgSO_4$. At this $MgSO_4$ concentration, only one aqueous phase was present, and the salt concentration was above the cfc, leading to the presence of visible flocs. It is clear from the image that the flocculated particles are arranged into a semi-structured particle network containing pore spaces which show similar structure to flocculated Ludox silica particles in the presence of a low molecular weight polymer (Hassander et al., 1989) and fumed silica particles dispersed in water (Juarez and Whitby, 2011).

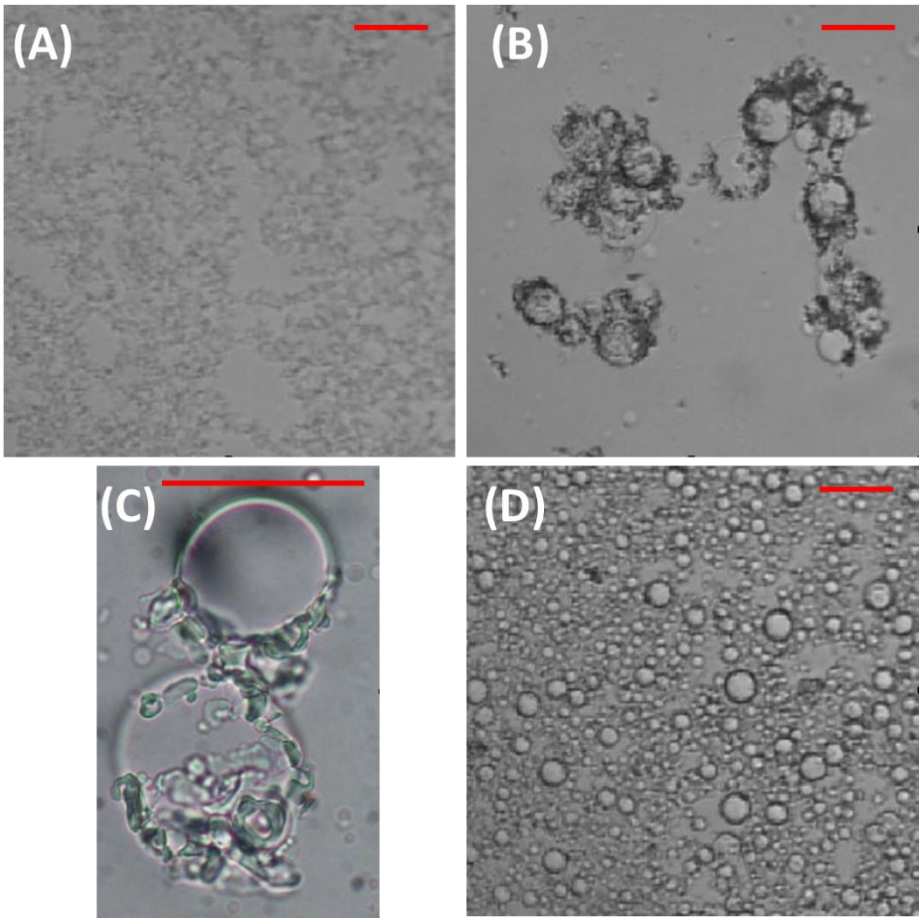

Figure 6.2 – Optical micrograph of: (A) 2 wt% flocculated 6nm PEGylated nanoparticles in a 20 wt% PEG and 0.5 wt% $MgSO_4$ dispersion. (B) Emulsified $MgSO_4$ drops with flocculated PEGylated particles/PEG polymer adsorbed to $MgSO_4$/PEG interface. (C) Zoomed in micrograph of (B), (D) Emulsified $MgSO_4$ drops with 6 wt% 6nm PEGylated particles. The red scale bar represents 50 µm.

Figure 6.2B is an optical micrograph of an $MgSO_4$-in-PEG emulsion made from a mixture with 20 wt% PEG, 4.0 wt% $MgSO_4$, and 2 wt% nanoparticles. The image shows flocculated particles/PEG at the interface of $MgSO_4$ drops. Comparison of Figure 6.2A and B illustrates that a large majority of the flocculated particles that were present in Figure 6.2A are no longer visibly present in the continuous phase of Figure 6.2B, which is due to their accumulation at the interface of $MgSO_4$ drops. Figure 6.2C is an image of

the same emulsion in B, however at 4x the magnification, and shows only partial coverage of the $MgSO_4$ with flocculated particles/PEG (at 2 wt%). The lack of static stability of these drops (with respect to time) is illustrated in Figure 6.3B which plots emulsion drop size vs. time. This plot shows the size the emulsion drops stabilized with 6 nm and 50 nm particles (at 2 wt%) grew rapidly over a periods of three days. However, when 6 wt% particles were used, the emulsion drops showed little change in drop size over a period of seven days (Figure 6.3B), which is due to a combination of increased particle coverage on the emulsion drop surface and due to the formation of a particle network in the continuous phase of the emulsion.

Figure 6.2D is an emulsion prepared from a mixture using 6 wt% particles and shows that flocculated particles are present the continuous phase of the emulsion. The increased particle concentration led to smaller emulsion drops (Figure 6.3A) which is frequently seen in particle stabilized emulsions (Chevalier and Bolzinger, 2013). The structure of the flocculated particles in this emulsion appears to be similar to the dispersion of flocculated particles in Figure 6.2A. The presence of flocculated particles in the continuous phase of Pickering emulsions is not unexpected and has been reported in w/w emulsions made from polyethylene oxide/dextran systems stabilized with high aspect ratio cellulose nanocrystals (Peddireddy et al., 2016; Ayed et al., 2018) and in traditional oil/water Pickering emulsions stabilized with fumed silica in the presence of salt (Katepalli et al., 2017).

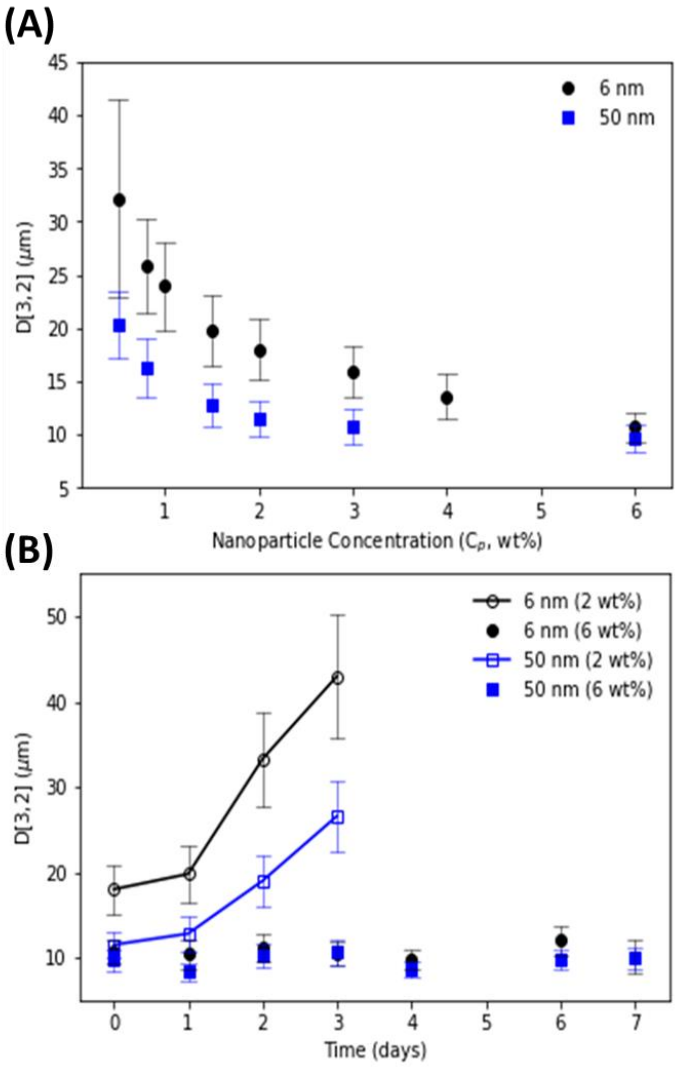

Figure 6.3 – (A) emulsion drop size vs. nanoparticle concentration using 6 nm (black markers) and 50 nm (blue markers) particles. (B) Drop size vs. time for 6 and 50 nm particle stabilized emulsions using 2 wt% and 6 wt% particles.

6.3.5 Rheology

Figure 6.4(A,B) are oscillatory strain sweep measurements of emulsions stabilized with 6 nm (black markers) and 50 nm (blue markers) particles at 2 wt%. At the range of strain amplitudes imposed (0.5-1000%), there was no evidence of viscoelastic

behavior in either sample as G”>G’ throughout the measurement. The loss moduli (G”) of the two emulsions are similar at all strain amplitudes (Figure 6.4B). This implies the samples have similar viscosities and that nanoparticle size does not significantly impact the viscosity of the emulsions. The storage moduli (G’) of the two samples deviate from one another at strain amplitudes greater than 3%. We did not investigate these emulsions any further because of their lack of static stability with time (Figure 6.3B).

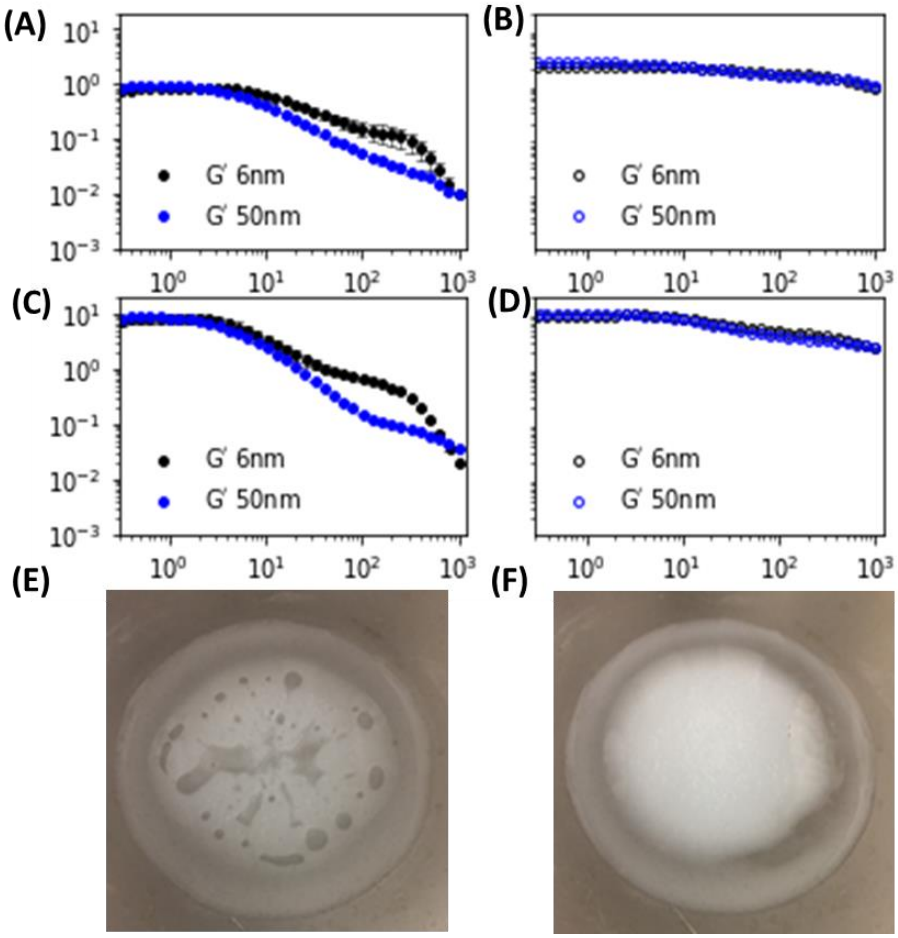

Figure 6.4 – Oscillatory rheology measurements of emulsions stabilized with 2 wt% particles (A,B) and 6 wt% particles (C,D). G’ (filled), G” (open) symbols. Image (E) is a 6 wt% 6nm emulsion after a shear sweep experiment. Image (F) is a 6 wt% 50nm emulsion after a shear sweep experiment.

Figure 6.4(C,D) show oscillatory strain sweep measurements of emulsions stabilized with 6 nm and 50 nm particles at 6 wt%. At this concentration, the loss and storage moduli are about an order of magnitude larger than emulsions stabilized with 2wt% particles. At low strain amplitudes (γ <1%), the emulsions show evidence of viscoelastic behavior as G' (Figure 6.4C) and G" (Figure 6.4D) are comparable to each other (~ 10 Pa). However, G' is never significantly larger than G" (for these two samples), implying the emulsions are only weakly viscoelastic. Similar in behavior to emulsions stabilized with 2 wt% particles, the 6 wt% emulsions show nearly identical loss moduli (G") throughout the measurement (Figure 6.4D), indicating that particle size does not have a large impact on viscosity. Deviation in the storage moduli (G') occurred at strain amplitudes greater than 19%.

Because these emulsions are dilute (17% by volume $MgSO_4$), the presence of viscoelasticity at 6 wt% nanoparticle loading was due to flocculated particles in the continuous phase of the emulsion. However, there was no evidence (from these measurements) to suggest the presence of a highly structured gel as the emulsions easily flowed in vials when they were tilted. Structured gels were reported in cellulose nanocrystal stabilized emulsions (Ayed et al., 2018) and would likely occur if bare nanoparticles were used instead of PEGylated particles.

Upon completion of rheological measurements, we observed significant differences in the physical appearance of the emulsions (Figure 6.4E,F). Figure 6.4E is an image of a 6 wt% emulsion stabilized with 6 nm particles after a shear sweep test. The image shows evidence of macroscopic coalescence which was shear induced. Figure 6.4F, on the other hand, is an image of a 6 wt% emulsion stabilized with 50 nm particles and shows no coalescence of the $MgSO_4$ emulsion drops.

Because oscillatory strain sweep measurements probe samples at small strain amplitudes for short time durations, we tested the stability of the 6 wt% emulsions by shearing at a fixed rate of 10 s^{-1}. We selected the 6 wt% formulation because the emulsions, regardless of the particle size, had similar viscosities (Figure 6.4D) and drop sizes (Figure 6.3B) which meant the dominant parameter affecting their stability was particle size. The shear test used here is referred to a simple shear test and has been used by others (Caserta et al., 2005; Whitby et al., 2011) to characterize emulsion stability.

During the shear stability experiment, a small volume of sample was periodically removed from the rheometer and imaged using light microscopy. This was done to quantify the change in emulsion drop size with respect to shearing time. Two characteristic parameters arise from these plots and are described by Whitby et al. (2011) as the lag time, which is the time required for >10% change in emulsion drop size, and t*, which is the time required for average emulsion drop size to double. We use these same definitions in our analysis.

Figure 6.5 plots emulsion drop size vs. shear time for the two different particle stabilized emulsions. The profiles of the two samples are qualitatively very different. After just one minute of shear, the average drop size of the 6 nm particle stabilized emulsions increased from 10.7 to 12.3 μm, suggesting the characteristic lag time is less than one minute whereas the lag time for emulsions stabilized with 50 nm particles was approximately 30 minutes. The time required for the emulsion drops to double in size was about 25 and 80 minutes for emulsions stabilized with 6 and 50 nm particles, respectively. The results obtained here demonstrate that the orthokinetic stability of w/w emulsions is highly dependent on the size of the particles used to stabilize the emulsion.

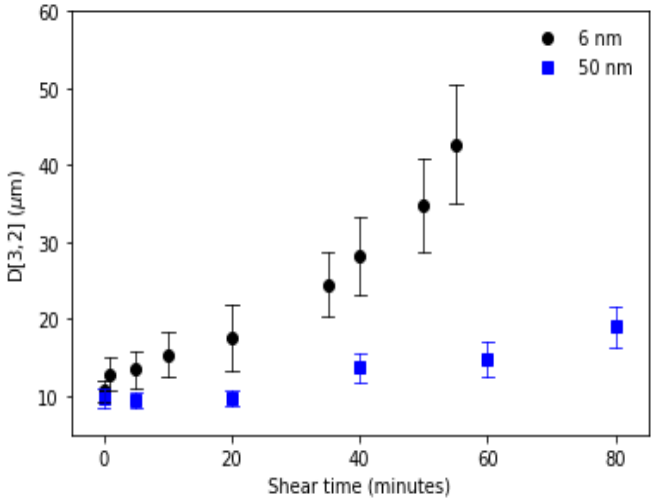

Figure 6.5 – Sauter diameters of emulsions stabilized with 6 nm (black) and 50 nm (blue) particles vs. shear time at 10 s-1.

6.4 Discussion

We have determined that it is possible to stabilize $MgSO_4$-in-PEG emulsions using PEGylated nanoparticles and that a necessary requirement for emulsion stabilization is the presence of flocculated particles. The mechanism likely responsible for this is a combination of nanoparticle charge screening from the partitioned $MgSO_4$ into the PEG rich phase and depletion flocculation of nanoparticles due to the presence of a high mass fraction of PEG polymer (Firoozmand et al., 2009). This is based on the observation that our PEGylated particles in PEG polymer solution are stable in the absence of $MgSO_4$ and because the particles do not immediate flocculate upon their addition into DI water with 0.5 wt% $MgSO_4$. The flocculated particles and PEG polymer showed the ability to localize at the PEG/$MgSO_4$ interface (Figure 6.2C). To highlight the importance of this, we performed two experiments to show the PEG/$MgSO_4$ interface cannot be stabilized without flocculated particles.

In the first experiment, we attempted to stabilize emulsions using particles with the same 6 nm silica core, but instead functionalized with (3-glycidyloxypropyl)trimethoxysilane (glymo). These particles were used in our previous work (Griffith and Daigle, 2018) and selected because of their stability in concentrated brine (Worthen et al., 2016). The particles (at 6 wt%) were stable upon their addition into an equilibrated PEG/ $MgSO_4$ phase, as there was no visible particle flocculation. The mixture was then homogenized and left to stand on the lab bench. Droplet coarsening and phase separation occurred on approximately the same time scale as phase separation of the ATPS in the absence of particles. This result implied that the stable glymo-coated particles did not show any affinity for the PEG/$MgSO_4$ interface and that they were unable to slow down phase separation (Figure C4).

In our second experiment, we prepared an ATPS mixture with a lower molecular weight PEG. We selected a 2,000 g mol^{-1} PEG in an attempt to minimize nanoparticle flocculation. The final composition of PEG and $MgSO_4$ (upon addition of silica) was 24 wt% and 7wt%. With this formulation, two phases were still present (Figure C5, left) and there was no visible particle flocculation upon addition of the PEGylated silica particles. This behavior was anticipated and in agreement with (Milling et al., 1991) which states that particle stability in polymer systems can be improved by decreasing the MW of polymer. The two phase mixture was homogenized and observed. The emulsion quickly coarsened and phase separated. This suggests that emulsion drops of $MgSO_4$ were not stable in the absence of non-flocculated particles (Figure C5, right).

The experiments performed above highlight the importance of flocculated particles and their role in stabilizing this emulsion. We believe the non-flocculated particles are unable to stabilize the $MgSO_4$ interface because of their small size which prevents them from straddling the entire interface (Balakrishnan et al., 2012). This allows

for rapid phase separation and coalescence. However, because the flocculated particles are larger in size, it is possible for them to span the interface (Balakrishnan et al., 2012) and prevent coalescence. This behavior of flocculated particles and their ability to stabilize w/w emulsion appears to be similar to Gonzalez-Jordan et al. (2017) which used fractal or microgel protein particles to stabilize w/w emulsions using high salt concentrations (0.1 and 0.3 M NaCl).

Using the results from our optical micrographs and rheological measurements, we selected an emulsion system that had similar viscosities and emulsion drop size regardless of nanoparticle size. This was intentionally done so we could directly probe the effect of particle size on the shear stability of these emulsions. This was an important step and worth highlighting because the stability of emulsion drops with respect to shear is proportional to the third power of the emulsion drop diameter (Whitby et al., 2011). Therefore, changes in drop size would have a large impact on the shear stability of different emulsions, which we have attempted to minimize.

The results from our shear coalescence experiments showed that the emulsion stabilized with 6 nm particles had a lag time of less than one minute. This implies the emulsion was very weak and required only several seconds of shear (at 10 s^{-1}) to remove particles from the w/w interface and induce drop destabilization. This was not the case for the emulsion stabilized with 50 nm particles, which had a lag time of 30 minutes.

Given the recent interest in w/w emulsions (Ganley et al., 2017) and the lack of information on their shear stability, the results presented here have quantified the stability of a w/w emulsion system under shear by monitoring the change in drop size with respect to shearing time. Moreover, these results show that relatively good orthokinteic stability can be achieved in these systems if larger particles are used to stabilize the interface. This

result was expected given that nanoparticle attachment energies scale with R^2 (equation (6.2)).

6.5 CONCLUSIONS

The goal of this work was to assess the stability of water-in-water Pickering emulsions (under simple shear flow) stabilized with nanoparticles of different size and to correlate the relationship between emulsion stability and particle size. We were interested in investigating this because during our literature survey it was apparent that many studies have quantified the static properties of low interfacial tension water-in-water emulsion systems (Vis et al., 2015; Nguyen et al., 2015; Ganley et al., 2017; Gonzalez-Jordan et al., 2018) but very few have studied their stability with respect to shear (Balakrishnan et al., 2012).

To study this relationship, we first demonstrated that it was possible to stabilize water-in water emulsions made from an aqueous, two-phase system of polyethylene glycol and magnesium sulfate with nanoparticles functionalized with 2-(methoxy(polyethyleneoxy)6-9propyl)trimethoxysilane. We determined that particle flocculation was a necessary requirement for emulsion stabilization. We characterized the static stability of different emulsions and showed that emulsions stabilized with 6 wt% particles (regardless of particle size) were statically stable for up to seven days. However, when the emulsions were sheared at a constant rate of 10 s^{-1}, the stability of the 6 nm and 50 nm emulsions were significantly different. We quantified this relationship by monitoring the change in emulsion drop size with respect to shearing time. We found that the orthokinetic stability of these emulsions could be greatly improved by using the larger particles. We determined the time required for the average Sauter mean diameter for the 50 nm particle stabilized emulsion to double was 80 minutes whereas it was only about

25 minutes for the 6 nm particle stabilized emulsions. This difference in emulsion doubling time was attributed to particle size.

The results presented here are important to the current work on water-in-water emulsions because they provide a framework in which the orthokinetic stability of these low interfacial systems can be evaluated, which to this point has been limited. Future work on this particular emulsion system could focus on understanding, in more detail, the mechanisms responsible for driving particles to the water/water interface. Additionally, flowing the emulsions through simple micromodels could provide useful information on their destabilization and coalescence behavior in real time. Lastly, there are opportunities to study the behavior of these water-in-water systems with respect to temperature fluctuations, which has practical implications for industrial use.

Chapter 7: Conclusions

SUMMARY

In this dissertation, I stabilized Pickering emulsions using silica nanoparticles modified with low and high surface concentrations of (3-glycidyloxypropyl)trimethoxysilane (glymo) or polyethylene glycol silane. I characterized the static and dynamic stability of different Pickering emulsions by measuring their demulsification pressures and by flowing them through glass capillary tubes. I performed a detailed rheological characterization on emulsions stabilized with nanoparticles with low and high surface concentrations of glymo in the presence of different ionic strength brines. I showed that the viscoelastic properties of these Pickering emulsions were dependent on interparticle interactions, which could be minimized by using nanoparticles with high surface concentration of glymo. I also characterized how to destabilize a very stable model Pickering emulsion using fumed silica particles combined with shear from a lab stir plate. I determined that destabilization was possible only when the fumed silica particles were sufficiently hydrophobic. Lastly, I characterized the shear stability of a water-in-water emulsion stabilized with 6 nm and 50 nm silica nanoparticles. I showed that the stability of this emulsion was improved by using larger nanoparticles which had large particle attachment energies than the smaller nanoparticles.

Static and dynamic stability of Pickering emulsions

My results show that the demulsification pressure can sufficiently capture differences in the stability of Pickering emulsions and that this method of assessing an emulsion's stability is superior to traditional emulsion characterization. I show that the demulsification pressure of a Pickering emulsion can be correlated to its dynamic

stability which has previously not been done in the literature. These results show that the demulsification pressure is sufficiently accurate as an emulsion screening tool and that it can allow for rapid assessment of different Pickering emulsion formulations.

Manipulation of Pickering emulsion rheology

I show through a detailed rheological characterization that for emulsions stabilized with silica nanoparticles, interparticle interactions between particles (in brine) can be minimized by optimally surface modifying the nanoparticles. The process of sterically stabilizing nanoparticles is responsible for reducing the zero-shear elastic storage modulus of a Pickering stabilized with 1 wt% particles in 0.25 wt% $CaCl_2$ from 200 Pa (for a non-optimally designed emulsion) to 20 Pa for an emulsion stabilized LSC glymo-modified nanoparticles. The zero-shear elastic storage modulus is further reduced to 2 Pa when when emulsions are stabilized with HSC glymo-modified nanoparticles. The implication of these results is that not only is the correct selection of a nanoparticle surface modifier an important design parameter but so too is the amount of modifier that is applied to the nanoparticle surface. This highlights the importance of surface modification for the successful deployment of nanoparticles for subsurface applications.

Destabilizing Pickering emulsions

I show that colloidal silica particles are capable of destabilizing a model Pickering emulsion. The extent of destabilization depends on the wettability of the colloidal particles with more hydrophobic particles showing a greater tendency to coalesce Pickering emulsions. Very hydrophobic particles with an oil/water/air contact angle of 117° destabilize 65% of an emulsion with just 0.01 wt%. The volume of coalesced oil increases to 85% when 0.05 wt% fumed silica was used. I observed that coalescence of a

Pickering emulsion was only possible with very hydrophobic particles and that when particles with lower oil/water/air contact angles were used (<23°) no coalescence was observed. The use of colloidal silica could be used as emulsion breakers when emulsions are produced from reservoirs.

Water-in-water emulsions

I determined that the shear stability of a water-in-water emulsion can be improved by using larger nanoparticles to stabilize the water/water interface. The improved stability results from larger particles having larger attachment energies. When particle attachment energies were on the order of 10 kT, water-in-water emulsions rapidly destabilized while sheared. However, when particle attachment energies were on the order of 100 kT or larger, markedly improved shear stability was observed.

The results presented here are important because they show that these low IFT emulsions can be designed to have adequate shear stability, which is important for their use in the subsurface.

FUTURE WORK

Natural future work should utilize the concept of the demulsification pressure and to flow emulsions with different demulsification pressures through bead packs and cores with different grain diameters so that the conditions for which Pickering emulsions remain dynamically stable in porous media can be established. Moreover, correlating the grain diameter and emulsion drop size to peak pressure drop, similar to the work of Yu et al. (2018), would make for useful work.

Past work has focused on generating emulsions in-situ by co-injecting and oil and an aqueous phase into bead packs to generate a Pickering emulsion. Characterizing the

stability of these emulsions and comparing their stability to emulsions generated by a tip sonicator or rotor stator would make for useful work. Additionally, characterizing the flowing stability of these emulsions through a glass capillary tube is also worthy of investigation.

An extension to the work listed above would be to characterize the stability of nanoparticles acting in synergy with surfactants using the demulsification pressure. This would help determine if Pickering emulsions stabilized with low concentrations of nanoparticles and surfactants are stable enough to retain their stability under dynamic conditions. This is important because Pickering emulsions stabilized with nanoparticles alone require relatively high concentrations of particles ~2 wt%. Therefore, minimizing the concentration of particles would minimize the overall cost of these emulsion formulations.

In this dissertation, I stabilized emulsions with surface modified silica nanoparticles and in all of these nano-dispersions; there was some free ungrafted silane. A detailed investigation into the contribution of the ungrafted silane and how it aids in emulsion stability is relevant to this work here but also to the general emulsion science community.

A current gap in the literature is that there is little detailed rheological data on Pickering emulsions at elevated temperatures. Measuring the rheology of Pickering emulsions is often difficult due to density differences between oil and water which leads to phase separation and because of water evaporation at elevated temperatures. Therefore, having a solvent trap and formulating emulsions with high specific gravity oils would enable for detailed rheological characterization of Pickering emulsions under different physicochemical conditions.

Crude oils often contain natural surfactants which are quantified in terms of the total acid number (TAN). It has previously been established that Pickering emulsions stabilized with silica particles modified with cationic surfactants can destabilize in the presence of anionic surfactants, which is due to a competition between the cationic surfactant binding with the negatively charged silica particle or binding to the negatively charged anionic surfactant. Contacting Pickering emulsions with crude oils that contain low, medium, and high concentrations of natural surfactants and assessing the stability of the Pickering emulsion would make for interesting work.

Appendices

Appendix A - Nanoparticle sols, silanes, and particle surface modification

Here I outline the steps that I used to functionalize silica nanoparticles with different silanes, which follows the work of Worthen et al. (2016).

NANOPARTICLES

In this work, I used silica nanoparticles that were purchased from Nyacol technologies (NexSil 5, 6, 8, 12, and 85) and from Nalco Champion (Nalco 1130, 2236, and DVSZN004). The properties of the particles are listed in Table A.1.

All of the particles from Nyacol Technologies (that I used) were sodium stabilized; the Nalco Champion 1130 particles were also sodium stabilized. The Nalco Champion 2236 and DVSZN004 particles were ammonium stabilized. Sodium and ammonium refer to the counterions that are used to stabilize the silica sol. Silica sols are electrostatically stabilized by deprotonating surface silanol groups. A hydroxide salt is used to increase the pH of the dispersion so that the silanol groups become deprotonated. Different hydroxide salts can be used – i.e., NaOH, NH_4OH. Therefore, the difference in stabilizing counterion is due to the different hydroxide salts that were used in the particle dispersions.

For some applications, the counterion can play an important role in a reaction or a subsequent process. This is apparently design parameter that is of practical interest for catalysis reactions (Ludox Technical Report). Later, I will show that I had issues in my reactions between (3-glycidyloxypropyl)trimethoxysilane (glymo) and silica sols that were stabilized with ammonium.

Particle Name	Size [nm]	Surface area [m^2/g]	% Solids	pH	$\%Na_2O$	Counterion	Surface Charge
Nalco 1130	8	375	30	10	0.45	Sodium	Negative
Nalco 2326	5	600	15	9	0.02	Ammonium	Negative
Nalco DVSZN004	44	70	70	9.5	0.04	Ammonium	Negative
NexSil 5	4-6	553	14.5-15.5	10.5-11	0.5-0.9	Sodium	Negative
NexSil 6	5-7.5	445	16-18	9.5-10.5	0.25-0.55	Sodium	Negative
NexSil 8	7-10	331	29-30	9.5-10.5	0.3-0.6	Sodium	Negative
NexSil 12	10-14	234	29-31	8.8-9.5	0.05-0.35	Sodium	Negative
NexSil 85	40-60	60	39-41	8.8-9.8	0.05-.2	Sodium	Negative

Table A.1 – Properties of the various silica nanoparticle sols used throughout this work.

SILANES

I used the following silanes: (1) (3-glycidyloxypropyl)trimethoxysilane (glymo), (2) 2-methoxy(polyethyleneoxy)6-9propyl)trimethoxysilane (PEG-silane), (3) 3-methoxypropyltrimethoxysilane, (4) 3-(trimethoxysilyl)propylmethacrylate, (5) 3-([dimethyl(3-trimethoxysilyl)propyl]-ammonio)propane-1-sulfonate. Table A.2 includes relevant information on each of the silanes. Figure A.1 shows the molecular structures of the different silanes that I tested.

Silane	MW [g/mol]	Source	Purity [%]	Catalog #	Price [$/g]
3-(trimethoxysilyl) propylmethacrylate	248.4	Sigma-Aldrich	98	440159	$ 0.4
(3-glycidyloxypropyl) trimethoxysilane	236.3	Sigma-Aldrich	98	4440167	$ 0.5
3-methoxypropyl trimethoxysilane	194.3	Gelest INC	100	SIM6493.0	$ 2.6
2-(methoxy(polyethyleneoxy)6-9propyl)trimethoxysilane	525	Gelest INC	90	SIM6492.7	$ 3.4
3-([dimethyl(3-trimethoxysilyl) propyl]-ammonio) propane-1-sulfonate	330	Gelest INC	95	SIM6492.7	$ 13.2

Table A.2 – Silane name, molecular weight, supplier, purity, catalog #, and price/gram for the different silanes used in this work.

(1) (3-glycidyloxypropyl)trimethoxysilane (glymo)

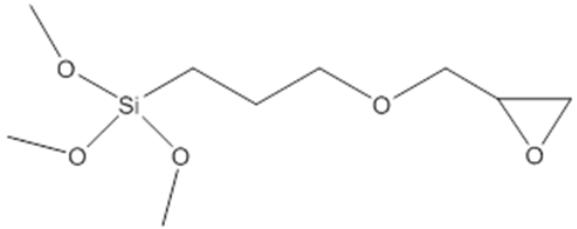

(4) (3-(trimethoxysilyl)propylmethacrylate

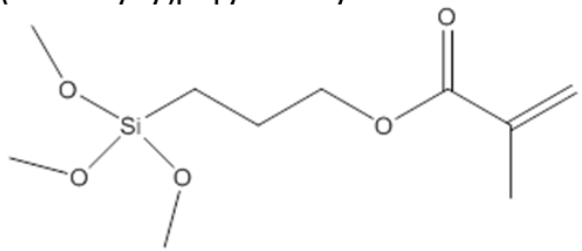

(2) 2-methoxy(polyethyleneoxy)6-9propyl)trimethoxysilane (PEG-silane)

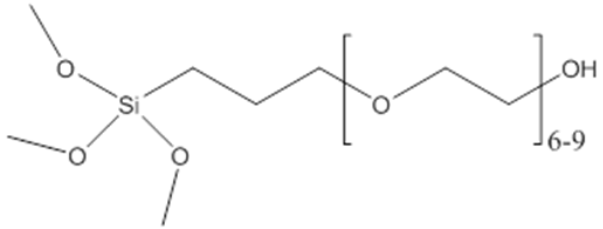

(5) 3-([dimethyl(3-trimethoxysilyl)propyl]-ammonio)propane-1-sulfonate

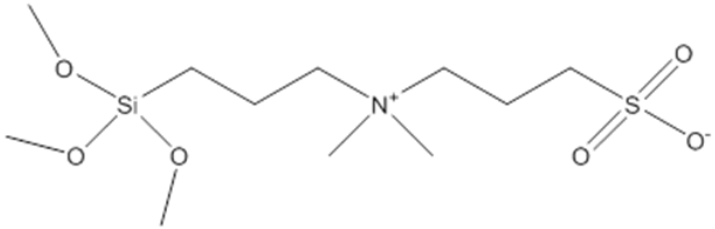

(3) 3-methoxypropyltrimethoxysilane

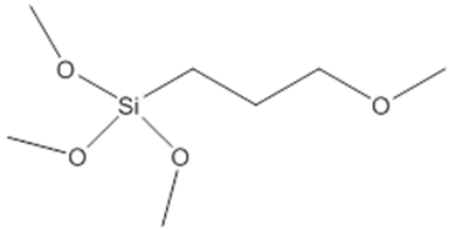

Figure A.1 – Molecular structures for the different silanes listed in Table A.2

SURFACE MODIFICATION

Determination of % solids

A certificate of analysis typically accompanies a silica sol. The analysis does not provide a specific mass % of nanoparticles, but instead only includes a mass % range, see for example Table A.1.

Therefore, upon receiving a new silica sol, the first step is to determine the mass fraction of nanoparticles in the dispersion. This is often referred to as the % solids. This is done by weighing a known mass of silica sol in a glass petri dish and heating the solution in an oven for at least 3 hours at 120°C so that all of the water has evaporated. The % solids is calculated using equation A.1

$$\% \, solids = \left(\frac{m_{3hrs,120^oC}}{m_{initial}}\right) x100, \quad \text{(A.1)}$$

where $m_{3hrs,\ 120°C}$ is the mass of solid particles after heating for 3 hours at 120°C and $m_{initial}$ is the initial mass of the silica sol in the petri dish. The NexSil 6 particles used in the chapter on "A comparison of the static and dynamic stability of Pickering emulsions" had a % solid content of 17.1 wt%, which is within the range specified in Table A.1

Determination of silane mass for reaction

Because the reaction between a silane and a silica nanoparticle is a surface area driven reaction, the amount of silane to include in a reaction is expressed as a concentration, with units of μmol silane/m² of nanoparticle surface area (Worthen et al., 2016; Bjorkegren et al., 2017) or as mmol/g of nanoparticle (Jang et al., 2018).

It is generally assumed that bare silica particles produced via precipitation (versus flame hydrolysis) contain 4.6 SiOH groups/nm² (Worthen et al., 2016), which means that a complete monolayer of silane on a particle surface is 7.6 μmol/m².

Therefore, a reaction between a silica nanoparticle and silane should contain no more than 7.6 μmol/m² silane. This is because at this concentration, there is more silane than available silanol sites.

For my initial reactions, I followed the steps that were outlined in Worthen et al. (2016).

Silane added versus silane grafted

During my initial surface salinization experiments, it was important to determine the optimal concentration of silane to add to a reaction mixture. This was done by varying the amount of silane in a reaction, filtering the reaction mixture, and quantifying the mass of silane that was actually bound to the particle surface. Once this data was obtained, a plot of bound silane versus added silane to a reaction mixture was made. On this plot, data that deviates from a straight line starting at the origin (with unit slope) indicates

saturation of a nanoparticle surface with silane. This also indicates the near optimum concentration of silane that should be added to a reaction mixture.

It is important to highlight the silane filtration step. This step filters ungrafted silanes from a reaction mixture that contains nanoparticle+silane and allows for the determination of silane that is actually bound to the particle surface. Filtration can be done passively or by using a centrifugal filter.

For this work, I used Amicon Centrifugal filters with a 30,000 molecular weight cut off (MWCO) filter that is housed within a standard 50 mL centrifuge tube (Figure A.2 A,B). These filters are convenient because they allow for nanoparticle/silane mixtures to be filtered in short time durations, ~1 hour. This is because filtration done with a centrifuge. Passive filtration, which is a diffusion driven process, can take days to weeks.

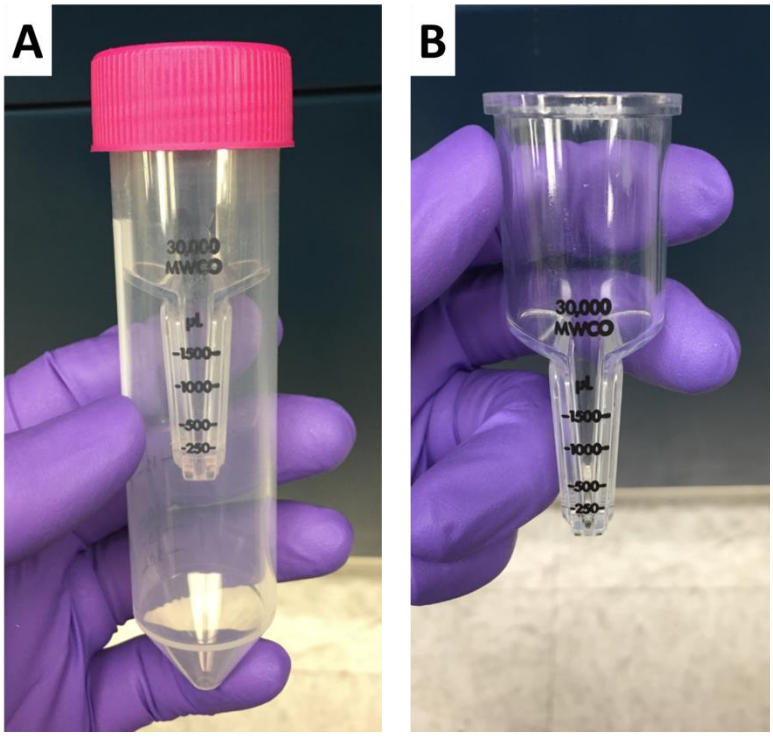

Figure A.2 – (A): 50 mL centrifuge tube with a 30,000 MWCO filter. (B) 30,000 MWCO filter removed from the centrifuge vial.

Approximately 10 mL of reaction mixture is placed into the 30,000 MWCO filter and the mixture is centrifuged for 15 minutes at 5,500 RPM (Worthen et al., 2016). After centrifugation, ~2 mL of concentrated nanoparticle dispersion remains in the 30,000 MWCO filter (Figure A.2 B). The other 8 mL of fluid passes through the filter and is collected in the bottom of the 50 mL centrifuge vial (Figure A.2A, bottom). This fluid is discarded. Fresh DI water is added to the concentrated nanoparticle dispersion and agitated to re-disperse the particles. This process is repeated three more times to remove ungrafted silanes.

Once the particles are free of ungrafted silane, they are dried in an oven at 80 °C, overnight, or until they are a solid powder.

To determine the mass of silane that is grafted to the nanoparticle surface, a thermogravimetric analyzer is used. Analysis is done by placing approximately 50 mg of dried nanoparticle sample into a 150 µL alumina crucible. The crucible is transferred into a Mettler-Toledo TGA/DSC 1 Thermogravimetric analyzer (TGA). The sample is heated at a rate of 20 °C/min from 30 °C to 110 °C . Inert nitrogen gas is used as the gaseous phase in the heating chamber and flows at 50 mL/min. Once the sample reaches a temperature of 110 °C, it is maintained there for 20 minutes. This is to remove any remaining water. Note that the sample loses about 6 wt% of its total mass when heated from just 30 °C to 110 °C. (Figure A.3 A) After being held at 110 °C for 20 minutes, the sample is heated from 110 °C to 800 °C and the mass that is lost during this heating cycle is attributed to the organic content from silanization.

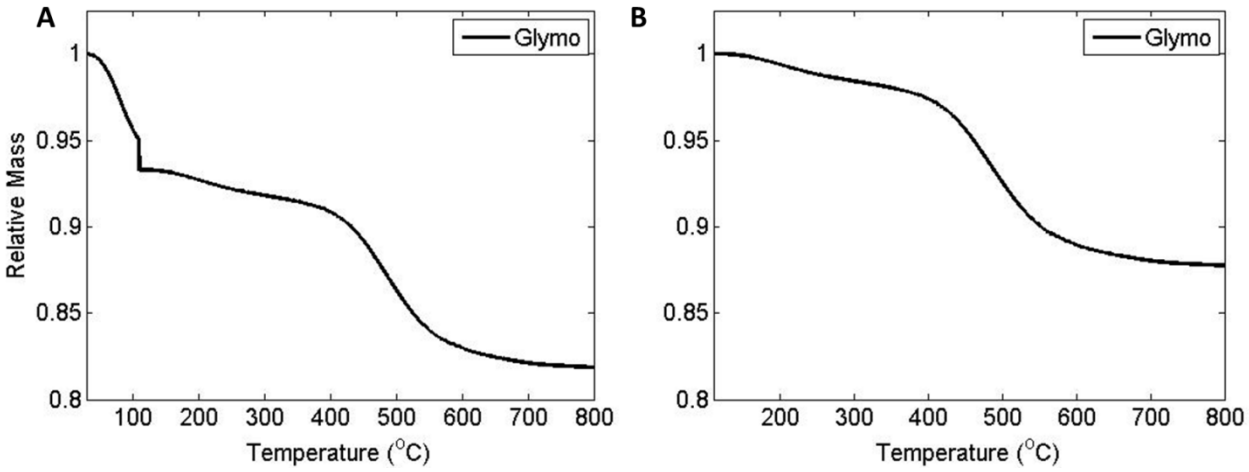

Figure A.3 – (A) raw relative mass versus temperature data from thermogravimetric analysis for a glymo-modified nanoparticle sample that was heated from 30 °C to 800 °C. (B) Relative mass versus temperature data from (A), where the data is normalized to the relative mass of the sample in (A) at 110 °C.

Figure A.3 (A) shows an example of raw data that is obtained from TGA. Figure A.3(B) is data from (A) that is normalized to the relative mass of the sample at a temperature of 110 °C. In this example, the sample had 12.3 wt% organic content.

Figure A.4 A,B show plots of silane added versus silane attached to the particle surface from Worthen et al. (2016) and Estephan et al. (2010), respectively. Worthen et al. (2016) functionalized silica nanoparticles with glymo and Estephan et al. (2010) was functionalized silica nanoparticles with a zwitterion called 3-(dimethyl(3-trimethoxysilyl)propyl)-ammonio)propane-sulfonate. For the data presented by Worthen et al. (2016) the optimum concentration of silane added is in the range of 3-5 µmol/m² and ~ 1.7 µmol/m² for Estephan et al. (2010).

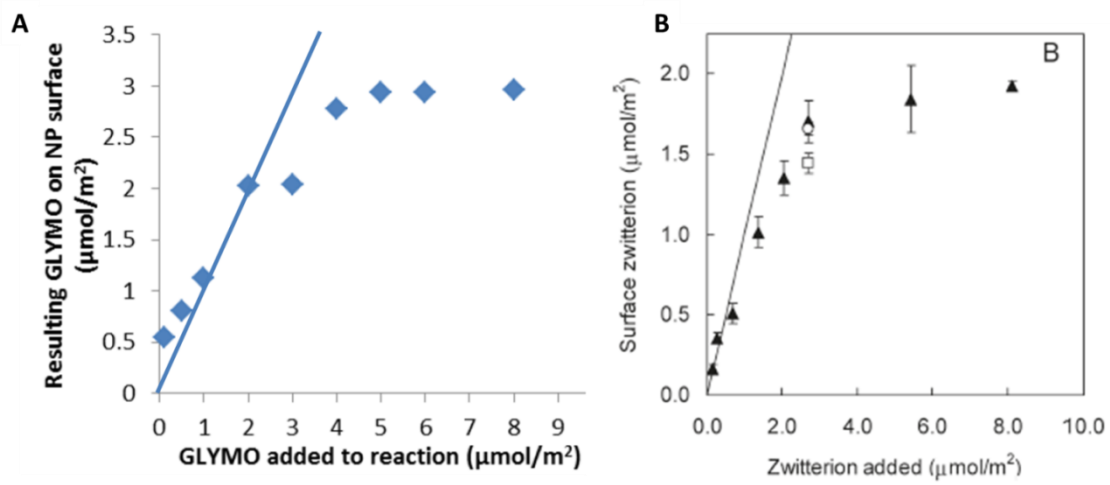

Figure A.4 – (A) Concentration of glymo attached to a nanoparticle surface versus concentration of glymo added (from Worthen et al., 2016). (B) Concentration of zwitterion attached to a nanoparticle surface versus concentration zwitterion added (from Estephan et al., 2010). Straight line in the plots represents one to one ratio of silane added to silane attached to particle surface.

Figure A.5 shows a plot of attached 2-methoxy(polyethyleneoxy)6-9propyl)trimethoxysilane (PEG-silane) versus PEG-silane that was added to reaction mixtures from my own experiments. In these experiments, I was trying to determine the optimum concentration of PEG-silane to add to a reaction mixture. Based on my data, the optimum concentration of PEG-silane to add ~1.07 µmol/m².

My data compares very favorably to PEG functionalized silica particle data that was presented in Bjorkegren et al. (2017). In their work, they showed that when PEG-silane was added to a reaction mixture at a concentration of 2 µmol/m², approximately 0.9 µmol/m² actually bound to the particle surface (45% efficiency). For my reactions, when PEG silane was added at a concentration of 2.14 µmol/m², 1.14 µmol/m² bound to the particle surface (53% efficiency).

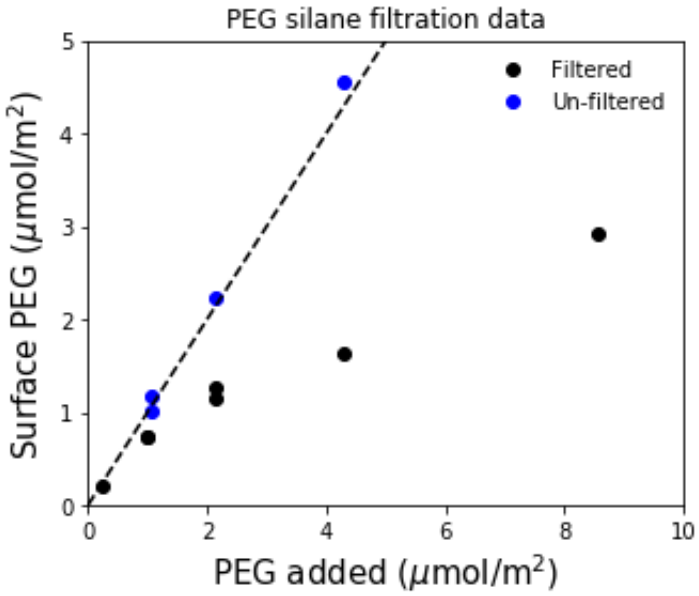

Figure A.5 – Concentration of PEG-silane attached to a nanoparticle surface versus concentration of PEG silane added. This plot comes from my reaction tests with NexSil 6 nanoparticles and 2-methoxy(polyethyleneoxy)6-9propyl)trimethoxysilane. The dashed straight line in plot represents one to one ratio of silane added to silane attached to particle surface.

PROCEDURE - GLYMO MODIFICATION – WITH SODIUM STABILIZED SILICA SOL

The reaction procedure outlined in Worthen et al. (2016) used a silane concentration of 5 μmol/m². This was used for all silanes that were tested in that study. So this is the same concentration that I used in my initial reactions.

All my reaction calculations are done on a mass ratio basis. My initial reactions were done in 20 gram batches. DI water was used to dilute the final nanoparticle concentration to ~10 wt%, which is based on the description given in Worthen et al. (2016). Below are my calculations for determining the required mass of nanoparticle dispersion and silane to satisfy the 10 wt% nanoparticle concentration and 5 μmol/m² requirement, respectively. Using Table A.1 and Table A.2, I get relevant nanoparticle properties that are required for the calculation.

Mass nanoparticle dispersion:

$$\text{m NP}_{\text{dispersion}} = \frac{(\text{Total Mass Reacion})(\text{Desired NP wt\%})}{\text{\% solids silica sol}} = \frac{(20\text{g})(10\text{ wt\%})}{17.1\text{ wt\%}}$$
$$= 11.7\text{ g silica sol}$$

Mass glymo silane

$$m_{glymo-silane} = \frac{(\text{mass NP})(\text{silane concentration})(\text{MW silane})(\text{SSA NP})}{\text{silane purity}} * 1e-6$$

$$m_{glymo-silane} = \frac{(2g)\left(5\frac{\mu mol}{m^2}\right)\left(236.3\frac{g}{mol}\right)\left(445\frac{m^2}{g}\right)\left(1E-6\frac{mol}{\mu mol}\right)}{0.98}$$

$$m_{glymo-silane} = 1.07 \text{ g glymo silane}$$

Reaction procedure

1. 11.8 g NexSil 6 dispersion and 1.13 g DI water were added to a 25 mL round bottom flask. The round bottom flask was equipped with a stir bar.
2. A water bath was placed onto a heated stir plate and the temperature was to 60 °C. The 25 mL round bottom flask, along with the nanoparticles and DI water, was placed in the water bath and stirred.
3. In a separate, 15 mL glass vial, 1.07 g of glymo was added to 6 g of 0.01 M HCl water (pH ~ 2).
4. The glymo/water mixture was stirred for 2 minutes to perform an acid catalyzed ring opening reaction. This reaction is required to open the glymo epoxide and convert it to a diol. If this step is not done (without including other reagents), the glymo silane cannot be dispersed into DI due to its hydrophobicity. During this reaction, the reaction mixture almost immediately transitioned from turbid solution to a clear one upon its to the pH 2 water, this was noted in Worthen et al. (2016).
5. After 2 minutes, the glymo/water mixture was added dropwise to the 25 mL round bottom flask using a 1 mL pipette. This was done over the course of ~ 1 minute.
6. The reaction was allowed to stir for 24 hours at 60 °C.

INITIAL REACTION RESULTS

Figure A.6 (left) shows the initial state of a nanoparticle/glymo reaction mixture with: 11.8 g NexSil 6 particles, 1.13 g DI water, 6 g pH 2 water, and 1.07 g glymo silane. The reaction mixture is clear and semi-translucent, which is expected at this time.
Figure A.6 (right), however, shows the reaction mixture after 2 hours. The mixture is turbid and no longer translucent. This indicates the silica nanoparticles and silane are no longer stable. Qualitatively, the particles and silane have increased in size to the point where they are now scattering light, which is inferred from the turbid solution.

This result was surprising, but consistent among all of my initial experiments with silica dispersions and glymo.

Glymo is a complicated molecule. This is because its final structure is very sensitive to reaction conditions (temperature, pH, solvent, and whether or not nucleophiles are present).

Therefore, going into detail on this subject is beyond the scope of this appendix, however, for interested readers, several good references on glymo chemistry are: Gabrielli et al. (2013), Gabriella et al. (2014), Guillory et al. (2016).

Most likely what happened during my reaction was: (1) the epoxide ring on the glymo molecule opened upon addition to pH 2 water, which was confirmed by the fact the solution went from turbid to clear. (2) the silica sols that I used are strongly buffered to ~ pH 10. (3) given that the concentration of glymo in these initial reactions is high (5 μmol/m²) in combination with the of high pH of the dispersion, these conditions favored the self-condensation of glymo molecules to form oligomers (Gabrielli et al., 2013) instead of condensing onto the silica particle surface. This means that the glymo molecules were only reacting with one another and not the silica nanoparticles, which we do not want.

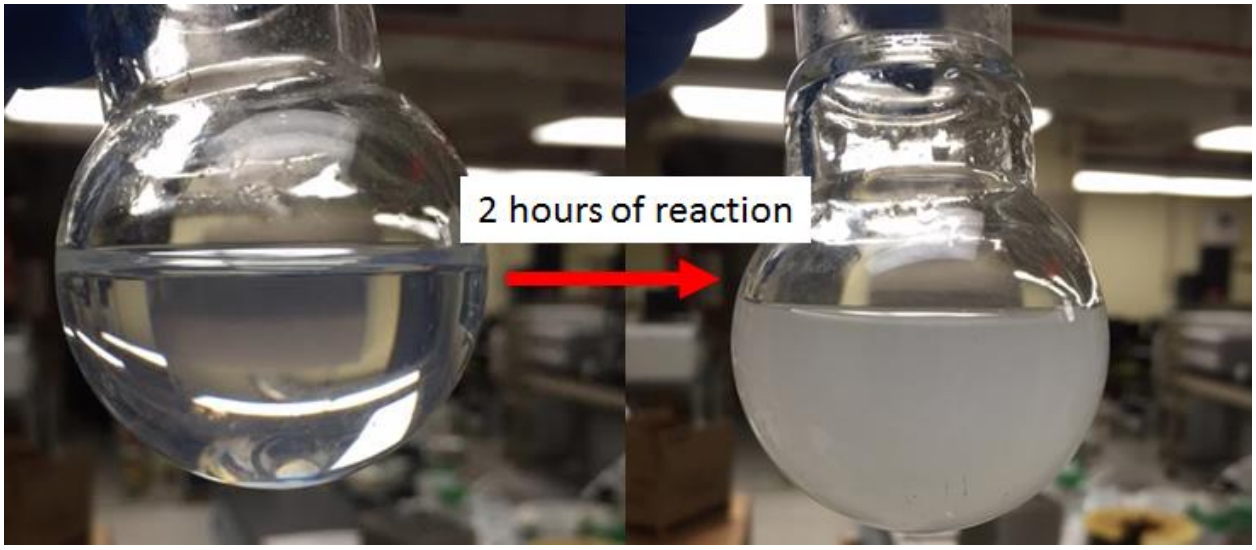

Figure A.6 – Left: 11.8 g NexSil 6 nanoparticles, 1.13 g DI water, 1.07 g glymo silane, and 6 g 0.01 M HCl water. Right: Reaction mixture after two hours of reaction at 60°C

PREVENTING GLYMO PRECIPITATION BY REDUCING GLYMO CONCENTRATION

To prevent the self-condensation of glymo oligomers, I performed experiments where I varied the concentration of glymo in my reaction mixtures from 1.5 – 3 μmol/m². This was done so that I could establish a concentration of glymo that did not precpirate from solution. For my 20 gram reaction batches, this corresponded to 0.32 – 0.64 g glymo silane.

Based on my results, 1.85 – 2 μmol/m² was the concentration of glymo where precipitation was absent (without addition of cosolvent). In my work, I refer to particles with this concentration of glymo as low surface coverage (LSC) glymo modified particles.

PREVENTING GLYMO PRECIPITATION BY INCLUDING A COSOLVENT

To prevent glymo oligomers from precipitating from a reaction mixture while using higher concentrations of glymo silane (> 2 μmol/m²), I used different cosolvents to help maintain the solubility of glymo in a reaction mixture.

I first had to determine the chemical compatibility between cosolvents and nanoparticle sols. I used: methanol, ethanol, and isopropyl alcohol as cosolvents. Ethanol caused the NexSil particles to destabilize – i.e., gel upon its addition. The NexSil particles were stable to both methanol and isopropyl alcohon.

I ran experiments where I varied the alcohol mass fraction from 10 wt% - 22 wt% using 6 wt% increments. I determined that 22 wt% methanol was optimal. This was based on the observation that no glymo precipitation was observed when 4-5 μmol/m² was used. Therefore, this is the mass fraction of methanol I used in my work.

My modified reaction procedure using methanol was:

1. 11.8 g NexSil 6 dispersion and 1.13 g DI water were added to a 25 mL round bottom flask equipped with a stir bar.
2. A water bath on a heated stir plate was set to a temperature of 60 °C. The 25 mL round bottom flask was placed in the water bath and stirred.
3. In a separate, 15 mL glass vial, 1.07 g of glymo was added to 2.73 g DI water and 4.4 g methanol, which had a combined pH ~2.
4. The glymo/water/methanol mixture was stirred for 2 minutes
5. After 2 minutes, the glymo/water/methanol mixture was added, dropwise, to the 25 mL round bottom flask using a 1 mL pipette. This was done over the course of ~ 1 minute.
6. The reaction was allowed to stir for 24 hours at 60 °C.
7. Upon completing the reaction, it was free of any precipitated material, and methanol was evaporated using a Dean-Stark reflux trap.

PROCEDURE - GLYMO MODIFICATION – WITH AMMONIUM STABILIZED SILICA SOL

In an attempt to use the same nanoparticle core that our department has used in the past (5 nm, ammonium stabilized) I tried to functionalize Nalco 2236 nanoparticles with glymo silane using my modified methanol reaction procedure.

As I mentioned earlier, in some cases the counterion in a silica sol can impact the behavior of a reaction. When reacting ammonium stabilized silica with glymo, the final product was a gelled particle/glymo mixture. The structure of this nanoparticle/glymo mixture is quite similar to previously published work that makes gels by adding ammonium hydroxide – see Chu et al. (1997).

There could be interest in using this reaction for a conformance gel, which is an environmentally accepted method for gelation in the North Sea (Boul et al., 2015)

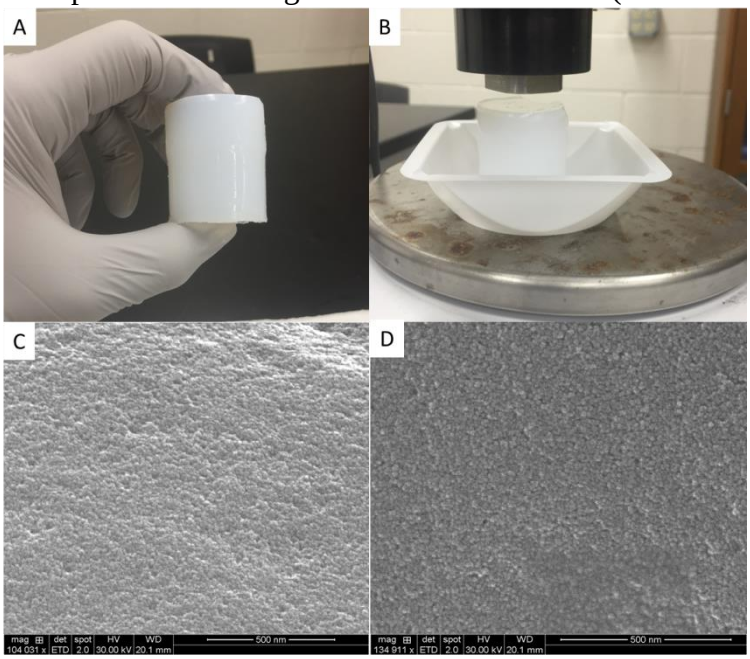

Figure A.7 – (A) Gelled Nalco 23260 nanoparticle dispersion with 5 μmol/m² glymo silane after 24 hours of reaction. (B) Gelled Nalco 2326 nanoparticle/glymo dispersion during an unconfined compression test. (C)-(D) SEM image of the Nalco 2326 nanoparticle/glymo surface.

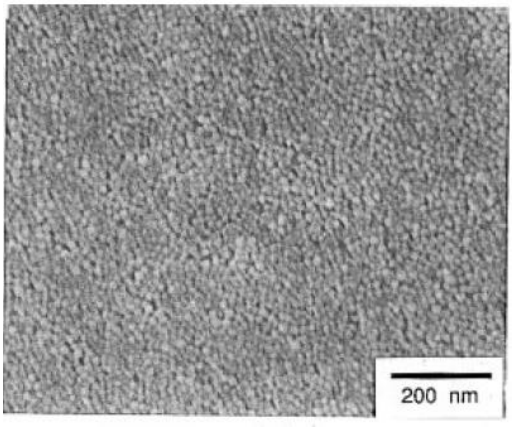

Figure A.8 – Ludox LS silica nanoparticles with glymo. pH adjust is performed with ammonium hydroxide. Note similar characteristics to our gelled nanoparticle glymo matrix. From Chu et al. (1997)

AQUEOUS STABILITY

Aquous stability tests were done with glymo modified nanoparticles at elevated temeparture and different salinities. For these tests, I used nanoparticles modified with 4 µmol glymo/m². Salt concentrations ranged from 1 wt% to 10 wt% (NaCl, $CaCl_2$, and $MgCl_2$). Particles were placed in an oven at 70°C and visually assessed for their aqueous stability after one week.

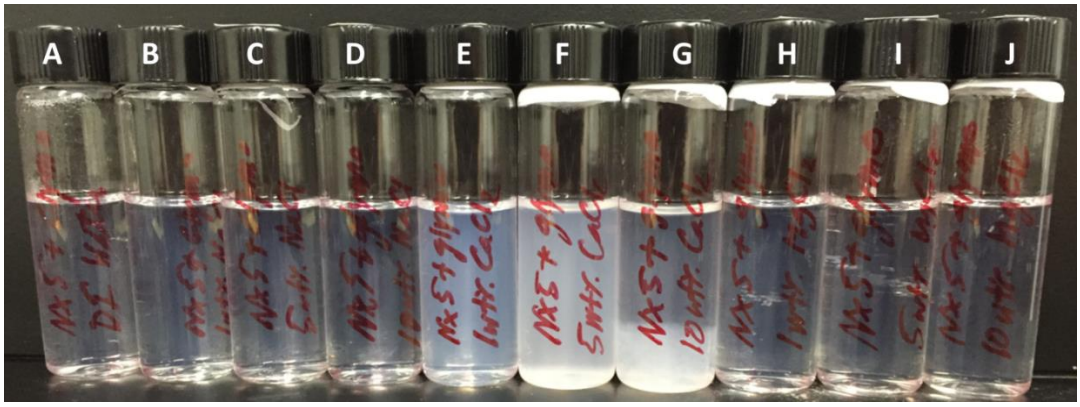

Figure A.9 – 5 wt% HSC glymo-modified particles after one week in a 70 °C oven with (A) DI, (B) 1 wt% NaCl, (C) 5 wt% NaCl, (D) 10 wt% NaCl, (E) 1 wt% $CaCl_2$, (F) 5 wt% $CaCl_2$, (G) 10 wt% $CaCl_2$, (H) 1 wt% $MgCl_2$, (I) 5 wt% $MgCl_2$, and (J) 10 wt% $MgCl_2$.

As we would expect, the dispersions in DI water showed no signs of particle agglomeration. The dispersion in NaCl, at all concentrations, did not show signs of agglomeration. The dispersions in magnesium chloride did not show signs of agglomeration. However, the nanoparticle dispersions in 1 wt% calcium chloride showed some turbidity, which indicates loss of aqeous satbility. This turbidity increased with increasing salt concertation. At 10 wt% calcium chloride, there were clear sings of particles completely settling out of diserpsion, indicating the particles were not aqueously stable (Figure A.9 G).

Appendix B – Emulsions

EMULSIFICATION ABILITY FOR DIFFERENT SURFACE MODIFIED NANOPARTICLES

I modified 6 nm NexSil 6 particles with the following silanes: (1) (3-glycidyloxypropyl)trimethoxysilane (glymo), (2) 2-methoxy(polyethyleneoxy)6-9propyl)trimethoxysilane (PEG-silane), (3) 3-methoxypropyltrimethoxysilane, (4) 3-(trimethoxysilyl)propylmethacrylate, (5) 3-([dimethyl(3-trimethoxysilyl)propyl]-ammonio)propane-1-sulfonate (zwitterionic silane).

Some pre-screening was done to test how well the different surface modified particles could stabilize emulsions. For these initial experiments, octane was used as the oil phase. Deionized water was used as the aqueous phase and 1 wt% nanoparticles were used. The pH of the dispersions was unaltered, and likely to be ~ 10.

Figure B.1 A,B show results from my initial emulsification tests. All of the particles, except for the zwitterionic modified particle were capable of stabilizing octane-in-water emulsions (Figure B.1A,B right most vial). These emulsions were stable for at least 24 hours.

Because the methyl acrylate silane is relatively hydrophobic, I was only able to modify particles with low concentrations of silane (< 1 μmol/m²). Moreover, the particles were not stable in low concentration brine waters. The particles precipitated out of solution in the presence of 3.5 wt% NaCl. Therefore, we did not explore these particles any further.

The glymo modified particles showed good emulsification ability. And as we would expect, the glymo modified particles were stable in brine water, making them a good candidate for further testing. The zwitterionic modified particles were unable to stabilize octane-in-water emulsions. We did not test these particles any further.

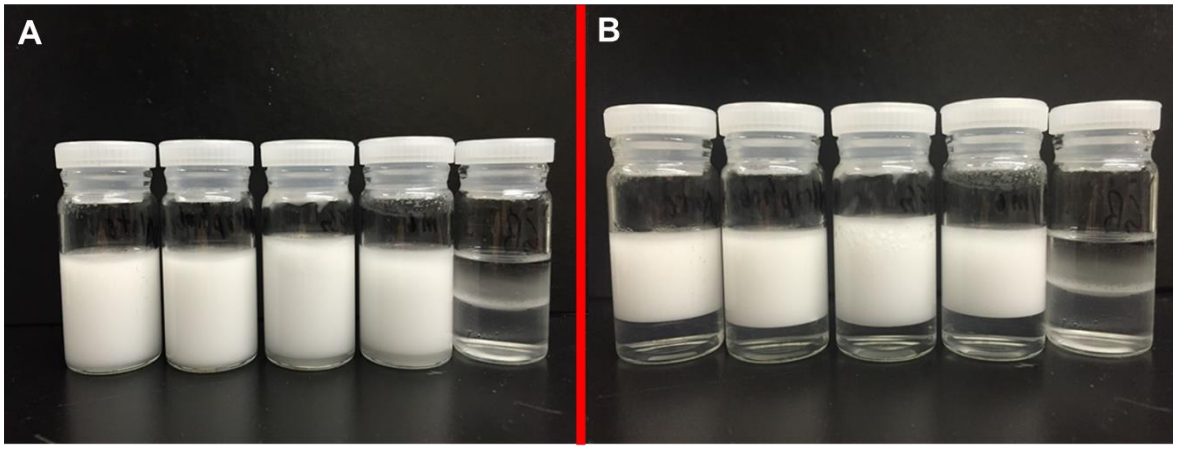

Figure B.1 – (A) octane-in-water emulsions immediately after formation, stabilized with 1 wt% (left to right): methyl acrylate-modified particles, LSC glymo-modified nanoparticles, PEG-silane modified nanoparticles, HSC glymo-modified nanoparticles, zwitterionic silane modified nanoparticles. (B) emulsions in (A), but 24 hours after formation.

EMULSION STABILITY: ROTOR STATOR VERSUS TIP SONICATOR

In this work, I prepared emulsions using a 30W Branson Digital Tip Sonifier with a 5 mm microtip (Figure B.2 A) or an IKA T18 Digital Ultra Turrax rotor stator homogenizer (Figure B.2 B).

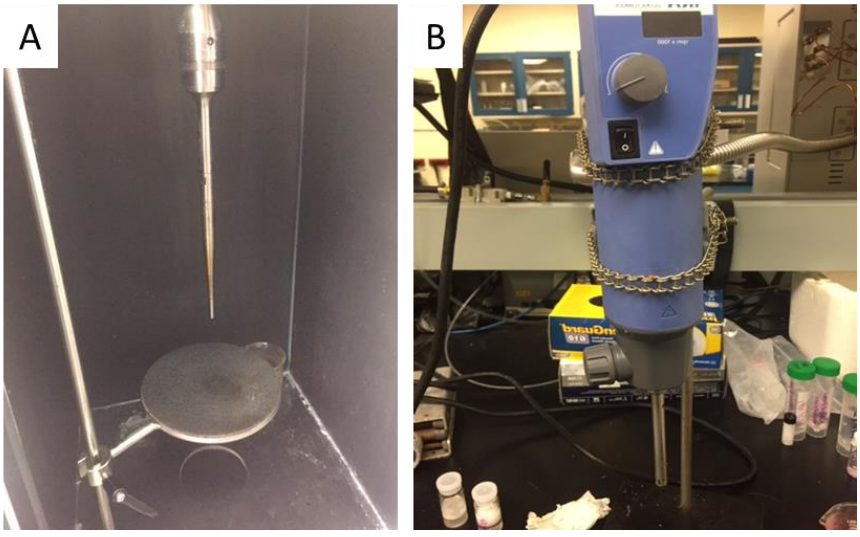

Figure B.2 – (A) 30W Branson Digital Tip Sonifier with a 5 mm microtip. (B) IKA T18 Digital Ultra Turrax rotor stator homogenizer.

In general, emulsions prepared with a tip sonicator are more stable (to coalescence) than emulsions prepared with a rotor stator homogenizer (Zhang et al., 2015).

Forced coalescence experiments were done to confirm this behavior; they were also done to quantify the differences in the relative stabilities for these different emulsification methods.

To test the relative stabilities based on emulsification method. Emulsions were prepared with 2.75 wt% HSC surface modified glymo particles dispersed in deionized water. Decane was used as the oil phase (50 volume %) and the total volume of oil and water in these formulations was 40 mL.

Emulsions that were generated with the tip sonicator were sonicated for 10 seconds at 50% amplitude (which is a variable that can be controlled on the sonicator), followed by gentle hand shaking. This process of sonication/hand shaking was repeated two more times so that all of the oil was emulsified.

Emulsions prepared with the IKA T18 Digital Ultra Turrax rotor stator homogenizer were homogenized for 2 minutes at 25,000 RPM.

Both emulsions were centrifuged at 5,000 g. The emulsion prepared with the rotor stator completely coalesced (no emulsion remained after centrifugation) whereas the emulsion prepared with the tip sonicator released ~14.6 mL of decane.

To find an appropriate gravitation acceleration that did not completely coalesce the rotor stator generated Pickering emulsion, a series of experiments were done where the gravitation acceleration was varied. After experimentation, it was determined that an acceleration of 250 x g would not completely coalesce and emulsion prepared with the rotor stator. This allowed for a demulsification pressure to be calculated.

The 2.75 wt% HSC glymo-stabilized emulsion prepared with the rotor stator released 4.65 mL of oil after centrifugation. The demulsification pressure, which determines the relative strength/stability of an emulsion, was calculated using equation (B.1):

$$P_{demulsification} = \frac{\Delta\rho g_k (V_{oil} - V_{released})}{A}, \tag{B.1}$$

where $\Delta\rho$ is the density difference between oil and aqueous phase, g_k is the gravitation acceleration of the centrifuge, V_{oil} is the total volume of oil in the emulsion, $V_{released}$ is the volume of oil released after centrifugation, and A is the cross sectional area of the centrifuge tube. Aqueous phase density was determined by measuring 10 mL of nanoparticle dispersion and recording its mass.

The 2.75 wt% HSC glymo stabilized emulsion that was made with the tip sonicator had a demulsification pressure of 10.2 kPa and the emulsion prepared with the rotor stator had a demulsification pressure of 1.6 kPa, this result suggests that the emulsion prepared with the tip sonicator is ~ 6 x more stable than the emulsion prepared with the rotor stator.

COMMENT ON EMULSIFICATION METHODS

Given that emulsions prepared with a tip sonicator are more stable than emulsions prepared with a rotor stator homogenizer, it would be interesting to compare the stability emulsions that are generated using these two methods to emulsions generated in-situ (for example in a bead back or core) by the co-injection method.

I anticipate that emulsions generated in a bead pack would be weaker than both of the emulsions prepared here. This is because the shear rates that are generated by co-injecting fluids at a rate of 24 mL/min in a bead pack (180 µm beads) is ~ 12,500 s^{-1} (Gabel, 2014). Emulsions prepared with a rotor stator homogenizer operating at 13,500 RPM have an estimated shear rate of 17,000 s^{-1} (Worthen et al., 2014).

Moreover, it would be important to quantify the actual stability of Pickering emulsions that are prepared in synergy using a combination of surfactants and nanoparticles, like in the work of Kim et al. (2017). In many cases, when using surfactants in synergy with nanoparticles to stabilize emulsions, their concentrations are very low, like in the case of Kim et al. (2017). In their work, emulsions were stabilized with 5 nm particles using only 0.01 wt% particles! Surfactants were also included but at very low concentrations ~0.0005 wt% - 0.1 wt% (depending on the surfactant).

IMAGE ANALYSIS

ImageJ (version 1.51j8) was used to process all images in this dissertation. Below are a general guidline for the steps I used to get drop sizes for my different emulsions:

1. Load image
2. Select Image, Type, 8-bit
3. Select Image, Adjust, Threshold (Ctrl + Shift + T) - Apply
4. Select Analyze, Analyze Particles…,
    a. Set Size (pixel^2): typically 20-infinity
    b. Circularity: typically 0.65-1.00
    c. Show: Outlines
    d. Select: Display Results, Clear Results
5. Below is an example sequence of what a raw image, thresholded, and analyzed image looks like from imageJ.

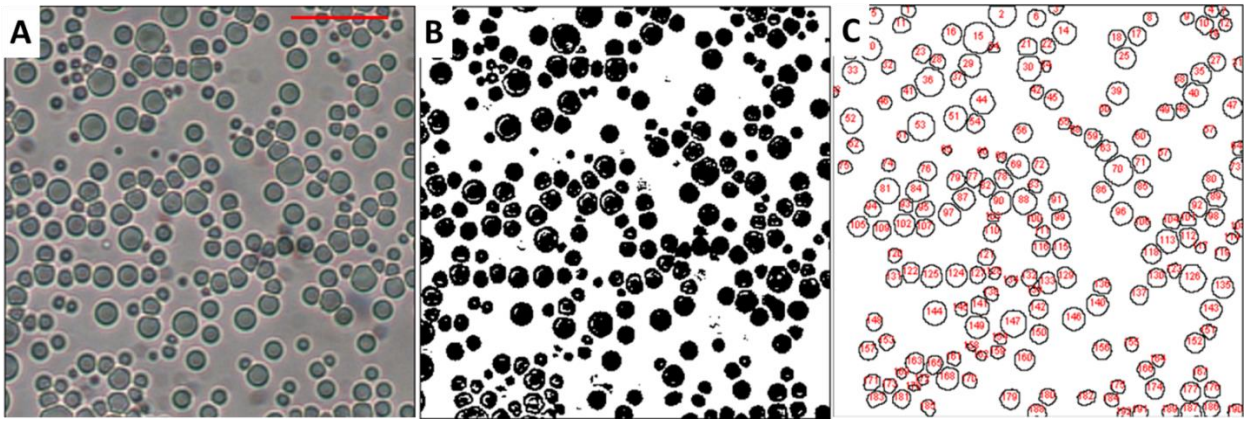

Figure B.3 – (A) Raw image of a nanoparticle stabilized emulsion. The scale bar is 25 µm. (B) Thresholded image, and (C) analyzed image with outlines around the emulsion drops.

6. The output of this process is the area of a circle given in square pixels. This data is exported to Excel where the mean Sauter diameter of the emulsion drops can be calculated.

EMULSION DYNAMIC STABILITY SUPPORTING INFORMATION

Here I include supporting information that was not included in the body of Chapter 3.

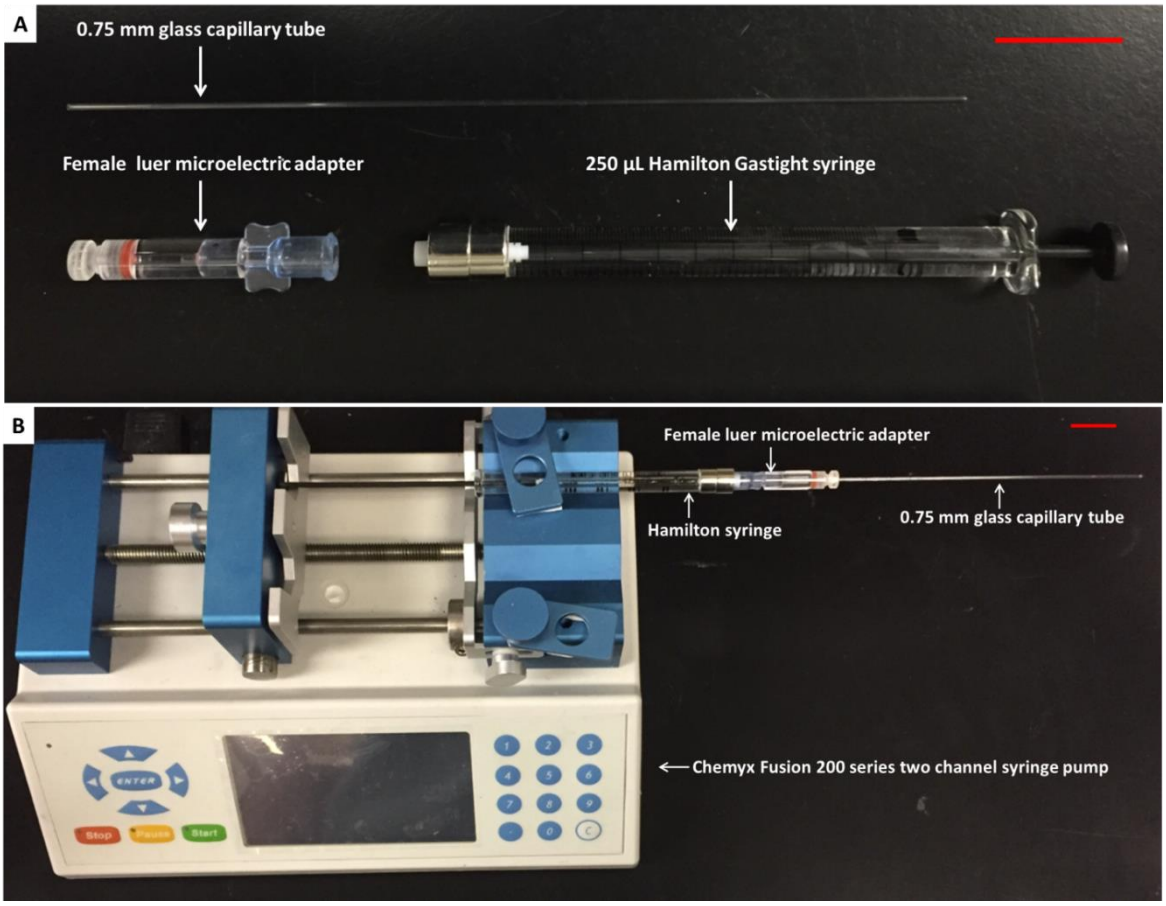

Figure B.4 – (A) A 250 µL Hamilton Gastight syringe (Part# 81120), a female luer microlectric adapter (1.0 mm OD) (Word Precision Instruments, Item# MPH6S10), and a 0.75 mm ID (1.0 mm OD, L = 152.4 mm) borosilicate glass capillary tube (World Precision Instrument, Item# TW100-6). (B) All of the components in (A) connected and mounted on a Chemyx Fusion 200 series two channel syring pum p (Model #720). Red scale bar is 2 cm.

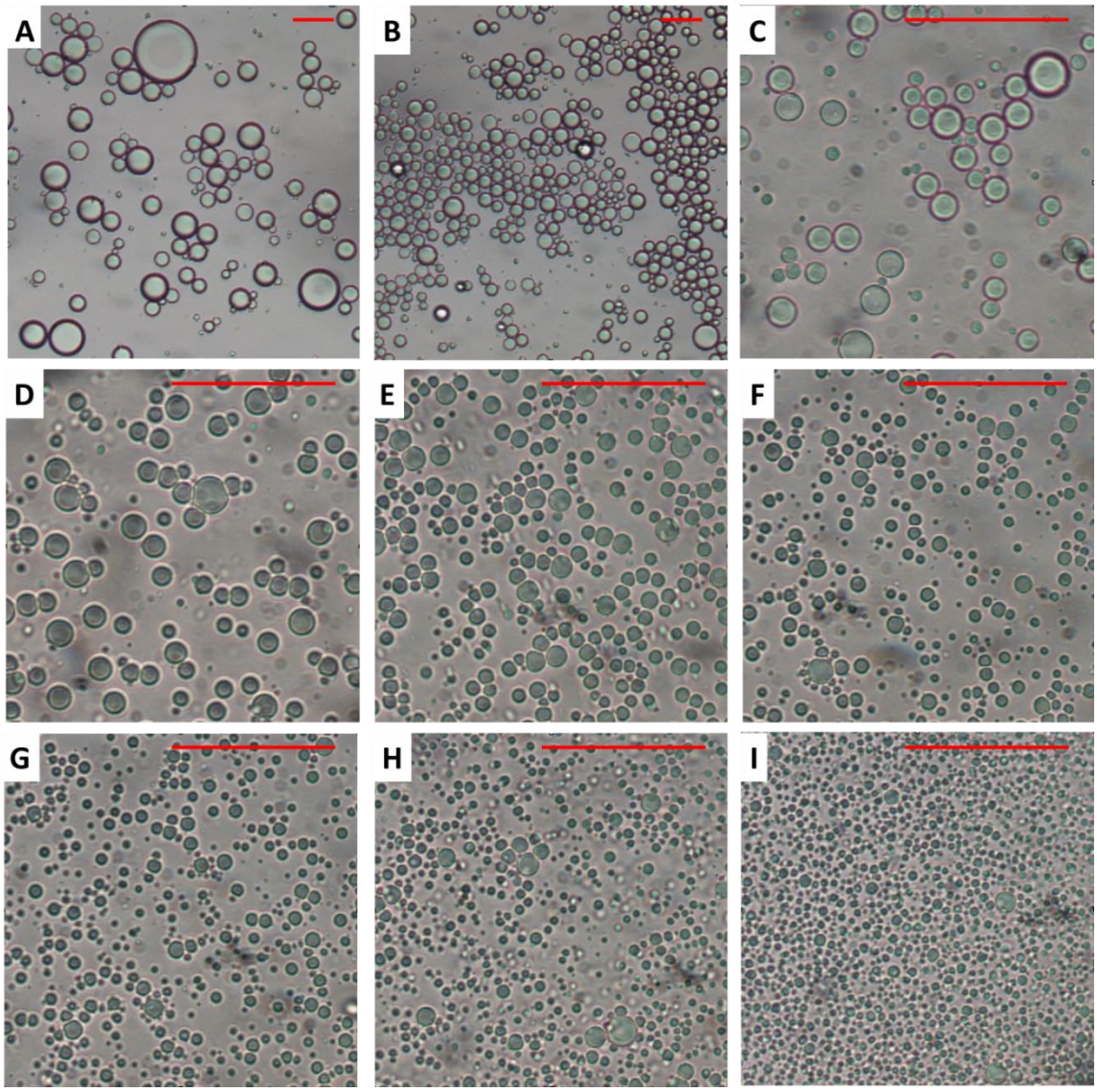

Figure B.5 – Optical micrographs for LSC glymo-stabilized emulsions immediately after formation using: (A) 0.34 wt%, (B) 0.69 wt%, (C) 1.4 wt%, (D) 2.1 wt%, (E) 2.8 wt%, (F) 3.4 wt%, (G) 4.1 wt%, (H) 5.5 wt%, and (I) 6.9 wt% LSC glymo-coated nanoparticles.

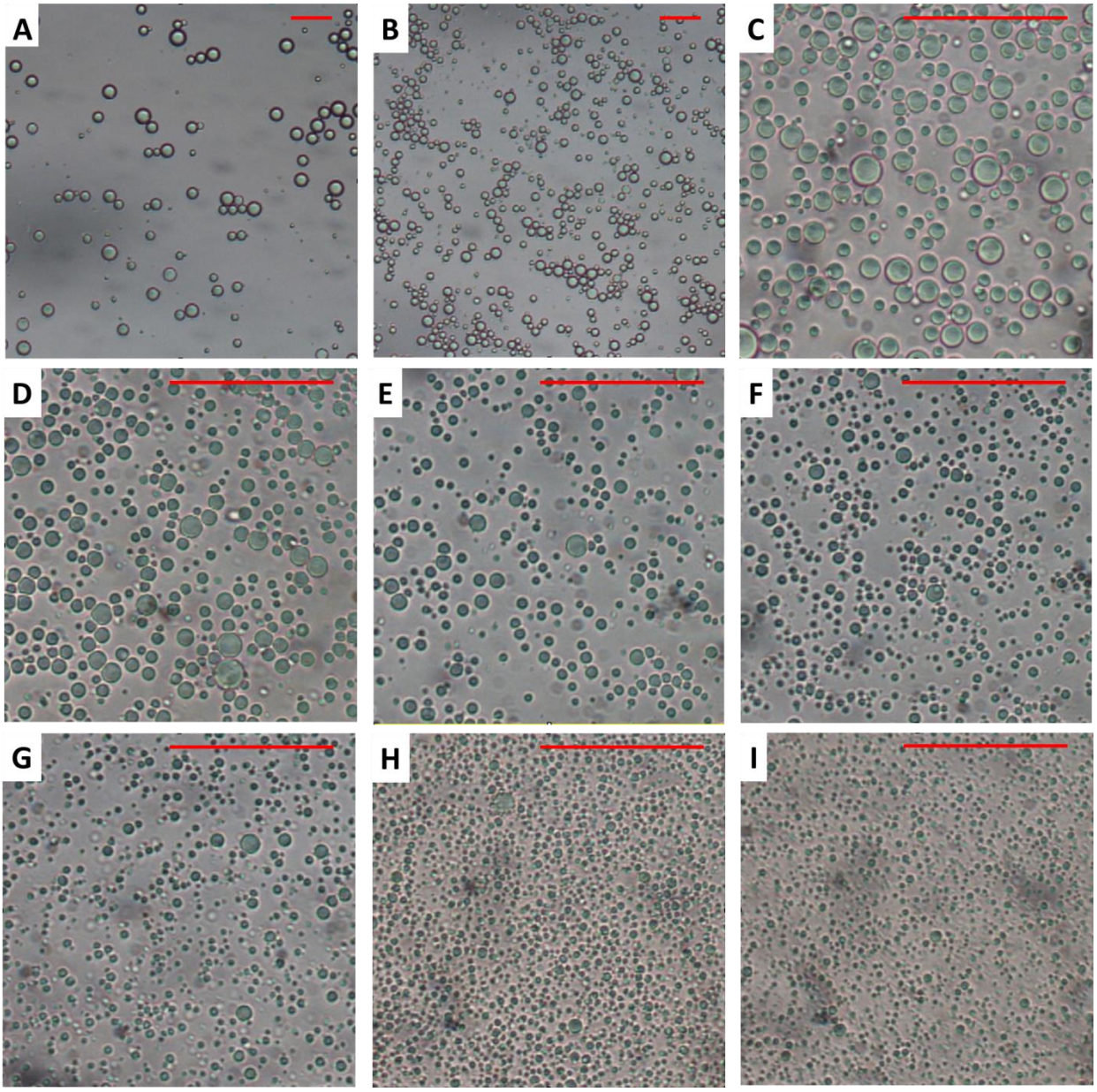

Figure B.6 – Optical micrographs for HSC glymo-stabilized emulsions immediately after formation using: (A) 0.34 wt%, (B) 0.69 wt%, (C) 1.4 wt%, (D) 2.1 wt%, (E) 2.8 wt%, (F) 3.4 wt%, (G) 4.1 wt%, (H) 5.5 wt%, and (I) 6.9 wt% HSC glymo-coated nanoparticles.

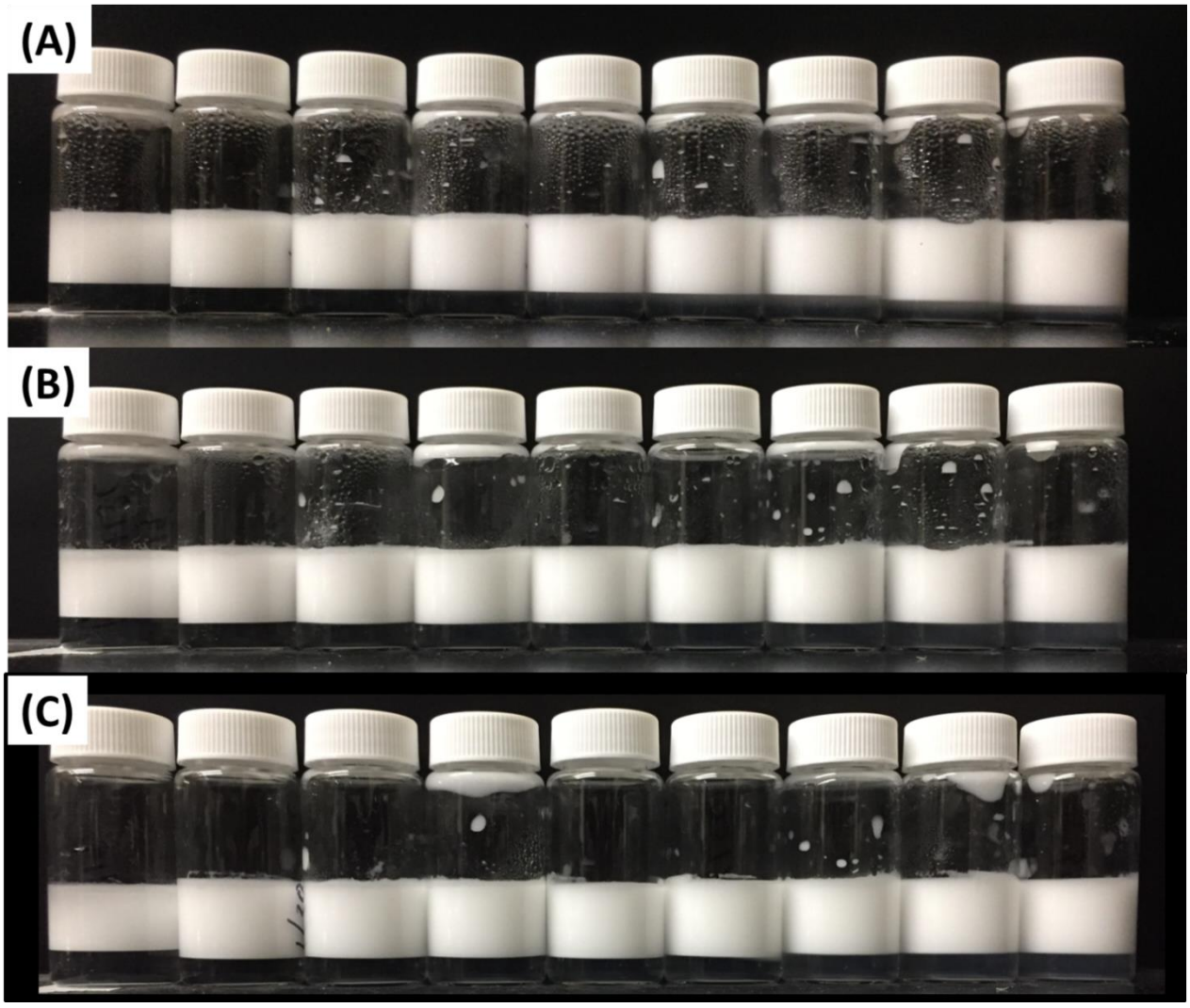

Figure B.7 – LSC glymo-stabilized emulsions (A) 24 hours, (B) 1 week after emulsification. From left to right: 0.34 wt%, 0.69 wt%, 1.4 wt%, 2.1 wt%, 2.8 wt%, 3.4 wt%, 4.1 wt%, 5.5 wt%, and 6.9 wt% LSC glymo-coated nanoparticles.

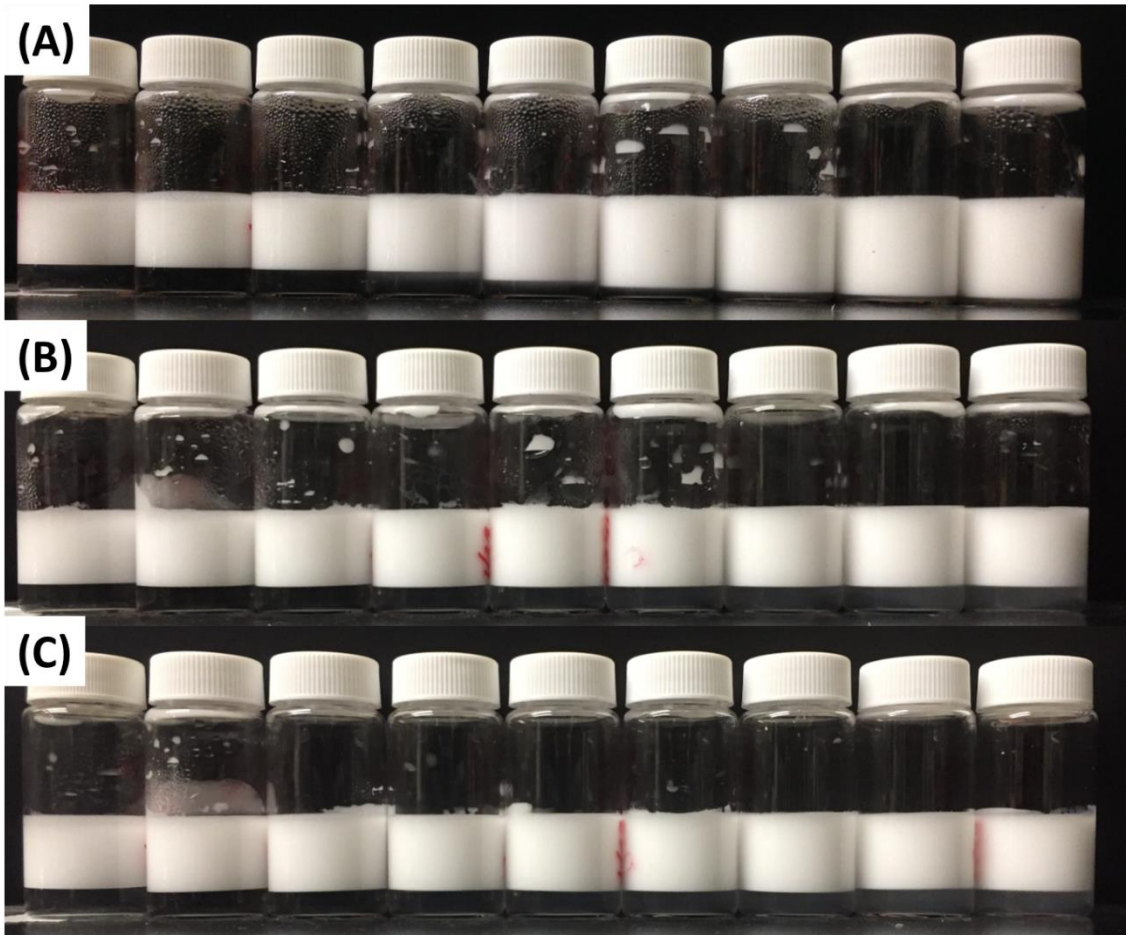

Figure B.8 – HSC glymo-stabilized emulsions (A) 24 hours, (B) 1 week after emulsification. From left to right: 0.34 wt%, 0.69 wt%, 1.4 wt%, 2.1 wt%, 2.8 wt%, 3.4 wt%, 4.1 wt%, 5.5 wt%, and 6.9 wt% HSC glymo-coated nanoparticles.

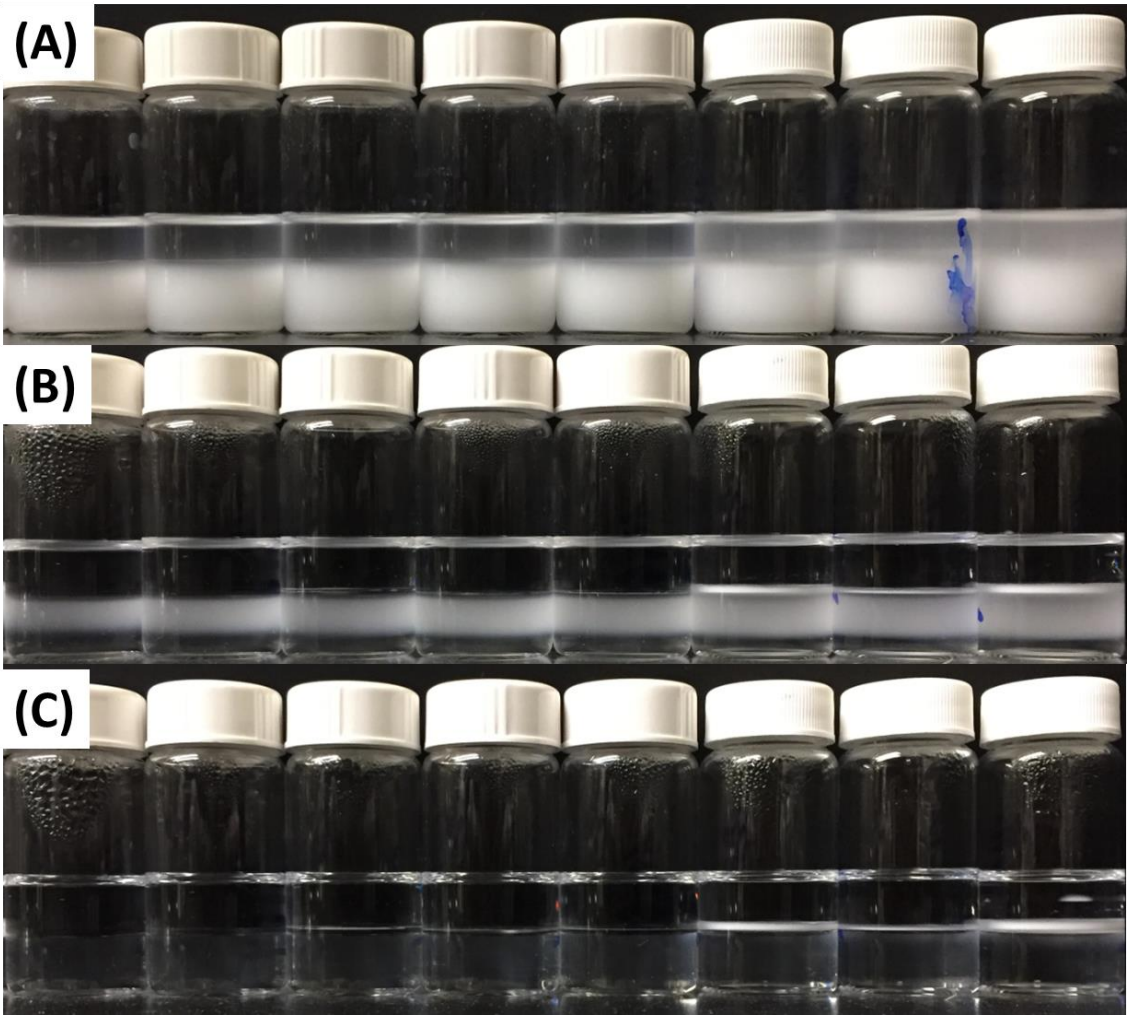

Figure B.9 – Decane-in-water emulsions stabilized with glymo silane (without nanoparticles) using the same emulsion formulation as the 0.69 wt%, 1.4 wt%, 2.1 wt%, 2.8 wt%, 3.4 wt%, 4.1 wt%, 5.5 wt%, and 6.9 wt% HSC glymo-modified nanoparticles. (A) Immediately after emulsification, (B) 24 hours after emulsification, (C) 48 hours after emulsification.

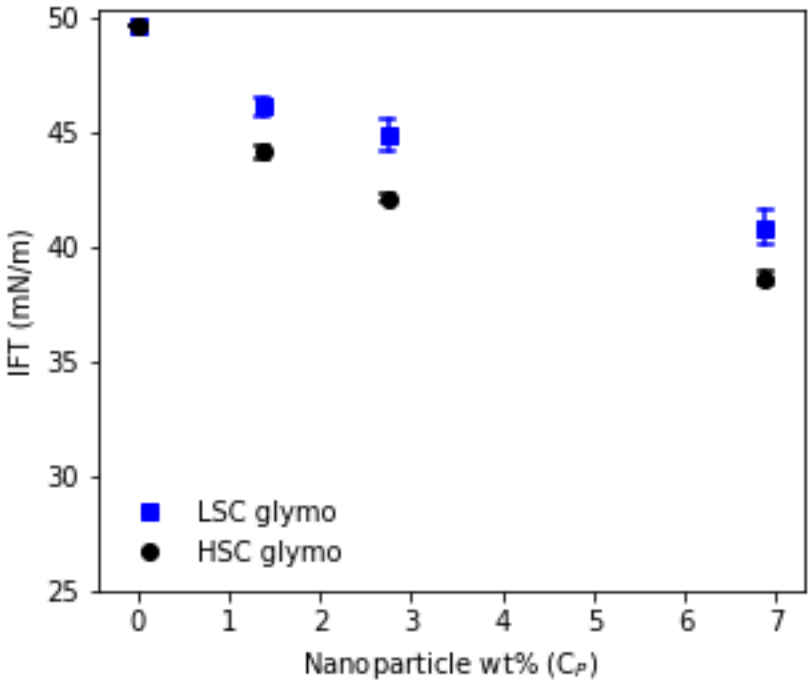

Figure B.10 – Interfacial tension (IFT) between decane and LSC (blue, squares) and HSC (black, circles) glymo-coated nanoparticles vs. nanoparticle concentration.

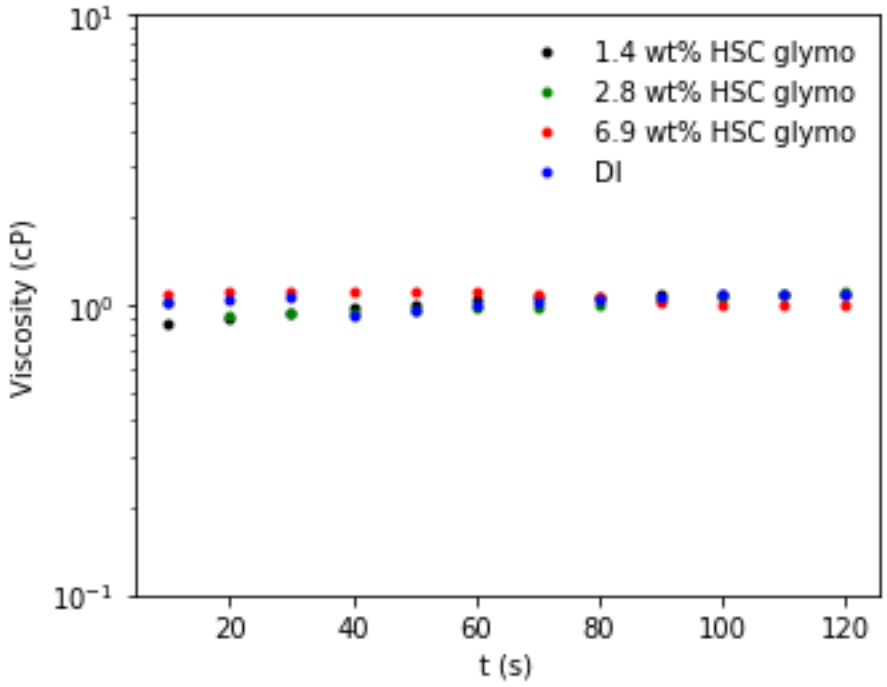

Figure B.11 – Dispersion rheology of: DI water (blue), 1 wt% (black), 2 wt% (green), and 5 wt% (red) HSC glymo nanoparticle dispersions. Samples were sheared for two minutes at 75 1/s (T = 23°C).

Sample	Viscosity	Stdev
DI	1.03	5E-02
1.4 wt% HSC	1.02	8E-02
2.8 wt% HSC	1.01	6E-02
6.9 wt% HSC	1.07	5E-02

Table B. 1 – Average viscosities for different nanoparticle dispersions.

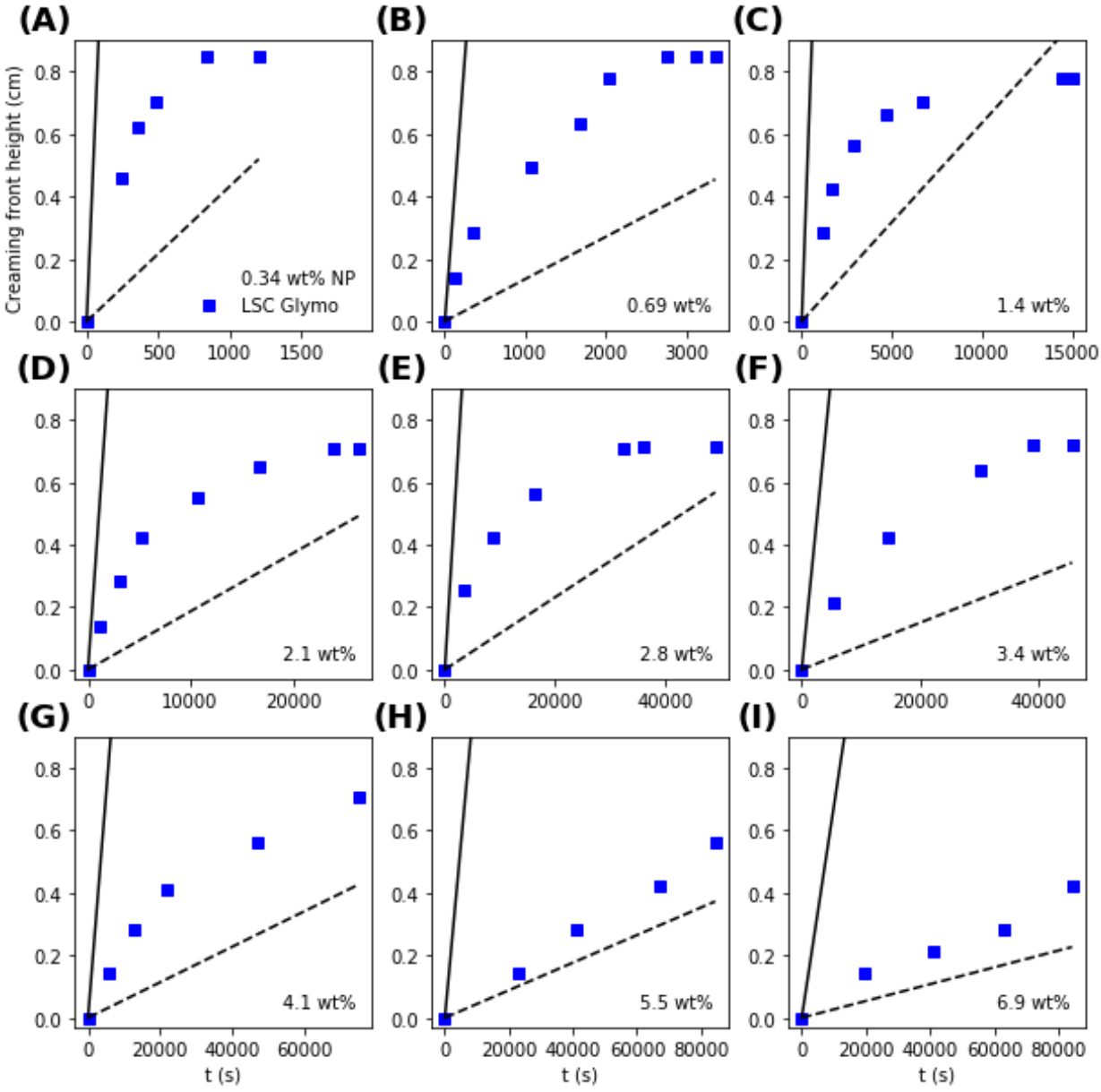

Figure B.12 – Creaming front velocities for LSC glymo-stabilized emulsions: (A) 0.34 wt%, (B) 0.69 wt%, (C) 1.4 wt%, (D) 2.1 wt%, (E) 2.8 wt%, (F) 3.4 wt%, (G) 4.1 wt%, (H) 5.5 wt%, and (I) 6.9 wt%. The solid, black line is the ideal Stokes law creaming front and the dashed, black line is the modified Richardson-Zaki model.

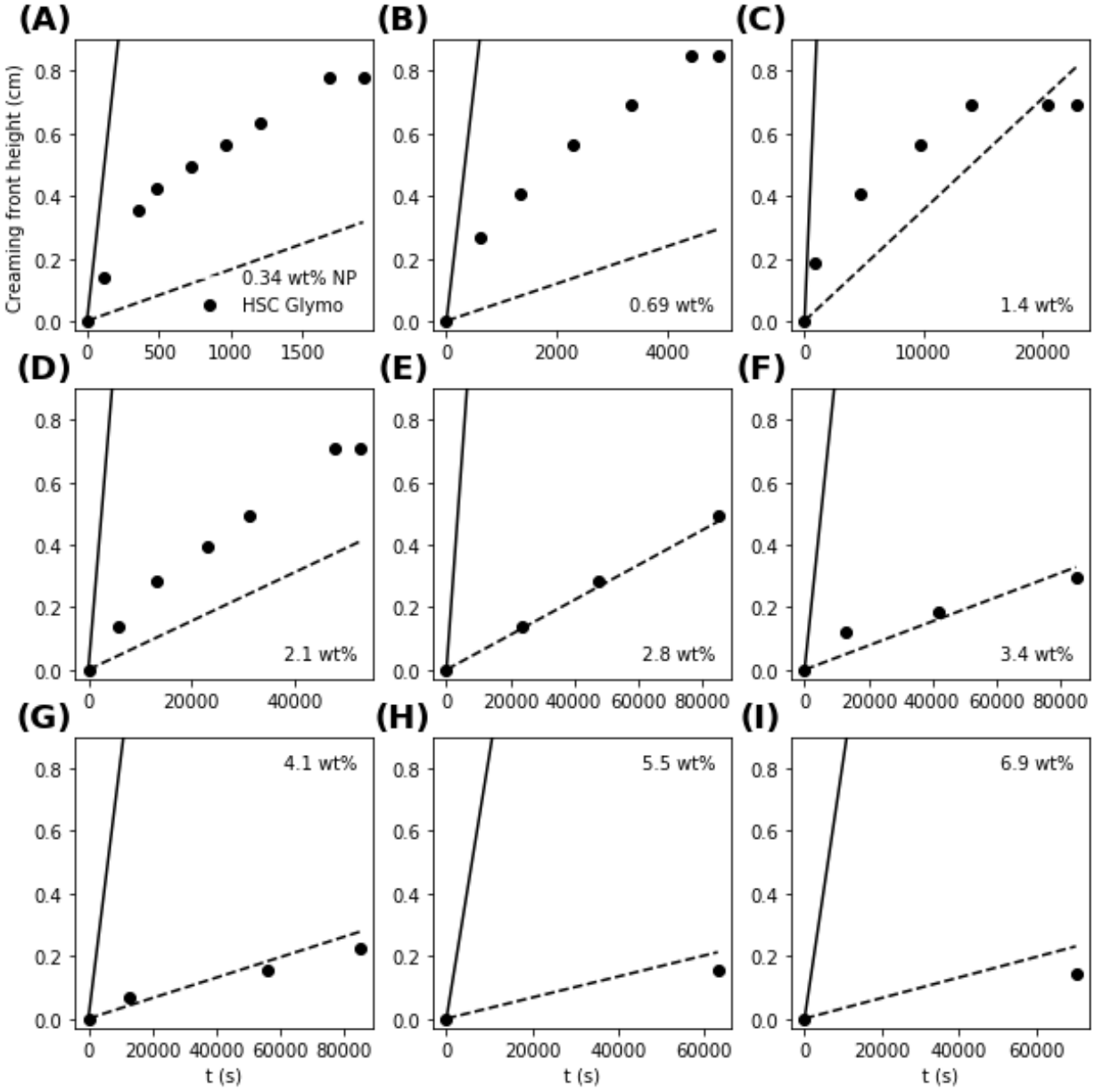

Figure B.13 – Creaming front velocities for HSC glymo-stabilized emulsions: (A) 0.34 wt%, (B) 0.69 wt%, (C) 1.4 wt%, (D) 2.1 wt%, (E) 2.8 wt%, (F) 3.4 wt%, (G) 4.1 wt%, (H) 5.5 wt%, and (I) 6.9 wt%. The solid, black line is the ideal Stokes law creaming front and the dashed, black line is the modified Richardson-Zaki model.

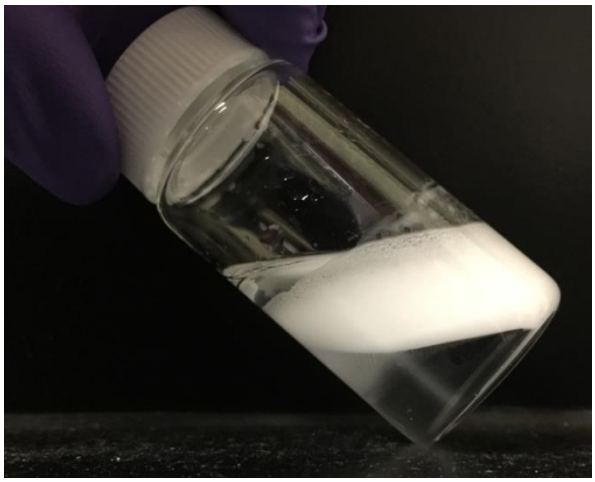

Figure B.14 – A vial with a decane-in-water emulsion stabilized with 0.34 wt% LSC glymo-coated particles. The image was taken two weeks after emulsification. Notice the clear coalesced oil that is resting on top of the emulsion.

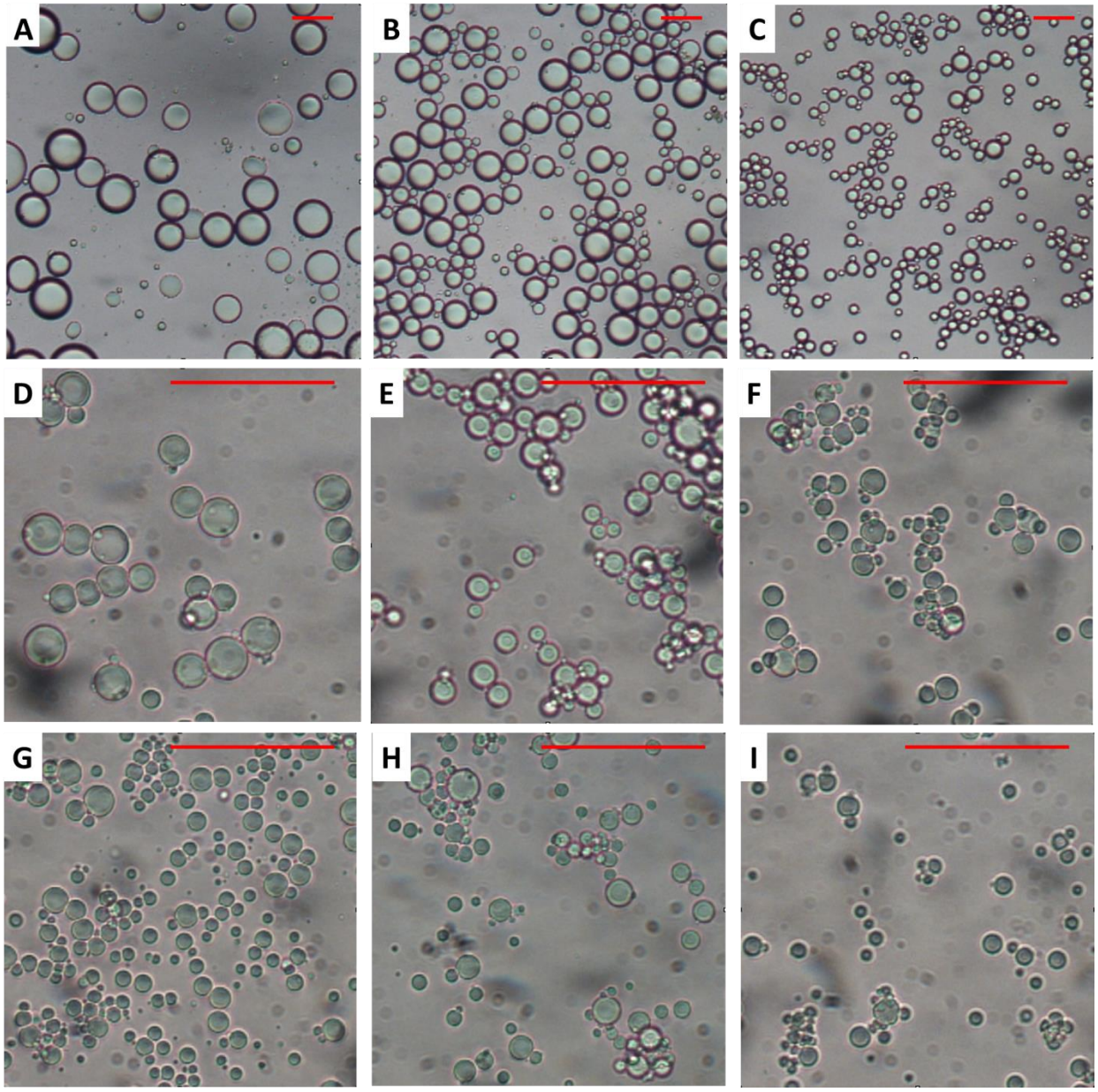

Figure B.15 – Optical micrographs for 3M PEG stabilized emulsions immediately after formation using: (A) 0.34 wt%, (B) 0.69 wt%, (C) 1.4 wt%, (D) 2.1 wt%, (E) 2.8 wt%, (F) 3.4 wt%, (G) 4.1 wt%, (H) 5.5 wt%, and (I) 6.9 wt% 3M PEG nanoparticles.

Appendix C – water-in-water emulsions

TWO PHASE BOUNDARY (BINODAL)

For an aqueous, two phase system (ATPS), establishing the two phase region (often referred to as the binodal) is important because it allows for the selection of appropriate incompatible solute concentrations that will form 2 phases. Determining the two phase region was the first step I took in this work.

I followed Kaul (2000) to determine the binodal for my polyethylene-glycol (20,000 g/mol)/magnesium sulfate ATPS. Kaul (2000) outlines two common techniques to determine the two-phase region, which are: (1) the turbidometric titration method and (2) the cloud point method. Both are very similar, however, I found the turbidometric titration to be easier to do in the lab, so it was the method that I used.

In the turbidometric titration method, a turbid, two phase solution is made and the mass of each species is recorded. Next, while the solutions is continually stirred, it is diluted with DI water (Figure C.1 blue dots) until the solution is no longer turbid and there is only one phase present. The mass fractions of each species can be calculated and the point at which one phase became present lies on the binodal of the ATPS (Figure C.1, red dot)

To determine the phase boundary for my PEG/ $MgSO_4$ system, I made a concentrated solution of $MgSO_4$ that was 23 wt%. The total mass of the solution was 250 g (57.5 g $MgSO_4$; 192.5 g DI). For my polymer solution, I made a concentrated stock solution that was 40 wt% 20,000 g/mol PEG. The total mass of this solution was also 250 g (100 g PEG; 150 g DI).

Next, I made 5 solutions with varying mass ratios of concentrated PEG and magnesium sulfate solutions (Figure C.1 black dots). The solutions that I made had the following mass of each stock solution (listed below). In parenthesis I am showing the mass fraction that each species represents as a fraction of the total solution mass:

1. 5 g 40 wt% PEG, 1 g 23 wt% $MgSO_4$ (33.3 wt% PEG, 3.8 wt% $MgSO_4$)
2. 4 g 40 wt% PEG, 2 g 23 wt% $MgSO_4$ (26.7 wt% PEG, 7.7 wt% $MgSO_4$)
3. 3 g 40 wt% PEG, 3 g 23 wt% $MgSO_4$ (20.0 wt% PEG, 11.5 wt% $MgSO_4$)
4. 2 g 40 wt% PEG, 4 g 23 wt% $MgSO_4$ (13.3 wt% PEG, 15.3 wt% $MgSO_4$)
5. 1 g 40 wt% PEG, 5 g 23 wt% $MgSO_4$ (6.7 wt% PEG, 19.2 wt% $MgSO_4$)

These solutions were diluted with DI water while stirring on a lab stir plate. Once there was only one phase was present, the experiment was stopped and mass fractions for each species were calculated. The end result is the two-phase boundary for this system (Figure C.1 black line).

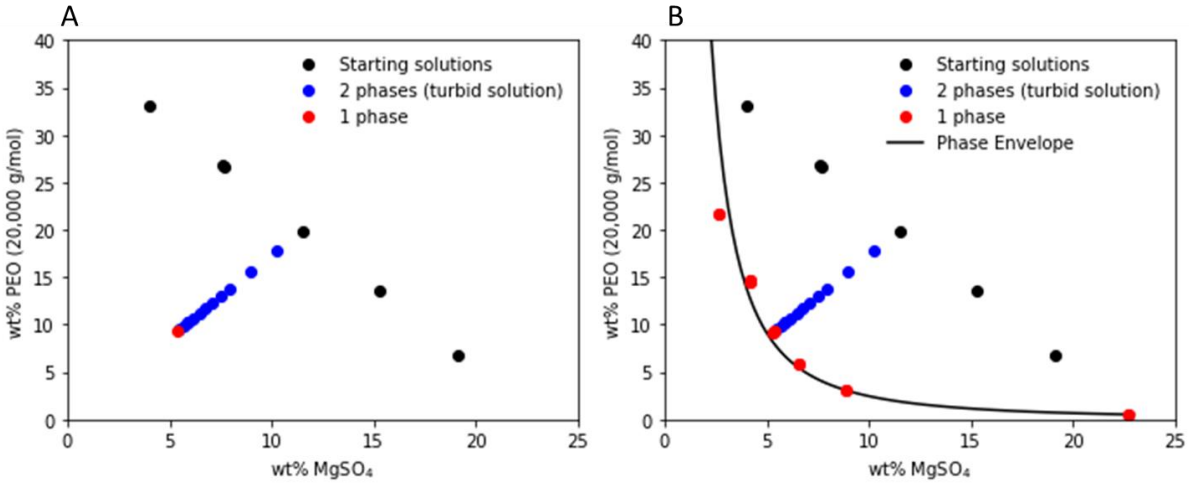

Figure C.1 – (A) black dots: starting solutions for my turbidometric titration experiments. Blue dots, data points associated with a turbidometric titration experiment to determine a point on the binodal. Red dot, a point that is on the binodal. (B) The same plot in (A), but including the two-phase envelope for this 20,000 g/mol PEG and $MgSO_4$ system.

IFT CORRELATION

Wu et al. (1996) presents a wide range of IFT data for different PEG/salt/water systems. I used their data to estimate the IFT between my PEG/ $MgSO_4$ ATPS. The interfacial tension (σ) was determined using the following correlation which is shown in equation (C.1)

$$\log(\sigma) = a_1 + b_1 \log(\mathrm{TLL}), \qquad \text{(C.1)}$$

where TLL is the tie-line length and has units of wt%, a_1 and b_1 are empirical constants. These constants were obtained by making log-log plots of the fitting parameter (a_1 or b_1) versus PEG molecular weight. We obtained a_1 to be 1.76 and b_1 to be 1.24. For a TLL of 38.8 wt% we get an estimated IFT of 1.6 mN/m and 0.77 mN/m for a TLL of 21.5 wt%.

Because I studied the behavior of an emulsion system that had a TLL of 21.5 wt%, I experimentally measured the IFT of this system using the pendent drop method. I did this by preparing a two-phase mixture by mixing 30 g 40 wt% PEG, 10.5 g 23 wt% $MgSO_4$, and 19.5 g DI water. This produced a two phase system with a PEG mass fraction of 20 wt% and ~ 4 wt% $MgSO_4$. The top and bottom phases were used for IFT measurements. I obtained IFTs that ranged from 0.98-1.54 mN/m, which is on the same order of magnitude from the correlations.

RHEOLOGY

When performing rheological measurements, it is important to make sure all samples are measured in the same way. This is important when samples are sensitive to shear (like water-in-water emulsions). A common experimental approach to overcome this issue is to perform a conditioning step on samples.

One potential concern with the conditioning step is that sometimes the sample is not given enough time (rest) before the actual measurement is made, which would suggest the samples rheological state is changing (i.e., it is in a transient state) prior to the measurement being made. Ideally, this should be avoided.

Enough time must pass before a measurement the measurement is done. For my rheology measurements, I used a conditioning step that was 10 seconds long and done rate of 10 s^{-1}. Upon completing this conditioning step; the sample was allowed to rest for one minute before the actual measurement was done.

To determine whether or not enough time had passed after the conditioning step, I had to monitor the response of the sample with time. In order to do this, a very low strain amplitude is used so the sample is in the linear viscoelastic regime (LVE regime) during the monitored response.

Figure C.2 shows how magnesium sulfate-in-polyethylene glycol water-in-water emulsions stabilized with 6 and 50 nm particles change with respect to time after completing the conditioning step conditioning step 10 seconds of shear at 10 s^{-1}. Figure C.2 A shows the response of the elastic storage moduli (G') while Figure C.2 B shows the loss moduli (G") of the emulsion. The elastic storage modulus of both emulsions changes with time up until about 30 seconds after the conditioning step. After this time, there is little to no change in the sample with respect to time.

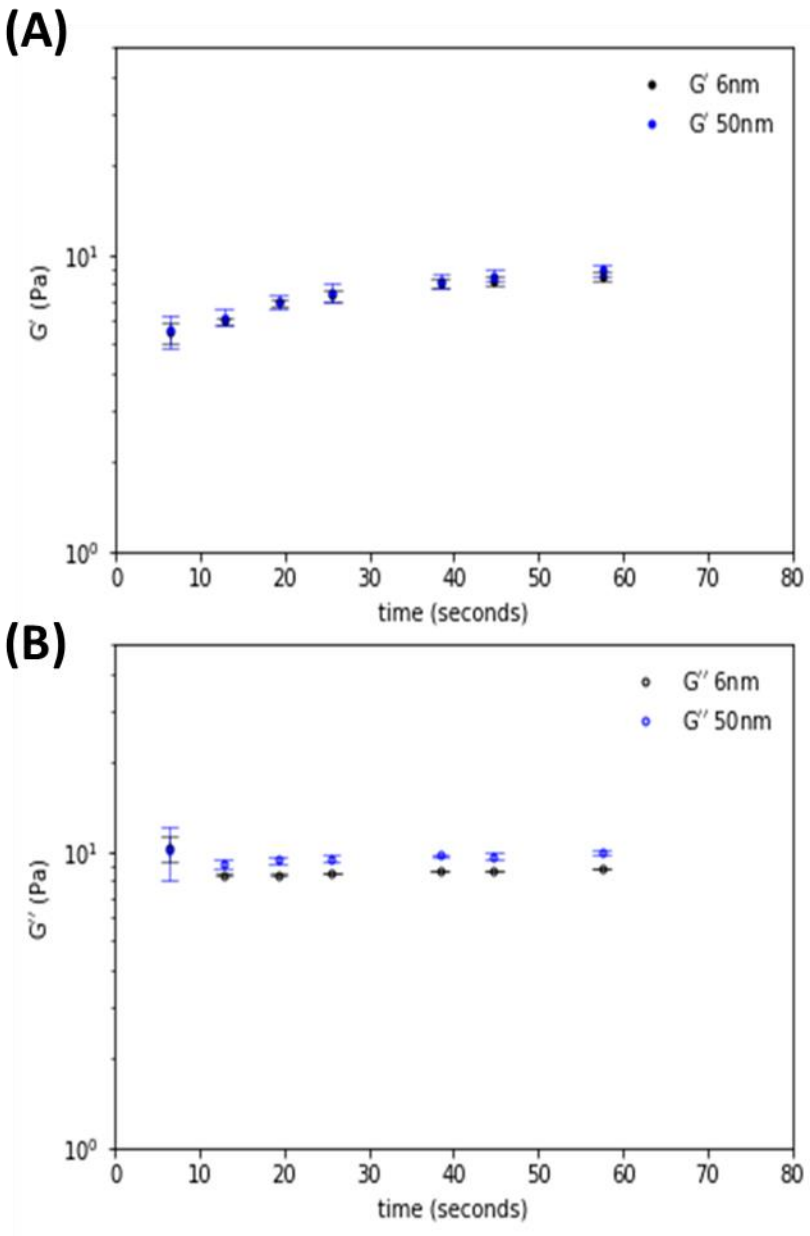

Figure C.2 – Response of (A) G' and (B) G" of 6 wt% 6 nm and 50 nm particle stabilized emulsions after they were pre sheared for 10 second at 10 s^{-1}. A strain amplitude of 0.1% and frequency of 1 Hz were used. Error bars represent the range in data collected for two experiments.

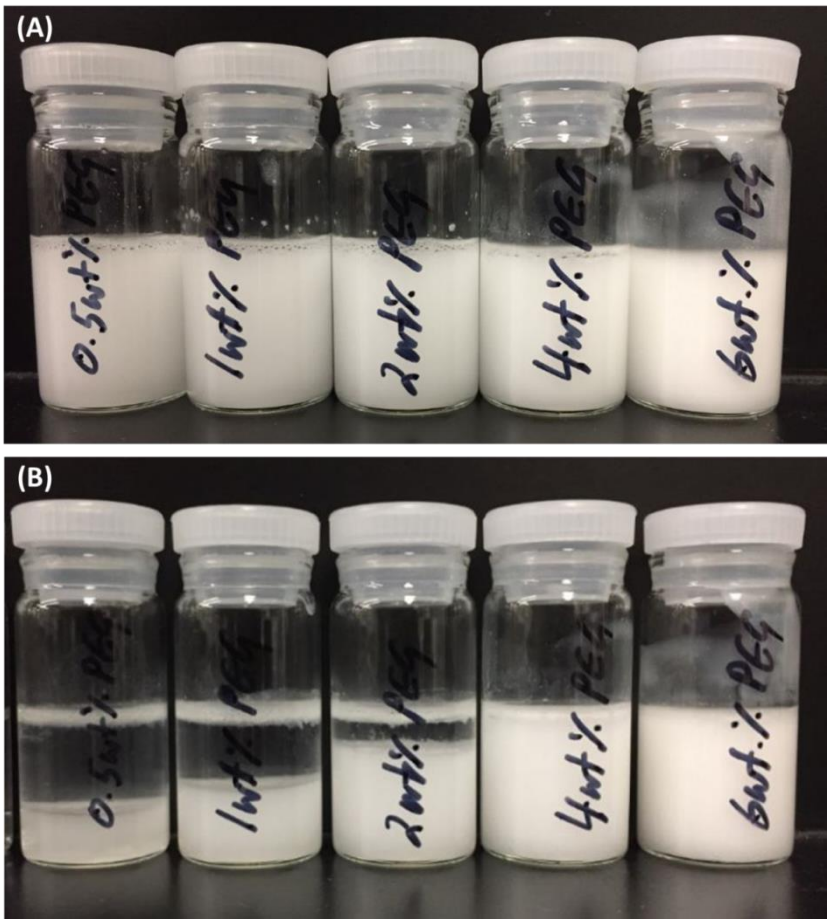

Figure C.3 – Emulsions stabilized with 6 nm PEGylated particles (A) immediately after homogenization, (B) one week after homogenization.

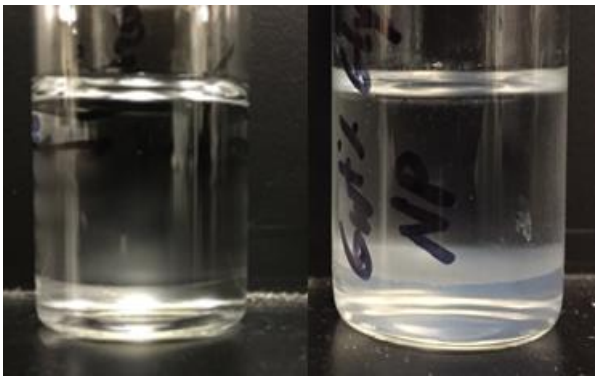

Figure C.4 – (left) Aqueous two phase system of 20,000 g/mol polyethylene glycol (20 wt%) and magnesium sulfate (4 wt%) without added nanoparticles. (Right) Aqueous two phase system of 20,000 g/mol polyethylene glycol (20 wt%) and magnesium sulfate (4 wt%) and 6 wt% glymo functionalized nanoparticles 24 hours after homogenization. There is no particle flocculation and no emulsion stabilization.

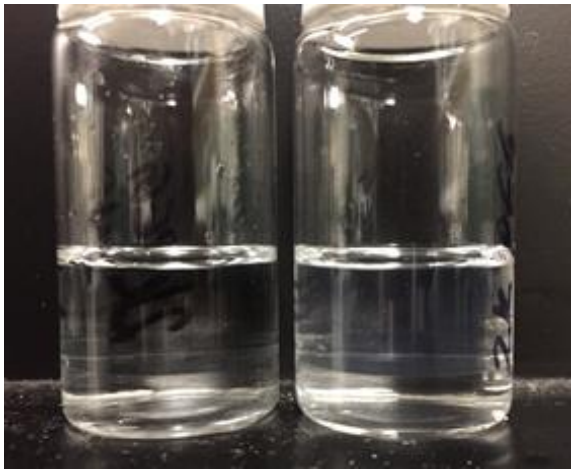

Figure C.5 – (left) Aqueous two phases of 2,000 g/mol polyethylene glycol (24 wt%) and magnesium sulfate (6.9 wt%) without added nanoparticles. (right) Aqueous two phases of 2,000 g/mol polyethylene glycol (24 wt%), magnesium sulfate (6.9 wt%) and 6 wt% PEGylated nanoparticles 24 hours after homogenization. There is no particle flocculation and no emulsion stabilization.

References

A. Azevedo, A. Gomes, P. Rosa, I. Ferreira, A. Pisco, M. Aires-Barros, Partitioning of human antibodies in polyethylene glycol-sodium citrate aqueous two-phase systems, Separation and Purification Technology. 65 (2009) 14-21.

A. Baldygin, D. Nobes, S. Mitra, Water-alternate-emulsion (WAE): A new technique for enhanced oil recovery, Journal of Petroleum Science and Engineering. 121 (2014) 167-173.

A. Behzadi, A. Mohammadi, Environmentally responsive surface-modified silica nanoparticles for enhanced oil recovery, Journal of Nanoparticle Research. 18 (2016) 265-284.

A. Drelich, F. Gomez, D. Clausse, I. Pezron, Evolution of water-in-oil emulsions stabilized with solid particles- Influence of added emulsifier, Colloids and Surfaces: A Physicochemical and Engineering Aspects. 365 (2010) 171-177.

A. Gonzalez-Jordan, L. Benyahia, T. Nicolai, Cold gelation of water in water emulsions stabilized by protein particles, Colloids and Surfaces A. 532 (2017) 332-341.

A. Gonzalez-Jordan, T. Nicolai, L. Benyahia, Enhancement of the particle stabilization of water-in-water emulsions by modulating the phase preference of the particles, Journal of Colloid and Interface Science. (2018)

A. Kaul, Chapter 2, The Phase Diagram, Aqueous two-phase systems: methods and protocols, Methods in Biotechnology. 11 (2000) 11-21.

A. Kumar, Y. Raman, C. Aichele, Demulsification of surfactant-stabilized water-in-oil (cyclohexane) emulsions using silica nanoparticles, Energy and Fuels. 32 (2018) 8121-8130.

A. Mandal, A. Samanta, A. Bera, K. Ojha, Characterization of oil-water emulsion and its use in enhanced oil recovery, Industrial & Engineering Chemistry Research. 49 (2010) 12756-12761.

A. Milling, B. Vincent, S. Emmett, A. Jones, Depletion flocculation in dispersions of sterically-stabilised silica particles 3. The effect of grafted chain length, Colloids and Surfaces. 57 (1991) 185-195.

A. Pandey, A. Telmadarreie, M. Trifkovic, S. Bryant, Cellulose nanocrystal stabilized emulsions for conformance control and fluid diversion in porous media, SPE Annual Technical Conference and Exhibition, September 2018.

A. Pandey, M. Derakhshandeh, S. Kedzior, B. Pilapil, N. Shomrat, T. Segal-Peretz, S. Bryant, M. Trifkovic, Role of interparticle interactions on microstructural and rheological properties of cellulose nanocrystal stabilized emulsions, Journal of Colloid and Interface Science. 532 (2018) 808-818.

A. Pena, G. Hirasaki, C. Miller, Chemically induced destabilization of water-in-crude oil emulsions, Industrial and Engineering Chemistry Research. 44 (2005) 1139-1149.

A. Saha, A. Nikova, P. Venkataraman, V. John, A. Bose, Oil emulsification using surface-tunable carbon black particles, ACS Applied Materials & Interfaces. 5 (2013) 3094-3100.

A. Schroder, J. Sprakel, K. Schroen, J. Spaen, C. Berton-Carabin, Coalesence stability of Pickering emulsions produced with lipid particles: A microfluidic study, Journal of Food Engineering. 234 (2018) 63-72.

A. Tyowua, S. Yiase, B. Binks, Double oil-in-oil-in-oil emulsions stabilized solely by particles, Journal of Colloid and Interface Science. 488 (2017) 127-134.

A. Umar, I. Saaid, A. Sulaimon, R. Pilus, A review of petroleum emulsions and recent progress on water-in-oil crude oil emulsions stabilized by natural surfactants and solids, Journal of Petroleum Science and Engineering. 165 (2018) 673-690.

A. Worthen, H. Bagaria, Y. Chen, S. Bryant, C. Huh, K. Johnston, Nanoparticle-stabilized carbon dioxide-in-water foams with fine texture, Journal of Colloid and Interface Science. 391 (2013) 142-151.

A. Worthen, L. Foster, J. Dong, J. Bollinger, A. Peterman, L. Pastora, S. Bryant, T. Truskett, C. Bielaski, K. Johnston, Synergist formation and stabilization of oil-in-water emulsions by a weakly interacting mixture of zwitterionic surfactant and silica nanoparticles, Langmuir. 30 (2014) 984-994.

A. Worthen, S. Bryant, C. Huh, K. Johnston, Carbon dioxide-in-water foams stabilized with nanoparticles and surfactant acting in synergy, AIChE. 59 (2013) 3490-3501.

A. Worthen, V. Tran, K. Cornell, T. Truskett, K. Johnston, Steric stabilization of nanoparticles with grafted low molecular weight ligands in highly concentrated brines including divalent ions, Soft Matter. 12 (2016) 2025-2039.

A. Worthen, V. Tran, K. Cornell, T. Truskett, K. Johnston, Steric stabilization of nanoparticles with grafted low molecular weight ligands in highly concentrated brines including divalent ions, Soft Matter. 12 (2016) 2025-2039.

AEROSIL – Technical bulletin number 11: Fumed silica, Basic characteristics and applications of AEROSIL fumed silica, 8th edition.

AEROSIL – Technical bulletin number 11: Fumed silica, Basic characteristics and applications of AEROSIL fumed silica, 4th edition.

B. Binks, A. Desforges, D. Duff, Synergistic stabilization of emulsions by a mixture of surface-active nanoparticles and surfactant, Langmuir. 23 (2007) 1098-1106.

B. Binks, C. Whitby, Nanoparticle silica-stabilized oil-in-water emulsions: improving emulsion stability, Colloids and Surface A: Physicochemical Engineering Aspects. 253 (2005) 105-115.

B. Binks, J. Philip, J. Rodrigues, Inversion of silica-stabilized emulsions induced by particle concentration, Langmuir. 21 (2005) 3296-3302.

B. Binks, J. Rodrigues, W. Frith, Synergistic interaction in emulsions stabilized by a mixture of silica nanoparticles and cationic surfactants, Langmuir. 23 (2007) 3626-3636.

B. Binks, Modern Aspects of Emulsion Science, The Royal Society of Chemistry. Cambridge, 1998.

B. Binks, Particles as surfactants – similarities and differences, Current Opinion in Colloid and Interface Science. 7 (2002) 21-41.

B. Binks, S. Lumsdon, Influence of particle wettability on the type and stability of surfactant-free emulsions, Langmuir. 16 (2000) 8622-8631.

B. Binks, S. Lumsdon, Pickering emulsions stabilized by monodisperse latex particles: effects of particle size, Langmuir. 17 (2001) 4540-4547.

B. Binks, S. Lumsdon, Stability of oil-in-water emulsions stabilized by silica particles, Physical Chemistry Chemical Physics. 1 (1999) 3007-3016.

B. Derjaguin, L. Landau, Theory of the stability of strongly charged lyophobic sols and the adhesion of strongly charged particles in solutions of electrolytes, Acta Physicochim. (1941).

B. Hoxha, E. van Oort, H. Daigle, How do nanoparticles stabilize shale? SPE International Conference on Oilfield Chemistry. April, 2017.

B. Madivala, S. Vandebril, J. Fransaer, J. Vermant, Exploiting particle shape in solid stabilized emulsions, Soft Matter. 5 (2009) 1717-1727.

B. Murray, N. Phisarnchananan, The effect of nanoparticles on the phase separation of waxy corn starch + locust bean gum or guar gum, Food Hydrocolloids. 42 (2014) 92-99.

B. Nguyen, W. Wang, B. Saunders, L. Benyahia, T. Nicolai, pH-responsive water-in-water Pickering emulsions, Langmuir. 31 (2015) 3605-3611.

B. Pilapil, H. Jahandideh, S. Bryant, M. Trifkovic, Stabilization of oil-in-water emulsions with noninterfacially adsorbed particles, Langmuir. 32 (2016) 7109-7116.

B. Spisak, Using nanoparticle stabilized foam to achieve wellbore stability in shales, MS Thesis, The University of Texas at Austin, 2011.

C. Berton-Carabin, K. Schroen, Pickering emulsions for food applications: background, trends, and challenges, Annual Review of Food Science and Technology. 6 (2015) 263-297.

C. Gao, Viscosity of partially hydrolyzed polyacrylamide under shearing and heat, Journal of Petroleum Exploration and Production Technology. 3 (2013) 203-206.

C. Griffith, H. Daigle, Manipulation of Pickering emulsion rheology using hydrophilically modified silica nanoparticles in brine, Journal of Colloid and Interface Science. 509 (2018) 132-139.

C. Griffith, H. Daigle, Stability of polyvinyl alcohol-coated biochar nanoparticles in brine, Journal of Nanoparticle Research. 19 (2017) 1-12.

C. Huh, G. Pope, Residual oil saturation from polymer floods: laboratory measurements and theoretical interpretation, SPE Improved Oil Recovery Symposium. April 2008.

C. Hwang, G. Ruan, L. Wang, H. Zheng, E. Samuel, C. Xiang, W. Lu, W. Kasper, K. Huang, Z. Peng, Z. Schaefer, A. Kan, A. Marti, M. Wong, M. Tomson, J. Tour, Carbon-based nanoreporters designed for subsurface hydrogen sulfide detection, ACS Applied Materials and Interfaces. 6 (2014) 7652-7658.

C. Knieke, A. Berger, M. Voigt, R. Taylor, J. Rohrl, W. Peukert, Scalable production of graphene sheets by mechanical delamination, Carbon. 48 (2010) 3196-3204.

C. McAuliffe, Oil-in-water emulsions and their flow properties in porous media, Journal of Petroleum Technology. 25 (1973) 727-733.

C. Metin, Characterization of nanoparticle transport in flow through permeable media, PhD Dissertation. UT Austin, 2012.

C. Metin, J. Baran, Q. Nguyen, Adsorption of surface functionalized silica nanoparticles onto mineral surfaces and decane/water interface, Journal of Nanoparticle Research. 14:1246 (2012).

C. Metin, L. Lake, C. Miranda, Q. Nguyen, Stability of aqueous silica nanoparticle dispersions, Journal of Nanoparticle Research. 13 (2011) 839-850.

C. Priest, M. Reid, C. Whitby, Formation and stability of nanoparticle-stabilized oil-in-water emulsions in a microfluidic chip, Journal of Colloid and Interface Science. 363 (2011) 301-306.

C. Vashisth, C. Whitby, D. Fornasiero, J. Ralston, Interfacial displacement of nanoparticles by surfactant molecules in emulsions, Journal of Colloid and Interface Science. 349 (2010) 537-543.

C. Wang, A. Bobba, R. Attinti, C. Shen, V. Lazouskaya, L. Wang, Y. Jin, Retention and transport of silica nanoparticles in saturated prous media: effect of concentration and particle size, Environmental Science and Technology. 46 (2012) 7151-7158.

C. Whitby, A. Onnink, Rheological properties and structural correlations in particle-in-oil gels, Advanced Powder Technology. 25 (2014) 1185-1189.

C. Whitby, D. Fornasiero, J. Ralston, Effect of adding anionic surfactant on the stability of Pickering emulsions, Journal of Colloid and Interface Science. 329 (2009) 173-181.

C. Whitby, E. Wanless, Controlling Pickering emulsion destabilisation: a route to fabricating new materials by phase Inversion, Materials. 9 (2016) 626.

C. Whitby, F. Fischer, D. Fornasiero, J. Ralston, Shear-induced coalescence of oil-in-water Pickering emulsions, Journal of Colloid and Interface Science. 361 (2011) 170-177.

C. Whitby, H. Anwar, J. Hughes, Destabilizing Pickering emulsions by drop flocculation and adhesions, Journal of Colloid and Interface Science. 465 (2016) 158-164.

C. Whitby, L. Lotte, C. Lang, Structure of concentrated oil-in-water Pickering emulsions, Soft Mater. 8 (2012) 7784-7789.

C. Whitby, M. Krebsz, Coalescence in concentrated Pickering emulsions under shear, Soft Matter. 10 (2014) 4848-4854.

C. Esquena, Water-in-water (W/W) emulsions, Current Opinion in Colloid and Interface Science. 25 (2016) 109-119.

D. Aarts, J. van der Wiel, H. Lekkerkerker, Interfacial dynamics and the static profile near a single wall in a model colloid-polymer mixture, Journal of Physics: Condensed Matter. 15 (2003) S245-S250.

D. Arab, A. Kantzas, S. Bryant, Nanoparticle stabilized oil in water emulsions: A critical review, Journal of Petroleum Science and Engineering. 163 (2018) 217-242.

D. Boverhof, C. Bramante, J. Butala, S. Clancy, M. Lafranconi, J. West, S. Gordon, Comparative assessment of nanomaterial definitions and safety evaluation considerations, Regulatory Toxicology and Pharmacology. 73 (2015) 137-150.

D. Buzza, P. Fletcher, T. Georgiou, N. Ghasdian, Water-in-Water Emulsions Based on Incompatible Polymers and Stabilized by Triblock Copolymers-Templated Polymersomes, Langmuir. 29 (2013) 14804-14814.

D. de Araujo Sampaio, L. Mafra, C. Yamanoto, E. de Andrade, M. de Souza, M. Mafra, F. De Castilhos, Aqueous two-phase (polyethylene glycol + sodium sulfate) system for caffeine extraction: Equilibrium diagrams and partitioning study, J. Chem. Thermodynamics. 98 (2016) 86-94.

D. Espinosa, D. Walker, D. Alexis, V. Dwarakanath, A. Jackson, D. Kim, H. Linnemeyer, T. Malik, D. McKilligan, P. New, A. Poulsen, G. Winslow, Dynamic field rheology, filterability and injectivity characterization using a portable measurement unit, SPE Improved Oil Recovery Conference. April 2018.

D. Espinosa, F. Caldelas, K. Johnston, S. Bryant, C. Huh, Nanoparticle-Stabilized Supercritical CO_2 Foams for Potential Mobility Control Applications, SPE Improved Oil Recovery Symposium. Tulsa, Oklahoma, 2010.

D. Lee, H. Cho, J. Lee, C. Huh, K. Mohanty, Fly ash nanoparticles as a CO_2 foam stabilizer, Powder Technology. 283 (2015) 77-84.

D. Levitt, G. Pope, Selection and screening of polymers for enhanced-oil recovery, SPE Improved Oil Recovery Symposium. April 2008.

D. Schmidt, H. Soo, C. Radke, Linear oil displacement by the emulsion entrapment process, Society of Petroleum Engineers. 24 (1984) 351-360.

D. Walker, C. Britton, D. Kim, S. Dufour, U. Weerasooriya, G. Pope, The impact of microemulsion viscosity on oil recovery, SPE Improved Oil Recovery Symposium. April 2012.

E. Ayed, R. Cochereau, C. Dechance, I. Capron, T. Nicolai, L. Benyahia, Water-in-Water emulsion gels stabilized by cellulose nanocrystals, Langmuir. 34 (2018) 6887-6893.

E. Dickinson, Food emulsions and foams: stabilization by particles, Current Opinion in Colloid and Interface Science. 15 (2010) 40-49.

E. Ruckenstein, J. Chi, Stability of microemulsions, Journal of the Chemical Society, Faraday Transactions 2: Molecular and Chemical Physics. 71 (1975) 1690-1707.

E. Verwey, J. Overbeek, Theory and stability of lyophobic colloids, Elsevier. (1948).

E. Vignati, R. Piazza, Pickering emulsions: Interfacial tension, colloidal layer morphology, and trapped-particle motion, Langmuir. 17 (2003) 6650-6656.

F. Gautier, M. Destribats, R. Perrier-Cornet, J. Dechezelles, J. Giermanska, V. Heroguez, S. Ravaine, F. Leal-Calderon, V. Schmitt, Pickering emulsions with stimulable particles: from highly- to weakly-covered interfaces, Physical Chemistry Chemical Physics. 9 (2007) 6455-6462.

F. Yang, S. Liu, J. Xu, Q. Lan, F. Wei, D. Sun, Pickering emulsions stabilized solely by layered double hydroxides particles: The effect of salt on emulsion formation and stability, Journal of Colloid and Interface Science. 302 (2006) 159-169.

G. Balakrishan, T. Nicolai, L. Benyahia, D. Durand, Particles trapped at the droplet interface in water-in-water emulsions, Langmuir. 28 (2012) 5921-5926.

G. Franks, Zeta potentials and yield stresses of silica suspensions in concentrated monovalent electrolytes: Isoelectric point shift and additional attraction, Journal of Colloid and Interface Science. 249 (2002) 44-51.

G. Frye, J. Berg, Antifoam action by solid particles, Journal of Colloid and Interface Science. 127 (1989) 222-238.

G. Howard, P. McConnell, Adsorption of polymers at the solution-solid interface: I. Polyethers on Silica, The Journal of Physical Chemistry. 71 (1967) 2974-2980.

G. Maitland, Oil and gas production, Current Opinion in Colloid & Interface Science. 5 (2000) 301-311.

G. Michael, W. Lortz, T. Ladwig, T. Gross, Dispersion comprising hydrophobized silicon dioxide particles, and paint preparation, United States Patent. US8882901B2, 2014.

G. Schmidt, M. Malwitz, Properties of polymer-nanoparticle composites, Current Opinion in Colloid and Interface Science. 8 (2003) 103-108.

H. Daigle, N. Griffith, Optimizing nanoparticles-stabilized emulsion behavior in porous media through electrostatic interactions, SPE Annual Technical Conference, September 2018.

H. Firoozmand, B. Murray, E. Dickinson, Interfacial structuring in a phase-separating mixed biopolymer solution containing colloidal particles, Langmuir. 25 (2009) 1300-1305.

H. Hassander, B. Johansson, B. Tornell, The mechanism of emulsion stabilization by small silica (Ludox) particles, Colloidsand Surfaces. 40 (1989) 93-105.

H. Jang, W. Lee, J. Lee, Nanoparticle dispersion with surface-modified silica nanoparticles and its effect on the wettability alteration of carbonate rocks, Colloids and Surfaces A. 554 (2018) 261-271.

H. Jang, W. lee, J. Lee, Nanoparticle dispersion with surface-modified silica nanoparticles and its effect on the wettability alteration of carbonate rocks, Colloids and Surface A. 554 (2018) 261-271.

H. Jennings, C. Johnson, C. McAuliffe, A caustic waterflooding process for heavy schools, Journal of Petroleum Technology. 26 (1974) 1343-1352.

H. Katepalli, A. Bose, T. Hatton, D. Blankschtein, Destabilization of oil-in-water emulsions stabilized by non-ionic surfactants: effect of particle hydrophilicity, Langmuir. 32 (2016) 10694-10698.

H. Katepalli, V. John, A. Tripathi, A. Bose, Microstructure and rheology of particle stabilized emulsions: effects of particle shape and itner-particle interactions, Journal of Colloid and Interface Science. 485 (2017) 11-17.

H. Koh, V. Lee, G. Pope, Experimental investigation of the effect of polymers on residual oil saturation, SPE Improved Oil Recovery Conference. April 2016.

H. Pei, Z. Shu, G. Zhang, J. Ge, P. Jiang, Y. Qin, X. Cao, Experimental study of nanoparticle and surfactant stabilized emulsions flooding to enhance heavy oil recovery, Journal of Petroleum Science and Engineering. 163 (2018) 476-483.

H. ShamsiJazeyi, C. Miller, M. Wong, J. Tour, R. Verduzco, Polymer-coated nanoparticles for enhanced oil recovery, Journal of Applied Polymer Science. 131 (2014) 1-13.

H. Soo, C. Radke, Flow of dilute, stable liquid and solid dispersions in underground porous media, AIChE Journal. 31 (1985) 1926-1928.

H. Soo, C. Radke, Velocity effects in emulsion flow through porous media, Journal of Colloid and Interface Science. 102 (1984) 462-476.

H. Zhang, T. Ramakrishnan, A. Nikolov, D. Wasan, Enhanced oil recovery driven by nanofluid structural disjoining pressure: flooding experiments and microvisualization, Energy and Fuels.

I. Kalashnikova, H. Bizot, B. Cathala, I. Capron, New Pickering emulsions stabilized by bacterial cellulose nanocrystal, Langmuir. 12 (2011) 7471-7479.

I. Kim, A. Taghavy, D. DiCarlo, C. Huh, Aggregation of silica nanoparticles and its impact on particle mobility under high-salinity conditions, Journal of Petroleum Science and Engineering. 133 (2015) 376-383.

I. Kim, A. Worthen, K. Johnston, D. DiCarlo, C. Huh, Size-dependent properties of silica nanoparticles for Pickering stabilization of emulsions and foams, Journal of Nanoparticle Research. 18:82 (2016).

I. Kim, A. Worthen, M. Lotfollahi, K. Johnston, D. Dicarlo, C. Huh, Nanoparticle-stabilized emulsions for improved mobility control for adverse-mobility waterflooding, 19th European Symposium on Improved Oil Recovery. April 2017.

J. Asenjo, B. Andrews, Aqueous two-phase systems for protein separation: Phase separation and applications, Journal of Chromatography A. 1238 (2012) 1-10.

J. Dong, A. Worthen, L. Foster, Y. Chen, K. Cornell, S. Bryant, T. Truskett, C. Bielawski, K. Johnston, Modified montmorillonite clay particles for stable oil-in-seawater emulsions, ACS Applied Materials and Interfaces. 6 (2014) 11502-11513.

J. Driver, Tailoring polymer molecular weight distribution to pore size distribution using filtration and mechanical degradation, MS Thesis, The University of Texas at Austin. 2017.

J. Felichowska, M. Bolzinger, Y. Chevalier, Effects of solid particle content on properties of o/w Pickering emulsions, Journal of Colloid and Interface Science. 351 (2010) 348-356.

J. Juarez, C. Whitby, Oil-in-water Pickering emulsion destabilization at low particle concentrations, Journal of Colloid and Interface Science. 368 (2012) 319-325.

J. Kirsner, D. Siems, K. Burrows-Lawson, D. Carbajal, I. Robb, D. Jamison, Invert drilling fluids for use in drilling in subterranean formation, United States Patent. (2009) US7488704B2.

J. Muth, J. Lewis, Microstructure and elastic properties of colloidal gel foams, Langmuir. 22 (2017) 6869-6877.

J. Rubio, J. Kitchener, The mechanism of adsorption of poly(ethylene oxide) flocculant on silica, Journal of Colloid and Interface Science. 57 (1976) 132-142.

J. San, S. Wang, J. Yu, N. Liu, R. Lee, Nanoparticle-stabilized carbon dioxide foam used in enhanced oil recovery: effect of different ions and temperature, SPE Journal. 22 (2017) 1416-1424.

J. Santos, N. Calero, L. Trujillo-Cayado, J. Munoz, Development and characterization of a continuous phase based on a fumed silica and a green surfactant with emulsion applications, Colloids and Surfaces A. 555 (2018) 351-357.

J. Sheng, Status of surfactant EOR technology, Petroleum. 1 (2015) 97-105.

J. Szczech, J. Higgins, S. Jin, Enhancement of the thermoelectric properties in nanoscale and nanostructured materials, Journal of Materials Chemistry. 21 (2011) 4037-4055.

J. Taber, F. Martin, R. Seright, EOR Screening criteria revisited – Part 1: Introduction to screening criteria and enhanced recovery field projects, SPE Reservoir Engineering. 12 (1997) 189-198.

J. Weston, R. Jentoft, D. Resasco, J. Harwell, Silica nanoparticle wettability: characterization and effects on the emulsion properties, Industrial and Engineering Chemistry Research. 54 (2015) 4274-4284.

K. Boode, P. Walstra, Partial coalescence in oil-in-water emulsions 1. Nature of the aggregation, Colloids and Surfaces A: Physicochemical and Engineering Aspects, 81 (1993) 121-137.

K. Edgehouse, M. Escamilla, L. Wang, R. Dent, K. Pachuta, L. Kendall, P. Wei, A. Sehirliolgu, E. Pentzer, Stabilization of oil-in-water emulsions with graphene oxide and cobalt oxide nanosheets and preparation of armored polymer particles, Journal of Colloid and Interface Science. 241 (2019) 269-278.

K. Jafarabad, S. Sawant, J. Joshi, Enzyme and protein mass transfer coefficient in aqueous two-phase systems-I. Spray extraction columns, Chemical Engineering Science. 47 (1992) 57-68.

K. Liu, J. Jiang, Z. Cui, B. Binks, pH-responsive Pickering emulsions stabilized by silica nanoparticles in combination with a conventional zwitterionic surfactant, Langmuir. 33 (2017) 2296-2305.

K. Panthi, R. Singh, K. Mohanty, Microencapsulation and stimuli-responsive controlled release of particles using water-in-air powders, Langmuir. 33 (2017) 3998-4010.

K. Peddireddy, T. Nicolai, L. Benyahia, I. Capron, Stabilization of Water-in-Water Emulsions by Nanorods, ACS Macro Letters. 5 (2016) 283-286.

K. Saleh, L. Forny, P. Guigon, I. Pezron, Dry water: from physico-chemical aspects to process-related parameters, Chemical Engineering Research and Design. 89 (2011) 537-544.

K. Xu, D. Agrawal, Q. Darugar, Hydrophilic nanoparticle-based enhanced oil recovery: microfluidic investigations on mechanisms, Energy and Fuels. 32 (2018) 11243-11252.

K. Xu, P. Zhu, T. Colon, C. Huh, M. Balhoff, A microfluidic investigation of the synergistic effect of nanoparticles and surfactants in macro-emulsion-based enhanced oil recovery, SPE Journal. 22 (2017) 459-469.

K. Xu, T. Liang, P. Qi, J. Lu, C. Huh, M. Balhoff, A 2.5-D glass micromodel for investigation of multi-phase flow in porous media, Lab on a Chip. 17 (2017) 640-646.

L. Chu, M. Daniels, L. Francis, Use of (Glycidoxypropyl)trimethoxysilane as a binder in colloidal silica coatings, Chemistry of Materials. 9 (1997) 2577-2582.

L. Gabrielli, L. Connell, L. Russo, J. Jimenez-Barbero, F. Nicotra, L. Cipolla, J. Jones, Exploring GPTMS reactivity against simple nucleophiles: chemistry beyond hybrid materials fabrication, RCS Advances

L. Gabrielli, L. Russo, A. Pveda, J. Jones, F. Nicotra, J. Jimenez-Barbero, L. Cipolla, Epoxide opening versus silica condensation during sol-gel hybrid biomaterial synthesis, Chemistry A European Journal. 19 (2013) 7856-7864.

L. Mei, D. Lin, Z. Shu, Z. Han, Densities and Viscosities of Polyethylene Glycol + Salt + Water Systems at 20°C, J. Chem. Eng. Data. 40 (1995) 1168-1171.

L. Mejia, M. Tagavifar, K. Xu, M. Mejia, Y. Du, Matthew Balhoff, Surfactant flooding in oil-wet micromodels with high permeability fractures, Fuel. 241 (2019) 117-1128.

L. Nicora, P. Pirovano, N. Blomberg, K. Taugbol, High-density invert-emulsion system with very low solids content to drill ERD and HPHT wells, SPE International Symposium on Oilfield Chemistry. February 2001.

L. Otero-Gonzalez, J. Field, I. Calderon, C. Aspinwall, F. Shadman, C. Zeng, R. Sierra-Alvarez, Fate of fluorescent core-shell silica nanoparticles during simulated secondary wastewater treatment, Water Research. 77 (2015) 170-178.

L. Ridel, M. Bolzinger, N. Gilon-Delepine, P. Dugas, Y. Chevalier, Pickering emulsions stabilized by charged nanoparticles, Soft Matter. 12 (2016) 7564-7576.

L. Yu, B. Ding, M. Dong, Q. Jiang, Plugging ability of oil-in-water emulsions in porous media: experimental and modeling study, Industrial & Engineering Chemistry Research. 57 (2018) 14795-14808.

M. Creighton, W. Zhu, F. van Krieken, R. Petteruti, H. Gao, R. Hurt, Three-dimensional graphene-based microbarriers for controlling release and reactivity in colloidal liquid phases, ACS Nano. 10 (2016) 2268-2276.

M. Daniels, J. Sefcik, L. Francis, A. McCormick, Reactions of a trifunctional silane coupling agent in the presence of colloidal silica sols in polar media, Journal of Colloid and Interface Science. 219 (1999) 351-356.

M. Daniels, L. Francs, Silane adsorption behavior, microstructure, and properties of glycidoxypropyltrimethoxysilane-modified colloidal silica coatings, Journal of Colloid and Interface Science. 205 (1998) 191-200.

M. Derakhshandeh, B. Pilapil, B. Workman, M. Trifkovic, and S. Bryant, Analysis and network formation and long-term stability in silica nanoparticle stabilized emulsions, Soft Matter. 14 (2018) 4268-4277.

M. Destribats, M. Rouvet, C. Gehin-Delval, C. Schmitt, B. Binks, Emulsions stabilized by whey protein particles: towards food-grade Pickering emulsions, Soft Matter. 10 (2014) 6941-6954.

M. Kaganyuk, A. Mohraz, Non-monotonic dependence of Pickering emulsion gel rheology on particle volume fraction, Soft Matter. 13 (2017) 2513-2522.

M. Lee, H. Chan, A. Mohraz, Characteristics of Pickering emulsion gels formed by droplet bridging, Langmuir. 28 (2012) 3085-3091.

M. Rincon-Fontan, L. Rodriguez-Lopez, X . Vecino, J. Cruz, A. Moldes, Study of the synergic effect between mica and biosurfactant to stabilize Pickering emulsions containing Viatmin E using a triangular design, Journal of Colloid and Interface Science. 537 (2019) 34-42.

M. Roberts, Shear-induced emulsions stabilized with surface-modified silica nanoparticles, MS Thesis, The University of Texas at Austin, 2011.

M. Tagavifar, S. Herath, U. Weerasooriya, K. Sepehrnoori, G. Pope, Measurment of microemulsion viscosity and its implications for chemical enhanced oil recovery, SPE Journal. 23 (2018) 65-83.

M. Vis, J. Opdam, I. van't Oor, G. Soligno, R. van Roij, R. Tromp, B. Erne, Water-in-Water Emulsions Stabilized by Nanoplates, ACS Macro Letters. 4 (2015) 965-968.

N. Ashby, B. Binks, Pickering emulsions stabilized by laponite clay particles, Physical Chemistry Chemical Physics. 2 (2000) 5640-5646

N. Briggs, A. Raman, L. Barrett, C. Brown, B. Li, D. Leavitt, C. Aichele, S. Crossley, Stable Pickering emulsions using mulit-walled carbon nanotubes of varying wettability, Colloids and Surfaces A: Physicochemical and Engineering Aspects. 537 (2018) 227-235.

N. Denkov, Mechanisms of foam destruction by oil-based antifoams, Langmuir. 20 (2004) 9463-9505.

N. Eskandar, S. Simovic, C. Prestidge, Synergistic effect of silica nanoparticles and charged surfactants in the formation and stability of submicron oil-in-water emulsions, Physical Chemistry Chemical Physics. 9 (2007) 6426-6434.

N. Griffith, Y. Ahmad, H. Daigle, C. Huh, Nanoparticle-stabilized natural gas liquid-in-water emulsions for residual oil recovery. SPE Improved Oil Recovery Conference, April 2016.

N. Kumar, T. Guar, A. Mandal, Characterization of SPN Pickering emulsions for application in enhanced oil recovery, Journal of Industrial and Engineering Chemistry. 54 (2017) 304-315.

N. Maurya, A. Mandal, Investigation of synergistic effect of nanoparticle and surfactant in macro emulsion based EOR applications in oil reservoirs, Chemical Engineering Research and Design. 132 (2018) 370-384.

N. Saleh, T. Sarbu, K. Sirk, G. Lowry, K. Matyjaskewski, R. Tilton, Oil-in-water emulsions stabilized by highly charged polyelectrolyte-grafted silica nanoparticles, Langmuir. 21 (2005) 9873-9878.

N. Yan, J. Masliyah, Characterization and demulsification of solids-stabilized oil-in-water emulsions. Part 2: Demulsification by the addition of fresh oil, Colloids and Surfaces A: Physicochemical and Engineering Aspects. 75 (1993) 123-132.

N. Yan, Y. Maham, J. Masliyah, M. Gray, A. Mather, Measurement of contact angles for fumed silica nanospheres using enthalpy of immersion data, Journal of Colloid and Interface Science. 228 (2000) 1-6.

N. Zhang, L. Zhang, D. Sun, Influence of emulsification process on the properties of Pickering emulsions stabilized by layered double hydroxide particles, Langmuir. 31 (2015) 4619-4626.

P. Ajayan, J. Tour, Nanotube composites, Nature Materials Science. 447 (2007) 1066-1068.

P. Boul, A. Ye, X. Pang, V. Goel, L. Eoff, B. Reddy, Nanosilica-based conformance gels, SPE European Formation Damage Conference, June 2015. SPE-174265-MS

P. Greenwood, B. Gevert, Aqueous silane modified silica sols: theory and preparation, Pigment & Resin Technology. 40 (2011) 275-284.

P. Kundu, A. Agrawal, H. Mateen, I. Mishra, Stability of oil-in-water macro-emulsion with anionic surfactant: effect of electrolytes and temperature, Chemical Engineering Science. 102 (2013) 176-185.

P. Lettieri, D. Newton, J. Yates, Homogeneous bed expansion of FCC catalysts, influence of temperature on the parameters of the Richardson-Zaki equation, Powder Technology. 123 (2002) 221-231.

P. Qi, D. Ehrenfired, H. Koh, M. Balhoff, Reduction of residual oil saturation in sandstone cores by use of viscoelastic polymers, SPE Journal. 22 (2017) 447-459.

P. Schonherr, A. Seifert, R. Lungwitz, F. Simon, N. Moszner, P. Burtscher, S. Spange, Modification of solid particles with epoxysilanes and characterization by the Preussmann-test, Progress in Organic Coatings. 75 (2012) 335-343.

P. Sullivan, G. Tustin, Y. Christanti, G. Kubala, B. Drochon, T. Hughes, Aqueous two-phase emulsion gel systems for zone isolation, United States Patent. (2010) US7703527 B2.

P. Walstra, Principles of emulsion formation, Chemical Engineering Science. 48 (1993) 333-349.

Q. Lan, F. Yang, S. Zhang, S. Liu, J. Xu, D. Sun, Synergistic effect of silica nanoparticle and cetyltrimethylammonium bromide on the stabilization of o/w emulsions, Colloids and Surfaces A: Physicochemical Engineering Aspects. 302 (2007) 126-135.

R. Aveyard, B. Binks, J. Clint, Emulsions stabilized solely by colloidal particles, Advances in Colloid and Interface Science. 100-102 (2003) 503-546.

R. Aveyard, B. Binks, J. Clint, P. Fletcher, Foams and emulsions: their stability and breakdown by solid Particles and liquid Droplets. In Foams and Emulsions, J. Sadoc, N. Rivier, Kluwar Academic Publishers (1999).

R. de Freitas, T. Nicolai, C. Chassenieux, L. Benyahia, Stabilization of Water-in-Water Emulsions by Polysaccharide-Coated Protein Particles, Langmuir. 32(5) (2016) 1227-1232.

R. Fortenberry, D. Kim, N. Nizamindin, S. Adkins, G. Arachilage, H. Koh, U. Weeasooriya, G. Pope, Use of cosolvents to improve alkaline/polymer flooding, SPE Journal. 20 (2015) 255-266.

R. Healy, R. Reed, Physicochemical aspects of microemulsion flooding, SPE Journal. 257 (1974) 492-501.

R. Hwan, C. Miller, T. Fort, Determination of microemulsion phase continuity and drop size by ultracentrifugation, Journal of Colloid and Interface Science. 68 (1979) 221-234.

R. Jiang, K. Li, R. Horne, A mechanism study of wettability and interfacial tension for EOR using silica nanoparticles, SPE ATCE, October 2017. SPE-187096-MS.

R. Kaminsky, R. Wattenbarger, J. Lederhos, S. Leonardi, Viscous oil recovery using solids-stabilized emulsions, SPE Annual Technical Conference and Exhibition, September 2010.

R. Pichot, F. Spyropooulos, I. Norton, Mixed-emulsifier stabilized emulsions: Investigation of the effect of monoolein and hydrophilic silica particle mixtures on the stability against coalescence, Journal of Colloid and Interface Science. 329 (2009) 284-291.

R. Seright, The effects of mechanical degradation and viscoelastic behavior on injectivity of polyacrylamide solutions, SPE Journal. 23 (1983) 474-485.

R. Singh, K. Panthi, K. Mohanty, Microencapsulation of acids by nanoparticles for acid treatment of shales, Energy and Fuels. 31 (2017) 11755-11764.

R. Torrico, S. Harb, A. Trentin, M. Uvida, S. Pulcinelli, C. Santilli, P. Hammer, Structure and properties of epoxy-siloxane-silica nanocomposite coatings for corrosion protection, Journal of Colloid and Interface Science. 513 (2018) 617-628.

S. Abedi, N. Suteria, C. Chen, S. Vanapalli, Microfluidic production of size-tunable hexadecane-in-water emulsions: effect of droplet size on destabilization of two-dimensional emulsions due to partial coalescence, Journal of Colloid and Interface Science. 533 (2019) 59-70.

S. Arditty, V. Schmitt, F. Lequeux, F. Leal-Calderon, Interfacial properties in solid-stabilized emulsions, The European Physical Journal B. 44 (2005) 381-393.

S. Bjorkegren, L. Nordstierna, A. Torncrona, A. Palmqvist, Hydropilic and hydrophobic modifications of colloidal silica particles for Pickering emulsions, Journal of Colloid and Interface Science. 487 (2017) 250-257.

S. Caserta, L. Sabetta, M. Simeone, S. Guido, Shear-induced coalescence in aqueous biopolymer mixtures, Chemical Engineering Science. 60 (2005) 1019-1027.

S. Gabel, Generation, stability, and transport of nanoparticle-stabilized oil-in-water emulsions in porous media, MS Thesis, The University of Texas at Austin. 2014.

S. Hann, K. Stebe, D. Lee, AWE-somes: All Water Emulsion Bodies with Permeable Shells and Selective Compartments, ACS Applied Materials and Interfaces. 9 (2017) 25023-25028.

S. Ko, C. Huh, Use of nanoparticles for oil production applications, Journal of Petroleum Science and Engineering. 172 (2019) 97-114.

S. Lee, D. Kim, C. Huh, G. Pope, Development of a comprehensive rheological property database for EOR polymers, SPE Annual Technical Conference. October 2009.

S. Melle, M. Lask, G. Fuller, Pickering emulsions with controllable stability, Langmuir. 21 (2005) 2158-2162.

S. Raja, V. Murty, V. Thivaharan, V. Rajasekar, V. Ramesh, Aqueous Two Phase Systems for the Recovery of Biomolecules – A Review, Science and Technology. 1 (2011) 7-16.

S. Simon, S. Theiler, A. Knudsen, G. Oye, J. Sjoblom, Rheological properties of particle-stabilized emulsions, Journal of Dispersion Science and Technology. 31 (2010) 632-640.

S. Simovic, C. Prestidge, Nanoparticles of varying hydrophobicity at the emulsion droplet-water interface: adsorption and coalescence stability, Langmuir. 20 (2004) 8357-8365.

S. Varanasi, L. Henzel, L. Mendoza, R. Prathapan, W. Batchelor, R. Tabor, G. Garnier, Pickering emulsions electrostatically stabilized by cellulose nanocrystals, frontiers in Chemistry. 6 (2018) 409.

S. Zhang, D. Sun, X. Dong, C. Li, J. Xu, Aqueous foams stabilized with particles and nonionic surfactants, Colloids and Surfaces A: Physicochemical and Engineering Aspects. 324 (2008) 1-8.

T. Fuma, M. Kawaguchi, Rheological responses of Pickering emulsions prepared using colloidal hydrophilic silica particles in the presence of NaCl, Colloids and Surfaces A: Physicochemical and Engineering Aspects. 465 (2015) 168-174.

T. Hariz, Nanoparticle-stabilized CO_2 foams for potential mobility control applications, MS Thesis, The University of Texas at Austin. 2012.

T. Horozov, B. Binks, Particle-stabilized emulsions: A bilayer or a bridging monolayer? Angewandte Chemi. 118 (2006) 787-790.

T. Horozov, B. Binks, T. Gottschalk-Gaudig, Effect of electrolyte in silicone oil-in-water emulsions stabilized by fumed silica particles, Physical Chemistry Chemical Physics. 9 (2007) 6398-6404.

T. Ngai, S. Bon, Particle-stabilized emulsions and colloids: formation and applications, Royal Society of Chemistry Soft Matter, London, UK 2014.

T. Sharma, G. Kumar, B. Chon, J. Sangwai, Thermal stability of oil-in-water Pickering emulsion in the presence of nanoparticle, surfactant, and polymer, Journal of Industrial and Engineering Chemistry. 22 (2015) 324-334.

T. Sharma, G. Kumar, J. Sangwai, Comparative effectiveness of production and performance of Pickering emulsion stabilized by nanoparticle-surfactant-polymer over surfactant-polymer (SP) flooding for enhanced oil recovery for Brownfield reservoir, Journal of Petroleum Science and Engineering. 129 (2015) 221-232.

T. Zhang, A. Davidson, S. Bryant, C. Huh, Nanoparticle-stabilized emulsions for applications in enhanced oil recovery, Society of Petroleum Engineers. SPE Improved Oil Recovery Symposium, April 2010.

W. Frith, Mixed biopolymer aqueous solutions – phase behavior and rheology, Advances in Colloid and Interface Science. 161(2010) 48-60.

W. Ganley, J. van Duijneveldt, Controlling the rheology of montmorillonite stabilized oil-in-water emulsions, Langmuir. 33 (2017) 1679-1686.

W. Ganley, P. Ryan, J. van Duijneveldt, Stabilisation of water-in-water emulsions by montmorillonite platelets, Journal of Colloid and Interface Science. 505 (2017) 139-147.

W. He, D. Wu, J. Loi, K. Zhang, Y. Xiang, L. Long, S. Qin, J. Yu, Q. Zhang, Surface modification of colloidal silica nanoparticles: controlling the size and grafting process, Bulletien of Korean Chemical Society. 34 (2013) 2747-2753.

W. Salathiel, T. Muecke, C. Cooke, N. Li, Well treatment with emulsion dispersions, United States Patent. (1980) 4233165.

X. Guillory, A. Tessier, G. Gratien, P. Weiss, S. Colliec-Jouault, D. Dubreuil, J. Lebreton, J. Le Bideau, Glycidyl alkoxysilane reactivities towards simple nucleophiles in organic media for improved molecular structure definition in hybrid materials, RCS Advances. 6 (2016) 74087-74099.

X. Ma, N. Lee, H. Oh, J. Kim, C. Rhee, K. Park, S. Kim, Surface modification and characterization of highly dispersed silica nanoparticles by a cationic surfactant, Colloids and Surfaces A: Physicochemical and Engineering Aspects. 358 (2010) 172-176.

X. Yang, Z. Liu, A kind of nanofluid consisting of surface-functionalized nanoparticles, Nanoscale Research Letters. 5 (2010) 1324-1328.

X. Zhao, B. Huang, M. El-Aooiti, D. Rousseau, Demulsification to control solute release from Pickering crystal-stabilized water-in-oil emulsions, Journal of Colloid and Interface Science. 509 (2018) 360-368.

Y. Ahmad, Nanoparticle-stabilized oil-in-water emulsions for residual oil recovery, MS Thesis, The University of Texas at Austin. 2015.

Y. Chevalier, M. Bolzinger, Emulsions stabilized with solid nanoparticles: Pickering emulsions, Colloids and Surfaces A: Physicochemical Engineering Aspects. 439 (2013) 23-34.

Y. Cui, M. Threlfall, J. van Duijneveldt, Optimizing organoclay stabilized Pickering emulsions, Journal of Colloid and Interface Science. 356 (2011) 665-671.

Y. Kharaka, D. Cole, J. Thordsen, E. Kakouros, H. Nance, Gas-water-rock interactions in sedimentary basis: CO_2 sequestration in the Frio Formation, Texas, USA, Journal of Geochemical Exploration. 89 (2006) 183-186.

Y. Song, A. Sauret, H. Shum, All-aqueous multiphase microfluidics, Biomicrofluidics. 7 (2013) 1-13.

Y. Wu, Z. Zhu, L. Mei, Interfacial Tension of Poly(ethylene glycol) + Salt + Water Systems, J. Chem. Eng. Data. 41 (1996) 1032-1035.

Y. Zhu, J. Jiang, K. Liu, Z. Cui, B. Binks, Switchable Pickering emulsions stabilized by silica nanoparticles hydrophobized in situ with a conventional cationic surfactant, Langmuir. 31 (2015) 3301-3307.

Z. Estephan, J. Jaber, J. Schlenoff, Zwitterion-stabilized silica nanoparticles: toward nonstick nano, Langmuir. 26 (2010) 16884-16889.

Z. Xue, A. Worthen, A. Qajar, I. Robert, S. Bryant, C. Huh, M. Prodanovic, K. Johnston, Viscosity and stability of ultra-high internal phase CO_2-in-water foams stabilized with surfactants and nanoparticles with or without polyelectrolytes, Journal of Colloid and Interface Science. 461 (2016) 393-395.